OBSIDIAN HYDRATION AND ITS CONSEQUENCES FOR THE AR-AR DATING METHOD

By

Ariel K. Dickens

Submitted in partial fulfillment
of the requirements for the degree of
Master of Science in Geology

New Mexico Institute of Mining and Technology

Department of Earth and Environmental Science

Socorro, New Mexico

December, 2007

ABSTRACT

Volcanic glass has been a problematic material in Ar-Ar geochronological studies, in part due to hydration and the resultant element mobility of K and Ar. Ar-Ar and electron microprobe results from a systematic investigation of obsidian show that obsidian hydration can affect the precision and accuracy of apparent Ar-Ar ages, but these effects can be mitigated by specialized sample preparation techniques.

A select suite of variably hydrated obsidian samples were collected from the No Agua Peaks volcanic complex, NM, to systematically investigate how four preparation and four Ar-Ar extraction techniques affect obsidian ages. Obsidian samples prepared by different preparation techniques were chemically imaged and analyzed by an electron microprobe to assess chemistry and element mobility. Microprobe results show that the hydration process does not cause significant element mobility, and most water is concentrated within the hydration rinds. A long ultrasonic bath in water or the air abrasion preparation technique were determined the best methods to remove hydration rinds. Multi-step laser or furnace extractions were shown to be the best extraction methods. Once preparation and extraction methods were established, all other samples were dated. At the No Agua Peaks volcanic complex two temporally distinct eruptive events, 3.86±0.06 Ma and 4.07±0.03 Ma, were dated. These events are chemically distinct, and the ages match stratigraphy with a meter-thick paleosol developed between the two eruptive events.

Six mapped lobes at Cerro del Medio were dated in this study; the age of Cerro del Medio brackets the resurgence of Redondo Peak with the eruption of the Bandelier Tuff. There are two probable scenarios for formation of Cerro del Medio, based on whether the oldest sanidine ages are influenced by xenocrystic material. In the first scenario Cerro del Medio started forming at 1.22± 0.02 Ma in up to three temporally resolvable pulses, periodic dome building was sustained for 0.08±0.04 Ma, and resurgence was completed within 0.08± 0.04 Ma after the eruption of the Bandelier Tuff. In the second scenario, which considers the oldest lobe ages being influenced by xenocrysts, Cerro del Medio formed in up to two temporally resolvable events starting at 1.18± 0.03 Ma. In this scenario dome building lasted for 0.05± 0.04 Ma, and resurgence was completed within 0.08± 0.04 Ma.

Four samples of post 0.5 Ma units associated with the Valles caldera were dated to determine the youngest ages of activity, and to assess volcanic hazards associated. Of the four samples dated in this study, only one age appears accurate at 0.257± 0.088 Ma. Using ages from the current and previous studies there are two preferred age scenarios: 1) the units are 0.25± 0.06 Ma, or 2) if xenocryst contamination is affecting Ar-Ar ages, then an age of 0.054± 0.005 Ma, based on results from four non-K-based methods, may be more accurate.

ACKNOWLEDGEMENTS

There are many people whom have helped me through my thesis over the years that I would like to thank. Joseph Levay and Michel Houseman of World Minerals, whom I met through Richard Chamberlin of the NMBMMR, made sample collection possible at the No Agua Peaks volcanic complex. The Valles Caldera National Preserve was very generous in granting me access to the park, and allowing me to collect samples from archaeologically important obsidian flows. I thank Ana Stephan and Bob Parmenter who provided assistance with access to the park.

Financially there are many people to thank as well. First I thank the Department of Earth and Environmental Sciences for granting me teaching assistantships for my first years here. I also thank the New Mexico Geochronology Research Laboratory (NMGRL), the Electron Microprobe Laboratory at NMIMT, and Virginia McLemore from the NMBMMR for granting me research assistantships to fund my education. The New Mexico Geological Society and Chevron both gave generous grants to me to fund my research as well.

There are many other people that helped me along the way that need to be recognized. Rich Esser and Lisa Peters were two people that I could always turn to for much needed help and support, not to mention the countless hours of mineral separation and technical assistance in the NMGRL. I'd like to thank Lynn Heizler for her insights to microprobe related matters. Frasier Goff spent days showing me around the Valles caldera helping with sample collection and teaching me some of his vast knowledge on

the caldera history; Cathy Goff was kind and insightful as well. Jamie Gardner helped me understand the geological mapping done at the Cerro del Medio and his interpretation of the eruptive history at the dome was extremely helpful. Erin Phillips generously allowed me to use two of her Cerro del Medio samples as well as all of her data for Cerro del Medio obsidians that she collected and analyzed. I thank Lewis Gillard, through Molycorp, helped me produce my two sample location figures. I thank my all my friends, especially those I met here (316!), whom gave me help and support with drafts (both beer and paper), insight, and stability. I thank Nova Meek for inspiring me to obtain a Master's degree. I thank my family for all their support over the years, for tolerating me, and not giving up. I acknowledge Ras Tafari, the Light I follow, for leading my life in, what I believe, a good direction.

My advisors were the people whom saw me grow the most, and without them I might not have grown so well. I thank Andrew Campbell for his mineralogical support, insightful comments on my thesis, and for helping me with the stable isotopic analysis of obsidian, although not used in this study. Nelia Dunbar spent maybe years of her life reading paper after paper with me so that I could learn the processes of glass hydration. She also helped immeasurably with my geochemical data, funding, and support throughout the years. Last I would like to thank my advisor and friend, Bill McIntosh, who rounded many of my rough (maybe even sharp) edges throughout the years. Bill was here for me since I came to Socorro. He extended himself and his family to me, and humbly gave countless hours of his time to reading my torturous thesis and helping me fix my VW buses. His patience, insight, support, and kindness all exceed what I ever expected from any individual. Bill is awesome.

TABLE OF CONTENTS

LIST OF FIGURES

LIST OF TABLES

This Thesis is accepted on behalf of the faculty
of the Institute by the following committee:

William C McIntosh
Academic Advisor

William C McIntosh
Research Advisor

Andrew Campbell
Committee Member

Welton W. Gunn
Committee Member

8/9/07
Date

I release this document to the New Mexico Institute of Mining and Technology

Ariel Dickens 8-9-07

Ariel Dickens Date

CHAPTER 1: INTRODUCTION

Although K-rich glass is a common product of volcanic eruptions, it has not been systematically investigated as an Ar-Ar dating material. Volcanic glass shards typically produce inaccurate ages, but some obsidians yield meaningful results (Phillips et al., 2007; Singer et al., 2004; Cerling et al., 1985; Gardner and Goff, 1984). Numerous studies have linked hydration of glass and element mobility to problems associated with Ar-Ar dating (Whitehead et al., 1995; Petit et al., 1990; Fiore et al., 1999; Mungall and Martin, 1994; Jezek and Noble, 1978). This study is an attempt to systematically investigate the suitability of obsidian for Ar-Ar dating. This study uses a combination of electron microprobe and Ar-Ar dating to quantitatively assess the effects of hydration on obsidian chemistry and Ar-Ar ages by using different preparation techniques to selectively remove hydrated components from glass samples.

Sample suites of sanidine, unhydrated obsidian, hydrated obsidian, and perlite were collected from the dome complex at No Agua Peaks, NM to establish how certain preparation and extraction techniques affected sample ages. Chemical analysis and imaging of glass and perlite was performed using an electron microprobe. The imaging, done with backscattered electrons (BSE), was used to visualize the relationship between obsidian and perlite, as well as to determine whether hydration rinds were removed using certain preparation techniques. Quantitative geochemical analyses were preformed to assess element mobility, hydration and augment BSE data. Samples were Ar-Ar dated by either a furnace or CO_2 laser to determine if extraction techniques affect apparent age.

The obsidian preparation techniques established using a select set of No Agua Peaks samples were then applied to date all other No Agua Peaks obsidian samples, as well as obsidian samples from the Valles caldera. Feldspar from the No Agua Peaks complex and Cerro del Medio dome were also Ar-Ar dated to obtain feldspar ages for some units; this was to assess the age data obtained from obsidian samples. The No Agua Peaks samples were dated to determine if there were temporally distinct eruptions at the complex. At the Valles caldera multiple lobes were dated from the oldest ring dome, Cerro del Medio, to constrain resurgence activity. The youngest eruptive products associated with the Valles caldera, the Banco Bonito lava, the El Cajete pumice, and Battleship Rock ignimbrite were also dated. These units were sampled to assess ages that have been disputed in the past due to variable results and high uncertainties in previous studies (Reneau et al., 1996; Toyoda et al., 1995; Spell and Harrison, 1993; Self et al., 1991; Goff et al., 1989; Goff et al., 1986; Miyachi et al., 1985; Gardner and Goff, 1984).

CHAPTER 2: PHYSIOCHEMICAL EFFECTS OF GLASS HYDRATION AND IMPLICATIONS FOR THE AR-AR METHOD

2.1 Glass and obsidian

There are many types of glass that are associated with volcanic eruptions and crystallization. Glass forms by quenching due to the large temperature gradient between magma and the surrounding environment. The most common types of volcanic glass are melt inclusions, pumice, glass shards, matrix glass, and obsidian. A melt inclusion is trapped within a crystal during crystal formation; these are useful for discerning the chemical evolution of magma chambers. Pumice is quickly cooled ejecta or pyroclastic material from an eruption that has undergone major vesiculation and has a high surface to volume ratio. Glass shards are primarily composed of shattered bubble walls and junctions formed by the destruction of pumice during an eruption. Matrix glass is interstitial material that adheres to the sides of grains and can act as a "cement" holding crystals together. All four of these glass types have large surface to volume ratios; this increases the rate that glass hydrates, converting the glass to perlite or clay. Obsidian is non-vesicular glass, usually forming domes and lobes during silicic volcanism. Obsidian is generally black in color with a glassy texture, is characterized by conchoidal fracture, and typically has a small surface area to volume ratio. Large obsidian flows are often associated with high-silica rhyolite magmatism, which has silica contents of 76 weight percent or higher. Obsidian is not defined as a mineral because there is no crystalline

structure, and does not behave the same way as minerals (in terms of element mobility) because of this.

2.2 Physical properties of hydration

Volcanic glass absorbs water over time in a process called hydration to form perlite. The perlitization process is a low-temperature alteration of glass by meteoric water (Cerling et al., 1985). This process is different from a higher temperature alteration because at low temperatures there can be major elemental changes without devitrification, a process that converts glass into crystalline material at high temperatures (Fieore et al., 1999; Mungall and Martin, 1994; Cerling et al., 1985). Studies have shown that the hydration process does not necessarily cause major changes in chemical composition (Fieore et al., 1999; Zielinski et al., 1977), although other studies have shown the opposite is true (Mungall and Martin, 1994; Cerling et al., 1985). Jezek and Noble (1978) showed that perlitic hydration rinds, as a result of volume change, break off of obsidian cores in a concentric pattern once the glass has absorbed between three to five weight percent water. From this observation, they suggested that there is a limited space available in hydration rinds for absorbed water. Friedman et al. (1966) not only discovered that the hydration front forms a sharp contact with the obsidian, but that the hydration rind will only get ~100 μm thick before it breaks off in this concentric pattern (Figure 2.1). This hydration habit has an associated texture called perlitic or "onionskin" texture, because it can look like a cut onion (Figure 2.2).

2.3 Simplified Model

The process of natural hydration can be illustrated in a simplified model (Figure 2.3). An unaltered obsidian core interacts with meteoric water as it diffuses into the core

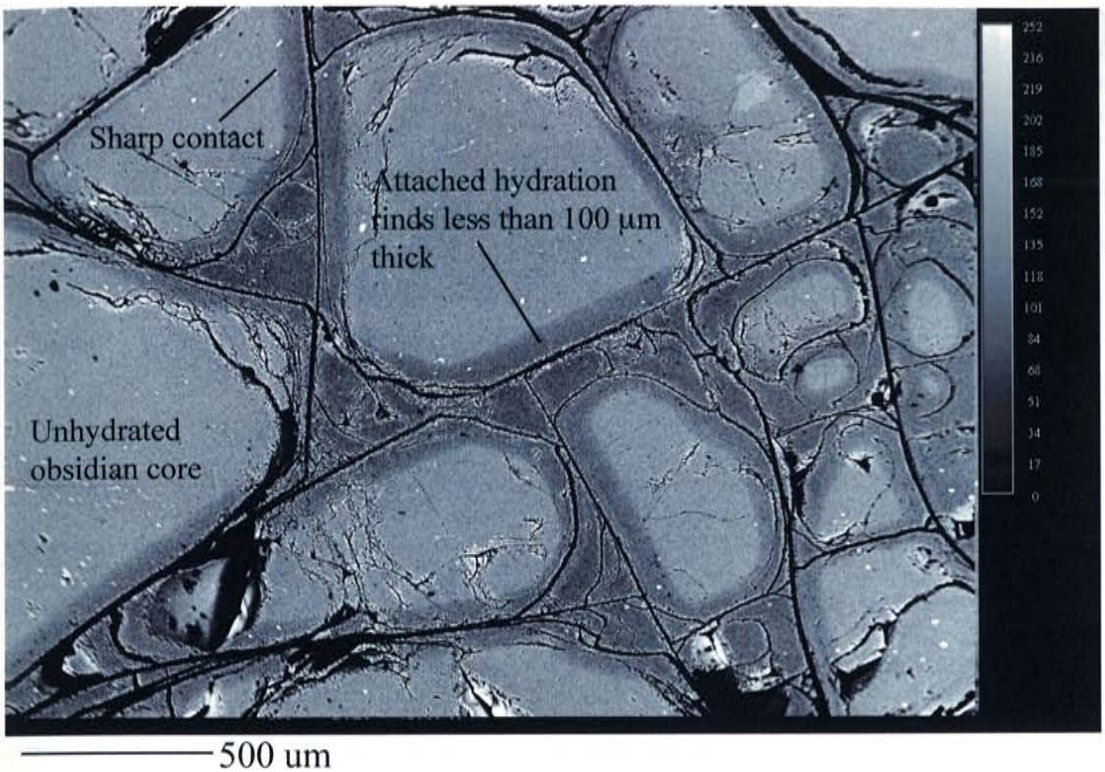

Figure 2.1. Backscattered electron image of obsidian sample AD-02 displaying dark gray perlite rinds still attached to the lighter-colored unaltered cores. Note how the perlite rind forms a sharp contact with the obsidian and the rind is no more than 100 μm thick.

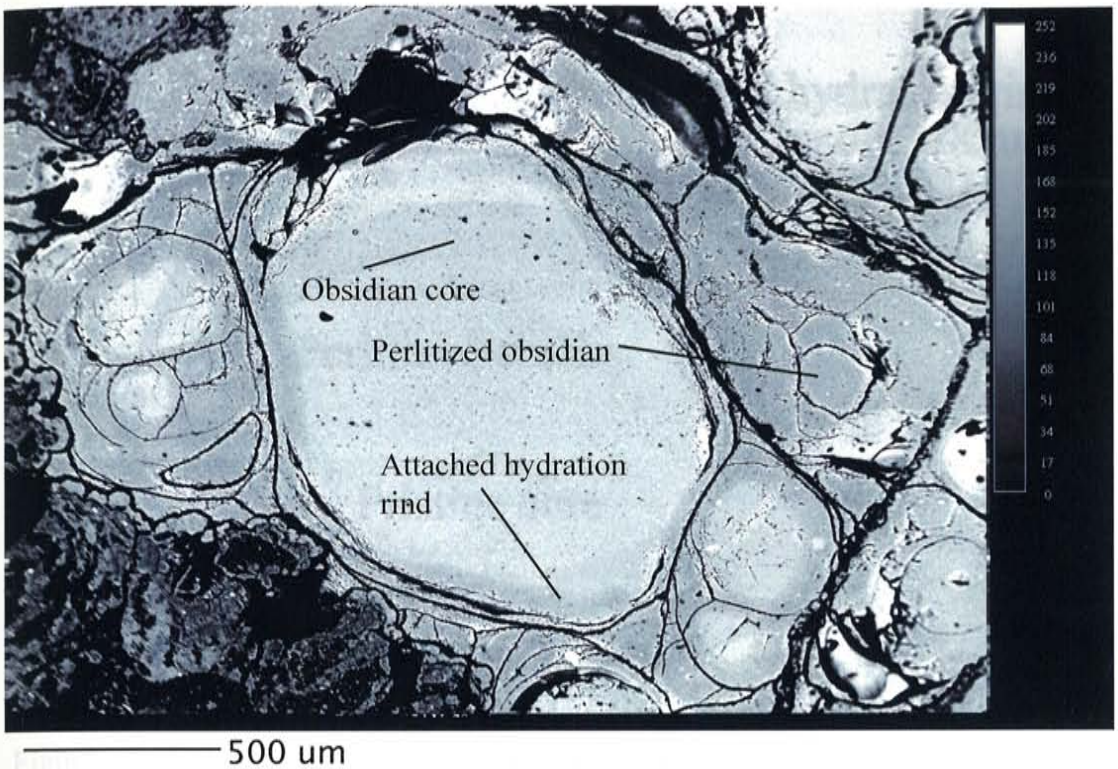

Figure 2.2. This is a BSE image of obsidian sample AD-02 displaying an unhydrated core (light in color). A concentric "onionskin fashion" perlite rind (dark gray in color) is surrounding the clast, either broken off or still attached.

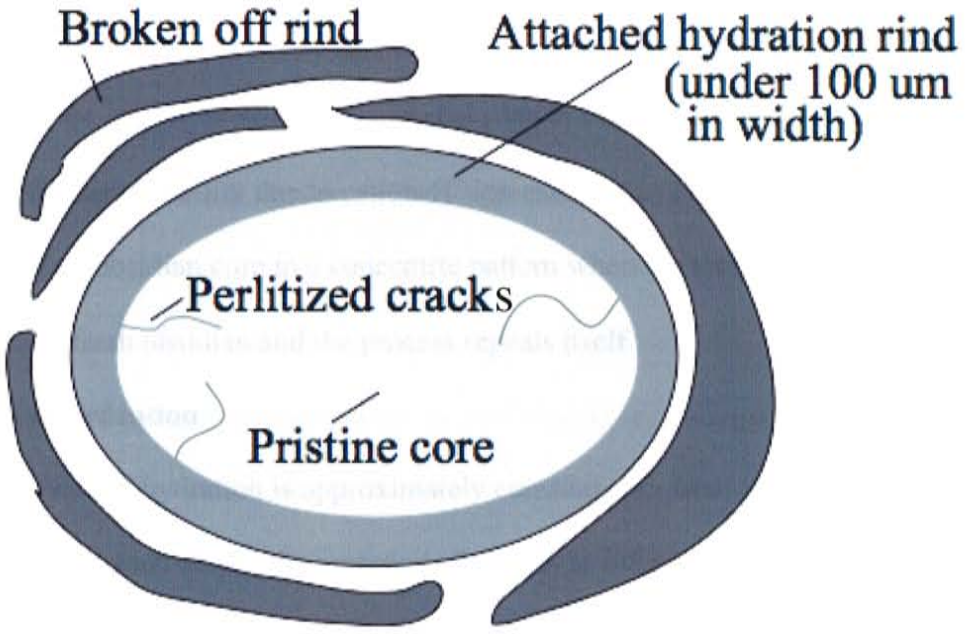

Figure 2.3. This is a simplified model that shows the hydration process. In the center of the picture there is a pristine obsidian core. This core is being hydrated on the surface of the grain, as well as along cracks that run through the grain. Darker colors represent more hydrated surfaces than lighter colors. Once the perlite rinds become ~100 μm thick it breaks off around the grain in an "onionskin" fashion, also known as perlitic texture. The broken off rind is more more hydrated than the rinds that are still attached.

from the surface of the grain and through cracks and vesicle walls. Over time a hydration layer is formed, which is attached to the grain and formed in part from the precipitation of hydrosilicates and hydroxides (Fieore et al., 1999; Petit et al., 1990), these processes can cause element mobility due to cation-H^+ ion exchange. The hydration rind will then break off of an obsidian core in a concentric pattern when the rind is ~100 μm thick. This exposes fresh obsidian and the process repeats itself.

2.4 Rates of hydration

The rate of hydration is approximately constant over time for a certain rock type, although factors such as pH, the presence of cations in infiltrating water, humidity, type of glass, and temperature can change the rate of hydration slightly. Freidman et al. (1976) showed that obsidian hydrates at a rate of approximately $T=kt^{1/2}$ over time, where T is the rind thickness in microns, k is a constant and t is time in years. A typical rate for pristine, unvesiculated obsidian is about 100 μm over a 10,000-year period. Hydration rind thickness has become a prominent dating method for archaeological materials, because it was believed that the rate of hydration for obsidian is not affected by relative humidity (Freidman et al., 1966). However, a recent paper by Anovitz et al. (2006) has suggested that obsidian hydration is affected by relative humidity and can be used to interpret paleoclimates. The hydration rate also varies slightly for different glasses (e.g. basalt versus rhyolite) and under different conditions (e.g. differences in pressure, temperature, or leaching solution). Slight changes in hydration rate as a function of leach chemistry were demonstrated by Petit et al. (1990) where basaltic and rhyolitic glasses were leached using D.I. water, or a 250 g/l NaCl brine at successively higher temperatures. When any glass was leached using the NaCl solution at temperatures

higher than 120° C, element mobility was hindered and the hydration rind was thinner compared to glasses leached in pure D.I. water. Petit et al. (1990) also found that after a short, 13-hour leaching period, there was little element mobility in all of the studied glasses. The conclusion that Pettit et al. (1990) made was that the difference between hydration rates of glass leached in D.I. water and a NaCl solution supports the theory of ion exchange between mobile alkalis and H^+-bearing species. This is due to the presence of Na reducing the chemical potential at the solid-liquid interface, thus retarding diffusion. However, the diffusion of water into obsidian is not a straightforward H^+ adsorption on the negatively charged surfaces of the grains because the uptake of H^+ extended much further into the grain than the surfaces alone (Petit et al., 1990). Also, during the hydration process, the H^+ uptake during ion exchange does not match the loss of cations on a charge-equivalent basis. Therefore, there must be ions other than H^+ absorbed into the obsidian during the hydration process in natural waters (Mungall and Martin, 1994). It was concluded by Petit et al. (1990) that the nature of the alkali in the solution does not matter, but the presence of cations in solution will inhibit ion exchange and slightly change the rate of hydration. In the current study the rate of hydration is not a primary concern, although understanding that glass can hydrate at slightly different rates and cause chemical changes over time is.

2.5 Complex hydration model

A more complex mechanism for absorption of water, network destruction and ion exchange explains the hydration process better than a simple model, and can account for the various degrees of element mobility, ion exchange, and hydration observed. Most studies conclude that hydration of obsidian is a non-uniform process and there are three

basic processes involved: 1) the absorption of molecular water into obsidian (Fieore et al., 1999; Yanagisawa et al., 1997; Petit et al., 1990), 2) a destruction of the silicate network (Petit et al., 1990), and 3) cation-H_3O^+ and cation-H^+ ion exchange accompanied with diffusion (Fieore et al., 1999). Since the process is not linear, all three processes can occur simultaneously and to different degrees. Differences in hydration rind thickness, ion exchange, and elemental mobility are the result of these variations.

2.5.1 Process 1: Water absorption

The diffusion of water into glass is always the dominant initial step, which can be the rate-determining step for the hydration process (Yanagisawa et al., 1997). Water is important because the diffusion of elements in glass has been shown to increase by up to two orders of magnitude by the presence of water alone (Mungall and Martin, 1994). Previous studies have determined ways to chemically measure the increase in water content on the surface of an obsidian grain to better understand the interactions between water and glass. The presence of meteoric water absorbed into obsidian can be chemically detected many ways including normalization of oxides and loss on ignition (L.O.I.) (Jezek and Noble, 1978; Mungall and Martin, 1994, respectively). Mungall and Martin (1994), in their comprehensive study, showed that there was no significant difference between measuring water content by L.O.I. or by normalization. Fieore et al. (1999) used L.O.I. to measure water absorption and found a gradient from core to rim as high as 1.16 wt. % H_2O. The gradient of meteoric water absorption can also be measured chemically because outer edges of obsidian have a higher concentration of OH^- and H^+ species compared to the magmatic percentages at the pristine obsidian cores (Yanagisawa et al., 1997; Petit et al., 1990, respectively). This increase in water content at the rind

will chemically affect structural and hydrochemical properties of the grain, which can alter the rates of ion exchange from dissolution and the degree of obsidian hydration. Meteoric water permeates glass and causes the glass to expand and fracture, thus allowing more water into the glass. Perlite along a fracture or plane has a higher concentration of water than massive perlite, and is characterized by increased ion exchange due to a higher frequency of dissolution along the plane (Jezek and Noble, 1978). This process can be seen in a BSE image of sample AD-11 from the current study, where highly perlitized planes run through the perlite itself (Figure 2.4). These planes are possibly due to flow banding, where certain bands perlitize faster than other bands and show different hydration habits. Petit et al. (1990) noted that the depths of perlitic fractures are dependent on the glass composition, solution chemistry, and temperature. The diffusion of molecular water and associated ion exchange are also accelerated in porous or vesiculated glass due to a higher surface area (Mungall and Martin, 1994). When no cracks or vesiculation are present within an obsidian grain the permeation of water into the grain will still occur. This was shown in an experiment using D.I. water to interact with obsidian at various temperatures and pressures (Yanagisawa et al., 1997). This experiment showed that rate of dissolution remained constant over the course of the experiment, where the hydration layer thickness increased parabolically at first and after 60 hours equaled the rate of dissolution (Figure 2.5). The parabolic thickness rate was proportional to the square root of time, and then reached a steady state when the dissolution rate became comparable to the hydration rate.

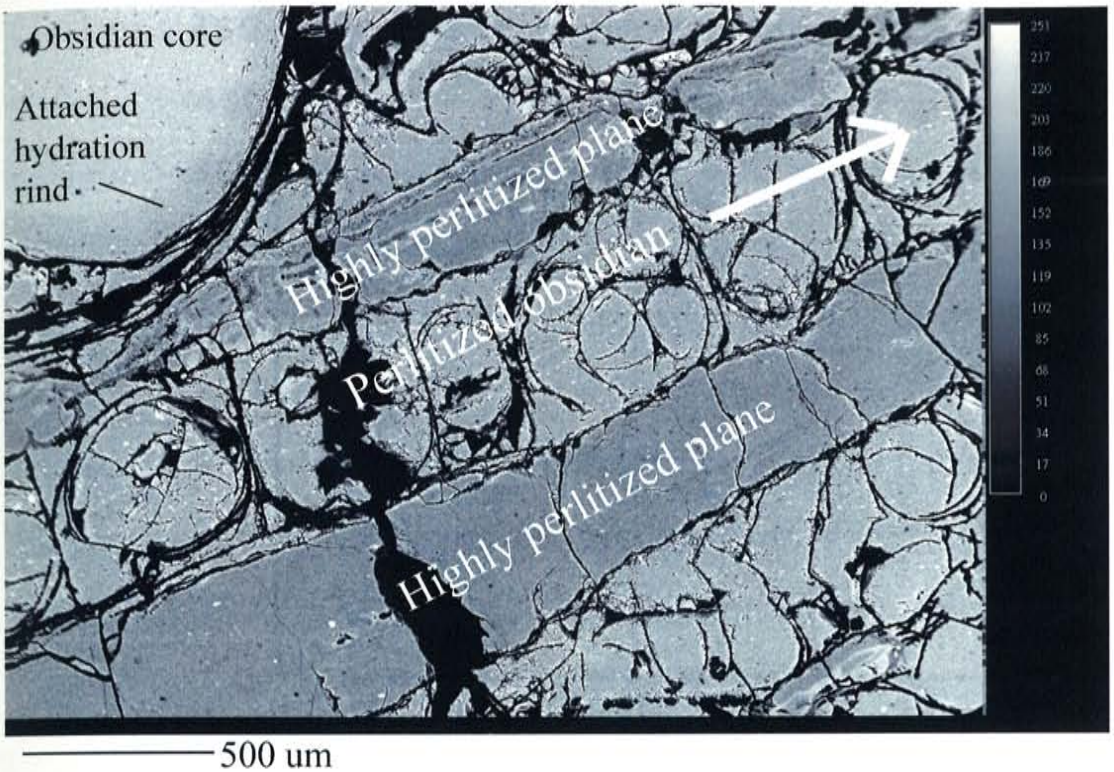

Figure 2.4. A BSE image of sample AD-11 that displays varying degrees of hydration. The large spheroid in the upper left hand corner of the image is obsidian, with a hydration rind still attached. The darker bands are perlitic planes running through less-hydrated perlitic material. Note the perlitic obsidian in the less-hydrated perlite. Darker shades of gray represent higher water contents than lighter gray areas in this image. The reasons for the highly perlitized planes are not fully undestood.

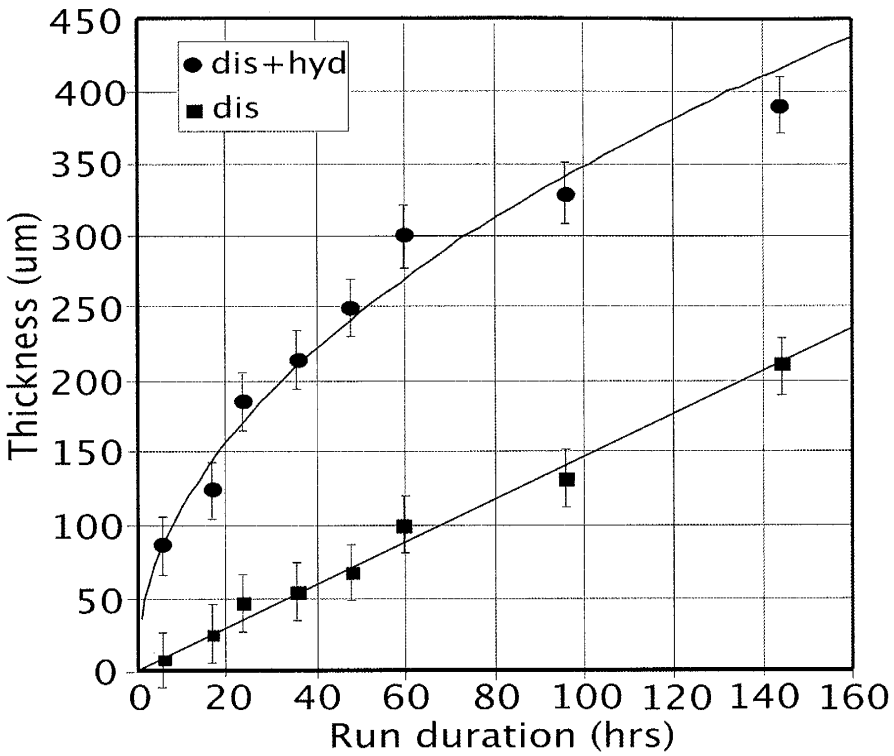

Figure 2.5. This graph from Yanagisawa et al. (1997) shows the thickness of the dissolved and hydrated layers versus the run duration of the experiment at 500°C and at 60 MPa. Squares represent the dissolved layer (dis), and the circles represent the thickness of the dissolved layer plus the hydrated layer (dis+hyd). Note that before 60 hours the hydration rind thickness increased parabolically before a steady state occurred, at this point the thickness rate of the dissolved layer became comparable to the hydrated layer.

2.5.2 Process 2: Destruction of the silica network

After the initial increase in water content, the dominant process becomes the destruction of the silicate network; this allows for ion exchange processes to occur. Hydration of glass results in a restructuring of the glass framework during the absorption of meteoric water. Destruction due to hydrolysis happens by generating an opening in the silicate structure by permeating water. This allows further penetration of water and ion exchange, while simultaneously creating hydroxides by selective dissolution of ions that results in a hydrated layer (Fieore et al., 1999; Petit et al., 1990). During this process OH^- groups, with a much lower diffusivity than molecular water, are formed by the hydrolysis of bridging oxygen atoms, further aiding the destruction of the glass framework (Zhang et al., 1991). Destruction of the silica structure happens at the grain surface where hydroxyl concentrations reach a critical value, causing surface silica to detach from the grain and equilibrate with the surrounding water (Yanagisawa et al., 1997; Mungall and Martin, 1994).

2.5.3 Process 3: Formation of hydroxides

The destruction due to hydrolysis allows for the formation of hydroxides on the surface of the grain (Petit et al., 1990). During this process hydroxyl groups continue to attack the silicate structure while breaking bridging oxygen bonds causing the framework to further weaken. This allows the selective leaching of alkalis by H^+-cation and H_3O^+-cation exchange, and the further permeation of molecular water (Mungall and Martin, 1994). This "late-stage" process is when ion exchange becomes the dominant mechanism, due to the dissolution process that initially weakened the silicic structure. The formation of hydroxides is also the most important mechanism affecting K mobility

(Fieore et al., 1999). When OH^- groups form and penetrate the silica structure ion exchange occurs, altering the original magmatic composition. To quantify the effect of element mobility in glass due to hydration, at seven weight percent water half of the cations present are hydrogen ions (Mungall and Martin, 1994).

2.6 Experiments relating leaching to element mobility and hydration rind formation

Elements in obsidian can be mobile, slightly mobile, or immobile as a function of various physiochemical conditions including, but not limited to, degree of hydration, temperature and pressure of the system, the texture and surface area of the obsidian grain such as vesiculation, the presence of organic acids, and the pH and composition of interacting water; slight differences in chemical composition and the framework of glass can lead to variations in element mobility as well (Fieore et al., 1999). In obsidian, chemical leaching is the process of dislodging an element from glass; mobile elements should be leached first and at a high diffusion rate (Fieore et al., 1999; Mungall and Martin, 1994). Potassium can be a mobile element and knowing the leaching behavior of it is important for Ar-Ar geochronology of glass. Studies on leaching have been performed on glass to determine which ions are the most mobile, as well as to understand the role of these elements during the earliest formation of the hydrated layer. For instance, Mungall and Martin (1994) studied severely leached glasses that displayed more than a 50% of loss in some elements. They compared normalized amounts of elements in the leached glass to concurrently erupted unaltered pumice to determine the order of element mobility in terms of diffusion rates. The order of alkaline mobility was Na>K>Ca being leached out of the glass and into the solution or adsorbed onto the hydration rinds, Si was mobile as well; Fieore et al. (1999) had the same result. These

two studies show that although physiochemical conditions can change leaching rates of elements, K can remain as a mobile element.

2.6.1 Leached elements and the early stages of clay formation

When hydrosilicates (Si-OH groups) leach out of an obsidian grain to form a hydrated layer, the molecules are organized in the early stages of clay formation (Petit et al., 1990). It has been seen that pristine glass is structureless and isotropic, whereas the hydration rind is optically anisotropic (Fieore et al., 1999; Yanagisawa et al., 1997). Using X-ray diffraction (XRD) to examine the hydration rind, Yanagisawa et al. (1997) was unable to determine the origin of the anisotropy. Fieore et al. (1999) however, used a high-resolution transmission electron microscope (HRTEM) and discovered that the altered glass formed flakes, needles, and leaf shaped aggregates; all three aggregate forms were interpreted to be early stages of clay formation. Petit et al. (1990) supports the observations of clay formation by Fieore et al. (1999) by finding that the hydrated layer did not lose a significant amount of H^+ during experimental heating at high temperatures, implying that the hydrated layer is a solid phase. The observations of early formation of clays elucidates why there is only a limited amount of space (~3-5 Wt. % H_2O) that water can occupy in the hydrated layer, as well as the origin of anisotropy for the hydrated layer.

2.7 Summary of hydration processes

In summary, the hydration of glass is non-uniform and involves multiple processes. The processes include the absorption of molecular water into the grain and the subsequent breaking of silicic bonds due to the hydrolysis of bridging oxygen atoms (Mungall and Martin, 1994). This weakens the framework of the glass allowing for H^+-

cation and H_3O^+-cation exchange between the water and obsidian (Fieore et al., 1999; Petit et al., 1990). The precipitation of hydroxides and hydrosilicates is a process where hydroxides will precipitate out of solution causing an increase of Si concentrations at the grain-water interface. This hampers the precipitation of hydroxides and allows for hydrosilicates to precipitate; the hydrosilicates will saturate the solution and again allow for the precipitation of hydroxides (Petit et al., 1990). When hydrosilicates and hydroxides form, they can either get washed away in solution or reorganize on or near the surface of a hydration rind to form clays; the early restructuring of hydrosilicates and hydroxides resembles the early stages of clay mineralization (Petit et al., 1990. The rate of absorption of molecular water into a grain is the rate-limiting step for this type of low-temperature alteration (Yanagisawa et al., 1997). Various factors including pH, temperature, pressure, solution and glass chemistry, and presence of vesiculation or organic acids can cause elements to be extremely mobile, slightly mobile, or immobile during the dissolution process (Fieore et al., 1999).

2.8 Hydration and its effect on Ar-Ar dating of glass

The potential problems of element mobility, especially K, associated with the formation of hydration rinds and subsequent absorption of atmospheric ^{40}Ar have made glass an undesirable material for Ar-Ar dating (Cerling et al., 1985). The presence of hydration rinds can be clearly imaged using BSE and water content and element mobility can be chemically quantified. It is the process of absorbing water to break down the silicic structure of glass that can cause the leaching of mobile elements and the formation of hydration rinds (Fieore et al., 1999; Petit et al., 1990). This process can affect Ar-Ar ages by 1) ^{40}Ar loss, 2) K loss, or by 3) absorption of atmospheric ^{40}Ar, as discussed in

Chapter 5, but it should be noted that some hydration can occur without any of these processes taking place. Argon loss can be caused by the loosening of the silicic structure during hydration, which will make it easier for argon to diffuse out of a grain. If potassium is lost during leaching, it can either be adsorbed onto a hydration rind or go into the leaching solution (Fieore et al., 1999; Mungall and Martin, 1994). This potential K loss cannot be accounted for and can result in an inaccurate apparent Ar-Ar age if hydration rinds are not removed. The absorption of atmospheric ^{40}Ar during rind and clay formation can lead to increased uncertainties in Ar-Ar ages and lower $^{40}Ar^*$ signals. Hydration rinds should be removed prior to dating glass because there is little way of knowing whether the formation of the rinds caused K or Ar mobility, which will yield imprecise or inaccurate ages.

2.8.1 Removal of hydration rinds

Problems associated with the formation of hydration rinds can be mitigated with certain preparation techniques, increasing the chances for glass to be an accurate and precise dating material by the Ar-Ar method. Only pristine obsidian should be used for Ar-Ar dating out of all glass types (obsidian, pumice, glass shards, matrix glass, and melt inclusions). This is because glass fragments need to be large enough so that hydration rinds can be removed while leaving enough pristine glass to be dated. Matrix glass, pumice, and glass shards all have a large surface to volume ratio, altering these forms of glass to clay or perlite faster than obsidian. Melt inclusions and matrix glass are generally not studied in an Ar-Ar analysis and should be removed, rather than dated. The crystal that the glass is trapped inside of or attached to has an isotopic ratio of K and Ar that is not representative of the true age. In cases where melt inclusions contain excess

^{40}Ar, a dated crystal will yield an inaccurate apparent age if the contaminant glass was not removed (Esser et al., 1997). For most argon geochronological studies, common mineral separation techniques (e.g. hydrofluoric acid treatment (HF) and crushing) are performed to remove contaminant matrix glass and melt inclusions associated with the mineral under study (van den Bogaard and Schirnick, 1995; Winick et al., 2001). Melt inclusions also have been known to have multiple reservoirs of trapped ^{40}Ar that are different from the atmospheric Ar-Ar value of 295, which can complicate an Ar-Ar analysis (Heizler and Harrison, 1988). Problems such as the ones stated above can be avoided by analyzing obsidian. Because obsidian clasts have small surface to volume ratios when cracks and vesiculation are absent, certain preparation treatments can be used to remove hydration rinds from obsidian while leaving enough pristine glass to be dated. An obsidian core, unaffected by hydration and ion exchange, should be the only remaining product when hydration rinds are properly broken off. Although the hydration process does not always cause K and Ar mobility resulting in inaccurate or imprecise ages, the rinds should be removed before dating because there is little way of knowing if the presence of hydration rinds will cause inaccurate or imprecise ages. The current study, as discussed in subsequent chapters, demonstrates that obsidian cores, after the removal of hydration rinds, can yield an accurate and precise Ar-Ar age.

CHAPTER 3: SAMPLE COLLECTION AND PREPARATION METHODS

3.1 Field Areas

3.1.1 Regional geologic setting

Samples were collected from two different localities, the No Agua Peaks volcanic complex and the Valles caldera, both located in north-central New Mexico. The No Agua Peaks volcanic complex is located in the Taos Plateau volcanic field within the largely basaltic Rio Grande rift; the other notable silicic volcanic region in the Rio Grande rift is associated with the Jemez Mountains volcanic field (JMVF). The Rio Grande rift an extensional structure that stretches from Leadville, CO into Texas and Mexico (Cordell, 1978). Volcanism associated with the rift began in the Cenozoic with two major pulses of volcanism occurring between 30-18 Ma and from 10 Ma to present; the longest lull in volcanism was during the mid-Miocene (Seager et al., 1984).

3.1.2 Geology of the No Agua Peaks volcanic complex

The rhyolitic volcanism that produced the dome complex at No Agua Peaks occurred in the larger regional setting of the Taos Plateau volcanic field. The Taos Plateau volcanic field consists of mainly units from young rift volcanism, although older, pre-Taos Plateau volcanic field units can be identified within the field. The older units are associated with the 26-22 Ma eruptions from the Latir volcanic field located southeast of the Taos Plateau volcanic field (Thompson and McMillan, 1992). The most common rock types within the Taos Plateau volcanic field are tholeiitic basalts, pyroxene dacites, and olivine andesites. The high-silicic rhyolite volcanism at No Agua Peaks appears to

be an isolated occurrence, as no similar lavas found elsewhere within the Taos Plateau volcanic field (Thompson and McMillan, 1992). Two separate eruptive sequences appear to be present at No Agua Peaks: the West Hills and North Hills stages. Both are the result of explosive silicic volcanism and consist of large tuff, pumice, and breccia deposits, followed by a rhyolite flow with the outer margins quenched to obsidian (Figure 3.1). Over time this obsidian has undergone hydration to form perlite. There is a meter-thick paleosol stratigraphically separating the two packages of units in the field (Figure 3.2). A third eruptive stage termed the Low Hills stage is believed to be a temporally intermediate event, but was not sampled during this study. The 3x5 km No Agua Peaks volcanic complex has been extensively mined for perlite, and unofficially boasts to be the largest perlite deposit in North America. The voluminous pumice fall and breccia deposits are the most economical units mined, although granular perlite has been mined in the past. A perlite mine such as the one at the No Agua Peaks complex is an excellent field area to test the methods presented in this paper because the well-exposed obsidian units display varying degrees of hydration (Figure 3.3).

Previous K-Ar and Ar-Ar ages for the No Agua Peaks have been imprecise or inaccurate. The complex was poorly dated at 3.3-7.8 Ma (Chamberlin and Barker, 1996) and 3.9 Ma (Lipman and Mehnert, 1979) by K-Ar dating. Previous Ar-Ar single crystal laser fusion (SCLF) dating of sanidine from the No Agua Peaks complex yielded results of 3.51± 0.12 Ma to 4.22± 0.14 Ma (Appelt, 1998). Appelt (1998) described a regional study and exact sample locations for the No Agua Peaks were not published; these ages either do not agree or poorly agree with the ages presented in the current study. In this

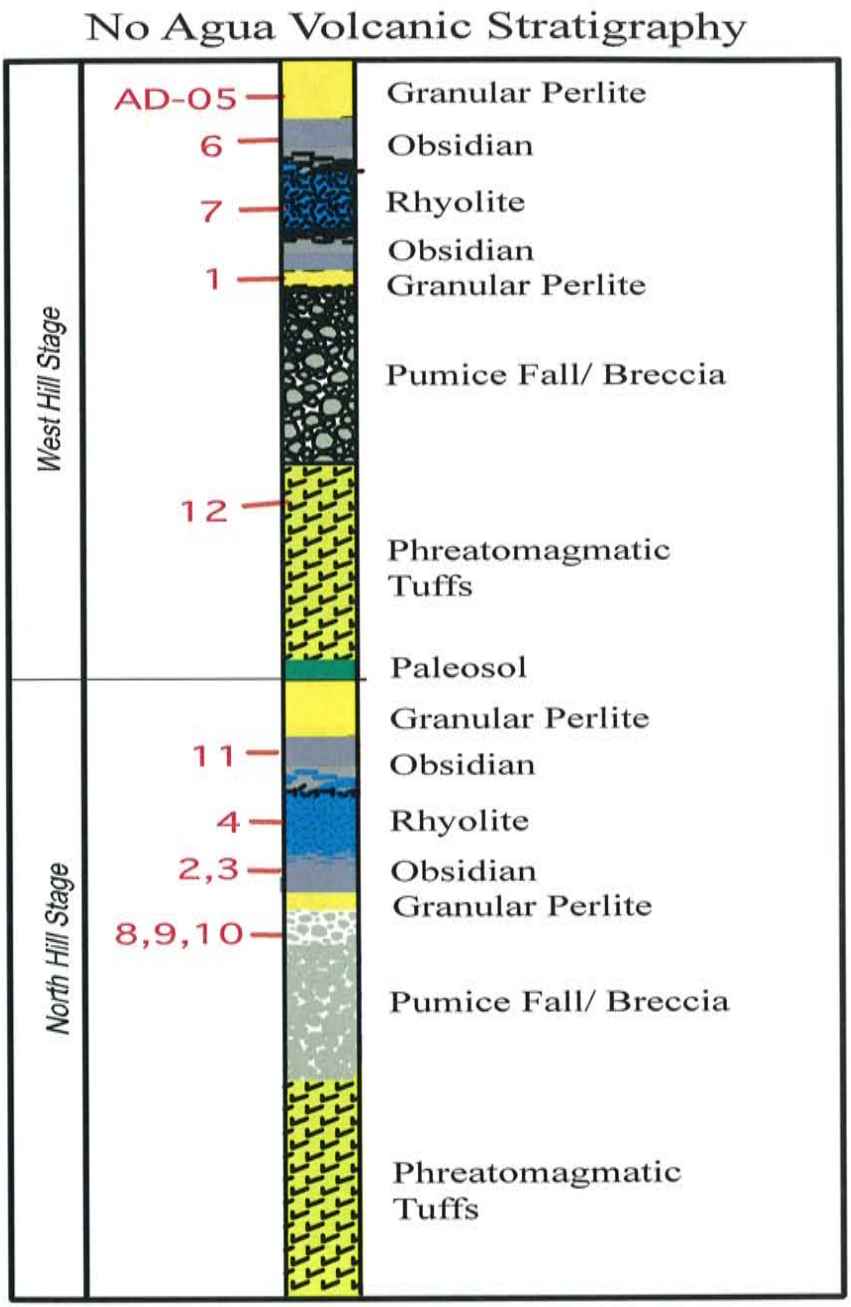

Figure 3.1. Stratigraphic column of the No Agua Peaks volcanic complex in northern New Mexico. The North Hills and West Hills events were dated in this study, sample numbers are shown in red. A meter-thick paleosol separates the two packages of units stratigraphically. Figure is adapted from Housman (unpublished).

3.2a

3.2b

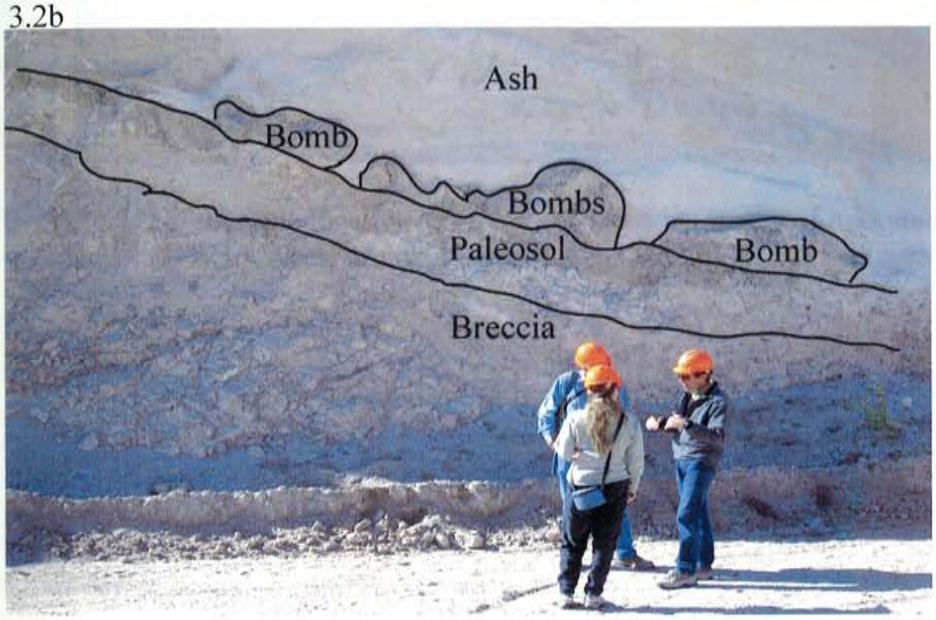

Figure 3.2. Both pictures show sample location AD-08, where moderately cemented breccia is unconformably overlain by a meter-thick paleosol; the paleosol is overlain by bombs and ash fall. Figure 3.2a shows the picture with no modification, where Figure 3.2b shows delineated features.

Figure 3.3. Sample locality AD-02, where various stages of hydration can be identified. Dark clasts are obsidian, whereas the lighter colored material is perlite.

study the West Hills and North Hills stages are shown to be two temporally and chemically distinct eruptive events.

3.1.3 Geology of the Valles caldera

The Valles caldera, a "super volcano", is located within the JMVF at the intersection between the Rio Grande rift and the Jemez lineament. The Jemez lineament is a NE-SW zone of focused volcanic activity that stretches from NE New Mexico into central Arizona. The lineament is believed to be of pre-Cambrian origin and seems to mimic the orientation of ancient terrain boundaries (Aldrich and Laughlin, 1984).

The Valles caldera has had multiple eruptive phases throughout its short history (Table 3.1). The initial rhyolite ignimbrite of the Lower Bandelier Tuff, formally known as the Otowi Member of the Tewa Group, erupted at 1.613± 0.011 Ma (Izett and Obradovich, 1994), which collapsed the Toledo caldera (Balsley et al., 1985). The Upper Bandelier Tuff, formally known as the Tshirege Member of the Tewa Group, has been Ar-Ar dated around 1.25± 0.03 Ma in multiple studies using sanidine (Phillips et al., 2007; Spell et al., 1996; Izett and Obradovich, 1994; Spell and Harrison, 1993). The eruption of the Upper Bandelier Tuff formed the Valles caldera, which is partially nested within the Toledo caldera. Shortly after explosive volcanism ceased, resurgence occurred. Within the Valles caldera is a central resurgent dome and seven rhyolite ring domes. The ring domes were Ar-Ar dated approximately at 1.18 to 0.54 Ma (Spell and Harrison, 1993; adjusted), and get progressively younger counterclockwise around the resurgent dome. The resurgent dome is Redondo Peak and the seven ring domes, from oldest to youngest, are Cerro del Medio, Cerros del Abrigo, Cerro Santa Rosa, Cerro San Luis, Cerro Seco, San Antonio Mountain and South Mountain. Cerro del Medio, a large

Group	Formations	Members and other units
Tewa Group ~3.6 - 0.05 Ma	Valles Rhyolite	Banco Bonito lava flow and minor pyroclastic beds
		VC-1 Rhyolite lava flow
		Battleship Rock ignimbrite
		El Cajete pumice beds, lava domes, and flows
		Valle Grande Member (includes ring domes)
		Redondo Creek Member
		Deer Canyon Member
	Bandelier Tuff	Tshirege Member (1.256± 0.010 Ma; Phillips et al., 1997)
		Cerro Toledo Rhyolite (1.38± 0.16 Ma; Spell et al., 1996)
	Bandelier Tuff	Otowi Member (1.613± 0.011 Ma; Izett and Obradovich, 1994)
		Cerro Rubio Quartz Latite
		Pre-Bandelier Silicic Tuffs

Table 3.1: Table showing the current interpretation of the youngest stratigraphic units in the Jemez volcanic field, based on Bailey et al. (1969), Gardner et al. (1986), and Self et al. (1991). Table is modified from Phillips et al. (2007)

ring dome located near the southeast caldera rim, was the primary focus for this study. This dome provides an upper time constraint on the rate of resurgence because it was the first of the seven ring domes to emerge after Redondo Peak (Phillips et al., 2007). Six eruptive lobes have been mapped at the Cerro del Medio dome (Gardner et al., 2006); sanidine from the oldest lobe of the Cerro del Medio dome was recently Ar-Ar dated at 1.23 Ma± 0.02 Ma (Phillips et al., 2007). The data from Phillips et al. (2007) imply that the timing of resurgence was within 0.027± 0.027 Ma.

Once the dome building of South Mountain ceased at 0.543± 0.004 Ma (Spell and Harrison, 1993, adjusted), explosive rhyolitic volcanism restarted sometime after 0.5 Ma (Reneau et al., 1996; Toyoda et al., 1995; Spell and Harrison. 1993). The three post-0.5 Ma volcanic units from the Valles Caldera dated in this study are the Banco Bonito formation, the El Cajete member, and the Battleship rock ignimbrite. Banco Bonito is a lava flow, Battleship Rock is a welded ignimbrite and the El Cajete member is composed of pyroclastic beds. Previous ages for El Cajete range from 1.3 Ma (Goff et al., 1986, 1989; Self et al., 1991) to as young as 0.05 Ma (Spell and Harrison, 1993; Toyoda et al, 1995; Reneau, 1996). Problems continue to arise when dating the post-0.5 Ma events of the Valles by any dating method. In this study, three obsidian-bearing samples from these units were dated in attempt to constrain the lower time limits of volcanic activity at the Valles Caldera, thus aiding in understanding the volcanologic hazard of the mountain.

3.2 Sample collection and preparation methods

Sample collection was performed in the following manner at both localities. The freshest material available was collected to minimize the effects of alteration, specifically hydration. The bulk of alteration rims were removed from samples in the field. Most

sample collection locations were situated on roadside outcrops, and GPS coordinates were taken at each location. Twelve different obsidian and feldspar-bearing samples were collected on the World Minerals property at No Agua Peaks (Figure 3.4); samples were collected from three obsidian flows (n=4), one pumice fall (n=3), two different perlite beds (n=2), a phreatomagmatic tuff (n=1), and two rhyolite flows (n=2). This was done to get the widest range of hydration possible, as well as to sample various stages of the hydration process.

In the Jemez Mountains volcanic field, nine obsidian and two feldspar samples were collected from Cerro del Medio (Figure 3.5). Two samples, EP-39 and EP-42, dated in Phillips et al. (2007) represent the age of the DM-S lobe in this study; all six lobes of the dome were sampled. Two obsidian flows (n=8), two feldspar-bearing rhyolite lavas (n=3), a feldspar-bearing breccia (n=1), and one obsidian-bearing breccia (n=1) were sampled. Five obsidian samples from the youngest volcanic units at the Valles caldera were collected for analysis. El Cajete obsidian samples were in the form of bread crust bombs (n=2), or from a pyroclastic surge (n=1). Obsidian from the Banco Bonito lava was sampled (n=1), and obsidian fiamme were sampled from the Battleship Rock ignimbrite (n=1).

Sample preparation was conducted in the following way for obsidian and feldspar-bearing samples. Samples were crushed, sieved (800-300 μm), and then handpicked under an optical microscope. Feldspar-bearing samples were also separated by a Frantz magnetic separator, heavy liquids, and treated with a 15% hydrofluoric acid (HF) solution for five minutes after crushing to remove melt inclusions and matrix glass on the surface of the grains.

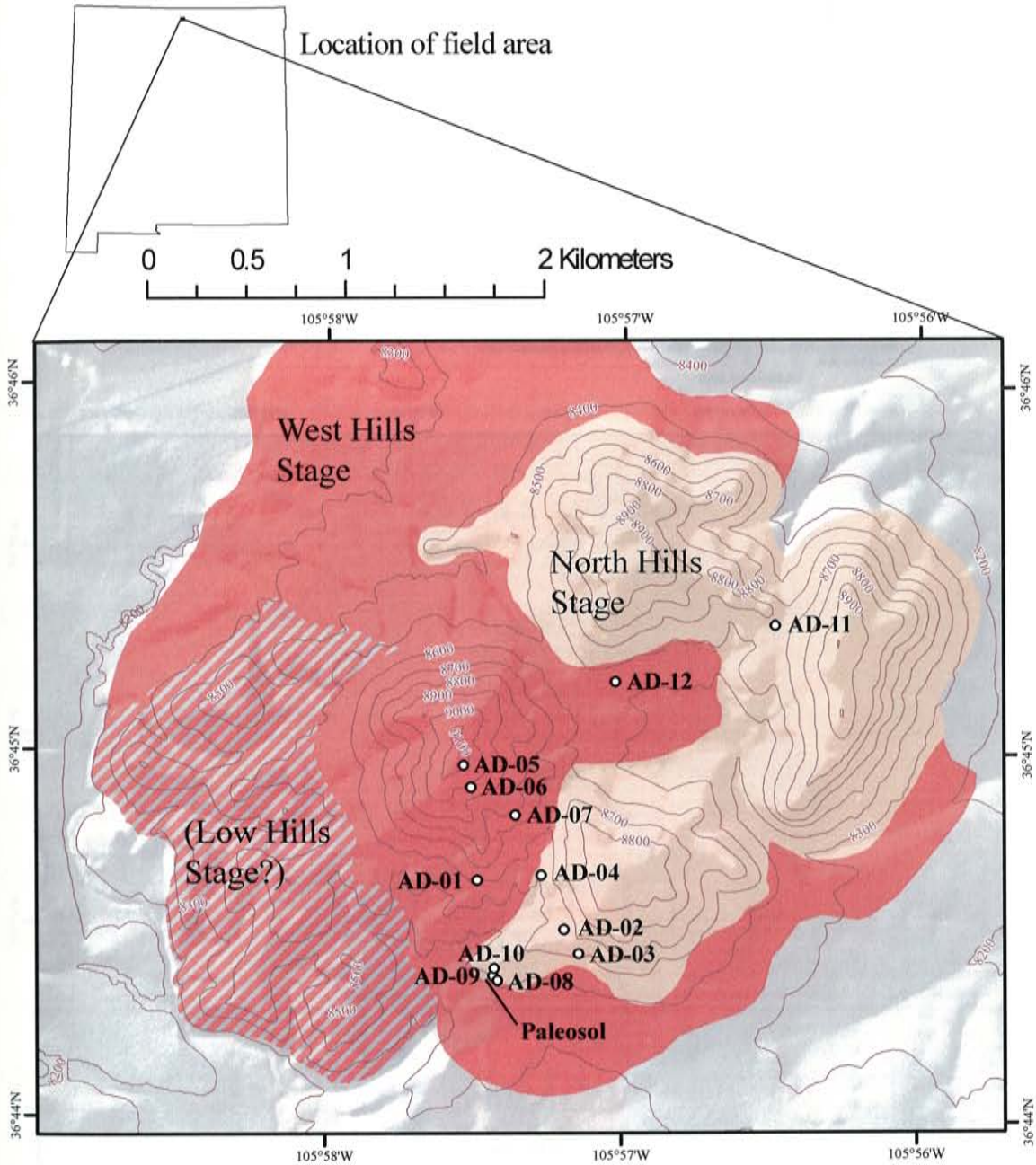

Figure 3.4. Geologic map of the No Agua Peaks volcanic complex including sample locations. The Low Hills Stage might be a third eruptive stage but was not sampled in this study. The North Hills Stage is stratigraphically older than the West Hills Stage.

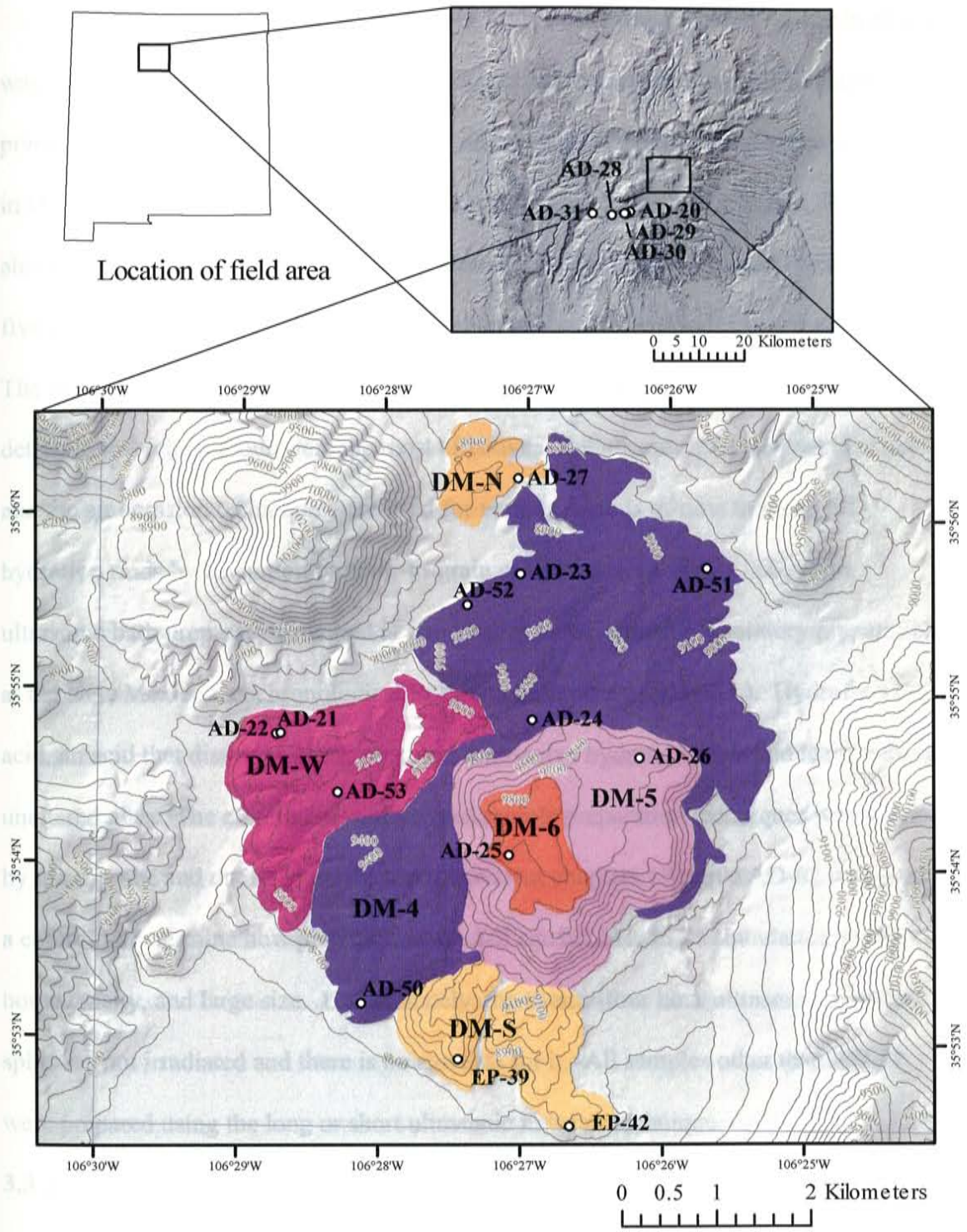

Figure 3.5. Shaded relief map of the Valles caldera including inset of the Cerro del Medio dome and sample locations. Unit names are included as well. Two samples dated by Phillips et al. (2007) from the DM-S lobe are included in the current study.

Obsidian sample AD-02 from the No Agua Peaks was prepared further in multiple ways to determine how the preparation technique affects apparent age. The various preparation methods applied to sample AD-02 were: 1) a five minute ultrasonic cleaning in D. I. water, and 2) a longer ultrasonic cleaning for 24 hours in D.I. water, 3) air abrasion, and 4) a five minute ultrasonic cleaning in HF. All preparations were rinsed for five minutes in D. I. water after the preparation process, unless water was used initially. The multiple preparation techniques were used to remove hydration rinds in order to determine which methods were the most effective. The ultrasonic treatments in water and the air abrasion technique were used for various periods of time to break off hydration rinds by cavitation or grain-to-grain collisions respectively. The short ultrasonic bath preparation method is also similar to the standard laboratory preparation at the New Mexico Geochronological Research Laboratory (NMGRL). Hydrofluoric acid, an acid that dissolves glass, was used to dissolve hydration rinds and leave behind unaltered glass. The effectiveness of various sample preparation techniques was assessed by microprobe and dating, described in subsequent chapters. Sample AD-02 was used as a control to determine how preparation affected age because of its abundance, purity, homogeneity, and large size. Unfortunately, the twenty-four hour ultrasonic in water split was not irradiated and there is no age data for it. All samples other than AD-02 were prepared using the long or short ultrasonic in water technique.

3.3 Ar-Ar dating procedures

3.3.1 Irradiation

Obsidian and feldspar separates were dated by the Ar-Ar method to determine how sample preparation and argon extraction techniques affect apparent age, and then to

obtain sample ages once the methods were established. Sample splits were irradiated for the Ar-Ar dating of glass and feldspar. For irradiation, samples were placed in machined aluminum disks in known geometries. For all irradiation packages, Fish Canyon Tuff sanidine was interspersed between samples as a flux monitor with an age of 28.02 Ma (Renne et al., 1998). The samples were irradiated in five different packages; four of the five were shielded against slow neutrons in the reactor. Packages were returned to the New Mexico Geochronology Research Laboratory (NMGRL) at the New Mexico Institute of Mining and Technology for the geochronological analysis of argon gas. For further information on irradiation see Appendix C.0.

3.3.2 Ar-Ar analysis

Four types of heating schedules were tried to determine the best heating schedule to use for analysis of obsidian. The four heating schedules consisted of 1) laser fusion, 2) a two-step laser-heating schedule, 3) multi-step incremental heating by a CO_2 laser, and 4) a multi-step incremental heating using a furnace. Laser fusion was the initial method of extraction for this study; gas was extracted using a Synrad 50 W CO_2 laser with a focused beam and grains were fused at either 2.8 or 3.2 W. Single crystal fusion analysis was used for all monitors, the HF split of sample AD-02, and for six of eight feldspar samples. The two-step laser-heating schedule consisted of a 20 second 0.55 W step to remove atmospheric argon from the obsidian sample followed by a second 20 second 2.8 to 3.2 W step to fuse the sample and extract the remainder of the argon gas; both steps used a defocused laser beam. Obsidian analyses generally employed the use of a two-step laser-heating schedule, but a laser step-heating schedule was used when more degassing information was needed. For laser multi-step heating schedules with more

than two steps, between 7.4 and 73.5 mg of obsidian were heated using a Synrad 50 W CO_2 laser fitted with a beam integrator to evenly distribute power over a 6x6 mm square. The samples were incrementally heated using heating schedules ranging between 3-35 W, in up to ten steps. Furnace incremental step heating analysis was used for select splits to compare with laser heating. Thirty milligrams of obsidian was used for each furnace analysis. Samples were heated for eight minutes per temperature step in a double-vacuum resistance furnace fitted with a Mo crucible and liner. A thirteen-step heating schedule, from 600° C to 1700° C, was used to degas the samples. For furnace samples, reactive gasses were initially removed using a SAES GP-50 getter in the first stage. All samples, furnace and laser, went through a second stage gettering process by using both a cold and hot SAES GP-50 getter for 120 seconds. Argon isotopes were analyzed with a MAP 215-50 mass spectrometer with extended geometry in static mode, and were measured by an electron multiplier. Multiplier sensitivity for the furnace was $2.48e^{-16}$ moles/pA and sensitivity ranged from $1.40e^{-16}$ to $1.69e^{-16}$ for the laser.

3.3.3 Data representation and criteria used for Ar-Ar data

Data are represented using age probability distribution diagrams (aka ideograms) or age spectra, depending on the extraction technique used. For the multi-step furnace and laser extractions, data are displayed using age spectra. An age spectrum displays apparent age on the Y-axis and percent $^{39}Ar_K$ released per temperature step on the X-axis. Three contiguous steps that agree at 2σ and comprise over 50% of the $^{39}Ar_K$ released during an analysis define a plateau age (Lanphere and Dalrymple, 1978; Fleck et al., 1977; Dalrymple and Lanphere, 1974). This criteria differs from other spectra criteria such as Foland et al. (1986) because the plateau steps do not need to agree at 1σ, or from

Snee et al. (1988) because $^{40}Ar^*$ is not included in the plateau criteria. Age spectra were used to evaluate Ar loss; total gas ages were used to compare results from integrated two-step and laser fusion ages. Data are plotted on ideograms for fusion and two-step laser extraction methods (McDougall and Harrison, 1999; Deino and Potts, 1992). All ideograms and age spectra have auxiliary graphs associated with them, which display additional data such as individual analyses and errors, % $^{40}Ar^*$, K/Ca ratio, and moles of $^{39}Ar_K$. The weighted mean age is reported in this study for each sample (Appendix C); uncertainty is reported at the 2σ-confidence level and is calculated by the weighed error of the mean (Taylor, 1982). When the MSWD of the population is greater than one, the uncertainty is multiplied by the square root of the MSWD.

Criteria were created to identify poor quality data because obsidian degasses variably; using criteria was a way to ensure quality age data from this material since little is known on how obsidian reacts in the reactor or how obsidian degasses in the extraction line. The K/Ca ratio, percent of $^{40}Ar^*$, and the moles of $^{39}Ar_K$ were used for this criteria. Obsidian analyses with K/Ca ratios vastly different from the mode were thrown out of data sets; a small scatter in K/Ca ratios was considered geologic. Analyses with $^{40}Ar^*$ yields lower than 5.0% were arbitrarily taken out of the data sets, these were analyses with little radiogenic gas and high uncertainties. Data with low $^{40}Ar^*$ yields often had small $^{39}Ar_K$ signals as well. Signal size is measured in moles of $^{39}Ar_K$; all analyses with $^{39}Ar_K$ signals lower than $0.1e^{-6}$ moles were rejected in this study. This arbitrary amount is typically two orders of magnitude lower than the highest signals. Data are not reported or represented graphically for points that do not meet the K/Ca, $^{40}Ar^*$, or signal size criteria. These data are often outliers and rejecting these points yielded a better mean

calculated age for a given sample. The sample analyses that were thrown out could be analytically flawed, have a low K content, be xenocrystic, or be contaminated with phenocrysts or melt inclusions. Rejected analyses are identified in tables and figures when they meet the criteria listed above, but removed from the mean age calculation for other reasons (e.g. xenocryst).

CHAPTER 4: ELECTRON MICROPROBE METHODS AND RESULTS

4.1 Methods

4.1.1 Introduction

The electron microprobe was used to image and geochemically characterize obsidian, perlite, and feldspar samples. Differently prepared glass splits were examined using backscattered electrons (BSE) to image hydration rinds, and to observe the effectiveness of the sample preparation in the removal of these rinds. Quantitative geochemical analyses were also carried out by the electron microprobe to determine the chemical composition of the samples at multiple points. All analyses were done at the New Mexico Institute of Mining and Technology on a Cameca SX-100 electron microprobe.

4.1.2 Backscattered electron analysis

Using backscattered electrons, obsidian and perlite can be imaged to understand the relationships between the two materials. This is possible because the mean atomic number of the two materials is different, and BSE is able to resolve the chemical difference. Backscattered electron analysis works by scanning a focused electron beam over a polished sample surface. The primary electron beam interacts with the sample and produces backscattered electrons. The brightness of the BSE signal is related to the mean atomic number, where the surfaces with high atomic number elements are brighter (e.g. Ni appears brighter than Si). The BSE analyses for obsidian were performed in high gain, which has a high sensitivity and can resolve 0.1 amu differences in Z. This

technique can help identify the interface between obsidian and its hydration rind because the mean atomic number of the materials is often only slightly different, which high gain can resolve. Perlite, which contains absorbed water, has a lower BSE intensity compared to obsidian due to the higher concentration of the low-Z element hydrogen. BSE imaging of feldspar crystals aided in determining whether contaminating phases were present within grains and to assess if crystals were resorbed, which could suggest a xenocrystic origin. Backscattered electron analysis was also used to assess chemical homogeneity during quantitative chemical analyses.

4.1.3 Quantitative X-ray analysis

Chemical data was collected by the electron microprobe using quantitative X-ray analysis. When accelerated electrons bombard a sample surface, electrons are ejected from the inner shells of the atoms. Electrons cascade from lower energy outer orbitals to fill the electrical void created by the ejected higher-energy inner shell electrons. When this occurs, energy is released in the form of an X-ray. The wavelength of the X-ray depends on the atomic number of the element. Quantitative analysis yields a chemical composition for each point analyzed. For glass analysis, a beam current of 10 nA, accelerating voltage of 15 kV, and a beam size that ranged from 20-25 μm was used in this study. The beam size was large to minimize electron beam-induced element mobility. For glasses, the following oxides and elements were analyzed: P, Si, S, Ti, Al, Mg, Ca, Mn, Fe, Na, K, F, and Cl. The standards used can be found in Appendix B. Quantitative results were all normalized to 100 wt. % to show unhydrated, initial percentages of each element present in a sample. Glass reference materials VG-568, KN18 and/or KE-12 were run to assess analytical precision and accuracy. Feldspar

samples were analyzed using a 20 nA beam, a 15 kV accelerating voltage and a 10 μm beam size. The oxides analyzed for feldspar were Na, K, Ca, Fe, Sr, Ba, Al, and Si. The standards used can be found in Appendix B. Reference samples of orthoclase, albite, and anorthite were analyzed to assess analytical precision and accuracy.

4.2 Electron Microprobe Results and Discussion

4.2.1 Major element chemistry

Quantitative analysis in this study was used to distinguish different eruptive events at the No Agua Peaks volcanic complex and the Valles caldera by geochemical variations in major elements; the characteristics of obsidian, hydration rinds, and water content were also documented. The average chemistry of obsidian and feldspar samples is summarized in Table 4.1. Obsidian characterization yielded the magmatic chemistry of an eruption, where a hydration rind represents the chemistry of the alteration product. By plotting mobile elements one cannot distinguish differences in original magmatic chemistries because the elements are mobile. However, two immobile elements plotted against each other, such as chlorine and calcium, make it evident that there are two distinct populations of elemental ratios for each locality (Figure 4.1). This shows that the original magma chemistries are different for the two events at No Agua Peaks, and between Cerro del Medio and the post-0.5 Ma volcanic units at the Valles caldera. Changes in magma chemistry might be attributed to long-term fractional crystallization or two distinct magma chambers; the cause for change in magma chemistry in both field areas is not a focus of this study.

Table 4.1. Table shows the average chemistry of obsidian and feldspar from the No Agua Peaks and the Valles caldera. For obsidian, oxide totals have been normalized to 100 wt. % where the total wt. % of oxides are unnormalized; this is to compare magmatic chemistries to one another, and to see how much a sample has hydrated.

Sample Number	Preparation	P2O5	SiO2	SO2	TiO2	Al2O3	MgO	CaO	MnO	FeO	Na2O	K2O	F	Cl	Total
AD-01	Short ultrasonic	0.01	76.32	0.01	0.06	13.16	0.06	0.44	0.16	0.51	4.08	4.74	0.38	0.04	97.55
AD-01	Long ultrasonic	0.01	76.36	0.02	0.06	13.03	0.09	0.47	0.14	0.52	4.17	4.86	0.20	0.05	98.84
AD-02	Short ultrasonic	0.01	76.29	0.01	0.07	13.37	0.03	0.73	0.08	0.45	4.07	4.67	0.13	0.07	98.39
AD-02	Long ultrasonic	0.02	76.09	0.02	0.07	13.21	0.13	0.80	0.07	0.56	4.04	4.80	0.07	0.08	98.80
AD-02	Air abrasion	0.01	76.18	0.02	0.07	13.24	0.05	0.80	0.08	0.42	4.12	4.81	0.10	0.08	99.42
AD-02	HF	0.01	76.30	0.02	0.07	13.10	0.05	0.77	0.06	0.44	4.16	4.82	0.10	0.08	100.00
AD-03	Short ultrasonic	0.00	76.00	0.01	0.05	13.24	0.08	0.75	0.07	0.45	4.05	4.83	0.36	0.11	96.77
AD-04	Short ultrasonic	0.02	76.28	0.01	0.06	13.35	0.03	0.78	0.06	0.34	4.22	4.67	0.14	0.03	98.82
AD-05	Short ultrasonic	0.01	76.68	0.01	0.06	13.18	0.02	0.46	0.14	0.5	4.26	4.42	0.22	0.04	97.18
AD-06	Short ultrasonic	0.01	76.19	0.01	0.05	13.13	0.02	0.40	0.16	0.48	4.26	4.68	0.54	0.06	97.68
AD-06	Long ultrasonic	0.00	76.67	0.02	0.06	12.86	0.03	0.46	0.13	0.41	4.19	4.83	0.27	0.04	100.01
AD-07	Short ultrasonic	0.03	75.95	0.01	0.06	13.03	0.02	0.47	0.11	0.30	4.34	4.94	0.65	0.08	98.68
AD-08	Short ultrasonic	0.02	76.06	0.01	0.07	13.35	0.02	0.62	0.08	0.39	3.68	5.49	0.14	0.09	95.52
AD-09	Short ultrasonic	0.03	76.32	0.03	0.06	13.24	0.01	0.59	0.11	0.48	3.97	4.97	0.09	0.10	94.34
AD-10	Short ultrasonic	0.02	76.11	0.01	0.06	13.40	0.04	0.75	0.08	0.54	4.01	4.82	0.09	0.07	95.79
AD-11	Short ultrasonic	0.01	76.40	0.01	0.07	13.43	0.03	0.75	0.06	0.41	4.33	4.33	0.10	0.07	96.67
AD-11	Long ultrasonic	0.01	76.29	0.01	0.07	13.13	0.04	0.76	0.07	0.35	3.85	5.17	0.13	0.09	99.46
AD-12	Short ultrasonic	0.01	76.47	0.01	0.06	13.09	0.01	0.46	0.16	0.51	4.22	4.52	0.40	0.04	97.18
AD-12	Long ultrasonic	0.01	76.67	0.01	0.06	13.06	0.05	0.46	0.14	0.41	4.34	4.51	0.22	0.04	99.41
AD-20	Long ultrasonic	0.04	76.02	0.00	0.20	13.00	0.16	0.84	0.03	0.92	3.86	4.83	0.03	0.06	98.35
AD-21	Long ultrasonic	0.02	76.70	0.01	0.10	12.37	0.03	0.35	0.07	0.88	4.23	5.01	0.11	0.12	98.26
AD-22	Long ultrasonic	0.01	76.42	0.00	0.09	12.56	0.31	0.35	0.05	0.87	4.06	5.08	0.09	0.11	98.88
AD-23	Long ultrasonic	0.01	76.63	0.01	0.10	12.52	0.02	0.35	0.04	0.99	4.26	4.84	0.11	0.11	99.53
AD-24	Long ultrasonic	0.02	76.66	0.01	0.10	12.48	0.03	0.34	0.06	1.00	4.3	4.77	0.09	0.13	99.36
AD-24	Long ultrasonic	0.01	76.71	0.01	0.09	12.45	0.03	0.35	0.06	0.99	4.26	4.79	0.12	0.12	99.27
AD-26	Long ultrasonic	0.00	76.36	0.01	0.09	12.71	0.04	0.37	0.06	1.02	4.28	4.81	0.13	0.12	99.83
AD-26	Short ultrasonic	0.01	76.42	0.01	0.12	12.67	0.03	0.34	0.07	0.81	4.38	4.92	0.10	0.12	99.28
AD-28	Long ultrasonic	0.03	76.46	0.02	0.20	12.96	0.06	0.70	0.04	0.71	3.74	4.97	0.05	0.06	99.07
AD-30	Long ultrasonic	0.02	75.82	0.01	0.23	13.16	0.13	0.80	0.04	0.98	3.79	4.90	0.05	0.07	98.31
AD-31	Long ultrasonic	0.02	76.38	0.02	0.20	12.95	0.12	0.84	0.04	0.55	3.27	5.49	0.05	0.07	96.22

Sanidine Data	Preparation	Na2O	K2O	CaO	FeO	SrO	BaO	Al2O3	SiO2	Total
AD-05	HF	9.55	1.07	2.26	0.12	0.03	0.03	22.13	66.73	101.92
AD-25	HF	5.86	3.36	0.71	0.15	0.01	0.01	14.86	76.74	101.71
AD-27	HF	7.61	5.33	0.95	0.18	0.02	0.04	20.34	66.74	101.21
EP-39	HF	6.64	6.87	0.57	0.12	0.05	0.07	19.70	65.88	99.89
EP-42	HF	6.75	6.90	0.59	0.12	0.06	0.10	19.84	66.32	100.68

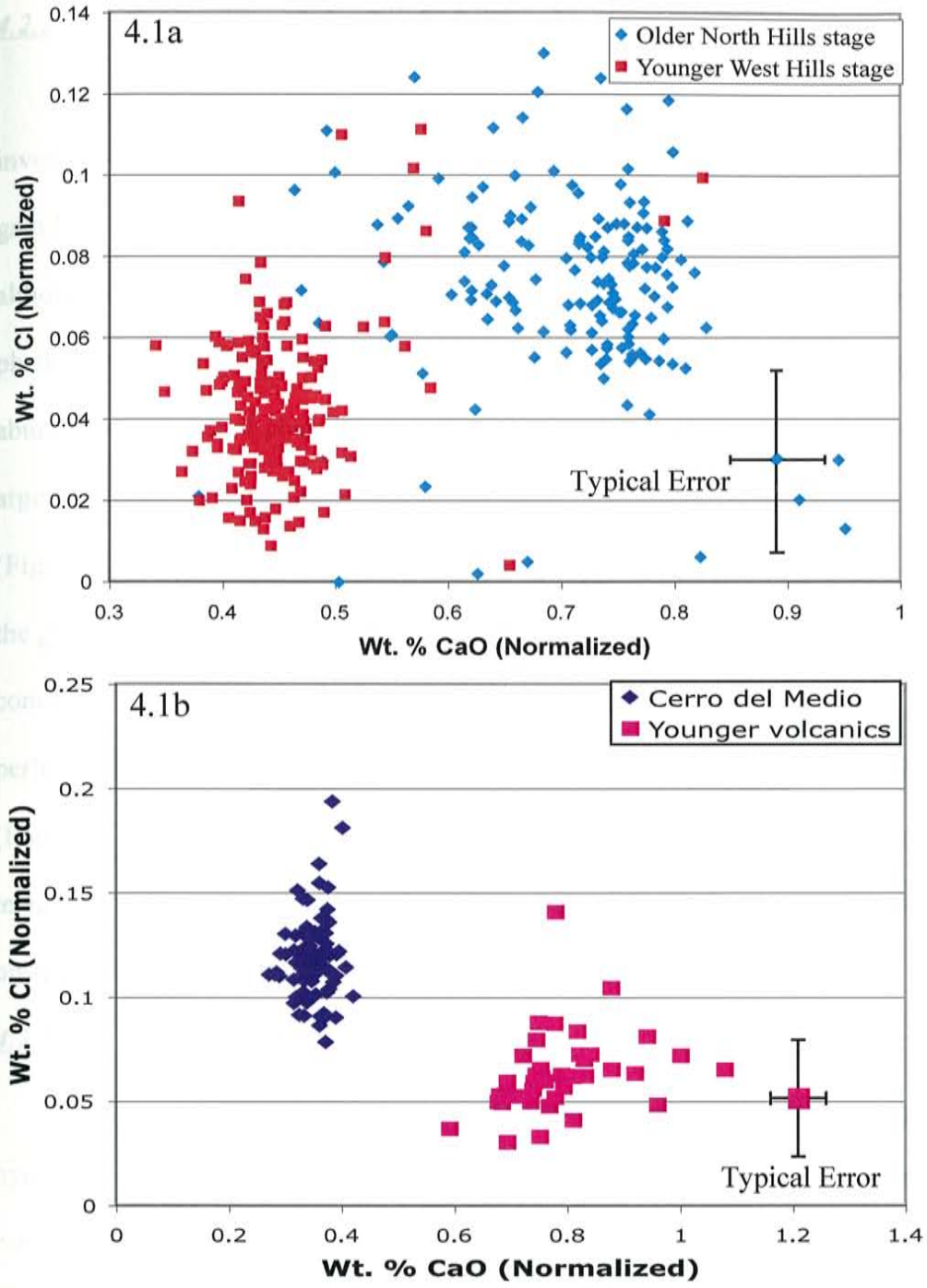

Figure 4.1. Graph of two normalized immobile elements, chlorine on the Y-axis and CaO on the X-axis, plotted against each other. The No Agua Peaks graph (4.1a) show some overlap between the two populations, North Hills and West Hills. The lower graph (4.1b) is between Cerro del Medio units and the younger Valles volcanic units where there are two chemically distinct populations. Typical errors are in the lower right-hand corner of each graph.

4.2.2 BSE observations of obsidian hydration

The relationship between glass and its hydrated counterpart, perlite, was investigated by chemically imaging the differences between the two materials using high-gain BSE. BSE imaging showed that no obsidian sample exhibited major vesiculation, although minor microvesiculation is present in some samples. Varying amounts of phenocrysts in all obsidian samples were observed using BSE; knowing the relative abundance and size of phenocrysts aided in determining what size fraction to use for argon analysis. In terms of alteration, five manifestations of hydration were observed (Figure 4.2). The manifestations include: obsidian with hydration rinds still attached to the grain (Figure 4.2a), perlite rinds broken off obsidian cores displaying an onion-skin concentric pattern with or without hydration rinds still attached to the core (Figure 4.2b), perlitized habits displaying relict obsidian cores showing nearly complete hydration (Figure 4.2c), obsidian cores with the hydration rinds broken off using certain preparation techniques (Figure 4.2d), and totally perlitized obsidian displaying no relict features of obsidian (Figure 4.2e).

4.2.3 BSE assessment of sample preparations

Backscattered electron images allow examination of the perlitization process and hydration relationships, as well as the effectiveness of the preparation treatment in removing hydration rinds from obsidian clasts. The process of perlitization may promote element mobility and affect resultant K-Ar and Ar-Ar ages (Cerling et al, 1985). Perlitization has been shown to only affect hydrated areas; only pristine obsidian should remain after hydrated areas are successfully broken off. A short ultrasonic treatment does not effectively remove hydration rinds, where the longer, twenty-four hour ultrasonic

4.2a

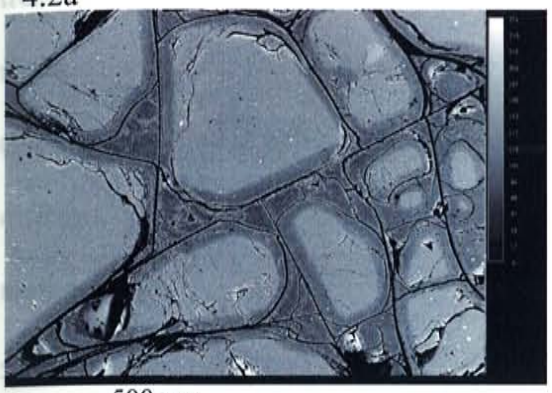

500 um

4.2d

1000 um

4.2b

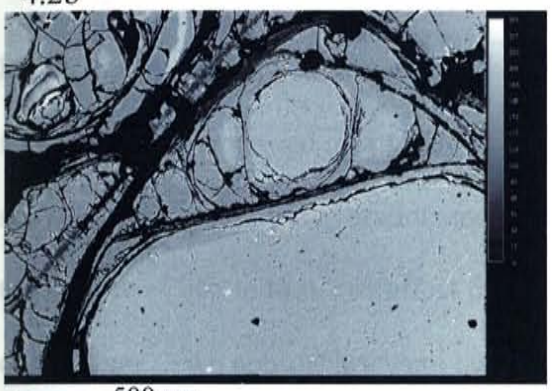

500 um

4.2e

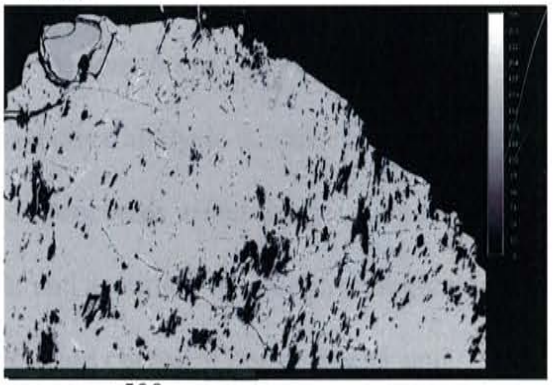

500 um

4.2c

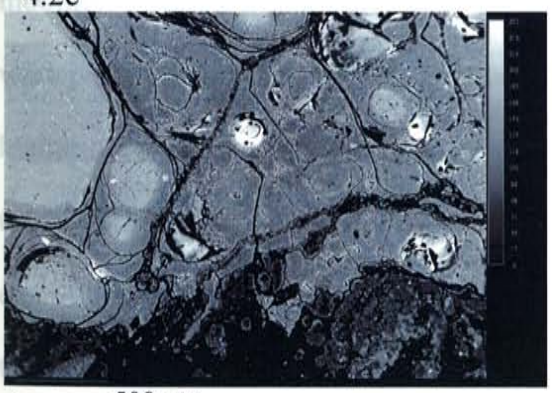

500 um

Figure 4.2: Five different manifestations of hydration habits for perlitic obsidian. All images are of obsidian and perlite with the perlite being darker in color due to absorbed water. Figure 4.2a is an image from sample AD-02 displaying hydration rinds still attached to the unaltered core obsidian clasts. Figure 4.2b is an image of sample AD-11 where the classic perlitic "onion-skin texture" is easily seen, because the perlite breaks off the obsidian core in a concentric pattern. Figure 4.2c is a different image from sample AD-02 where obsidian has almost totally altered to perlite. The massive perlite still shows the onionskin texture without the obsidian present; the obsidian core at left has very thin hydration rind implying that the hydration rind had recently broken off. Figure 4.2d is an image of AD-02 where the twenty-four hour ultrasonic treatment has effectively broken off the hydration rinds. The last image, 4.2e, is from AD-05 where the obsidian has totally altered into perlite displaying little indication of the presence of obsidian. The apparent texture of the grain might be from the polishing process and not a feature of the grain itself.

treatment does remove the rinds (Figure 4.3). The air abrasion and HF preparation methods were also found to effectively remove hydration rinds from obsidian cores (Figure 4.4); the HF splits were the least hydrated. No other apparent chemical differences were seen between the long ultrasonic, HF, and air abrasion preparation methods.

4.2.4 Glass homogeneity and element mobility

Quantitative analysis of obsidian was used to determine if the glass is chemically homogeneous, as well as to analyze what happens to elements as the glass hydrates to form hydration rinds and eventually perlite. Quantitative analysis is important because it shows, chemically, how hydration and preparation processes affect the geochemistry of the sample. This, in turn, can affect the precision and accuracy in geochronological work of obsidian. Two approaches were taken to investigate chemical homogeneity and mobility. First, to examine chemical homogeneity, pairs of normalized elemental oxides were plotted against each other. Second, to examine element mobility as a function of hydration, normalized element oxides were plotted against analytical totals. Analytical totals were used as a proxy for hydration because H_2O is not analyzed directly by the electron microprobe; the difference between the analytical total and 100% was assumed to represent the weight percent of water in the sample (Jezek and Noble, 1978; Fiore, 1999). So, an analytical point with an oxide total of 100 wt. % was assumed to be unhydrated glass, whereas a point with an oxide total of 97 wt. % was assumed to have undergone a three weight percent hydration of the glass.

Potassium is known to be a mobile element (Cerling et al., 1985) and it is pertinent for the Ar-Ar method; therefore, this element was used in many of the

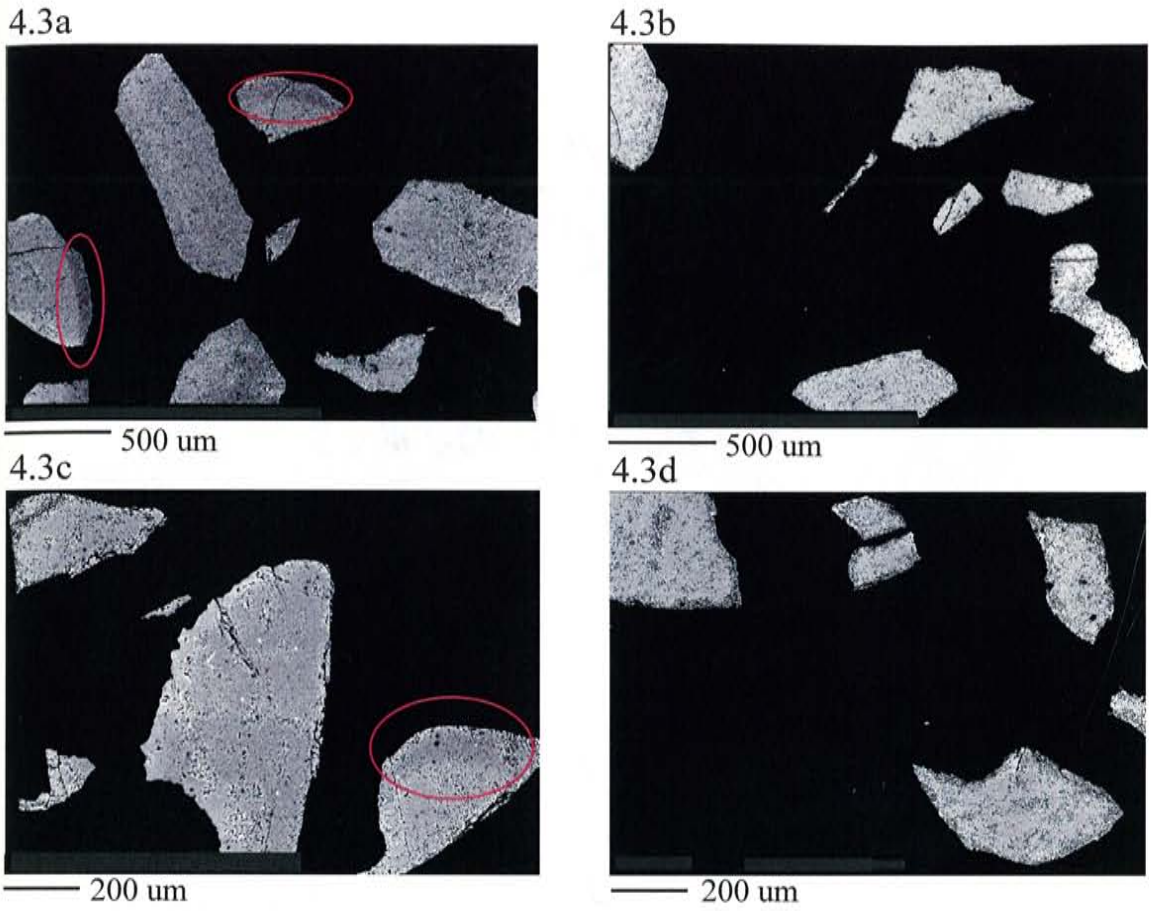

Figure 4.3. This figure shows BSE images of samples AD-01 and AD-11 that underwent two different preparation techniques. Figures 4.3a and 4.3c show the short ultrasonic bath splits of samples AD-01 and AD-11, respectively, where hydration are still attached to the grains (circled in red). Figures 4.3b and 4.3d show the long ultrasonic bath splits of samples AD-01 and AD-11, respectively, where hydration rinds have been sucessfully removed. All images are from irradiated splits.

4.4a

1000 um

4.4b

1000 um

Figure 4.4. BSE images of the air abraded (4.4a) and the HF prepared (4.4b) splits of sample AD-02. These images show that the hydration rinds have been effectively removed from the obsidian cores.

microprobe quantitative plots to determine the effects of hydration and preparation. By plotting a mobile oxide, such as K_2O, against weight percent water (proxy for hydration), it can be seen that for sample AD-02 there is little element mobility associated with hydration (Figure 4.5). The hydration level in this sample ranges between 0.0 and 3.5 wt. % H_2O, yet there is no statistical correlation between K_2O and H_2O. Chemical analysis of all unaltered obsidian cores examined in this study show that the glasses are nearly homogeneous within uncertainty in terms of element distribution.

4.2.5 Cross section through a hydrated obsidian grain

To understand the relationship between element mobility and hydration in more detail, a set of analyses was performed in a cross-section across an obsidian grain from sample split AD-10 (Figure 4.6). Twenty-one points were taken starting outside of the obsidian in the broken off hydration rind, progressing through the grain itself, and terminating on the other side. Hydration is greatest in the outer perlitized rinds (~6 wt. % H_2O), decreases through the still attached hydration rind (~3.5 wt. % H_2O), and is lowest at the inner core of the grain (~1.5 wt. % H_2O). The variations in hydration correspond well with the mean atomic number observed in the BSE image of the sample. In contrast to H_2O, there is no systematic elemental variation throughout the cross-section of the grain as represented by K_2O. These results are starkly different from those of Cerling et al. (1985), where the same degree of hydration (2.2-6.0 wt. % H_2O) resulted in a high degree of element mobility (K_2O amounts varied from 4.86-1.76 wt. %) in the African tephras studied.

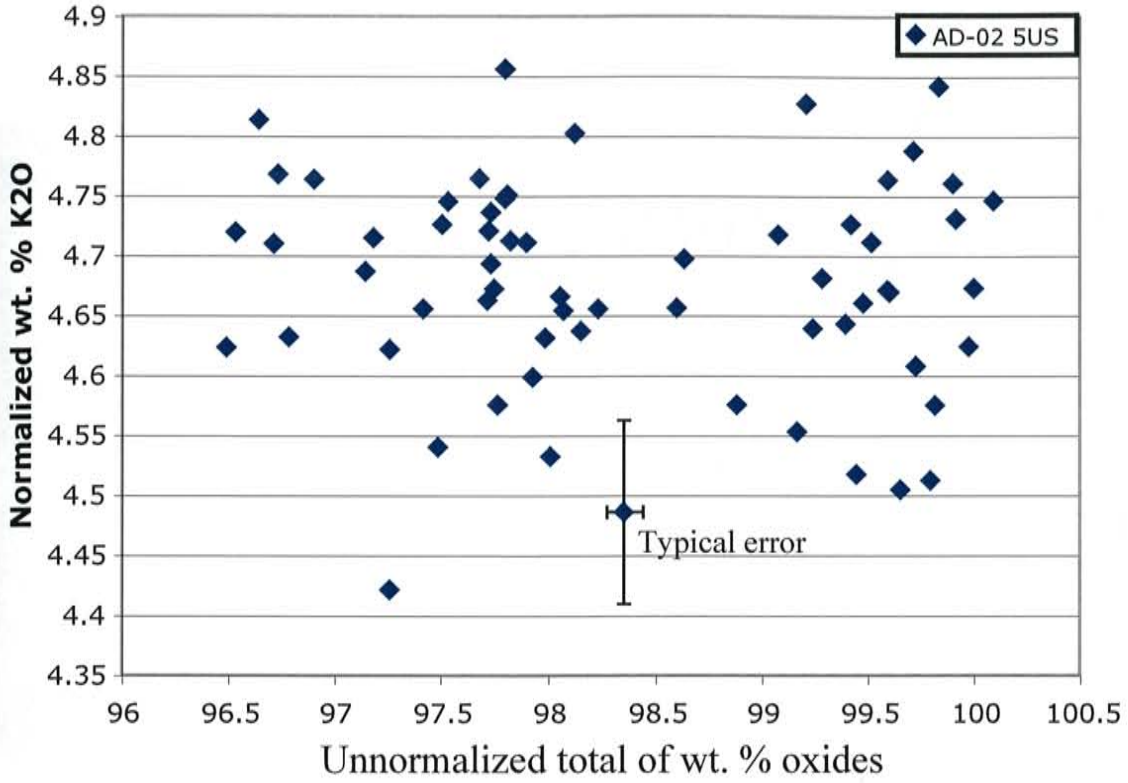

Figure 4.5. Shown here is a quantitative plot of sample AD-02 representing the normalized total of K_2O versus the unnormalized total of wt. % oxides. This shows that with increasing hydration there is little statistical evidence for element mobility associated with the hydration rind beyond natural geologic scatter. All samples behaved in a similar fashion in regard to hydration and mobility.

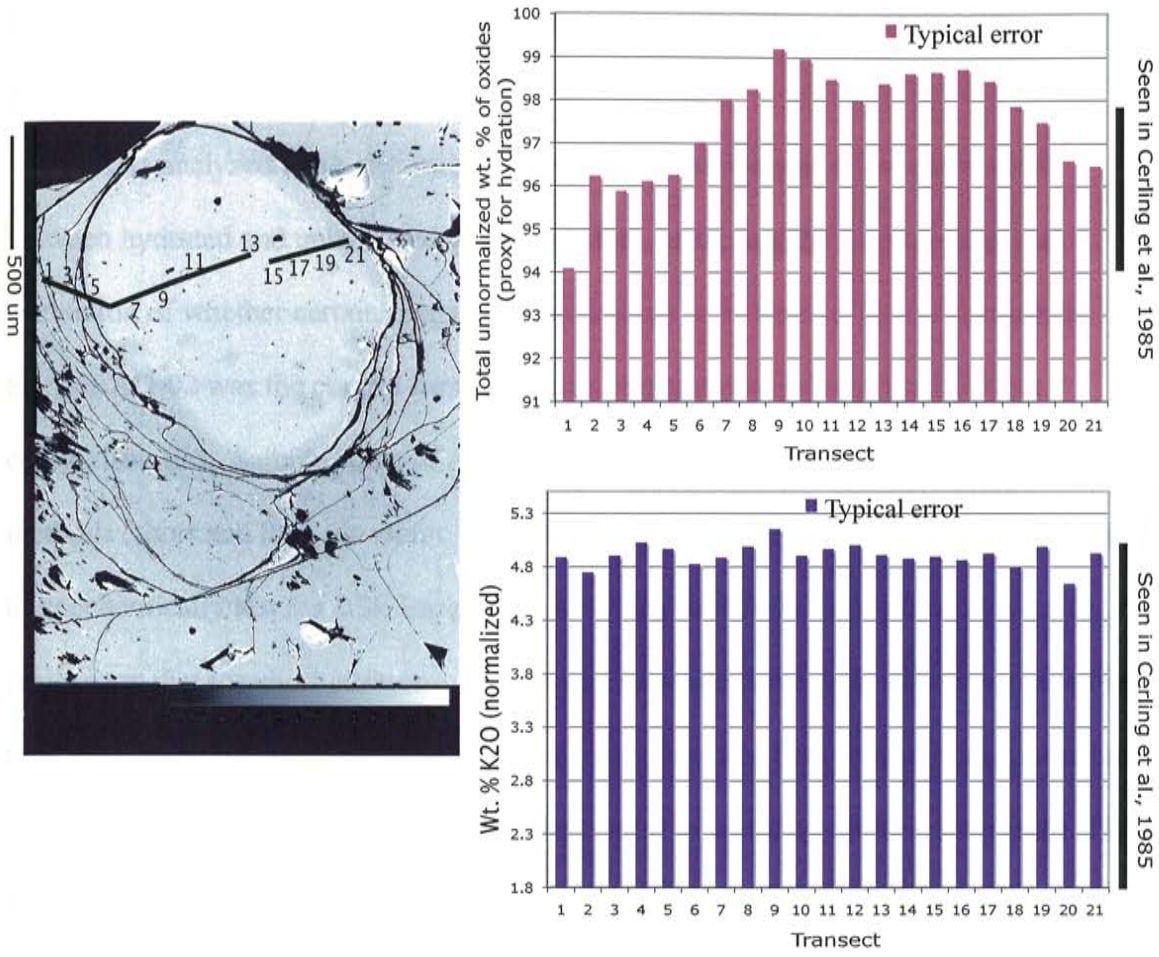

Figure 4.6: A transect through a grain of obsidian from sample AD-02 from No Agua Peaks, NM. The image shows a transect, numbered 1-21 from left to right, going through an obsidian grain starting at the outer, hydrated, broken off rind. The transect then goes through the unhydrated core and out the other side. The scale bar in the upper left is 500 um. On the right there are two graphs; both graphs represent the transect of the grain on the X-axis. The upper graph has the proxy for hydration on the Y-axis, showing that the inner obsidian is not significantly hydrated and hydration increases further away from the core. The lower graph has wt. % K_2O on the Y-axis showing that there is little element mobility associated with the hydration. On the right side of each graph there is a line representing the case study by Cerling et al. (1985) where there is an extensive amount of element mobility (4.86-1.76 wt. % K_2O) with a similar increase in water content (2.2-6.0% hydration by meteoric water). The high element mobility seen in the Cerling et al., 1985 study is not present in the obsidians from the No Agua Peaks.

4.2.6 Comparison between the short and long ultrasonic, HF, and air abrasion preparation methods

The analyzed totals determined by geochemical analysis allow distinction between hydrated and unhydrated glass; therefore, analyzing the data can allow an evaluation of whether certain preparation techniques were more effective that others. Sample AD-02 was the control for the various preparations and was used for this comparison test. Sample splits of AD-02 that had undergone four different preparation methods (short and long ultrasonic in water, ultrasonic in HF, and air abrasion) were used to geochemically test the BSE image results. Using the total weight percent of water, it is easily seen that the short ultrasonic bath in water sample is the least effective method in removing hydration rinds (Figure 4.7). The long ultrasonic bath in water, ultrasonic bath in HF, and air abrasion methods were all successful in breaking off hydration rinds. This proves that the preparation method chosen is important for the successful removal of the hydration rind. The HF split chemically appears to remove hydration rinds better than the long ultrasonic bath and air abrasion splits, but there is a significant amount of absorbed atmospheric ^{40}Ar that is seen in the argon analysis; this affects the precision and the accuracy of the obtained age. The overabundance of atmospheric ^{40}Ar for the HF split will be discussed later, but is noted here because the pursuit of the hydrofluoric preparation technique was abandoned in favor of the long ultrasonic bath preparation technique.

The difference in weight percent water between the short and long ultrasonic bath preparation methods is seen in every sample analyzed. No Agua samples AD-11 and AD-12 display a large range of hydration (up to >5 wt. % H_2O); the short and long

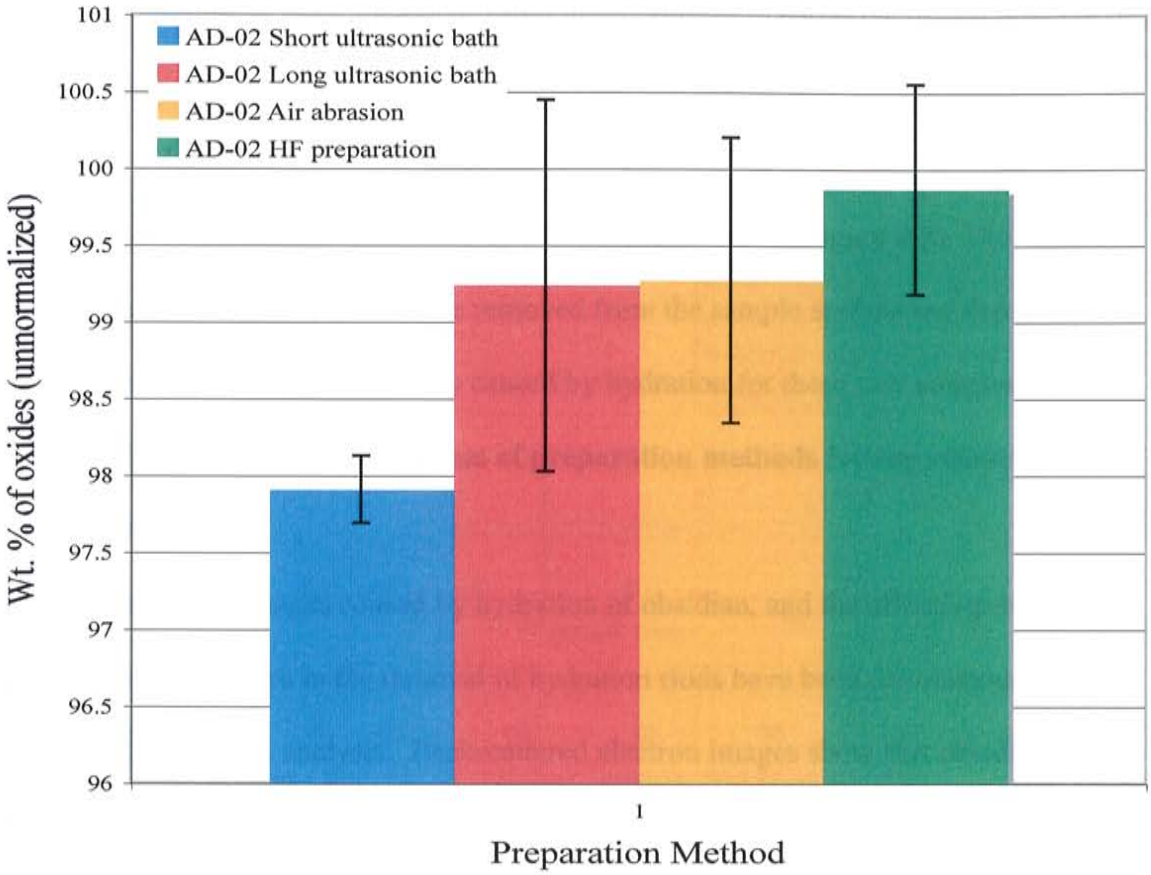

Figure 4.7. In this figure the X-axis represents the four different preparation methods where the Y-axis represents the unnormalized weight percent of total oxides; the difference between the wt. % total of oxides and 100 % represents the degree of hydration. Therefore the figure shows the effectiveness of rind removal for four splits of sample AD-02. Thirteen points from the outsides of grains of each sample were used in this anaylsis. The low degree of hydration is similar for the air abraded and long ultrasonic bath splits, and the HF split is the least hydrated. The short ultrasonic bath split of sample AD-02 has a much higher percent of absorbed water because hydration rinds were not effectively removed from the sample. Standard deviations are shown for each sample as well.

ultrasonic treatments were compared using these samples to better determine how the two preparation methods work with poor-quality obsidian. By comparing the unnormalized totals of oxide weight percents (H_2O proxy) between the short and long ultrasonic preparation treatments the difference in water content is seen (Figure 4.8). The results demonstrate that hydration rinds are removed from the sample surface and there is little element mobility within uncertainty caused by hydration for these two samples.

4.3 Conclusions on the effectiveness of preparation methods for the removal of hydration rinds

Chemical changes caused by hydration of obsidian, and the effectiveness of preparation techniques in the removal of hydration rinds have been demonstrated using BSE and quantitative analysis. Backscattered electron images show that obsidian can have a range of hydration characteristics from rinds attached to obsidian cores, to being broken off, to being totally perlitized. Using BSE, the differences between the short and long ultrasonic baths, HF, and air abrasion preparation techniques can be imaged. The short ultrasonic bath method does not break off hydration rinds where the other three preparation methods do. These observations are supported by quantitative analysis. A cross-section through a grain of obsidian showed that the hydration rinds and outer edges of a grain have the highest amounts of absorbed water. Quantitative analysis chemically showed that the short ultrasonic preparation method did not successfully remove hydration rinds and had the most absorbed water. The air abrasion and the long ultrasonic preparation techniques removed hydration rinds and have less water than the short ultrasonic bath method; the HF method had the least amount of water after breaking hydration rinds off the grains. Quantitative analysis also showed that no sample from the

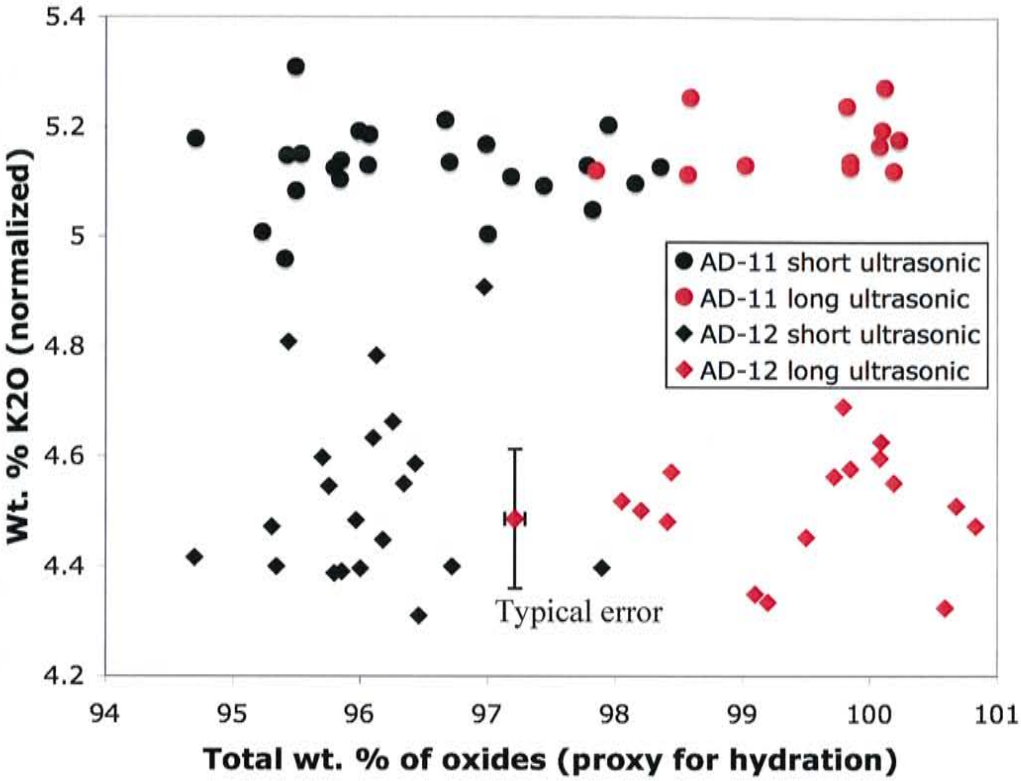

Figure 4.8. In this figure the unnormalized total weight percent of oxides is used as a proxy for hydration on the X-axis, and the normalized weight percent of K_2O is on the Y-axis. Two samples are shown, AD-11 and AD-12, with the black symbols representing a short ultrasonic preparation treatment and the red symbols representing a long ultrasonic treatment. It is clearly demonstrated that with a long ultrasonic treatment the hydrated portion of the sample is gone, thus leaving behind an unhydrated obsidian clast as the end result of the treatment.

No Agua Peaks or Valles caldera was severely affected by element mobility during hydration. After determining the best preparation technique for obsidian, samples used for age calculations were prepared by the long ultrasonic technique for argon dating because this technique breaks off hydration rinds while preserving a pristine obsidian core. The HF sample preparation technique was not used due to absorption of atmospheric ^{40}Ar during the preparation process (to be discussed in Chapter 5); the further pursuit of sample preparation by the air abrasion method was also abandoned for the long ultrasonic bath in water preparation method. There was no evidence in this study to determine that the air abrasion method is inferior to the long ultrasonic bath in water method, the ultrasonic bath method was used because it easier and took less time.

CHAPTER 5: ANALYTICAL RESULTS FROM AR-AR GEOCHRONOLOGY OF GLASS AND FELDSPAR

5.1 Introduction

The results from the Ar-Ar analyses are presented in three sections. The first section is the assessment of preparation and extraction experiments performed on obsidian splits to determine the best methods for dating glass. The second section presents the results from the Agua Peaks volcanic complex, and the final section gives the results from the Valles caldera.

5.2 Ar-Ar assessment of the preparation and extraction experiments

5.2.1 Introduction

A set of experiments was performed on glass to determine the best preparation and extraction methods to use to assure precision and accuracy of data. Sample AD-02 was the primary sample used for these experiments and was subjected to the most preparation and extraction techniques, as described in Chapter 3; samples AD-01 and AD-11 were also used in these experiments. Sample AD-02 was prepared for Ar-Ar analysis using a five-minute ultrasonic bath in water, air abrasion, and five-minute ultrasonic bath in hydrofluoric acid. The extraction techniques performed on sample AD-02 included laser fusion, a two-step laser extraction, and multi-step laser and multi-step furnace incremental heating. Because the long ultrasonic preparation split of AD-02 was not irradiated, samples AD-01 and AD-11 were used to compare the short and long ultrasonic bath preparation treatments. Argon gas for both of these samples was extracted by a two-step laser extraction. The comparison among multiple preparation and

extraction techniques helped to identify the most effective methods for obsidian dating. Comparing the short ultrasonic preparation method to other methods was important in this study because BSE and quantitative analysis both showed that the short ultrasonic method was not effective in removing hydration rinds, which can affect Ar-Ar ages, as discussed below.

5.2.2 Comparison between all preparation and extraction methods

5.2.2.1 Results

There are slight differences in results amongst all preparation and extraction methods for the AD-02 splits, even though ages from all methods overlap within uncertainty (Figure 5.1). The K/Ca and the moles of ^{39}Ar yields are roughly the same for all splits. The average % $^{40}Ar^*$ yield is the highest for the air abraded, two-step extracted split of AD-02. All two-step extraction data that met the criteria are used for age calculation in Figure 5.1 (Refer to Chapter 3 for criteria). The short ultrasonic preparation split yielded a low % $^{40}Ar^*$, and the HF-prepared, fusion-extracted split yielded a low average of % $^{40}Ar^*$ for 9 of 12 analyses. By comparing integrated ages from samples that used the two-step extraction with laser fusion sample ages it can be seen that the HF preparation method causes low % $^{40}Ar^*$ yields, and not the extraction method chosen (Figure 5.2). This allows the comparison between the total gas ages of both methods by using all data for the two-step extraction, which is a more accurate comparison between the two extraction methods.

Samples AD-01 and AD-11 were used to compare the short and long ultrasonic preparation treatments, in both cases using a two-step laser extraction (Figure 5.3). For both preparation methods of samples AD-01 and AD-11 the moles of ^{39}Ar, and K/Ca

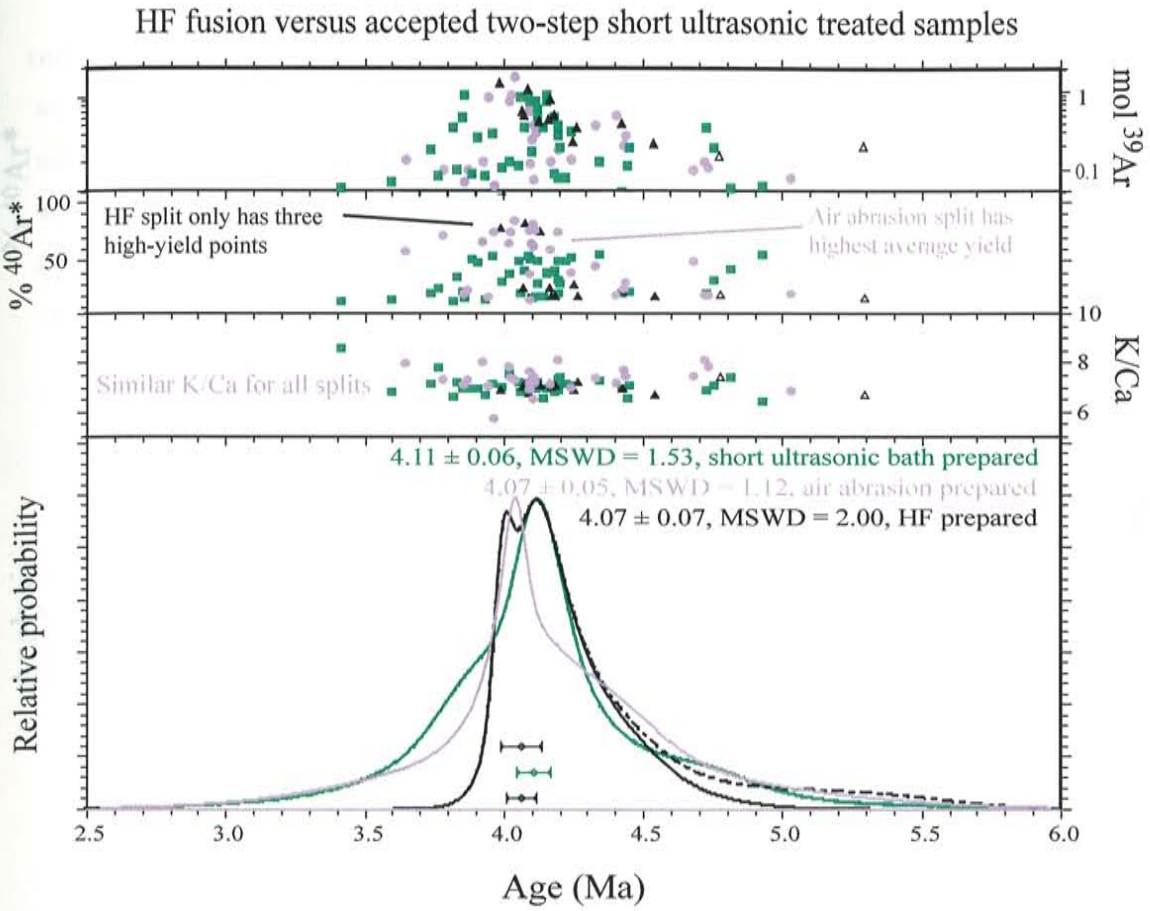

Figure 5.1. This is an ideogram that shows apparent ages for the short ultrasonic preparation treatment in water, HF, and air abrasion preparation methods, as well as two different extraction methods for obsidian sample AD-02. Fusion was used for the HF sample split, where a two-step laser heating schedule was used for the short ultrasonic bath and air abrasion splits. Only data that met the criteria were plotted. All ages overlap within uncertainity.

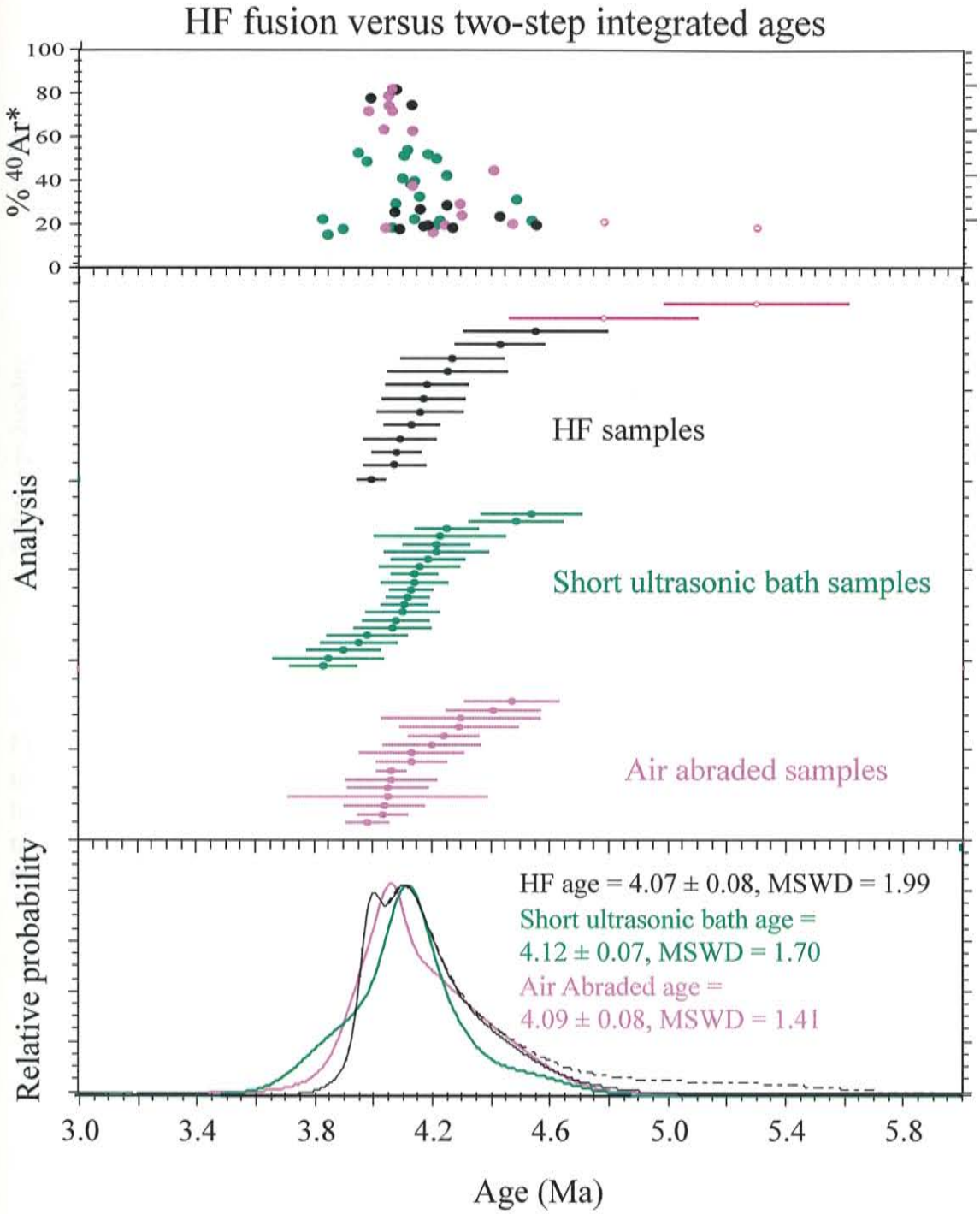

Figure 5.2. Comparison of integrated ages for the air abraded and short ultrasonic two-step samples to age data from the HF fusion split. The HF, short ultrasonic bath, and air abraded sample splits of AD-02 all overlap within uncertainty.

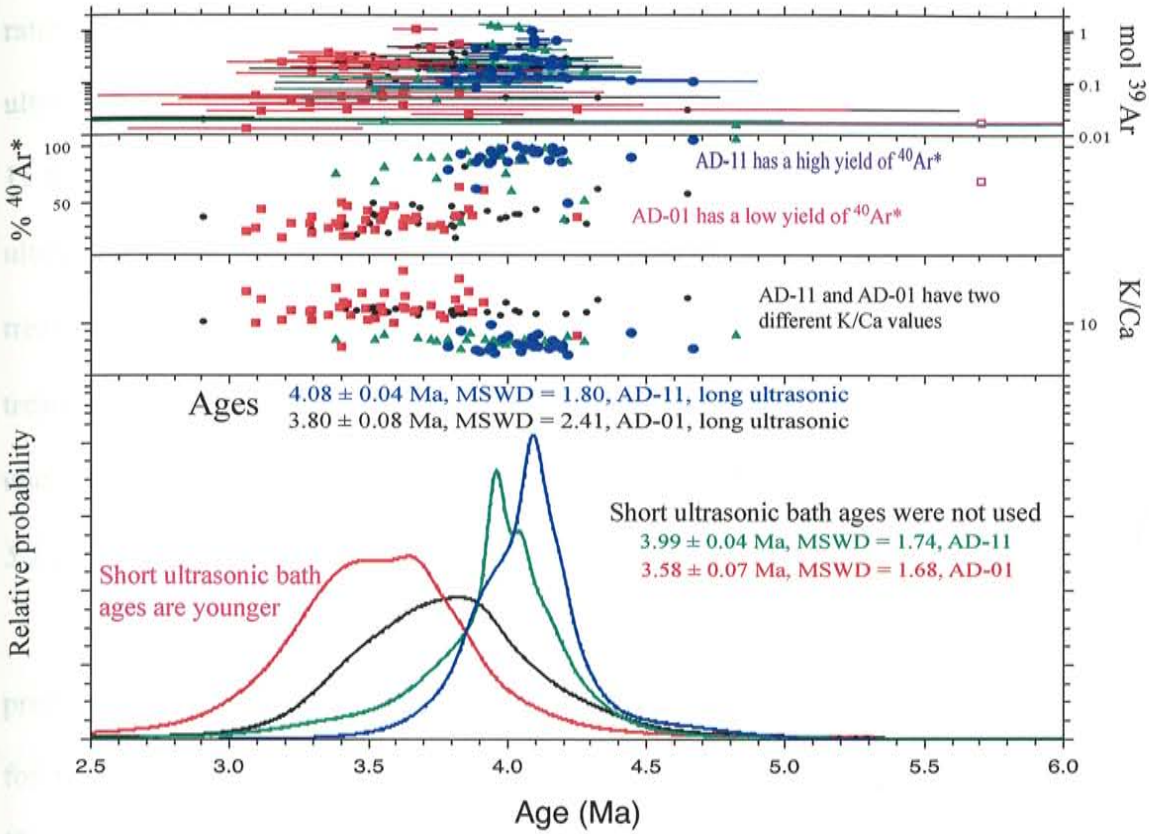

Figure 5.3. This figure represents the differences in age between the short and long ultrasonic preparation methods for obsidian samples AD-01 and AD-11. Sample AD-11 has a higher yield of % ^{40}Ar* because it is older than AD-01. The longer ultrasonic treatments yielded higher % ^{40}Ar* and slightly older apparent ages, which is attributed to the removal of hydration rinds.

ratios are similar, although the % $^{40}Ar^*$ yield is four to seven percent higher for both long ultrasonic bath splits when compared to the short ultrasonic bath splits. For sample AD-11 there is a 0.09± 0.08 Ma difference in age within uncertainty between the short ultrasonic preparation treatment (3.99± 0.04 Ma) and the long ultrasonic preparation treatment (4.08± 0.04 Ma). Also, at 2σ the age of the short ultrasonic preparation treatment (3.58± 0.07 Ma) for sample AD-01 is 0.22± 0.15 Ma younger within uncertainty than the long ultrasonic preparation treatment age (3.80± 0.08 Ma).

5.2.2.2 Interpretation

The differences in % $^{40}Ar^*$ yields are a result from the combinations of the preparation and extraction methods used. Effectiveness in the removal of hydration rinds for all four preparation methods is seen in BSE images (Figures 4.3 and 4.4). The low % $^{40}Ar^*$ and $^{39}Ar_K$ yields for the HF split of AD-02 implies the absorption of various amounts of atmospheric ^{40}Ar, or a reduction in grain size during the HF process. The HF split was also the only split that was extracted by laser fusion; this extraction method was abandoned early for the two-step laser extraction because the atmospheric and radiogenic ^{40}Ar components could not be separated using laser fusion. In this experiment the effects of fusion cannot be isolated from the effects of the HF process, although it was shown that the HF process reduces the % $^{40}Ar^*$ yield. The air abraded and short ultrasonic bath splits of AD-02 were both degassed using the two-step laser extraction method, here the difference in % $^{40}Ar^*$ yield of the higher temperature steps can be attributed to the ineffective removal of hydration rinds by the short ultrasonic preparation method. The low % $^{40}Ar^*$ yield for the short ultrasonic preparation split is attributed to the absorption of atmospheric ^{40}Ar and a loss of $^{40}Ar^*$ during the formation of hydration rinds. The high

% $^{40}Ar^*$ for the air abraded split of AD-02 is attributed to the hydration rinds being removed during the preparation process without causing absorption of atmospheric ^{40}Ar during preparation, unlike the HF preparation method.

Samples AD-01 and AD-11 show differences in Ar-Ar apparent ages between the short and long ultrasonic preparation treatments. The % $^{40}Ar^*$ yield increases and the age appears older for the longer ultrasonic bath splits. This is due to the removal of hydration rinds, which absorbed atmospheric ^{40}Ar and lost $^{40}Ar^*$ during formation. The difference in age between the two methods can be attributed to the character and degree of alteration of the hydration rinds, and that the rinds were not removed during the short ultrasonic preparation method. When there are 1) small hydration rinds, 2) low element mobility, and 3) little absorption of atmospheric argon, the presence of hydration rinds apparently causes only a slight change in precision or accuracy for the age of the sample; large rinds, high element mobility, or the absorption of atmospheric argon can affect the precision and accuracy of a sample. Sample AD-11 was apparently less affected by these factors than sample AD-01, and the presence of hydration rinds only slightly affected the precision and accuracy of the apparent age. Sample AD-01 was deeply hydrated and slightly vesiculated, which is likely why the presence of hydration rinds affected the sample age so much.

5.2.2.3 Conclusions

Although all four preparation methods yield similar ages, they vary in effectiveness. The air abraded and long ultrasonic bath splits have less absorbed atmospheric ^{40}Ar because both methods broke off hydration rinds from the obsidian grains. The short ultrasonic preparation method samples were affected by absorbed

atmospheric ^{40}Ar and $^{40}Ar^*$ loss due to the presence of hydration rinds, which can lower the precision or accuracy in an analysis. Although the HF preparation process removes hydration rinds, the process also causes absorption of atmospheric argon thereby lowering the radiogenic yield of a sample.

The two extraction methods used in this experiment produced similar ages, although the two-step laser extraction method appears better. The laser fusion split yielded a low % $^{40}Ar^*$, but this is attributed to the HF preparation method. Nonetheless, laser fusion cannot split up gas between radiogenic and atmospheric components where a two-step extraction schedule can. Separating the two components is important to drive off absorbed atmospheric argon from the surfaces of grains because the presence of atmospheric ^{40}Ar can lower the precision in an analysis, although this did not occur with the sample analyzed in the current study. Because of the problems associated with laser fusion and the HF preparation method, the air abrasion or long ultrasonic preparation treatment combined with the two-step laser extraction technique is the best way to prepare a sample of the above-mentioned preparations.

5.2.3 Laser and furnace multiple-step heating experiments

Furthering the preparation and extraction experiments, the short ultrasonic preparation and HF sample splits of AD-02 were degassed by multiple-step furnace or multiple-step laser incremental heating for comparison between the two extraction methods (Figure 5.4). This was to determine if there were differences between multi-step laser and multi-step furnace extraction ages, as well as between the ages from the two preparation methods. Step heating was also used to determine if there was an argon loss problem, which can be identified from detailed age spectra.

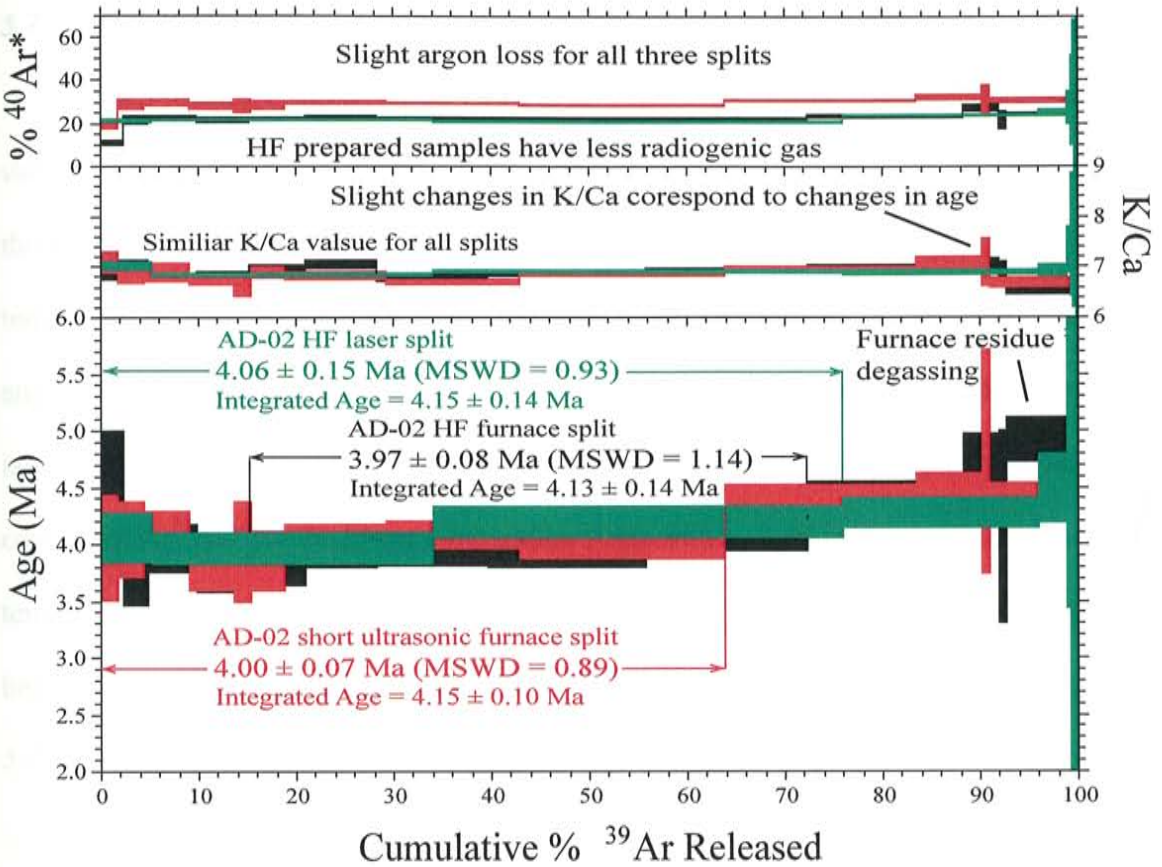

Figure 5.4. This is a spectra of three different AD-02 splits. In green is the HF split that was heated using the CO_2 laser, in black is the HF split that was heated using the furnace, and in red is the short ultrasonic furnace-heated split. All plateau and integrated ages overlap within uncertainity. All spectra display an upward stepping pattern during the later temperature steps. This pattern suggests that there are either microphenocrysts within obsidian that are degassing at higher temperatures or that the entire curves are affected by minor argon loss.

5.2.3.1 Results

Step-heating sample AD-02 allowed an evaluation of how the splits degassed at various temperature steps. Plateau and integrated ages overlap within uncertainty for all three splits. For all three spectra most of the gas is released during the lower temperature-steps, but there is a slight stepping upward trend in the age for the entire analysis. The K/Ca remains nearly constant for all three splits with slight increases in the later temperature steps. Other than the first temperature step, all three splits yielded consistent % $^{40}Ar^*$ for the lower temperature steps with a slight increase at the higher temperatures. However, the HF prepared sample splits for the laser and furnace step heating extractions both yielded lower % $^{40}Ar^*$ than the short ultrasonic bath split.

5.2.3.2 Interpretation

Age spectra show the degassing patterns of argon at increasing temperature steps, which helps to determine if there are differences between the preparation and extraction methods used. Both preparation and extraction methods produced similar K/Ca values during the lower temperature steps, but the K/Ca ratios change during the higher temperature steps. Although all preparation methods yielded a fairly consistent % $^{40}Ar^*$, both extraction methods for the HF split produced a low % $^{40}Ar^*$ yield. This confirms the results of previously described experiments, showing that atmospheric ^{40}Ar was incorporated into the grains during preparation. This also suggests that for this sample the short ultrasonic preparation method is better than the HF method in spite of the incomplete removal of hydration rinds.

A pattern exists for all three age spectra where the ages step upward with increasing temperature. At higher temperatures there is a slight increase in apparent age

for all three splits, accompanied by an increase in the % ^{40}Ar* yields and changes in the K/Ca ratios. This could be caused by low-K microxenocrysts within the obsidian degassing at successively higher temperature steps. The furnace split also displays the degassing of residue material at the highest temperature steps, which is interpreted as a laboratory artifact and not the degassing of xenocrysts within the obsidian. If argon loss were severe, a dramatic argon loss curve would be expected. None of the AD-02 sample splits display this kind of curve, although the curves do display what could be interpreted as a slight argon loss.

5.2.3.3 Conclusions

The use of multi-step age spectra can help identify xenocryst contamination, argon loss, and differences caused by the preparation method used. All plateau and integrated ages overlap within uncertainty, and there seems to be little difference between the multi-step laser and multi-step furnace extraction methods. There appears to be a slight argon loss problem for sample AD-02 and a problem with microxenocrysts degassing at higher temperatures, which affected the K/Ca, % ^{40}Ar* yield, and apparent age of the higher temperature steps. Although the two preparation methods produced similar ages, the short ultrasonic preparation method is preferred over the HF method because it yielded higher % ^{40}Ar* than the HF method. Either extraction method can be used because both yielded the same age result; residual degassing in the furnace is the only real difference between the two methods.

5.2.4 Preparation and extraction method experiment conclusions

Preparation and extraction methods can affect obsidian samples in various ways. Certain techniques can improve the chances of obtaining accurate data. All preparation

and extraction methods produced ages that overlapped within uncertainty for sample AD-02 (Figure 5.5), although the presence of hydration rinds have affected the apparent age of other samples. Since there is no way of knowing how the presence of hydration rinds will affect a sample, if at all, the rinds should be removed from obsidian grains before analysis. This is because hydration rinds can be affected by element mobility, and may have absorbed atmospheric ^{40}Ar or lost $^{40}Ar^*$ during formation, which can change the precision or accuracy of an apparent age. Therefore, the short ultrasonic preparation treatment is not recommended for age analysis, nor is the HF preparation method. HF prepared samples have been shown to absorb atmospheric ^{40}Ar during preparation and have low $^{40}Ar^*$ yields, this can affect the precision or accuracy of apparent ages. Preparation by air abrasion or by a long ultrasonic bath in water will break off hydration rinds without incorporating atmospheric ^{40}Ar during the process; BSE images from the electron microprobe confirm that hydration rinds are broken off. In the current study the long ultrasonic preparation technique was used instead of the air abrasion method because it was faster and easier.

Of the four extraction methods used, three are recommended for obsidian. A two-step extraction can break up gas between atmospheric and radiogenic ^{40}Ar, and was the preferred method of extraction for the current study. There is little difference between the degassing of obsidian between a multi-step laser and multi-step furnace incremental heating. Multiple-step incremental heating can show how obsidian degasses as a function of temperature, which can help identify argon loss and phenocryst contamination of a sample. Laser fusion of samples is not recommended because ^{40}Ar cannot be split between its radiogenic and atmospheric components. In hindsight, multiple-step

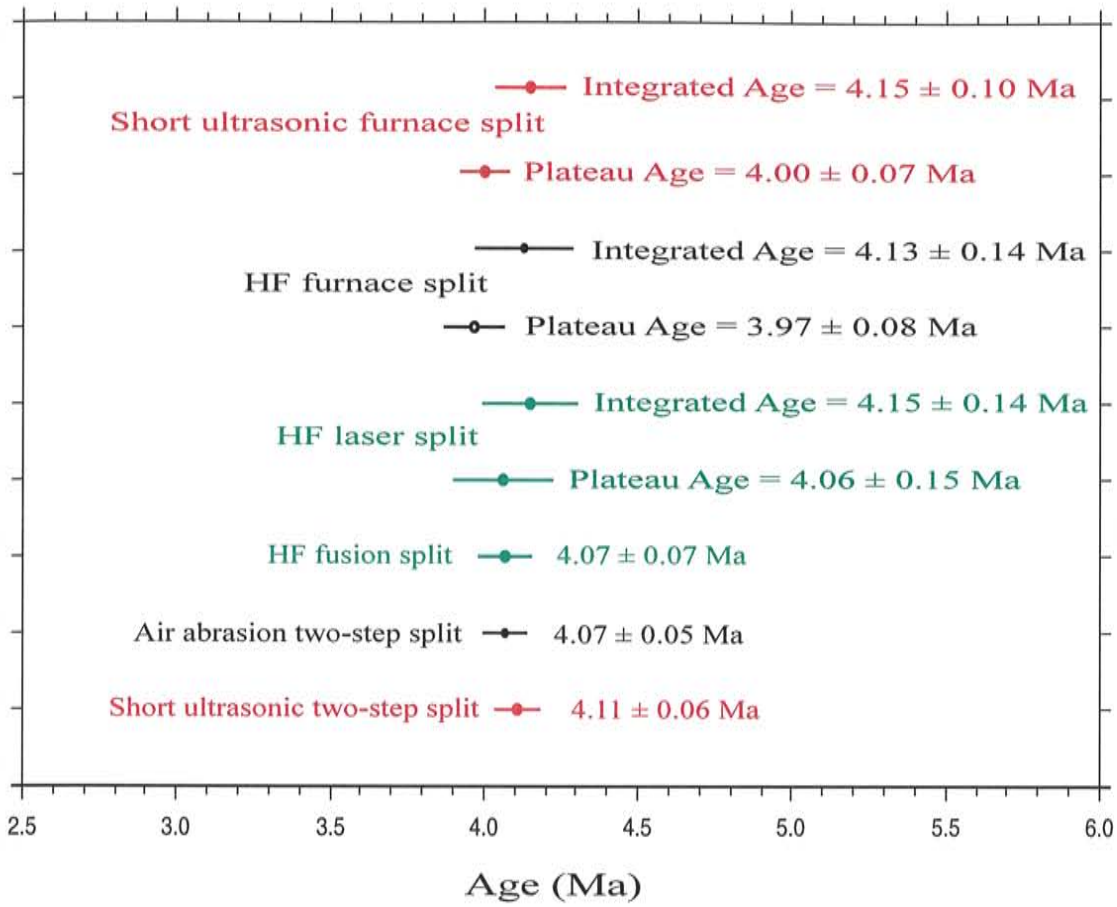

Figure 5.5. Plot displaying ages and uncertainties from all preparation and extraction methods for sample AD-02. All ages overlap within uncertainty at 2 sigma.

incremental heating is the best extraction method to use on obsidian for the above-mentioned reasons. The drawbacks of multiple-step heating are time and high costs for analyses. Pristine unaltered obsidian can be dated using a two-step method to save time and reduce costs, but some data will be lost.

5.3 Ages from the No Agua Peaks volcanic complex

Nine samples were dated from the No Agua Peaks volcanic complex to determine eruption ages. Three of the samples were feldspar and six were obsidian; of the three feldspar samples, two samples were from feldspar-bearing obsidian units and one was from a breccia. Feldspar-bearing obsidian samples were obtained to get accurate ages from eruptions using sanidine to determine if an obsidian age deviates from it. Feldspar data will be discussed first, then the obsidian ages of the complex. Individual sample age data are reported in Appendix C.

5.3.1 Results

Although K-feldspar phenocrysts typically yield precise and accurate eruption ages, the feldspars from the No Agua Peaks yielded less than perfect results. Three feldspar samples were collected from the No Agua Peaks complex, two from the older (AD-03 and AD-09), and one from the younger stratigraphic unit (AD-12). Of the three laser fusion analyses, only sanidine sample AD-09 produced a reasonable age of eruption at 4.04± 0.11 Ma with an MSWD of 10.65. The analysis for feldspar sample AD-03 was stopped early because the mineral analyzed was plagioclase instead of sanidine, as shown by low K/Ca ratios. The sanidines from sample AD-12 were xenocrysts, but yielded a geologically meaningful age from another event. After all outlier populations were removed from the main population of points, the sample yielded an age of 25.19± 0.13

Ma (Figure 5.6). This suite of crystals is from a pre-Taos Plateau volcanic field origin and does not relate to volcanism at the No Agua Peaks. However, the age precisely reflects the age of a large-scale volcanic eruption from the Latir range. The sanidines are xenocrysts from the Amalia Tuff, which crops out ~16 km south of the No Agua Peaks (Smith et al., 2002). These sanidines help to identify the northern extent of this outflow sheet, which is apparently present in the subsurface beneath No Agua Peaks.

5.3.2 Eruption ages

Of the nine samples analyzed, results from one sanidine and six obsidian samples were used to determine the age of the No Agua Peaks volcanic complex. Results from one sanidine and three obsidian samples were used to calculate the age of the oldest eruption, and three obsidian samples were used to calculate the age of the younger eruption. Data from the older and younger eruptions form distinct clusters with ages at 3.86± 0.06 Ma and 4.07± 0.03 Ma (Figure 5.7). Both curves are Gaussian and sample ages for each event agree within uncertainty.

5.3.3 Interpretation

Two distinct groups of ages were formed by the seven samples, coinciding with the North Hills and West Hills eruptive stages. Sanidine and obsidian ages agree within units, and mean unit ages agree with stratigraphy. In the field, a break in ages coincides with a meter-thick paleosol that formed along the contact between the oldest and youngest unit. The West Hills stage is not only temporally distinct, but the samples also have different immobile element chemistry from the North Hills stage. The observations of a paleosol stratigraphically separating the two packages of units along with changes in

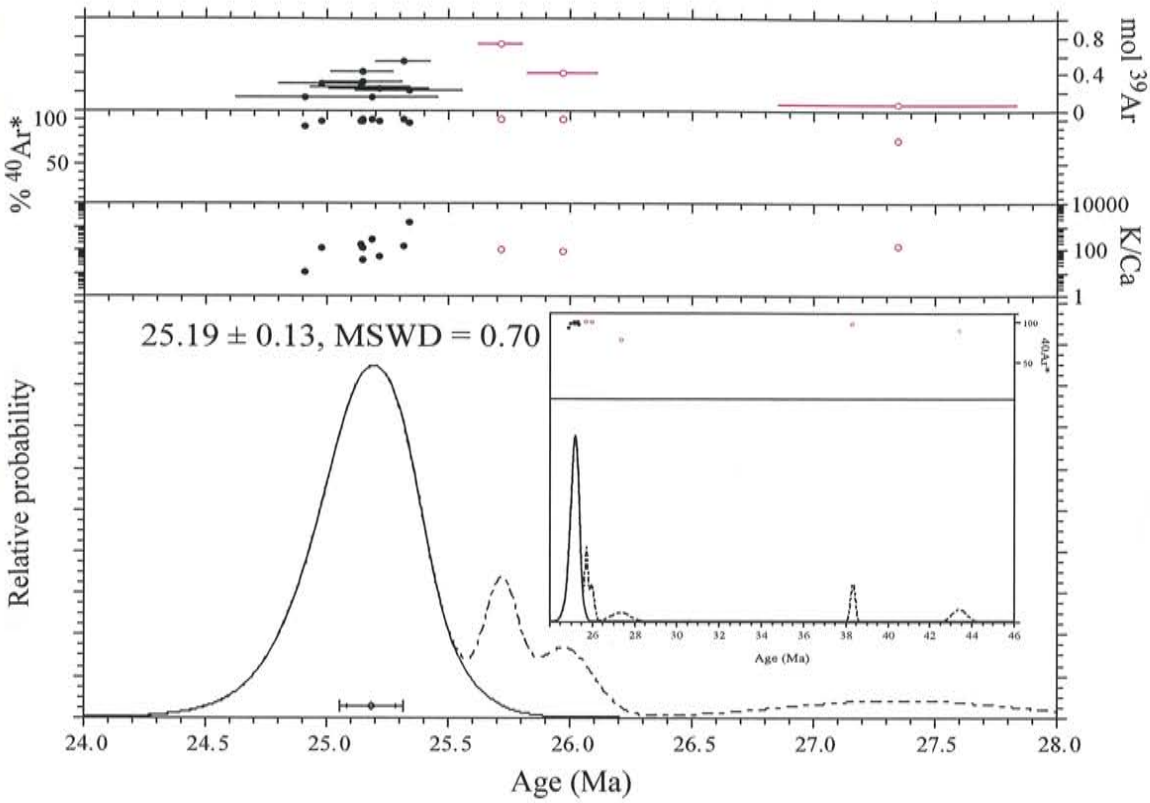

Figure 5.6. An ideogram of sanidine sample AD-12 where a xenocrystic population is identified (inset). After outliers (in red) were removed from the data set, an age of 25.19± 0.13 Ma was yielded with a MSWD of 0.70. This population represents an eruption from the Questa caldera, which outcrops as Amalia tuff ~16 km south of the No Agua Peaks complex.

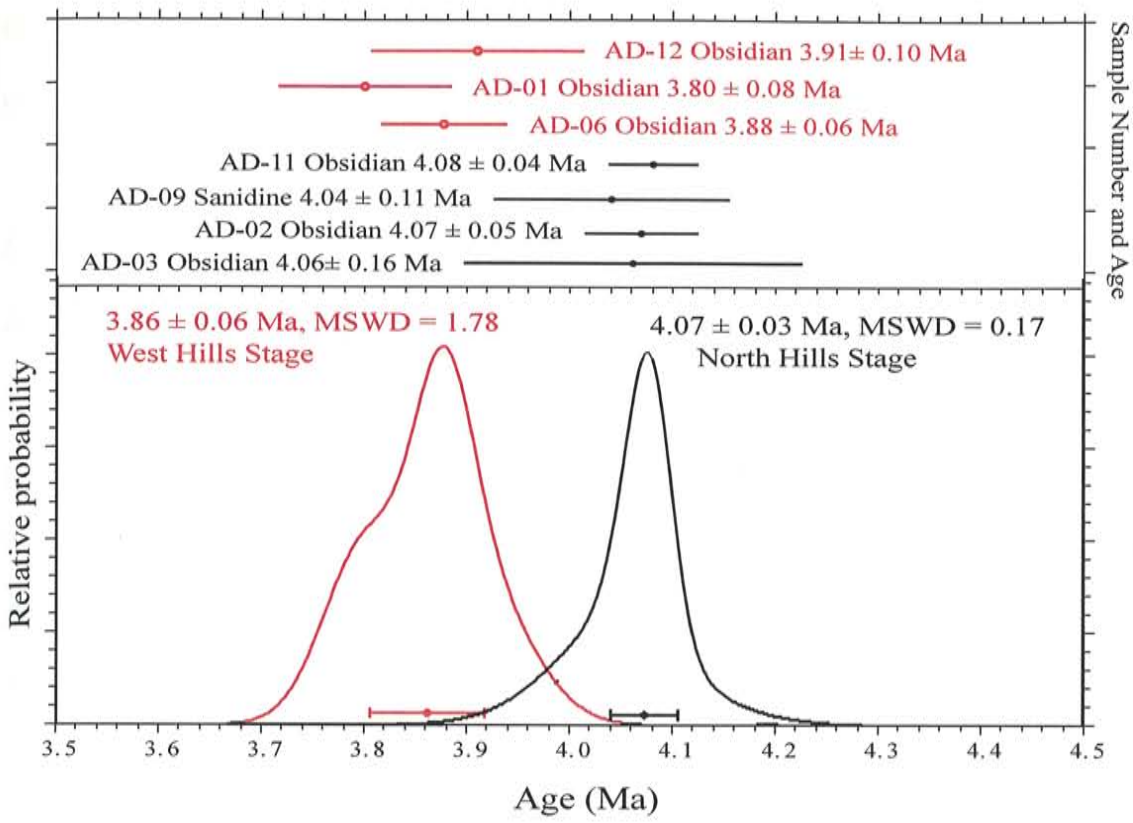

Figure 5.7. Ideogram displays the two eruption ages for the No Agua Peaks volcanic complex. All ages are from obsidian except for sample AD-09, which is from sanidine.

chemistry are good evidence that the two age populations are correct, and that both eruptions are temporally distinct from one another at 2σ.

Two samples yielded inaccurate apparent ages and were not used to calculate age for the No Agua Peaks volcanic complex. Low K/Ca ratios showed that feldspar sample AD-03 was plagioclase; this sample was not used because the apparent age of 2.2± 0.9 Ma is much too young for the eruption age. The inaccurate age also reemphasizes why plagioclase feldspar, in many cases, is a poor material for Ar-Ar dating. Sanidine sample AD-12 was not used because it yields an age influenced by xenocrysts that is appropriate for the Amalia Tuff.

5.3.4 Conclusions

Obsidian from the No Agua Peaks volcanic complex in this study have yielded ages that are more precise than previously published ages for this complex. This shows that obsidian can be used as a viable dating material for the Ar-Ar method. Different age populations of sampled units correspond to geochemical changes and the formation of a paleosol in the field. The ages of 3.86± 0.06 Ma for the West Hills stage and 4.07± 0.03 Ma for the North Hills stage allow a time gap between the two eruptive episodes of 0.21±0.09 Ma. This is enough time to allow chemical changes in magma chemistry and the formation of a meter-thick paleosol after the first episode of volcanism. The two-step extraction method coupled with a long ultrasonic cleaning of the grains yielded accurate and precise ages for the two events. If the history of the volcano were more complex (e.g. intrusions and late-stage hydrothermal activity), then a multiple-step heating schedule would have been more appropriate.

5.4 Dating of the Cerro del Medio dome and the <0.5 Ma volcanic units of the Valles caldera

Two distinct eruptive periods from the Valles caldera were investigated during the current study. Cerro del Medio dome building is the older activity and is discussed first; ages from this dome provide an upper time constraint for resurgent activity from the Valles caldera (Phillips et al., 2007). The second part of this section pertains to the post-0.5 Ma volcanic eruptions associated with the Valles caldera. Knowing the ages of the youngest eruptions aids in assessing the volcanic hazard of the volcano.

5.4.1 Cerro del Medio

Thirteen samples, four feldspar and nine obsidian, were dated in this study to obtain an age for the Cerro del Medio dome, the first in a series of rhyolite domes thought to have formed following the eruption of the Upper Bandelier Tuff at 1.256± 0.010 Ma (Phillips et al., 2007; Phillips, 2004). Samples were collected from six eruptive lobes that were previously mapped in the field (Gardner and Goff, 2006). From field mapping, the geologic relationships amongst these lobes give the stratigraphic order of events, from youngest to oldest, as DM-6, DM-5, DM-4, DM-North (DM-N), DM-West (DM-W), and DM-South (DM-S). There is some uncertainty in the stratigraphic order for the DM-S, DM-W, and DM-N lobes. The samples in this study were dated by lobe, and ages were combined to determine if lobe-forming events were temporally resolvable (Figure 5.8). The sanidine age for the outflow facies of the Upper Bandelier Tuff from Phillips et al. (2007) also appears in Figure 5.8. Four feldspar samples were dated in the current study, two by laser fusion (AD-25 and AD-27) and two by multi-step laser heating (EP-39 and EP-42). Sanidine samples EP-39 and EP-42 were dated by Phillips et al. (2007), but are

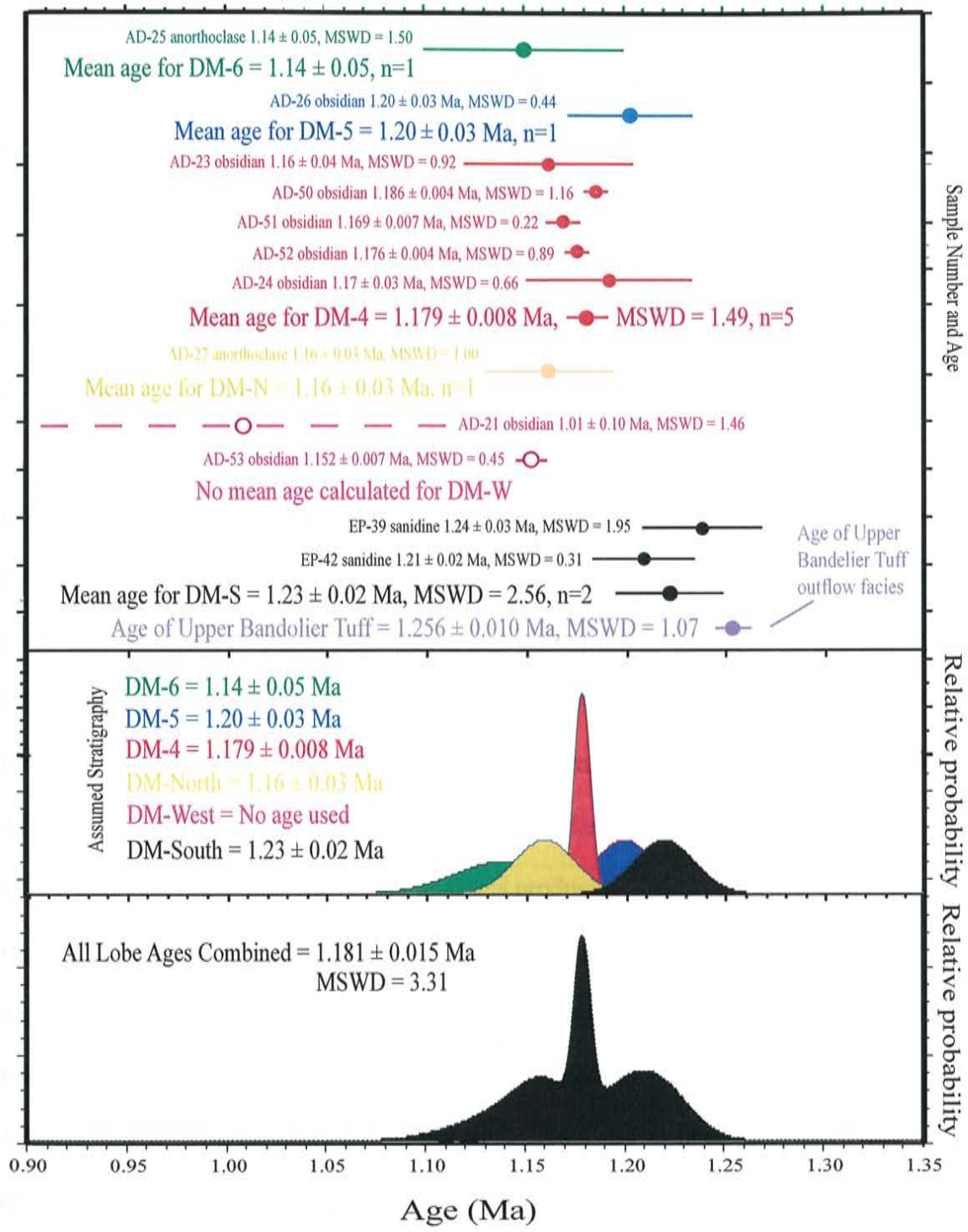

Figure 5.8. Ideogram displays the sample ages for Cerro del Medio by lobe as well as a composite probability curve for all lobes togeather. Hollow points are ages not used in calculations. The DM-6, DM-N and DM-S are feldspar ages. The age for the DM-S lobe and the Upper Bandelier Tuff are from Phillips et al. (2007).

used in this study for the age of the DM-S lobe; obsidian samples AD-50 to AD-54 are unpublished obsidian data from Phillips (2004) that are used in this study. Four of the nine obsidian samples (AD-50, AD-51, AD-52, and AD-53) were multi-step laser heated and the other five obsidian samples (AD-21, AD-22, AD-23, AD-24, and AD-26) were heated by a two-step laser extraction method. The DM-6 and DM-S lobes were dated by feldspar because the lobes do not have any associated obsidian.

5.4.1.1 Results and ages

Ten samples were used to calculate the age of the Cerro del Medio dome. An isochron age was used for the feldspar sample AD-25 from the DM-6 lobe because the sample appears to be affected by excess argon. Three of the six lobes were dated using only one sample per lobe (DM-6= 1.14± 0.05 Ma, DM-5= 1.20± 0.03 Ma, DM-N= 1.16± 0.03 Ma). The two lobes dated by multiple samples had MSWD's of 1.49 for the DM-4 lobe (n=5) and 2.56 for the DM-S lobe (n=2). No samples from the DM-W lobe (AD-21, AD-22, and AD-53) were used for age calculation. Samples AD-21 and AD-22 were affected by severe Ar loss, with many analyses producing little to no argon gas; this resulted in large uncertainties with geologically unreasonable ages. Sample AD-53 experienced analytical problems during extraction and the apparent sample age is not used. When all samples are grouped together the mean age is 1.181± 0.015 Ma with a MSWD of 3.31. A probability plot of the six lobes appears to have three partly overlapping age populations, which accounts for the poor MSWD.

5.4.1.2 Interpretation

Five of six lobes dated yielded apparent ages that are geologically reasonable, although these apparent ages have a potential to be inaccurate. Three of the six lobe ages

were calculated by using only one sample; having more samples dated would have increased the precision of these lobe ages. Neither of the two lobes dated using anorthoclase feldspar appear to be affected by excess argon. The two lobes that were dated by multiple samples were both dated using only one material each, feldspar for the DM-S lobe and obsidian for the DM-4 lobe; both lobe ages agree with stratigraphy. However, if there was a problem such as argon loss or xenocryst contamination for either the sanidine or obsidian, it might go unnoticed because only one type of material was dated for each lobe. The sanidine age from the DM-S lobe is questionable because in BSE the grains include patchy anorthoclase and appear slightly resorbed, indicating that the crystals may be xenocrystic (Figure 5.9). The obsidian ages for DM-5 and DM-4 are assumed to be accurate because the age is based on ages from multiple samples, agree with stratigraphy, and no analyses displays unreasonably young and imprecise ages implying argon loss, as in the case of samples AD-21 and AD-22. Assuming that the precise age for the DM-4 lobe is accurate and has not been affected by $^{40}Ar^*$ loss, the ages of the other five lobes can be compared to the stratigraphic order. The ages for the DM-6 and DM-5 lobe do not conflict because the ages agree with stratigraphy. The anorthoclase age for the DM-N lobe and the sanidine age for the DM-S lobe both fit with the stratigraphy as well because both ages are older than the DM-4 lobe. The ages obtained in this study are geologically reasonable because the ages agree with stratigraphy, although these ages differ from some previously published ages.

5.4.1.3 Comparison to previous ages of the Cerro del Medio dome

Previous Ar-Ar ages of the Cerro del Medio dome are from either sanidine or obsidian, and have produced varying results for lobe ages (Table 5.1). The ages from the

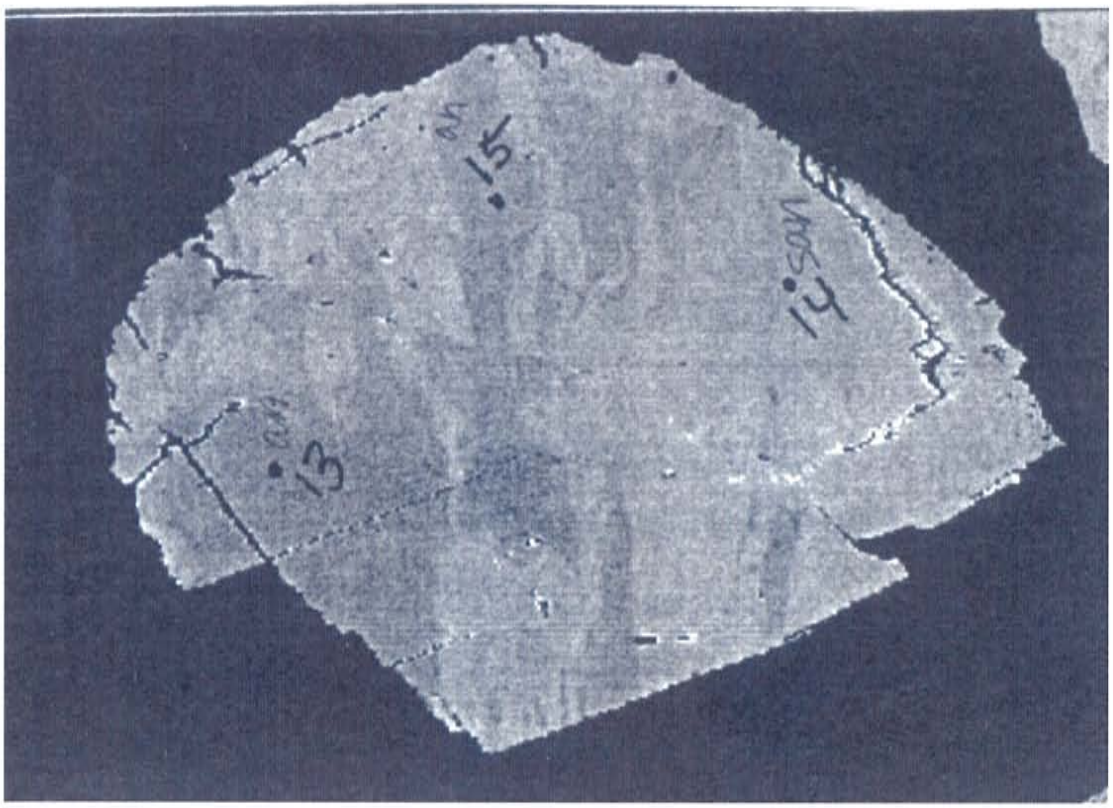

200 um

Figure 5.9. BSE image of EP-42 where patches of anorthoclase are imaged within sanidine crystals, the sanidine crystal also appears slightly resorbed. These observations could mean that the sanidines have been altered after they have formed, implying that the crystals may be xenocrysts.

Table 5.1. Table shows all ages of the Cerro del Medio dome from the current and previous studies. Previous ages have been corrected for monitor ages and changes in decay constants.

Author	Method	Dome, previous dome names are in parentheses.		
		DM-W (DM-I)	**DM-N (DM-II)**	**DM-S (DM-II)**
Doell (1968)	K-Ar	1.07±0.05 OBS		
Spell and Harrison (1993)	Ar/Ar	1.102±0.012 OBS		1.140±0.011 SAN
Izett and Obradovich (1994)	Ar/Ar	1.207±0.03 SAN		
Phillips et al. (2007)	Ar/Ar			1.229±0.017 SAN
This study	Ar/Ar		1.16±0.03 ANO	
		DM-4 (DM-II)	**DM-5 (DM-II)**	**DM-6 (DM-III)**
Doell (1968)	K-Ar	1.18±0.03 OBS		
Spell and Harrison (1993)	Ar/Ar			1.140±0.011 SAN
Izett and Obradovich (1994)	Ar/Ar	1.161±0.01 OBS		
Phillips et al. (2007)	Ar/Ar			
This study	Ar/Ar	1.179±0.008 OBS	1.20±0.03 OBS	1.14±0.05 ANO

Note: OBS=obsidian, SAN= sanidine and ANO=anorthoclase

current study are the only ages available for the DM-5 and DM-N lobes. Using data from all studies, the ages for the DM-4, DM-5, and DM-6 lobes agree within uncertainty with the current stratigraphy. The sanidine age for the DM-6 lobe from Spell and Harrison (1993) agrees with the anorthoclase age for this lobe from the current study, and this age is considered to be accurate and precise. The DM-4 and DM-5 obsidian ages are considered accurate and precise because three different studies yielded the same age results for this lobe and there does not appear to be an argon loss problem for these lobes in any study. There is uncertainty in the stratigraphy for the oldest lobes of Cerro del Medio, DM-W, DM-N, and DM-S, due to a large scatter in published ages and because the lobes do not have observable contact relationships. Since the DM-4 lobe overlies all three of these lobes, it is known that all three of these lobes are older than the DM-4 lobe. The DM-N lobe age is irresolvable from the DM-4 and DM-5 lobes because the geologically reasonable yielded age for the DM-N sample forms a population with the DM-4 and DM-5 lobes; this age is assumed to be accurate. There are two different published Ar-Ar sanidine ages for the DM-S lobe, one age is apparently older and the other age is apparently younger than the DM-4 lobe. The older age for this lobe is geologically reasonable because it agrees with the stratigraphy of the dome, and the DM-S lobe is believed to be the oldest lobe of the dome (Phillips et al., 2007; Phillips, 2004). There are three different ages for the DM-W lobe from previous K-Ar and Ar-Ar studies; no age was obtained in the current study due to argon loss and analytical problems during extraction. There are two age populations for this lobe, sanidine yields the oldest apparent age and obsidians yield the younger apparent ages for this lobe. Two obsidians in the current study were affected by severe argon loss and it is assumed that the two

previous obsidian ages for this dome are also incorrect because they yield ages that are younger than the DM-6 lobe. The sanidine age for this dome agrees with stratigraphy and with the sanidine age for the DM-S lobe as well. However, there is a possibility that the sanidines from the DM-S and DM-W lobes are xenocrystic and do not represent the ages of lobe-forming events.

5.4.1.4 Conclusions

Ages from the current and previous studies form three overlapping age populations, which permit two slightly different interpretations suggesting that Cerro del Medio formed six lobes over a short time period (Figure 5.10). The first scenario includes the DM-W and DM-S lobe ages, where the second scenario does not include these two lobes because the ages for these two domes may be influenced by xenocrysts; for both scenarios the youngest two lobe forming events appear to overlap in age, and may not be resolvable in age at 2σ. In the first scenario it appears that the DM-S and DM-W lobes concurrently formed the first two lobes, then the DM-N, DM-4, and DM-5 lobes were formed, and the DM-6 lobe formed on top of the dome last. The age for the DM-6 lobe might not be resolvable from the combined age of the DM-5, DM-4 and DM-N lobes. This scenario suggests that Cerro del Medio formed in up to three temporally distinct pulses starting at 1.22± 0.02 Ma and the duration of Cerro del Medio lasted for 0.08± 0.04 Ma. In the second scenario the age for the DM-S and DM-W lobes is influenced by xenocrystic material and is not used, where the youngest two ages are not fully resolvable at 2σ and can represent one or two temporally distinct pulses of volcanism. In this scenario lobe building at Cerro del Medio began at 1.18± 0.03 Ma and the duration of lobe forming events is 0.05± 0.04 Ma. The ages for Cerro del Medio from

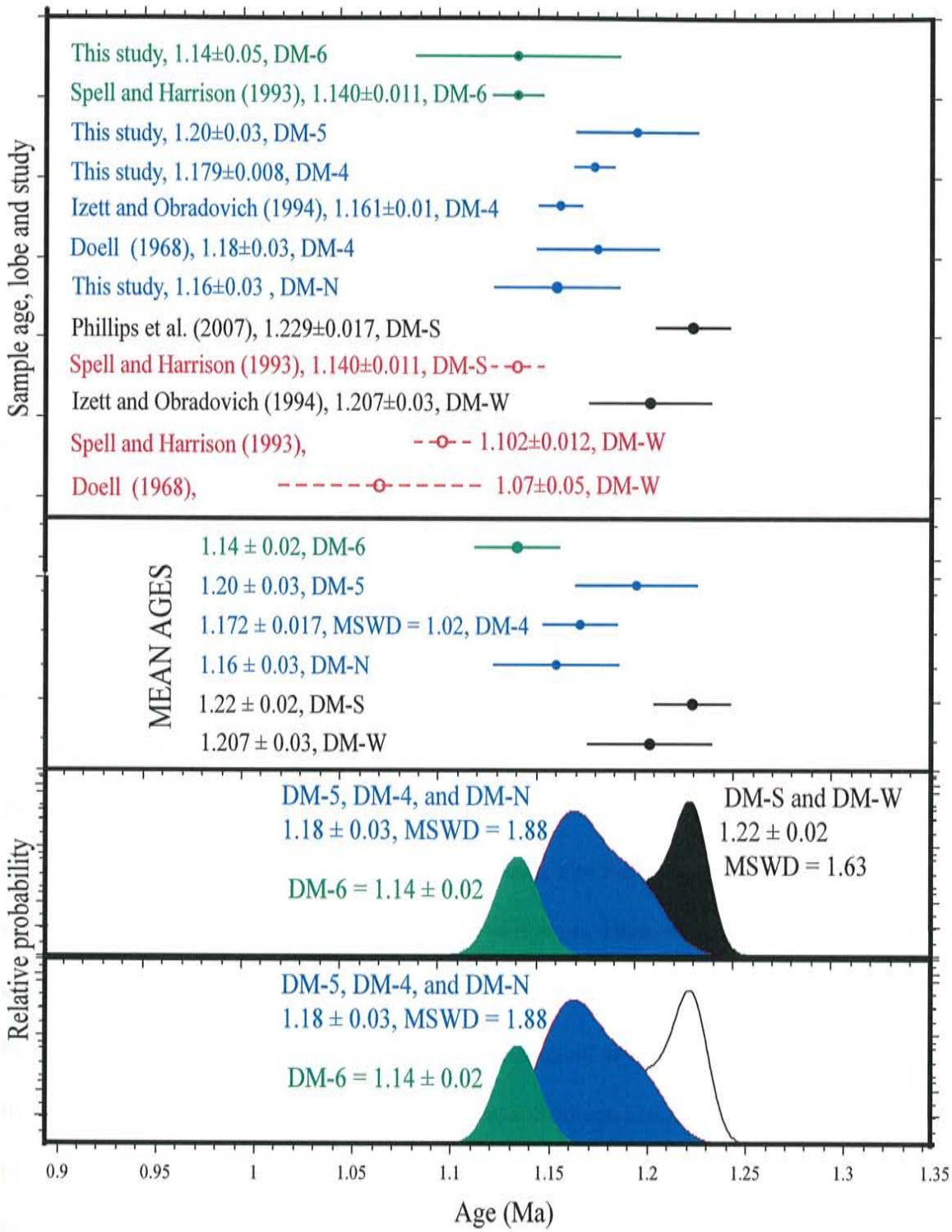

Figure 5.10. Figure shows all current and previous ages for the Cerro del Medio dome on top, ages in red were not used in the mean age calculation. The mean ages that were used for age calculation are shown in the center plot, and the two scenario curves for the ages of the domes are shown on the bottom. Ages in green are to show the youngest event, ages in blue show three lobes that formed concurrently, and ages in black show the oldest two lobes.

this study agree with most previously published ages, and show that obsidian can be used as an Ar-Ar dating material.

There are two different timings for resurgence based on the two scenarios for Cerro del Medio. The oldest age for Cerro del Medio is important because the age brackets the timing of resurgence of Redondo Peak with the age of the Upper Bandelier Tuff. In the first scenario the ages from the combined studies suggest that resurgence of the Valles caldera was completed within 0.04± 0.03 Ma after the initial eruption of the Bandelier Tuff, which agrees with the 0.027± 0.027 Ma timing of resurgence from Phillips et al. (2007). In the second scenario, where the ages for the DM-S and DM-W sanidines are influenced by xenocrysts, then the timing of resurgence for Cerro del Medio is 0.08± 0.04 Ma.

5.4.2 Results for the post-0.5 Ma volcanic units associated with the Valles caldera

The youngest volcanic units from the Valles caldera were analyzed to determine the lower time limit of volcanism, which aids in volcanological hazard assessments. The Banco Bonito formation overlies El Cajete deposits, and the Battleship Rock ignimbrite is an intermediate event (Toyoda et al., 1995; Self et al., 1991; Gardner and Goff, 1987; Goff et al., 1986). All units are believed to have erupted over a short time interval because of field relationships and chemical, petrological and isotopic similarities amongst the three units (Spell and Harrison, 1993). These units are also known to be <0.5 Ma because all units overlie the pumice beneath South Mountain, which formed ~0.5 Ma (Spell and Harrison, 1993, Self et al., 1991; Spell and Kyle, 1989; Doell et al., 1968). Obsidian was sampled from a Banco Bonito lava flow (AD-28), obsidian fiamme were sampled from the Battleship Rock ignimbrite (AD-31), and obsidian clasts from a

pyroclastic surge deposit (AD-20) as well as bread crust bombs (AD-29 and AD-30) were sampled from the El Cajete member. Sample grains were rigorously handpicked in attempt to minimize phenocryst contamination.

5.4.2.1 Results

Four of the five samples were analyzed; one El Cajete bread crust bomb sample (AD-29) was not analyzed due to extensive perlitic alteration. All samples were laser step-heated except for Banco Bonito sample AD-28, which was extracted using the two-step method. The phenocryst-rich Banco Bonito obsidian sample yielded an anomalously old age of 1.19± 0.03 Ma (Figure 5.11a), which is similar in age to the earliest Cerro del Medio dome building activity. The Banco Bonito sample was the first sample analyzed in this sample suite and it was two- step laser extracted, a multi-step laser extraction was used for the three other samples once the problem of xenocrystic material was noticed in this sample. Obsidian from the pyroclastic surge deposit of El Cajete yielded a stair-stepping downward pattern in age and % $^{40}Ar^*$ with increasing temperatures, forming an anomalously old plateau age of 1.62± 0.06 Ma comprised of only two temperature steps (Figure 5.11b). Obsidians from one El Cajete bread crust bomb sample had a plateau age of 0.257± 0.088 Ma and the Battleship Rock ignimbrite yielded a plateau age of 0.010± 0.015 Ma. Both plateau ages were from all temperature steps and have consistent % $^{40}Ar^*$ yields, although the K/Ca decreases with higher temperature steps for the El Cajete sample (Figure 5.12).

5.4.2.2 Preliminary interpretation of sample ages

Only one of the four post-0.5 Ma Valles obsidian samples yielded a geologically reasonable age; apparent ages of the remaining samples are either anomalously old or

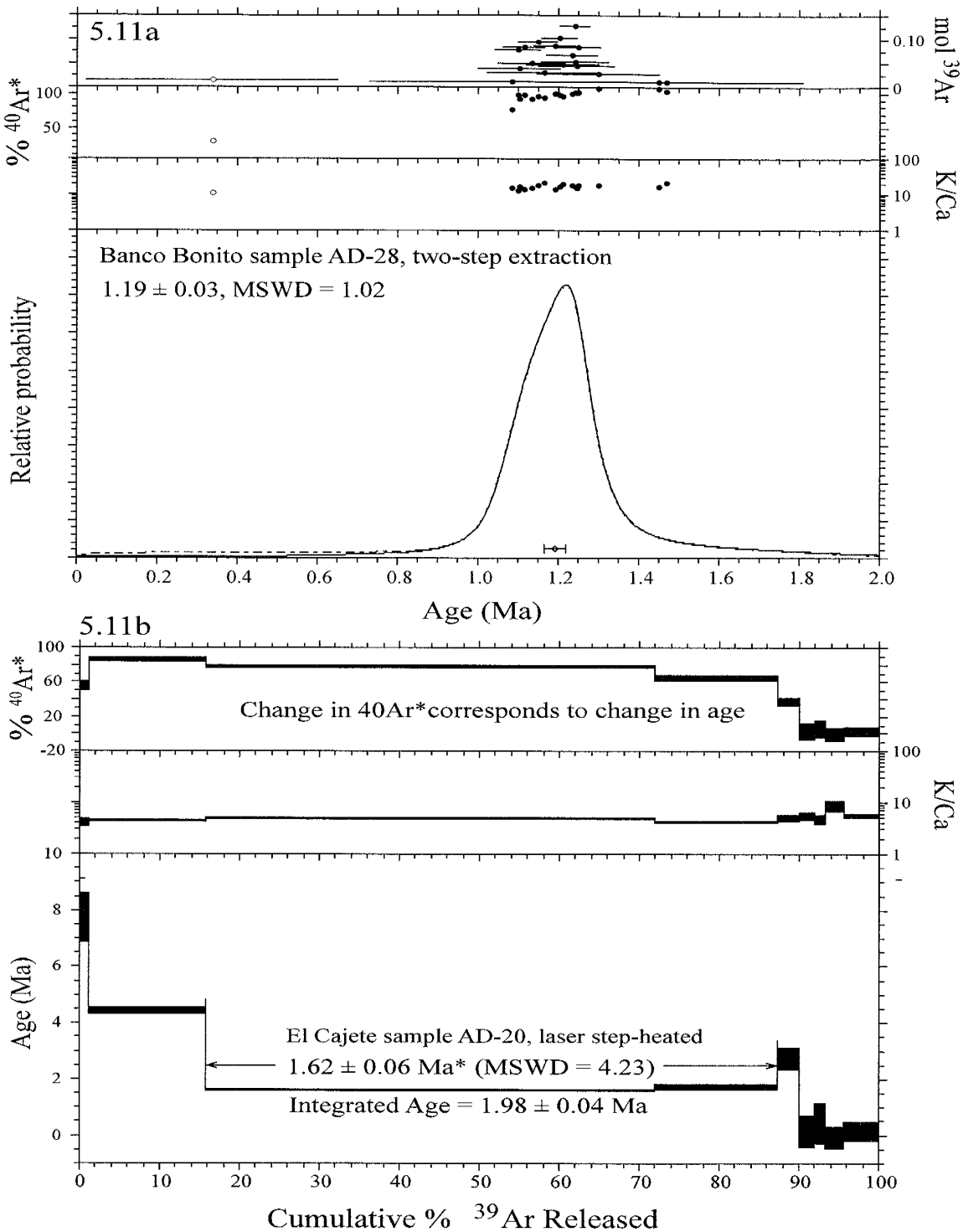

Figure 5.11. Figure shows the xenocrystic ages from Banco Bonito (above) and for El Cajete (below). The hollow red point was removed from the age calculation.

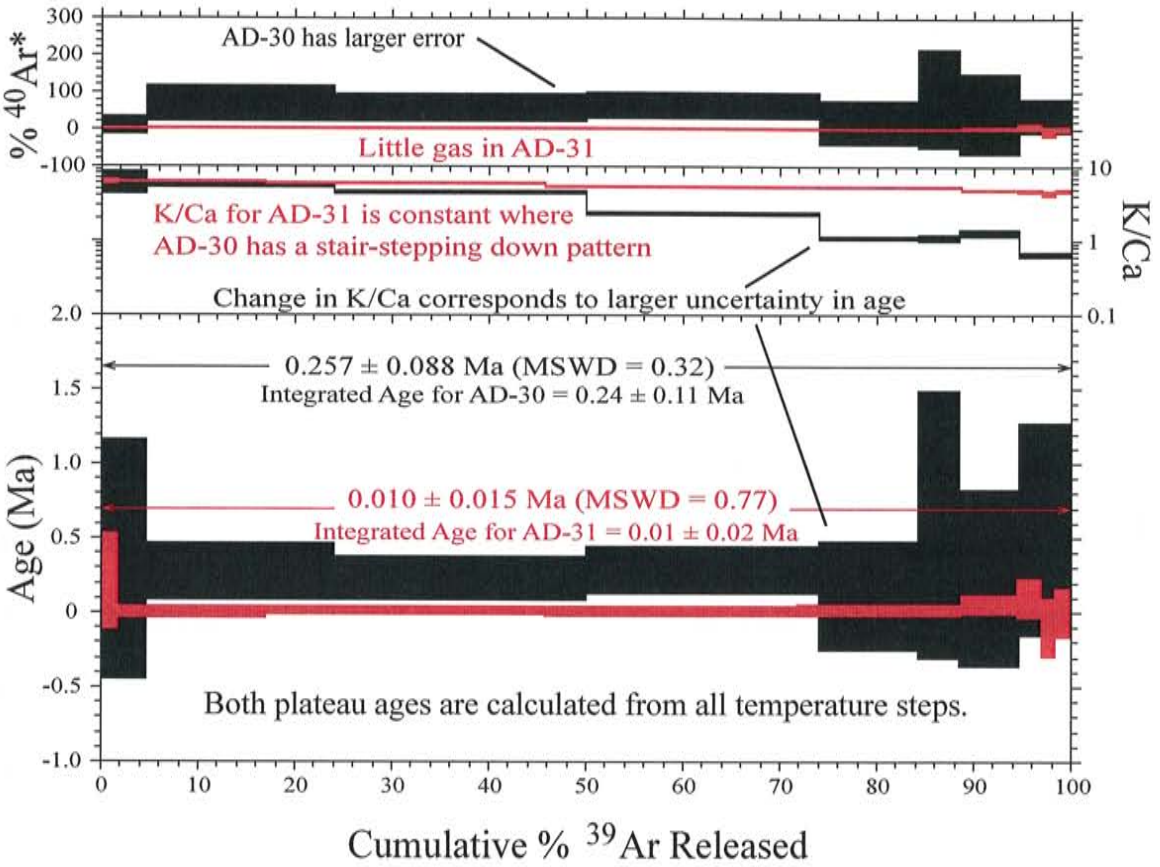

Figure 5.12. Laser step-heated spectra from two post-0.5 Ma units associated with the Valles caldera dated in this study. Obsidian sample AD-30 (in black) is from the El Cajete member, and obsidian sample AD-31 (shown in red) is from the Battleship Rock ignimbrite.

anomalously young. The plateau age of El Cajete sample AD-30 (0.257± 0.088 Ma) is analytically reasonable because this low-precision date yielded a high % $^{40}Ar^*$ and the age at all temperature steps overlap at 2σ. A decrease in K/Ca during the latter steps of the analysis could be from low-K phenocrysts degassing at higher temperatures, thus decreasing the K/Ca but not the age or % $^{40}Ar^*$ yield of the sample. The large uncertainties for the entire analysis might be due to lesser amounts of low-K microphenocrysts degassing earlier on in the analysis. The age is also geologically reasonable because the age agrees with stratigraphy and is younger than 0.5 Ma. The Battleship Rock sample yielded the most startling age of all the analyses. Although the age of 0.010± 0.015 Ma is much younger than previously thought (Spell and Harrison, 1993; Reneau et al., 1996), the consistent K/Ca, % $^{40}Ar^*$, and age make the age appear analytically accurate. A low % $^{40}Ar^*$ yield would be expected for such a young eruption because not enough time has past to accumulate a significant amount of $^{40}Ar^*$. However, if this age were accurate it would mean that the Banco Bonito formation is younger than 0.025 Ma. A uniform loss of $^{40}Ar^*$ could explain why the Battleship Rock age is so young; this date is assumed inaccurate and is not used for determining the age this event. The other two samples dated, one from Banco Bonito and one from El Cajete, yielded ages older than 0.5 Ma, which violates the observed stratigraphy. These ages were not used for analysis because the ages are influenced by microxenocrystic material, even though grains were rigorously handpicked in attempt to assure the quality of the analyses.

5.4.2.3 Previous ages of the post-0.5 Ma volcanic units associated with the Valles caldera

The permissible age from an El Cajete bread crust bomb presented in this study agrees with the stratigraphy for the youngest units of the Valles caldera, although numerous studies have published a wide range of ages (0.0-0.5 Ma) for the units (Table 5.2). Ages for the post-0.5 Ma volcanic units have been obtained using many different techniques including Ar-Ar (Spell and Harrison, 1993, Self et al., 1991), K-Ar (Goff et al., 1989), electron spin resonance (E.S.R.) (Toyoda et al., 1995), thermoluminescence (T.L.) (Reneau et al., 1996), fission track (Miyachi et al., 1985, Marvin and Dobson, 1979), radiocarbon (Reneau et al., 1996), and stratigraphic relations from the VC-1 core (Goff et al., 1986). Previous ages for the El Cajete member range from 0.05± 0.02 Ma to 0.57± 0.13 Ma; the three K-based ages form a population at 0.4± 0.2 Ma, where the radiocarbon, E.S.R., and T.L. dating methods form a tightly grouped population at 0.054± 0.011 Ma. Ages for the Battleship Rock ignimbrite range from 0.010± 0.015 Ma to 0.278± 0.104 Ma, the oldest age for Battleship Rock is from K-Ar dating. Previous studies have yielded ages for the Banco Bonito lava around 0.30± 0.18 Ma (Spell and Harrison, 1993; Self et al., 1991; Miyachi et al., 1985; Marvin and Dobson, 1969), forming two age populations at 0.16± 0.09 Ma (non-K-based dating methods) and 0.43± 0.17 Ma (K-based dating methods). The ages for Banco Bonito from Spell and Harrison (1993) form two distinct age populations, and are represented as two age populations instead of one. Fission track ages were not used to calculate any of these ages because they are repeatedly older than 0.5 Ma; incomplete annealing of fission tracks was suggested as a reason for these consistently inaccurate ages (Reneau et al., 1996).

Table 5.2. Table showing previous ages for Banco Bonito, Battleship Rock, and El Cajete units. All ages are presented at 2σ uncertainty.

Author	Dating method	Unit	Age (Ma)	Error (2σ)
Spell and Harrison (1993)	Ar-Ar	Banco Bonito	0.23	0.09
Spell and Harrison (1993)	Ar-Ar	Banco Bonito	0.43	0.05
This study	Ar-Ar	Banco Bonito	1.19	0.03
Self, et al. (1991)	Ar-Ar	Banco Bonito	0.42	0.06
Miyachi, et al. (1985)	Fission track	Banco Bonito	0.14	0.05
Marvin and Dobson (1979)	Fission track	Banco Bonito	0.13	0.1
This study	Ar-Ar	Battleship Rock	0.01	0.015
Goff, et al. (1989)	K-Ar	Battleship Rock	0.278	0.104
Miyachi, et al. (1985)	Fission track	Battleship Rock	0.14	0.05
Toyoda, et al. (1995)	E.S.R.	Battleship Rock	0.059	0.012
Spell and Harrison (1993)	Ar-Ar	El Cajete	0.57	0.13
This study	Ar-Ar	El Cajete	0.257	0.088
Self, et al. (1991)	Ar-Ar	El Cajete	0.57	0.13
Toyoda, et al. (1995)	E.S.R.	El Cajete	0.052	0.01
Miyachi, et al. (1985)	Fission track	El Cajete	0.17	0.08
Reneau, et al. (1996)	T.L.	El Cajete	0.054	0.006
Reneau, et al. (1996)	Radiocarbon	El Cajete	0.05	0.02

5.4.2.4 Four different scenarios for ages of the post-0.5 Ma volcanic units

Six different dating methods have been applied to the post-0.5 Ma volcanic units associated with the Valles caldera resulting in a spread of ages for these units. Assuming that the three units were formed concurrently, based on field relationships and chemical, petrological and isotopic similarities amongst the three units (Spell and Harrison, 1993), all three units should have a similar age. There are two possibilities, with four different scenarios for interpreting the accuracy of the ages of these units: 1) non-K-based dating methods (T.L., E.S.R., fission track, and radiocarbon) provide accurate ages, or 2) K-based methods (Ar-Ar and K-Ar) are accurate ages.

If the four non-K-based dates provide accurate ages, it suggests that the post-0.5 Ma units are quite young. Using T.L., E.S.R., fission track, and radiocarbon ages, the age of El Cajete is 0.054± 0.011 Ma, Battleship Rock is 0.06± 0.04 Ma, and Banco Bonito needs to be dated. These ages are consistent with the established stratigraphy for these units. Ages from radiocarbon dating may be questionable because these ages are at the upper limit of resolution for this method. T.L. and E.S.R. are fairly new dating methods, which have the potential to have unrecognized flaws in the methods.

There are three scenarios for event ages using K-based dating mechanisms, and one scenario from non-K-based dating (Figure 5.13). The first scenario is that all three units erupted at relatively the same time, with El Cajete forming at 0.57± 0.09 Ma, no age from Battleship Rock, and Banco Bonito erupting at 0.43±0.04 Ma. These two ages are temporally distinct at 2σ, but xenocrystic contamination could be causing older apparent ages for this scenario, as seen by two samples yielding xenocrystic ages from the current study. The second scenario is that all three units erupted at 0.25± 0.06 Ma. All three

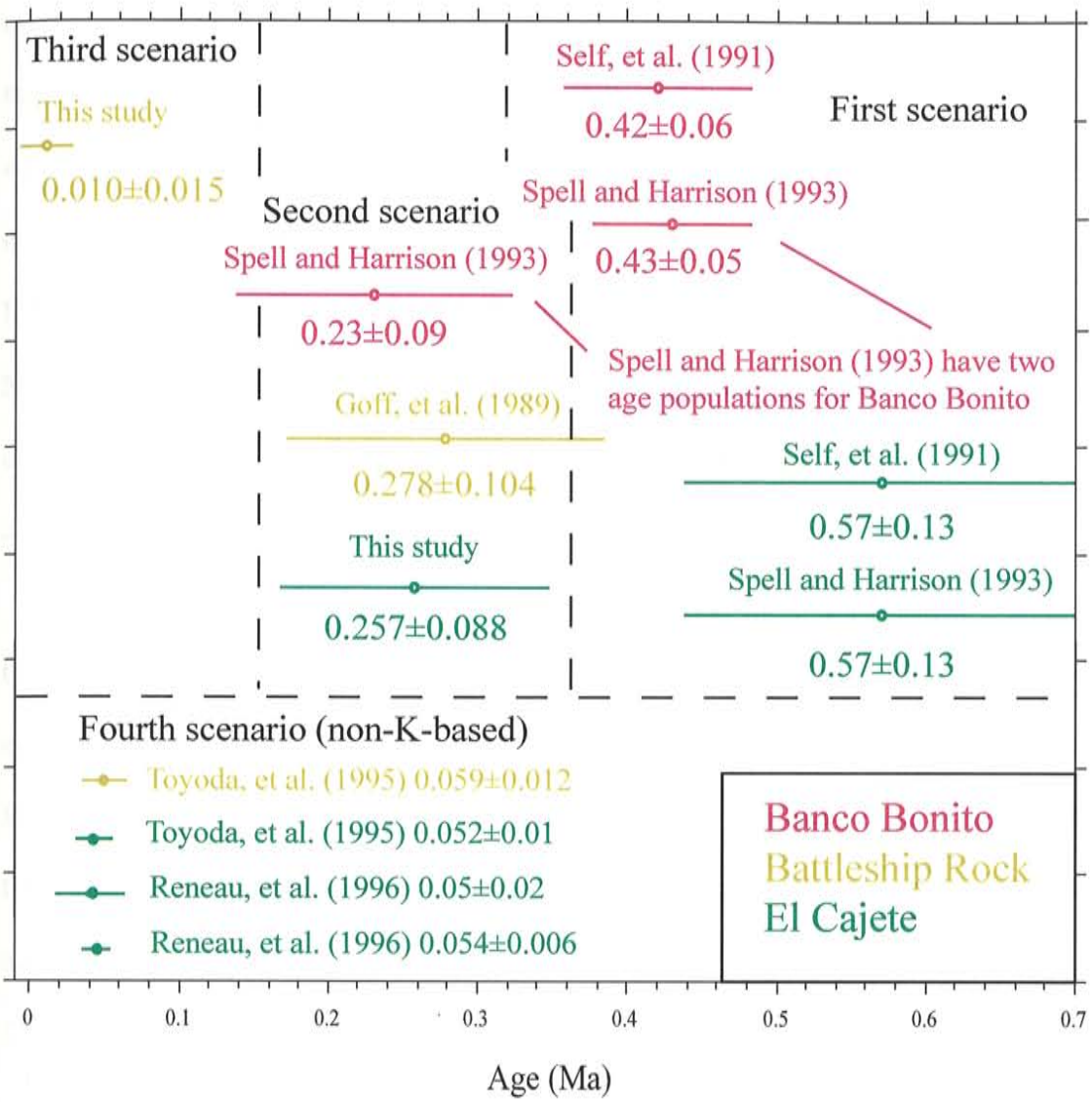

Figure 5.13. Figure shows four different scenarios for eruptive timings of the post-0.5 Ma volcanic eruptions associated with the Valles caldera. The first scenario could be affected by xenocrysts, resulting in an old apparent age. The second scenario is preferred, based on dates from the current and previous studies, and is considered to be the most accurate age for these eruptions at this time. The third scenario is based from one sample age of the current study which is believed to have experienced argon loss; this age is also the youngest age from all of the dating methods used and is not preferred as well. The fourth scenario is from non-K-based dating methods and could be accurate if the ages from K-based methods are influenced by xenocrysts.

units in this scenario overlap in age and agree with stratigraphy. The third possibility is that the 0.010± 0.015 Ma age for the Battleship Rock from the current study is correct, which would mean that all three units are younger than the ages from the non-K-based methods; this theory is not preferred. The fourth age scenario is based on ages from E.S.R., T.L., and radiocarbon, forming a tightly grouped age population at 0.054± 0.011 Ma. This age could be accurate if all K-based ages are affected by xenocryst contamination.

5.4.2.5 Ages from the current study revisited

In light of ages from previous studies, it appears that El Cajete sample AD-30 is the only age from the current study that is geologically reasonable. Two samples yielded ages that were older or concurrent with the initial eruptive activity of the Valles caldera. Battleship Rock sample AD-31 yielded a very young and improbable age, which results from a slight but uniform loss of $^{40}Ar^*$ to yield a highly precise, but inaccurate plateau age of 0.010± 0.015 Ma.

5.4.2.6 Conclusions

Four different geologically meaningful age scenarios are presented using ages from six different dating methods. The youngest scenario is from non-K-based dating methods producing a tight age population for the three units at 0.054± 0.005 Ma. The two older scenarios, from K-based dating methods, produced two different age populations for the events dated at 0.25± 0.06 Ma and at 0.45± 0.07 Ma. A problem with xenocryst contamination may exist for the Ar-Ar ages presented in this study, although numerous problems exist for the multiple non-K-based dating methods as well. Considering that Spell and Harrison (1993) obtained two age populations for the Banco

Bonito lava the issue of xenocryst contamination may be more of a problem for the oldest K-based age scenario, but this does not mean that the youngest K-based scenario is free from xenocryst contamination. The result of one geologically reasonable sample from this study suggest that the ages for the post-0.5 Ma eruptions associated with the Valles are no older than 0.25± 0.06 Ma, and if xenocryst contamination is affecting this sample then the non-K-based age of 0.054± 0.005 Ma may be more appropriate.

Chapter 6: Discussion

There are many factors involved in obtaining an accurate and precise age from volcanic glass using the Ar-Ar method. The type and characteristics of the glass used is important to minimize hydration effects. After choosing the correct type of glass, the precision in age can be enhanced by the preparation and extraction methods used. Although hydration does not always promote element mobility, breaking off hydration rinds with proper preparation techniques can increase the chances of obtaining precise and accurate ages from obsidian using the Ar-Ar method.

6.1 Type of glass

The type of glass chosen for Ar-Ar analysis is very important. Volcanic glass can take the form of obsidian, matrix glass, glass shards, pumice, or melt inclusions. Ideally, non-vesicular obsidian should be used as a dating material because it typically has a small surface to volume ratio. Obsidian can be prepared to remove hydration rinds while leaving behind enough unaltered obsidian to be dated. Xenocryst contamination can affect an obsidian age, so obsidian must be chosen that is crystal-poor.

6.2 Effects of hydration

Obsidian hydration can affect obsidian grains by causing K mobility, argon loss, and the incorporation of atmospheric argon into the hydration rinds. Any of these factors can affect the precision and accuracy of an apparent age from obsidian. Care must be taken to use obsidian that does not have a high surface to volume ratio to minimize the effects of hydration. The rate at which obsidian hydrates will increase with higher surface

areas, such as with cracks and vesiculation. There is no way of knowing whether hydration rinds will affect Ar-Ar ages prior to dating, therefore it is recommended that hydration rinds be removed prior to dating. Certain preparation techniques can mitigate the effects of argon loss, argon absorption, and element mobility by breaking off hydration rinds while leaving behind pristine obsidian to be dated. However, if K and Ar are not severely affected by hydration and the formation of rinds, then the presence of a hydration rind may not cause a significant change in age.

6.3 Preparation methods

In order to alleviate the problems associated with hydration rinds, the rinds need to be removed from the surfaces of obsidian grains. Pristine, unaltered glass is the only product remaining once the hydration rinds are removed. Certain preparation methods work better than others when preparing obsidian for Ar-Ar analysis. The HF, air abrasion, and long ultrasonic preparation methods all remove hydration rinds, but air abrasion or long ultrasonic preparation work the best because they do not cause adsorption of atmospheric ^{40}Ar. The air abrasion method was shown to work, but it was not pursued because the long ultrasonic preparation method was faster and easier. A short ultrasonic bath in water does not effectively remove hydration rinds from grains, and the problems associated with the rinds are not mitigated. The HF preparation treatment is not advised because the method causes absorption of atmospheric argon during preparation, which can increase the uncertainty and lower the apparent $^{40}Ar^*$ yield. After the initial preparation method experiment, the long ultrasonic preparation method was used for nearly all Ar-Ar obsidian analyses.

6.4 Extraction methods

The extraction method can affect the accuracy and precision of an apparent obsidian age. The four extraction methods used in this experiment include 1) laser fusion, 2) a two-step laser extraction, 3) multi-step laser incremental heating extraction, and 4) a multi-step furnace incremental heating extraction. Laser fusion was abandoned early because radiogenic and atmospheric ^{40}Ar components cannot be separated from each other, thus increasing uncertainties in an analysis. A two-step laser-heating extraction method was used to overcome this obstacle for obsidian analyses. The initial step was to drive off the atmospheric ^{40}Ar from the grain and the second step was to fuse the grain and drive off the radiogenic ^{40}Ar. Although this extraction method did not always split the gas between radiogenic and atmospheric components, the results were better than the fusion of grains. A two-step extraction method can obtain precise and accurate results when an obsidian sample is free of phenocrysts and has a simple geologic history, such as when the obsidian has only been subjected to atmospheric conditions since deposition. A multi-step laser or furnace incremental heating extraction method was used for young samples to better determine the degassing pattern of a sample and minimize uncertainty. A step-heated extraction by either the laser or furnace can be used to detect Ar loss or the degassing of xenocrysts, which can improve the accuracy and precision of Ar-Ar ages. Obsidian can have problems such as argon loss or absorption of atmospheric argon due to hydration and alteration, or contain microphenocrysts that degas at high temperatures. Age spectra allow resolution of these problems that might otherwise go unnoticed in laser fusion or a two-step laser extraction. A multiple-step extraction method will yield more information about the degassing pattern of obsidian

and in many cases can yield ages with higher precision and accuracy than the other heating methods discussed. However, a multiple-step extraction has higher costs and takes more time.

6.5 No Agua Peaks volcanic complex

The No Agua Peaks complex was used as a field area because of its varying degrees of hydrated obsidian and the presence of sanidine within some samples. Initially, sanidine-bearing obsidian units were to be dated to get an accurate feldspar age and then determine how, or if, an obsidian age differed from the feldspar age. Unfortunately this did not work well because the sanidine was either xenocrystic, the analyzed mineral was plagioclase feldspar, or that the obsidian ages were more precise than the feldspar ages. The precise and accurate obsidian data from this study record two distinct eruptive events at the No Agua Peaks complex; the ages are more precise and accurate than previous ages, and also agree with stratigraphy and field observations. The two ages of 3.86± 0.06 Ma and 4.07± 0.03 Ma are distinct at 2σ. The eruptive hiatus of 0.21±0.09 Ma between the two eruptions at No Agua Peaks provided enough time for a change in magma chemistry to occur, and for a soil horizon to form on the North Hills flow before the second eruption. This meter-thick paleosol is important because it takes thousands of years to develop soils in the arid deserts of the American southwest (Brady and Weil, 2002). The obsidian ages presented in this study are more precise and accurate than previous ages published for this volcanic complex, and demonstrate the potential for obsidian to be a robust dating material for the Ar-Ar method.

6.6 Cerro del Medio ring dome

The Cerro del Medio ring dome ages constrain the timing of resurgence for the Valles caldera. Field evidence supports the model that Cerro del Medio was the first ring dome to form after the initial resurgent dome, Redondo Peak, and that both events are temporally distinct. In the field there are six different mapped lobes for the dome (Gardner et al., 2006), but there is not enough difference in geochemical composition amongst the lobes to distinguish events by chemistry. Multiple ages have previously been obtained for the six different lobes of the Cerro del Medio ring dome using the K-Ar and Ar-Ar methods (Gardner et al., 2006; Phillips, 2004; Izett and Obradovich, 1994, Spell and Harrison, 1993, Doell, 1968). Using ages from the current and previous studies it is shown that there are two scenarios for one lobe-forming time period at 1.18± 0.06 Ma, with up to three distinguishable pulses at the Cerro del Medio ring dome. The ages determined for the three events in this study (1.14± 0.02 Ma, 1.18± 0.03 Ma, and 1.22± 0.02 Ma) overlap in part within uncertainty at 2σ. In the first scenario, the oldest age for the Cerro del Medio dome, 1.22± 0.02 Ma, constrains the timing of resurgence for Redondo Peak within 0.04± 0.03 Ma after the initial caldera forming eruption of the Upper Bandolier Tuff at 1.26±0.01 Ma (Phillips, 2004). The second scenario addresses the possibility that the 1.22± 0.02 Ma age for the DM-S and DM-W lobes are influenced by xenocryst contamination and that the 1.18± 0.03 Ma age is the accurate age for the start of Cerro del Medio. In this scenario resurgence lasted for 0.08± 0.04 Ma.

6.7 Post-0.5 Ma volcanic units associated with the Valles caldera

The post-0.5 Ma volcanic units associated with the Valles caldera have been dated by numerous dating methods, which have produced a wide range of results. The El

Cajete pumice, Battleship Rock ignimbrite and Banco Bonito lava were all dated in this study to determine ages of the last eruptive stages associated with the Valles caldera. All three of these units are believed to have erupted concurrently because of chemical, petrological and isotopic similarities amongst the units (Spell and Harrison, 1993). In the current study one sample yielded a geologically reasonable sample age for the El Cajete pumice; the other sample from the El Cajete member, the sample of the Battleship Rock ignimbrite, and the Banco Bonito lava sample were all unsuccessfully dated. Two samples yielded anomalously old ages (1.62± 0.06 and 1.19± 0.03 Ma, respectively), apparently due to microxenocrysts that were imbedded in the obsidian, as seen in BSE images of the samples. The young, and assumed inaccurate, age of 0.010± 0.015 Ma for the Battleship Rock ignimbrite is best explained by argon loss that occurred uniformly to the obsidian grains. Numerous different dating methods in previous studies have been used to date these post-0.5 Ma volcanic units including K-Ar, Ar-Ar, thermoluminescence, fission track, radiocarbon, and electron spin resonance (Reneau et al., 1996; Spell and Harrison, 1993; Self et al., 1991; Miyachi et al., 1985; Marvin and Dobson, 1969). Comparing all previous ages provides insight for the ages of these units. It appears that the K-based dating methods all yield the oldest ages for the post-0.5 Ma units, with some ages being anomalously old. Fission track dating yields the oldest ages for all the units dated by this method, which could be a result from incomplete annealing (Reneau et al., 1996). In this study it is concluded that the ages for the post-0.5 Ma eruptions associated with the Valles are no older than 0.25± 0.06 Ma (including the 0.257± 0.88 Ma age from this study), and that the older apparent Ar-Ar ages are influenced by xenocryst contamination. If xenocryst contamination is also affecting the

~0.25 Ma Ar-Ar ages, then the age of 0.054± 0.005 Ma, based of T.L., E.S.R., and radiocarbon dating, may be more accurate for the three events. These age scenarios imply that volcanism associated with the Valles caldera has occurred within the last 0.25± 0.06 Ma and there is no evidence to suggest that the volcano is anything but dormant.

Chapter 7: Conclusions

There are many factors that can affect the quality Ar-Ar ages of obsidian. The three main factors affecting an age are geological conditions, sample preparation, and the extraction method used. Accurate obsidian age data can be used to determine volcanic history, including rates of resurgence, volcanic hazards and associated problems. The conclusions from this study are:

1) Nonvesicular, phenocryst-free obsidian glass can be an accurate and precise material for Ar-Ar dating because it has a small surface to volume ratio. The glass should not be in the form of matrix glass, melt inclusions, or glass shards. Glass that has been completely hydrated, or perlite, should not be dated.

2) Hydration rinds should be removed for obsidian grains to be dated accurately, even though hydration does not necessarily cause element mobility. Air abrasion and a 24-hour ultrasonic preparation treatment both remove hydration rinds without incorporating atmospheric argon into the sample or decreasing the $^{40}Ar^*$ yield. Brief ultrasonic cleaning does not remove the hydration rind, and hydrofluoric acid causes atmospheric argon to be absorbed into the sample, thereby decreasing the radiogenic yield.

3) Laser or furnace step-heating of multiple grains is more accurate than single-grain laser fusion because laser fusion does not separate atmospheric from radiogenic argon. There is little difference in the yielded age or the behavior of gas between the furnace and laser extraction methods. A multiple-step extraction method can image contaminating

phases and argon loss or absorption when dating obsidian, and will yield an age more accurate and precise than an integrated or fusion age.

4) High-precision, accurate dates obtained from obsidian analysis distinguish two eruptive events at the No Agua Peaks complex, dated at 3.86± 0.06 Ma (MSWD= 1.78) and 4.07± 0.03 Ma (MSWD= 0.17). These eruptive events have chemically distinctive immobile element signatures and there is a meter-thick paleosol that formed after the first eruption, stratigraphically separating the two events in the field. The No Agua peaks volcanic complex is geologically important because it is the only high-silica volcano in the Taos Plateau volcanic field and it is mined extensively for its voluminous perlite deposits.

5) There are two different scenarios for the ages of Cerro del Medio ring dome; ages for the Cerro del Medio dome from this study are consistent with ages from other studies (Doell et al., 1968; Spell and Harrison, 1993; Izett and Obradovich, 1994). The age of Cerro del Medio is important because the age constrains the timing of resurgence for the resurgent dome, Redondo Peak. The three low-resolution ages used in this study (1.14± 0.02 Ma, 1.18± 0.03 Ma, and 1.22± 0.02 Ma) could potentially reflect only one eruptive period, especially the youngest two lobe forming events. In the first scenario the first lobe of Cerro del Medio dome formed at 1.22± 0.02 Ma and the entire dome had a duration of 0.08± 0.04 Ma. The second scenario addresses the possibility that the oldest age for the Cerro del Medio dome has been influenced by xenocrystic material. If this is true then Cerro del Medio began lobe forming at 1.18± 0.03 Ma and the lifespan of the dome was 0.05± 0.04 Ma. In the first scenario resurgence was completed within 0.04±

0.03 Ma after the eruption of the Bandelier Tuff; the second scenario implies the duration of resurgence is 0.08± 0.04 Ma.

6) Of the four samples from the post-0.5 Ma volcanic units associated with the Valles caldera dated in this study, only one sample yielded a geologically reasonable age: the El Cajete pumice age of 0.257± 0.088 Ma; all other samples displayed ages that were either influenced by xenocrysts or had suffered argon loss. The three units, from stratigraphically youngest to oldest, are the Banco Bonito lava, Battleship Rock ignimbrite, and El Cajete pumice; these units represent the youngest activity associated with the Valles caldera and aid in determining the volcanological hazards of the volcano. The El Cajete age from this study forms a population of ages with other ages from K-Ar and Ar-Ar dating studies at 0.25± 0.06 Ma, which is the preferred eruption age for the three units. An older population from K-based dating methods is considered to reflect ages of xenocrystic material, but there is a possibility that all Ar-Ar ages have been influenced by xenocrystic material. If the age of 0.25± 0.06 Ma reflects xenocryst contamination as well, then the 0.054± 0.005 Ma age for the three units, derived from radiocarbon, E.S.R., and T.L., could be more accurate. The age for Battleship Rock of 0.010± 0.015 Ma from this study is assumed to have lost $^{40}Ar^*$, yielding a precise but inaccurate age. Ages from the current and previous studies suggest that the Valles caldera is currently dormant and could erupt again.

REFERENCES CITED

Aldrich, M.J., Laughlin, A.W., 1984, A model for the tectonic development of the southeastern Colorado Plateau boundary: J. Geophys. Res., v. 89, p. 10,207-10,218.

Anovitz, L.M., Riciputi, L.R., Cole, D.R., Fayek, M., Elam, J.M., 2006, Obsidian hydration: a new paleothermometer: Geology, v. 34, p. 517-520.

Applet, R.M., 1998, 40Ar/39Ar geochronology and volcanic evolution of the Taos Volcanic Field, northern New Mexico and southern Colorado: Master's Thesis.

Bailey, R.A., Smith, R.L., Ross, C.S., 1969, Stratigraphic nomenclature of volcanic rocks in the Jemez Mountains, New Mexico: U.S. Geol. Surv Bulletin, v. 1274-P, p. 1-19.

Brady, N.C., Weil, R.R., 2002, The Nature and Properties of Soils: Upper Saddle River, N.J., Prentice Hall.

Cerling, T.E., Brown, F.H., and Bowman, J.R., 1985, Low-temperature alteration of glass: hydration, Na, K, 18O and Ar mobility: Chemical Geology, v. 52, p. 281-293.

Chamberlin, R.M., and Baker, J.M., 1996, Genetic aspects of commercial perlite deposits in New Mexico: New Mexico Bureau of Mines and Min. Resources Bulletin, v. 154, p. 171-185.

Cordell, L., 1978, Regional geophysical setting for the Rio Grande rift: Geol. Soc. Am. Bull., v. 89, p. 1073-1090.

Dalrymple, G.B. and Lanphere, M.A., 1974, 40Ar/39Ar age spectra of some undisturbed terrestrial samples: Geochim. Cosmochim. Acta, v. 38, p. 715-738.

Deino, A., Tauxe, L., Monaghan, M., and Drake, R., 1990, 40Ar/39Ar age calibration of the litho- and paleomagnetic stratigraphies of the Ngorora Formation, Kenya: Journal of Geology, v. 98, p. 567-587.

Doell, R.R., Dalrymple, G.B., Smith, R.L., and Bailey, R.A., 1968, Paleomagnetism, potassium-argon ages, and geology of the rhyolites and associated rocks of the Valles caldera, New Mexico: Geol. Soc. Am. Memoir, v. 116, p. 211-248.

Esser, R.P., Kyle, P.R., McIntosh, W.C., and Heizler, M.T., 1997, Excess argon in melt

inclusions in zero-age anorthoclase feldspar from Mt. Erebus, Antarctica, as revealed by the 40Ar/39Ar method: Geochimica et Cosmochimica Acta, v. 61, p. 3789-3801.

Fiore, S., Huertas, F.J., Tazaki, K., Huertas, F., and Linares, J., 1999, A low temperature experimental alteration of a rhyolitic obsidian: Eur. J. Mineral., v. 11, p. 455-469.

Fleck, R.J., Sutter, J.F., Elliot, D.H., 1977, Interpretation of discordant 40Ar/39Ar age-spectra of Mesozoic tholeiites from Antarctica: Geochim. Cosmochim. Acta, v. 41, p. 15-32.

Foland, K.A., Gilbert, L.A., Sebring, C.A., Chen, J.F., 1986, 40Ar/39Ar ages for plutons of the Monteregian Hills, Quebec: evidence for a single episode of Cretaceous magmatism: Geol. Soc. Am. Bull., v. 97, p. 966-974.

Freidman, I., and Long, W., 1976, Hydration rate of obsidian: Science, v. 191, p. 347-352.

Friedman, I., Smith, R.L., Long, W.D., 1966, Hydration of natural glass and formation of perlite: Geological Society of America Bulletin, v. 77, p. 323-328.

Gardner, J.N., and Goff, F., 1984, Potassium-argon dates from the Jemez volcanic field: Implications for tectonic activity in the north-central Rio Grande Rift: NMGS Guidebook, v. 35, p. 173-190.

Gardner, J.N., Goff, F., Garcia, S., Hagan, R.C., 1986, Stratigraphic relations and lithologic variations in the Jemez Volcanic Field, New Mexico: J. Geophys. Res., v. 91, p. 1763-1778.

Gardner, J.N., Goff, F., Reneau, S.L., Sandoval, M.M., Drakos, P.G., Katzman, D., Goff, C.J., 2006, Preliminary geologic map of the Valle Toledo quadrangle, Los Alamos and Sandoval Counties, New Mexico, New Mexico Bureau of Geology and Mineral Resources open-file geologic map series.

Goff, F., Gardner, J., Woldegabriel, G., Geissman, J.W., Hulen, J.B., Sasada, M., Shevenell, L., Sturchio, N.C., and Trainer, F.W., 1989, Dating of hydrothermal events in active geothermal systems; example from the Valles Caldera, New Mexico, USA, General assembly of the International Association of Volcanology and Chemistry of the Earth's Interior: Santa Fe, NM, June 25-July 1.

Goff, F., Rowley, J., Gardner, J.N., Hawkins, W., Goff, S., Charles, R., Wachs, D., Maassen, L., Heiken, G., 1986, Initial results from VC-1, first continental scientific drilling program core hole in Valles caldera, New Mexico: Journal of Geophysical Research, v. 91, p. 1742-1752.

Heizler, M.T., and Harrison, T.M., 1988, Multiple trapped argon isotope components revealed by 40Ar/39Ar isochron analysis: Geochimica et Cosmochimica Acta, v. 52, p. 1295-1303.

Housman, M., unpublished data. No Agua Peaks stratigraphy, World Minerals.

Izett, G.A. and Obradovich, J.D., 1994, 40Ar/39Ar age constraints for the Jaramillo Normal Subchron and the Matuyama-Brunhes geomagnetic boundary: Journal of Geophysical Research, v. 99, p. 2925-2934.

Jezek, P.A., and Noble, D.C., 1978, Natural hydration and ion exchange of obsidian: an electron microprobe study: American Mineralogist, v. 63, p. 266-273.

Lanphere, M.A., 2000, Comparison of conventional K-Ar and 40Ar/39Ar dating of young mafic volcanic rocks: Quaternary Research, v. 53, p. 294-301.

Lanphere, M.A., and Dalrymple, G.B., 1978, The use of 40Ar/39Ar data in evaluation of disturbed K-Ar systems: U.S. Geol. Surv Open-file Report 78-701, p. 241-243.

Lipman, P.W., Mehnert, H.H., 1979, The Taos Plateau volcanic field, northern Rio Grande rift, New Mexico: Washington, D.C., AGU, 289-311 p.

Marvin, R.F., and Dobson, S. W., 1979, Radiometric ages: Compilation B: U.S. Geol. Surv: Isochron/West, v. 26, p. 25.

McDougall, I., and Harrison, T.M., 1999, Geochronology and thermochronology by the 40Ar/39Ar method: New York, Oxford University Press, p. 269.

Miyachi, M., Izett, G. A., Naeser, C. W., Naeser, N. D., Andreissen, P. A. M., 1985, Zircon fission-track ages on some volcanic rocks and pryoclastic flow deposits of the Jemez Mountains, New Mexico: Volcanological Society of Japan Bulletin, v. 30, p. 90.

Mungall, J.E., and Martin, R.F., 1994, Severe leaching of trachytic glass without devitrification, Terceira, Azores: Geochem. Cosmochim. Acta, v. 52, p. 1295-1303.

Petit, J.-C., Della Mea, G., Dran, J.-C., Magonthier, M.-C., Mando, P.A., and Paccagnella, A., 1990, Hydrated-layer formation during dissolution of complex silicate glasses and minerals: Geochem. Cosmochim. Acta, v. 54, p. 1941-1955.

Phillips, E., 2004, Collapse and resurgence of the Valles caldera, Jemez mountains, NM:40Ar/39Ar age constraints on the timing and duration of resurgence and ages of megabreccia blocks: Master's Thesis, p. p. 200.

Phillips, E., Goff, F., Kyle, P.R., McIntosh, W.C., Dunbar, N.W., and Gardner, J.N., 2007, The 40Ar/39Ar age constraints on the duration of resurgence at the Valles caldera, New Mexico: *J. Geophys. Res.*, In press.

Reneau, S.L., Gardner, J.N., and Forman, S.L., 1996, New evidence for the age of the youngest eruptions in the Valles Caldera, New Mexico: Geology, v. 24, p. 7-10.

Renne, P.R., Owens, T.L., DePaolo, D.J., Swisher, C.C., Deino, A.L., and Karner, D.B., 1998, Intercalibration of standards, absolute ages and uncertainties in 40 Ar/39Ar dating: Chemical Geology, v. 145, p. 117-152.

Seager, W.R., Shafiqullah, M., Hawley, J.W., Marvin, R.F., 1984, New K-Ar dates from basalts and the evolution of the southern Rio Grande rift: Geol. Soc. Am. Bull., v. 95, p. 87-99.

Self, S., Goff, F., Gardner, J.N., Wright, J.V., and Kite, W.M., 1986, Explosive rhyolitic volcanism in the Jemez Mountains: vent locations, caldera development, and relation to regional structure: J. Geophys. Res., v. 91, p. 1779-1798.

Self, S., Wolff, J.A., Spell, T.L., Skuba, C.E., and Morrissey, M.M., 1991, Revisions to the stratigraphy and volcanology of the Post-0.5 Ma units and the volcanic section of VC-1 core hole, Valles caldera, New Mexico: J. Geophys. Res., v. 96(B3), p. 4107-4116.

Singer, B.S., Ackert Jr., R.P., and Guillou, H., 2004, 40Ar/39 Ar and K-Ar chronology of Pleistocene glaciations in Patagonia: Bulletin of the Geological Society of America, v. 116, no. 3-4, p. 434-450.

Smith, G.A., Moore, J.D., McIntosh, W.C., 2002, Assessing roles of volcanism and basin subsidence in causing Oligocene- Lower Miocene sedimentation in the northern Rio Grande rift, New Mexico, U.S.A.: Journal of Sedimentary Research, v. 72, p. 836-848.

Snee, L.W., Sutter, J.F., Kelly, W.C., 1988, Thermochronology of economic mineral deposits: dating the stages of mineralization at Panaqueira, Portugal, by high-precision 40Ar/39Ar age spectrum techniques on muscovite: Econ. Geol., v. 83, p. 335-354.

Spell, T.L., and Harrison, T. M., 1993, 40Ar/39Ar geochronology of post-Valles caldera rhyolites, Jemez volcanic field, New Mexico: Journal of Geophysical Research, v. 98, p. 8031-8051.

Taylor, J.R., 1982, An Introduction to Error Analysis: The Study of Uncertainties in Physical Measurements: Mill Valley, CA, Univ. Sci. Books, p. 270 p.

Thompson, R.A., McMillan, N.J., 1992, A geologic overview and one-day field guide of the Taos Plateau volcanic field, Taos County, NM: U.S. Geol. Surv. Open-file Report 92-528.

Toyoda, S., Goff, F., Ikeda, S., and Ikeya, M., 1995, ESR dating of quartz phenocrysts in the El Cajete and Battleship Rock members of Valles rhyolite, Valles caldera, New Mexico: J. Volc. Geotherm. Res., v. 67, p. 29-40.

Van Den Bogaard, P., and Schirnick, C., 1995, 40Ar/39Ar laser probe ages of Bishop tuff

quartz phenocrysts substantiate long-lived silicic magma chamber at Long Valley, United States: Geology, v. 23, p. 759-762.

Whitehead, N.E., Seward, D., and Veselsky, J., 1993, Mobility of trace elements and leeching rates of rhyolitic glass shards from some New Zealand tephra deposits: Applied Geochemistry, v. 8, p. 235-244.

Winick, J.A., McIntosh, W.C., and Dunbar, N.W., 2001, Melt-inclusion-hosted excess 40Ar in quartz crystals of the Bishop and Bandelier magma systems: Geology, v. 29, p. 275-278.

Yanagisawa, N., Fujimoto, K., Nakashima, S., Kurata, Y., and Sanada, N., 1997, Micro FT-IR study of the hydration-layer during dissolution of silica glass: Geochem. Cosmochim. Acta, v. 61, p. 1165-1170.

Zielinski, R.A., P.W., L., and Millard, H.T., Jr., 1977, Minor-element abundances in obsidian, perlite, and felsite of calc-alkalic rhyolites: American Mineralogist, v. 62, p. 426-437.

APPENDIX A: ADDITIONAL ANALYTICAL METHODS

A.1 Field geology

Multiple 7.5-minute topographic maps were used in the field. La Segita Peaks and Tres Piedras were used for the No Agua sample suite. Jamez Springs, Redondo Peak, Bland, and Valle Toledo were used for the Valles caldera samples. Sample locations were taken by GPS in the UTM coordinate system with the WGS84 datum (Table A.1). Large obsidian and sanidine-bearing samples were collected from fresh outcrops appearing to be the least weathered; perlite is weathered obsidian and therefore sampled weathered.

A.2 Electron microprobe preparation and analysis

A.2.1. Sample preparation

All samples were prepared and analyzed at the New Mexico Institute of Mining and Technology. Samples were placed in single, four, and nine hole grain mounts. Grain mounts were then covered in epoxy and baked at 80° C for approximately 12 hours to cure. Samples were polished with 163, 68 and 30 μm grinding wheels for 3 minutes per wheel and then hand polished for 3 to 6 minutes on 15, 6 and <1 μm polishing cloths with diamond powder. Grain mounts were cleaned with petroleum ether to remove foreign matter (i.e. fingerprints) and then carbon coated before analysis.

A.2.2. Sample analysis

Samples analysis was performed on a CAMECA SX-100 electron microprobe using high-speed backscattered electron detectors for BSE work and three wavelength

dispersive spectrometers for quantitative analysis. BSE was used to image grains, textures and hydration rinds. Quantitative analysis was performed to determine mean sample chemistry at multiple points. Electron microprobe precision is tabled in Appendix Table B.4.

A.3. Ar-Ar sample preparation methods

All preparation and extraction methods were performed at the New Mexico Institute of Mining and Technology. A hammer, prior to crushing, removed weathered rinds from raw samples. Samples were crushed by a jaw crusher and then run through a disk grinder for final sizing of the grains. Samples were sieved to appropriate sizes; an 800 μm sieve size was preferred although the 300 μm sieve size was used when abundant clean material was not available from the larger size.

All samples were separated into magnetic and non-magnetic fractions using a Franz magnetic separator. Non-magnetic fractions were used for all obsidian samples unless otherwise noted. Sanidine samples were ultrasonically washed in a 15% HF solution to remove contaminant grains and matrix glass prior to magnetic separation. All samples were ultrasonically rinsed using distilled water after magnetic separation to break off anything adhering to the side of a grain. Grains were isolated by density using lithium metatungstate. Samples were once again ultrasonically rinsed after density separation to remove heavy liquid adhering to the samples. The various preparation methods for obsidian splits were performed after the use of heavy liquids. After preparation, all grains were handpicked using an optical microscope to assure purity of the separate.

Table A.1: Sample locations of No Agua Peaks and Valles caldera samples

No Agua Sample	Zone	Easting	Northing	Collector
AD-01	13N	414420	4066720	Dickens
AD-02	13N	414882	4066485	Dickens
AD-03	13N	414954	4066392	Dickens
AD-04	13N	414818	4066749	Dickens
AD-05	13N	414359	4067338	Dickens
AD-06	13N	414434	4067227	Dickens
AD-07	13N	414588	4067074	Dickens
AD-08	13N	414512	4066235	Dickens
AD-09	13N	414512	4066235	Dickens
AD-10	13N	414512	4066235	Dickens
AD-11	13N	415941	4068015	Dickens
AD-12	13N	415094	4067768	Dickens
Valles Caldera				
Cerro del Medio				
AD-21	13N	366495	3975243	Dickens
AD-22obs	13N	366495	3975243	Dickens
AD-23obs	13N	369153	3976766	Dickens
AD-24obs	13N	369245	3975212	Dickens
AD-25san	13N	368952	3973949	Dickens
AD-26obs	13N	370389	3974858	Dickens
AD-27san	13N	369103	3977741	Dickens
AD-50obs	13N	367385	3972385	Spell
AD-51obs	13N	370985	3976775	Spell
AD-52obs	13N	368525	3976600	Spell
AD-53obs	13N	367100	3974450	Spell
AD-54san	13N	368450	3971650	Phillips
AD-55san	13N	369802	3970174	Phillips
Post-0.5 Ma volcanic units				
AD-20	13N	360124	3966520	Dickens
AD-28obs	13N	356106	3965864	Dickens
AD-29obs	13N	359201	3966078	Dickens
AD-30obs	13N	358863	3966204	Dickens
AD-31obs	13N	351850	3966270	Dickens

APPENDIX B.1: EXPLANATION OF APPENDIX B

Appendix B contains additional data concerning the electron microprobe. Table B.1 is a list of all samples examined by the electron microprobe according to the preparation method used for the sample. Included in this list is the type of material analyzed, as well as the beam size used during analysis. Table B.2 is all the analytical data from the quantitative analysis of variously prepared glass. This is broken down into three sections: No Agua Peaks obsidian samples, the Valles caldera obsidian samples, and transects performed on obsidian sample AD-10 are reported last. Table B.3 is the analytical data from the quantitative analysis of feldspar. Table B.4 shows the precision of standards, as well as their accepted values.

Appendix B. Table B.1. Sample preparation list of materials analyzed by electron microprobe.

Sample	Material	5US	24US	AA	5HF	Beam Size
AD-01	Obsidian	X	X			20, 25
AD-01	Quartz				x	20
AD-02	Obsidian	X	X	X	X	25
AD-03	Obsidian	X				20
AD-03	Plagioclase				x	20
AD-04	Perlite	X				25
AD-05	Perlite	X				25
AD-06	Obsidian	X	X			20, 25
AD-07	Perlite	X				20
AD-08	Obsidian	X				25
AD-09	Obsidian				x	25
AD-09	Sanidine	X				20
AD-10	Obsidian	X				25
AD-11	Obsidian	X	X			25
AD-12	Obsidian	X	X			20
AD-12	Sanidine				x	20
AD-20	Obsidian		X			25
AD-21	Obsidian		X			25
AD-22	Obsidian		X			25
AD-23	Obsidian		X			25
AD-24M	Obsidian		X			25
AD-24NM	Obsidian		X			25
AD-25	Anorthocite				x	25
AD-26	Obsidian	X	X			25
AD-27	Anorthocite				x	25
AD-28	Obsidian		X			25
AD-29	Obsidian					
AD-30	Obsidian		X			25
AD-31	Obsidian	X				25
AD-40	Obsidian		X			25
AD-41	Obsidian		X			25
AD-50	Obsidian				x	25
AD-51	Obsidian				x	25
AD-52	Obsidian				x	25
AD-53	Obsidian				x	25
AD-54	Sanidine				x	25
AD-55	Sanidine				x	25

Note: 5US, 24US, AA, and 24HF refer to the preparation methods of the five minute and 24 hour ultrasonic treatments in distilled water (US), hydroflouric acid (HF), and air abrasion (AA) techniques. M and NM refer to a magnetic and non-magnetic sample split, all samples without reference are from the non-magnetic fraction of a sample.

Table B.2: Electron Microprobe Analyses of glass

Sample Number	P2O5	SiO2	SO2	TiO2	Al2O3	MgO	CaO	MnO	FeO	Na2O	K2O	F	Cl	N. Total
No Agua Peaks obsidian data														
AD-01-5US-01	0.00	76.58	0.04	0.01	13.30	0.00	0.45	0.15	0.50	4.42	4.49	0.00	0.05	97.54
AD-01-5US-02	0.06	76.86	0.00	0.04	12.95	0.00	0.44	0.22	0.54	4.04	4.73	0.10	0.04	97.81
AD-01-5US-03	0.00	76.67	0.02	0.08	13.20	0.05	0.42	0.18	0.48	3.96	4.72	0.18	0.04	96.82
AD-01-5US-04	0.00	76.61	0.05	0.07	13.06	0.01	0.44	0.18	0.48	4.09	4.77	0.19	0.04	97.20
AD-01-5US-05	0.00	76.54	0.01	0.03	13.03	0.00	0.44	0.17	0.47	4.20	4.72	0.34	0.05	97.39
AD-01-5US-06	0.00	74.36	0.01	0.09	12.82	0.00	0.41	0.09	0.45	4.12	4.54	3.06	0.05	98.78
AD-01-5US-07	0.01	76.15	0.00	0.03	13.33	0.01	0.47	0.15	0.49	4.14	4.95	0.22	0.04	95.65
AD-01-5US-08	0.00	76.54	0.00	0.08	13.14	0.00	0.49	0.15	0.44	4.28	4.51	0.33	0.03	97.08
AD-01-5US-09	0.00	76.71	0.00	0.06	13.04	0.00	0.44	0.15	0.56	4.02	4.72	0.25	0.04	97.93
AD-01-5US-10	0.04	75.95	0.01	0.04	13.45	0.02	0.36	0.21	0.51	4.21	4.81	0.36	0.03	96.32
AD-01-5US-12	0.01	76.38	0.02	0.08	13.25	0.00	0.39	0.14	0.53	4.38	4.59	0.19	0.04	99.75
AD-01-5US-13	0.04	75.89	0.00	0.10	13.12	0.02	0.41	0.16	0.57	4.17	4.70	0.76	0.06	100.43
AD-01-5US-14	0.00	76.72	0.05	0.11	13.03	0.00	0.48	0.16	0.48	4.21	4.51	0.20	0.05	98.74
AD-01-5US-15	0.06	75.82	0.01	0.03	12.92	0.09	0.45	0.18	0.56	4.00	4.65	1.21	0.03	99.20
AD-01-5US-17	0.03	76.54	0.01	0.06	13.18	0.00	0.42	0.20	0.52	4.09	4.68	0.23	0.04	98.13
AD-01b-5US-01	0.00	75.90	0.01	0.08	13.04	0.92	0.43	0.13	0.52	4.06	4.69	0.14	0.07	100.38
AD-01b-5US-02	0.00	76.31	0.01	0.07	13.18	0.02	0.45	0.18	0.56	4.06	4.87	0.24	0.04	97.88
AD-01b-5US-03	0.00	76.72	0.01	0.10	13.04	0.00	0.42	0.14	0.47	4.23	4.60	0.25	0.04	97.15
AD-01b-5US-04	0.00	76.14	0.01	0.01	13.47	0.03	0.45	0.11	0.56	4.21	4.79	0.17	0.05	95.38
AD-01b-5US-05	0.04	75.35	0.02	0.05	13.11	0.73	0.51	0.18	0.56	3.81	5.15	0.44	0.03	90.98
AD-01b-5US-06	0.00	76.36	0.00	0.06	13.21	0.02	0.45	0.16	0.45	4.17	4.76	0.31	0.04	99.61
AD-01b-5US-07	0.00	76.27	0.01	0.11	13.19	0.00	0.43	0.15	0.54	4.14	4.81	0.30	0.04	99.64
AD-01b-5US-09	0.01	76.72	0.02	0.09	13.25	0.00	0.42	0.13	0.55	3.99	4.72	0.08	0.04	96.64
AD-01b-5US-10	0.00	76.56	0.04	0.08	13.06	0.00	0.44	0.18	0.55	4.18	4.71	0.14	0.05	99.38
AD-01b-5US-11	0.00	76.29	0.00	0.02	13.28	0.01	0.47	0.21	0.50	4.24	4.76	0.17	0.06	98.87
AD-01b-5US-12	0.00	76.71	0.00	0.06	12.95	0.04	0.46	0.14	0.53	4.22	4.68	0.18	0.04	97.67
AD-01b-5US-13	0.00	76.09	0.02	0.05	13.32	0.00	0.44	0.18	0.53	4.30	4.82	0.19	0.05	97.53
AD-01b-5US-14	0.01	76.72	0.02	0.06	13.15	0.04	0.40	0.11	0.47	4.14	4.78	0.05	0.05	97.31
AD-01b-5US-15	0.01	76.31	0.04	0.07	13.20	0.04	0.46	0.19	0.50	4.22	4.80	0.11	0.04	96.14
AD-01b-5US-16	0.01	76.53	0.00	0.03	13.06	0.01	0.41	0.20	0.49	4.15	4.78	0.29	0.03	97.84
AD-01b-5US-17	0.04	76.30	0.02	0.08	13.21	0.00	0.46	0.19	0.55	4.20	4.78	0.12	0.04	99.30
AD-01d-5US-01	0.04	76.67	0.03	0.07	13.10	0.02	0.46	0.16	0.55	3.80	4.96	0.09	0.06	96.58
AD-01d-5US-02	0.05	76.50	0.00	0.04	13.17	0.00	0.44	0.16	0.50	4.08	4.72	0.31	0.03	95.70

Sample Number	P2O5	SiO2	SO2	TiO2	Al2O3	MgO	CaO	MnO	FeO	Na2O	K2O	F	Cl	N. Total
AD-01d-5US-03	0.02	76.63	0.00	0.07	13.44	0.00	0.43	0.18	0.51	2.41	4.66	1.62	0.03	95.50
AD-01d-5US-04	0.00	75.84	0.03	0.06	13.36	0.02	0.51	0.18	0.55	3.94	5.02	0.44	0.06	96.06
AD-01a-24US-02	0.00	76.40	0.02	0.08	13.03	0.01	0.50	0.11	0.54	4.23	4.88	0.14	0.04	100.01
AD-01a-24US-03	0.01	76.15	0.05	0.06	12.94	0.24	0.48	0.17	0.55	4.10	5.06	0.13	0.04	98.25
AD-01a-24US-04	0.00	76.26	0.02	0.06	13.16	0.05	0.46	0.14	0.43	4.31	4.69	0.30	0.12	94.26
AD-01a-24US-05	0.00	76.26	0.01	0.08	13.16	0.06	0.45	0.14	0.52	4.43	4.64	0.21	0.04	101.56
AD-01a-24US-06	0.00	76.54	0.00	0.03	13.01	0.05	0.49	0.12	0.57	4.19	4.86	0.10	0.05	98.40
AD-01a-24US-07	0.00	76.53	0.00	0.06	12.95	0.05	0.43	0.14	0.52	4.07	4.90	0.30	0.02	98.48
AD-01a-24US-08	0.00	76.69	0.05	0.04	12.92	0.23	0.47	0.15	0.44	4.02	4.90	0.00	0.05	96.52
AD-01a-24US-09	0.06	76.48	0.01	0.04	12.99	0.04	0.46	0.11	0.54	4.29	4.73	0.19	0.04	98.76
AD-01a-24US-10	0.00	77.97	0.01	0.05	13.24	0.00	0.45	0.08	0.50	2.35	5.01	0.26	0.04	96.62
AD-01a-24US-11	0.01	76.26	0.00	0.03	13.02	0.11	0.47	0.14	0.58	4.31	4.77	0.26	0.05	98.49
AD-01a-24US-13	0.01	76.06	0.00	0.09	13.00	0.11	0.47	0.15	0.58	4.23	4.88	0.34	0.05	99.92
AD-01a-24US-14	0.00	75.98	0.11	0.07	13.12	0.27	0.48	0.12	0.51	4.21	4.86	0.21	0.04	98.48
AD-01a-24US-15	0.07	76.21	0.01	0.03	12.98	0.03	0.46	0.12	0.55	4.31	4.93	0.23	0.07	99.83
AD-01b-24US-01	0.00	76.27	0.00	0.03	13.08	0.05	0.48	0.13	0.52	4.39	4.83	0.14	0.05	98.85
AD-01b-24US-02	0.01	76.05	0.03	0.09	12.95	0.18	0.47	0.18	0.53	4.42	4.90	0.10	0.04	99.54
AD-01b-24US-03	0.00	76.23	0.00	0.12	13.03	0.04	0.48	0.17	0.46	4.43	4.81	0.14	0.05	99.97
AD-01b-24US-04	0.00	76.23	0.00	0.08	13.16	0.03	0.46	0.16	0.49	4.12	4.89	0.30	0.04	98.58
AD-01b-24US-05	0.06	76.17	0.04	0.04	13.04	0.07	0.49	0.13	0.55	4.30	4.86	0.18	0.07	100.36
AD-01b-24US-06	0.00	76.00	0.02	0.06	13.00	0.05	0.51	0.14	0.52	4.31	4.99	0.29	0.07	100.06
AD-01b-24US-07	0.02	76.33	0.09	0.03	12.87	0.04	0.49	0.11	0.54	4.34	4.88	0.18	0.04	98.99
AD-01b-24US-08	0.00	76.50	0.00	0.05	12.89	0.08	0.47	0.14	0.52	4.25	4.84	0.18	0.06	99.79
AD-02-5US-01	0.02	76.36	0.00	0.13	13.27	0.02	0.80	0.07	0.51	3.94	4.73	0.09	0.07	99.42
AD-02-5US-02	0.04	76.35	0.00	0.08	13.33	0.05	0.74	0.06	0.39	4.14	4.62	0.16	0.05	99.98
AD-02-5US-03	0.00	76.02	0.00	0.02	13.40	0.05	0.75	0.11	0.54	4.03	4.75	0.27	0.07	100.09
AD-02-5US-04	0.02	76.05	0.00	0.14	13.28	0.03	0.75	0.05	0.37	4.24	4.86	0.14	0.07	97.80
AD-02-5US-05	0.00	76.42	0.02	0.09	13.39	0.04	0.76	0.08	0.32	4.03	4.71	0.05	0.08	97.90
AD-02-5US-06	0.02	76.31	0.03	0.04	13.18	0.04	0.79	0.05	0.50	4.07	4.75	0.15	0.09	97.53
AD-02-5US-07	0.02	76.46	0.00	0.09	13.24	0.02	0.79	0.06	0.44	3.97	4.72	0.11	0.08	96.53
AD-02-5US-08	0.02	76.25	0.00	0.08	13.38	0.02	0.80	0.07	0.55	4.08	4.69	0.00	0.05	97.15
AD-02-5US-09	0.00	76.20	0.00	0.05	13.40	0.04	0.78	0.11	0.53	4.07	4.62	0.17	0.04	97.26
AD-02-5US-10	0.02	76.20	0.02	0.07	13.29	0.03	0.74	0.08	0.57	4.04	4.71	0.14	0.07	97.18
AD-02-5US-11	0.00	76.42	0.01	0.05	13.27	0.05	0.76	0.11	0.39	4.08	4.75	0.07	0.05	97.80
AD-02-5US-12	0.02	76.29	0.00	0.07	13.43	0.05	0.74	0.07	0.44	4.00	4.76	0.05	0.06	97.68
AD-02-5US-13	0.01	76.12	0.00	0.08	13.41	0.05	0.75	0.09	0.47	3.98	4.80	0.14	0.10	98.12

Sample Number	P2O5	SiO2	SO2	TiO2	Al2O3	MgO	CaO	MnO	FeO	Na2O	K2O	F	Cl	N. Total
AD-02-5US-14	0.05	76.30	0.00	0.09	13.37	0.05	0.70	0.07	0.39	4.06	4.63	0.10	0.08	97.99
AD-02-5US-15	0.03	76.33	0.01	0.09	13.32	0.04	0.76	0.07	0.47	4.09	4.67	0.07	0.06	98.05
AD-02-5US-16	0.00	76.15	0.03	0.09	13.53	0.02	0.78	0.09	0.43	3.95	4.49	0.35	0.08	98.35
AD-02-5US-17	0.00	76.12	0.00	0.04	13.38	0.03	0.74	0.11	0.52	4.07	4.79	0.12	0.08	99.72
AD-02-5US-18	0.00	76.14	0.00	0.10	13.41	0.03	0.76	0.05	0.39	4.06	4.84	0.15	0.06	99.83
AD-02-5US-19	0.00	76.05	0.00	0.07	13.47	0.05	0.81	0.12	0.45	4.21	4.61	0.09	0.08	99.73
AD-02-5US-20	0.02	76.34	0.00	0.14	13.28	0.02	0.76	0.06	0.38	4.07	4.64	0.22	0.06	99.39
AD-02-5US-21	0.05	76.09	0.01	0.07	13.34	0.04	0.77	0.08	0.52	4.12	4.58	0.26	0.07	99.82
AD-02-5US-22	0.06	76.04	0.01	0.07	13.59	0.07	0.81	0.05	0.44	3.79	4.76	0.22	0.09	96.90
AD-02-5US-23	0.00	76.18	0.00	0.06	13.36	0.00	0.76	0.09	0.56	3.99	4.62	0.28	0.08	96.49
AD-02-5US-24	0.00	76.52	0.00	0.04	13.22	0.05	0.74	0.08	0.42	4.03	4.71	0.12	0.07	96.71
AD-02-5US-25	0.00	76.26	0.03	0.10	13.30	0.01	0.71	0.10	0.49	4.05	4.71	0.15	0.08	97.82
AD-02-5US-26	0.04	76.06	0.00	0.06	13.39	0.03	0.74	0.08	0.45	4.02	4.74	0.32	0.08	97.73
AD-02-5US-27	0.03	76.40	0.00	0.05	13.43	0.03	0.76	0.09	0.33	4.01	4.66	0.15	0.06	98.23
AD-02-5US-28	0.02	76.22	0.01	0.07	13.27	0.04	0.78	0.07	0.52	4.14	4.66	0.14	0.08	99.48
AD-02-5US-29	0.00	76.12	0.02	0.12	13.36	0.04	0.77	0.05	0.62	4.13	4.67	0.05	0.06	99.59
AD-02-5US-30	0.03	76.86	0.00	0.05	13.46	0.04	0.72	0.09	0.26	3.98	4.42	0.00	0.08	97.26
AD-02-5US-31	0.05	76.41	0.02	0.07	13.43	0.00	0.76	0.08	0.30	4.06	4.77	0.00	0.04	96.73
AD-02-5US-32	0.00	76.15	0.00	0.08	13.46	0.03	0.79	0.06	0.56	3.99	4.58	0.24	0.08	97.77
AD-02-5US-33	0.00	76.28	0.02	0.05	13.56	0.03	0.73	0.08	0.50	4.02	4.67	0.00	0.07	97.75
AD-02-5US-34	0.00	76.12	0.00	0.06	13.72	0.02	0.73	0.06	0.47	4.01	4.53	0.21	0.06	98.01
AD-02-5US-35	0.00	76.35	0.00	0.03	13.31	0.04	0.75	0.11	0.51	4.17	4.65	0.00	0.07	98.07
AD-02-5US-36	0.00	76.41	0.00	0.06	13.35	0.02	0.77	0.07	0.43	4.07	4.51	0.22	0.09	99.79
AD-02-5US-37	0.00	76.66	0.02	0.10	13.43	0.02	0.68	0.08	0.32	4.07	4.55	0.00	0.06	99.17
AD-02-5US-38	0.00	76.07	0.00	0.11	13.40	0.07	0.79	0.05	0.46	4.10	4.83	0.06	0.07	99.21
AD-02-5US-39	0.00	76.99	0.00	0.10	12.37	0.03	0.78	0.05	0.44	4.25	4.70	0.23	0.06	98.64
AD-02-5US-40	0.01	75.84	0.00	0.05	14.16	0.01	0.63	0.09	0.43	3.94	4.75	0.00	0.08	97.81
AD-02-5US-41	0.00	76.32	0.00	0.08	13.38	0.01	0.66	0.09	0.47	4.12	4.63	0.14	0.08	96.79
AD-02-5US-42	0.00	76.06	0.00	0.08	13.60	0.03	0.56	0.10	0.54	4.18	4.76	0.00	0.09	99.59
AD-02-5US-43	0.02	76.04	0.01	0.10	13.42	0.00	0.62	0.09	0.51	4.19	4.73	0.19	0.09	99.92
AD-02-5US-44	0.00	76.27	0.01	0.13	13.31	0.04	0.55	0.08	0.42	4.12	4.72	0.29	0.06	97.72
AD-02-5US-45	0.00	76.49	0.02	0.06	13.42	0.04	0.60	0.11	0.34	4.15	4.66	0.04	0.07	97.72
AD-02-5US-46	0.01	76.42	0.00	0.07	13.38	0.02	0.62	0.08	0.48	4.14	4.71	0.00	0.07	99.52
AD-02-5US-47	0.00	76.13	0.00	0.09	13.35	0.04	0.71	0.08	0.41	4.23	4.76	0.14	0.07	99.90
AD-02-5US-48	0.02	76.24	0.01	0.10	13.38	0.02	0.68	0.10	0.46	4.08	4.60	0.26	0.06	97.93
AD-02-5US-49	0.00	76.74	0.00	0.05	13.30	0.01	0.65	0.03	0.31	3.99	4.81	0.00	0.09	96.64

Sample Number	P2O5	SiO2	SO2	TiO2	Al2O3	MgO	CaO	MnO	FeO	Na2O	K2O	F	Cl	N. Total
AD-02-5US-50	0.03	76.25	0.00	0.06	13.19	0.03	0.56	0.12	0.54	4.05	4.66	0.41	0.09	97.42
AD-02-5US-51	0.00	76.23	0.01	0.06	13.41	0.02	0.61	0.10	0.32	4.17	4.73	0.27	0.07	97.51
AD-02-5US-52	0.00	76.44	0.04	0.11	13.28	0.02	0.66	0.08	0.39	4.11	4.54	0.22	0.09	97.49
AD-02-5US-53	0.00	76.08	0.02	0.05	13.80	0.04	0.64	0.09	0.47	4.08	4.67	0.00	0.07	100.00
AD-02-5US-54	0.04	76.47	0.00	0.07	13.38	0.05	0.62	0.10	0.45	4.09	4.64	0.00	0.08	98.15
AD-02-5US-55	0.00	76.23	0.03	0.07	13.45	0.05	0.58	0.09	0.39	4.13	4.67	0.28	0.05	99.60
AD-02-5US-56	0.02	76.16	0.00	0.03	13.47	0.05	0.73	0.14	0.53	4.00	4.50	0.29	0.07	99.65
AD-02-5US-57	0.03	76.05	0.01	0.07	13.36	0.03	0.79	0.06	0.61	4.14	4.68	0.09	0.08	99.28
AD-02-5US-58	0.02	76.15	0.00	0.10	13.54	0.04	0.73	0.06	0.47	4.12	4.58	0.14	0.05	98.88
AD-02-5US-59	0.00	76.33	0.01	0.06	13.57	0.04	0.74	0.05	0.30	4.13	4.64	0.08	0.06	99.24
AD-02-5US-60	0.00	76.51	0.02	0.07	13.17	0.03	0.83	0.09	0.42	4.03	4.69	0.07	0.06	97.73
AD-02-5US-61	0.00	76.52	0.00	0.06	13.38	0.00	0.76	0.08	0.52	4.05	4.52	0.04	0.08	99.45
AD-02-5US-62	0.01	76.59	0.01	0.07	13.05	0.03	0.77	0.09	0.49	4.04	4.72	0.06	0.08	99.08
AD-02-5US-63	0.00	76.64	0.01	0.05	13.08	0.04	0.82	0.04	0.41	4.04	4.66	0.15	0.08	98.60
AD-02a-24US-01	0.00	75.83	0.02	0.10	13.04	0.69	0.78	0.06	0.58	4.08	4.67	0.00	0.09	98.67
AD-02a-24US-02	0.05	76.08	0.00	0.05	13.38	0.05	0.77	0.06	0.50	4.17	4.76	0.05	0.07	99.77
AD-02a-24US-03	0.00	76.08	0.00	0.10	13.34	0.00	0.81	0.08	0.46	4.13	4.87	0.03	0.07	100.16
AD-02a-24US-04	0.00	75.97	0.03	0.09	13.38	0.04	0.72	0.05	0.43	4.22	4.86	0.12	0.06	98.16
AD-02a-24US-05	0.03	77.22	0.00	0.10	13.17	0.18	0.82	0.06	0.62	2.60	4.93	0.13	0.09	98.60
AD-02a-24US-06	0.00	76.10	0.02	0.08	13.25	0.00	0.81	0.09	0.45	4.14	4.84	0.13	0.07	100.31
AD-02a-24US-07	0.00	75.92	0.00	0.11	13.33	0.04	0.85	0.06	0.55	3.99	4.85	0.13	0.10	98.03
AD-02a-24US-08	0.06	75.90	0.02	0.03	13.35	0.06	0.82	0.08	0.53	4.14	4.92	0.00	0.09	96.75
AD-02b-24US-01	0.02	75.65	0.04	0.08	13.14	0.06	0.72	0.07	1.15	4.12	4.84	0.00	0.06	100.38
AD-02b-24US-02	0.00	76.32	0.00	0.12	13.15	0.06	0.79	0.07	0.41	4.20	4.76	0.06	0.08	100.47
AD-02b-24US-03	0.03	75.94	0.06	0.03	12.89	0.06	0.82	0.08	0.57	4.21	4.84	0.25	0.17	89.29
AD-02b-24US-04	0.05	76.06	0.00	0.06	13.32	0.07	0.82	0.12	0.36	4.16	4.82	0.04	0.08	99.54
AD-02b-24US-05	0.03	75.96	0.00	0.08	13.35	0.04	0.82	0.08	0.61	4.00	4.73	0.23	0.07	98.72
AD-02b-24US-06	0.02	76.33	0.01	0.07	13.13	0.05	0.76	0.05	0.54	4.19	4.75	0.00	0.06	99.79
AD-02b-24US-07	0.00	76.10	0.08	0.01	13.15	0.23	0.78	0.07	0.60	4.19	4.74	0.00	0.06	101.07
AD-02b-24US-08	0.05	75.99	0.14	0.05	13.06	0.45	0.79	0.04	0.60	4.05	4.66	0.00	0.07	99.75
AD-02b-24US-09	0.02	76.10	0.00	0.04	13.17	0.05	0.85	0.05	0.60	4.08	4.82	0.09	0.10	100.16
AD-02a-AA-01	0.00	76.34	0.00	0.09	13.11	0.04	0.81	0.08	0.40	4.17	4.73	0.11	0.06	98.43
AD-02a-AA-02	0.00	75.78	0.04	0.04	13.29	0.08	0.90	0.08	0.53	4.10	4.88	0.18	0.10	99.76
AD-02a-AA-03	0.00	76.08	0.02	0.04	13.39	0.03	0.76	0.06	0.32	4.15	4.87	0.18	0.07	99.89
AD-02a-AA-04	0.00	76.14	0.03	0.03	13.29	0.03	0.76	0.04	0.61	4.10	4.80	0.05	0.08	98.71
AD-02a-AA-05	0.03	76.63	0.03	0.04	13.16	0.05	0.73	0.05	0.35	3.98	4.68	0.19	0.05	98.14

Sample Number	P2O5	SiO2	SO2	TiO2	Al2O3	MgO	CaO	MnO	FeO	Na2O	K2O	F	Cl	N. Total
AD-02a-AA-06	0.01	76.24	0.01	0.08	13.22	0.02	0.72	0.14	0.22	4.04	4.94	0.26	0.07	98.36
AD-02a-AA-07	0.03	76.13	0.04	0.12	13.29	0.04	0.83	0.07	0.38	4.15	4.80	0.06	0.07	100.24
AD-02a-AA-08	0.02	76.40	0.01	0.09	13.25	0.04	0.81	0.07	0.31	4.09	4.81	0.00	0.08	100.49
AD-02a-AA-09	0.00	76.02	0.00	0.05	13.29	0.06	0.77	0.09	0.54	4.19	4.82	0.08	0.09	99.53
AD-02a-AA-10	0.04	75.98	0.01	0.11	13.17	0.07	0.84	0.09	0.49	4.10	4.90	0.08	0.09	100.29
AD-02b-AA-01	0.02	76.47	0.03	0.10	13.15	0.04	0.80	0.08	0.45	4.14	4.63	0.00	0.07	98.95
AD-02b-AA-02	0.00	76.44	0.00	0.13	13.12	0.06	0.73	0.09	0.25	4.01	4.81	0.22	0.07	98.15
AD-02b-AA-03	0.04	76.07	0.02	0.06	13.28	0.06	0.80	0.12	0.42	4.24	4.76	0.00	0.08	99.94
AD-02b-AA-04	0.00	75.92	0.01	0.06	13.44	0.06	0.84	0.09	0.44	4.25	4.82	0.00	0.07	100.17
AD-02b-AA-05	0.02	76.22	0.02	0.06	13.26	0.05	0.80	0.07	0.40	4.04	4.78	0.17	0.09	98.21
AD-02b-AA-06	0.00	76.01	0.03	0.08	13.21	0.04	0.79	0.06	0.55	4.20	4.87	0.05	0.10	100.53
AD-02b-AA-07	0.00	76.22	0.02	0.06	13.13	0.04	0.83	0.04	0.50	4.04	4.95	0.00	0.08	100.42
AD-02a-HF5US-01	0.02	76.02	0.00	0.08	13.25	0.04	0.85	0.05	0.48	4.18	4.94	0.00	0.08	100.75
AD-02a-HF5US-02	0.00	76.45	0.03	0.12	12.99	0.03	0.82	0.03	0.43	4.08	4.89	0.00	0.11	99.79
AD-02a-HF5US-03	0.00	76.32	0.01	0.06	13.18	0.05	0.74	0.06	0.51	4.19	4.65	0.19	0.06	100.57
AD-02a-HF5US-04	0.00	76.20	0.03	0.10	13.15	0.02	0.82	0.05	0.49	4.08	4.92	0.03	0.08	99.92
AD-02a-HF5US-05	0.00	76.19	0.02	0.09	12.92	0.08	0.75	0.08	0.61	4.15	4.88	0.12	0.08	100.26
AD-02a-HF5US-06	0.00	76.10	0.06	0.08	13.03	0.05	0.79	0.05	0.54	4.19	4.85	0.17	0.08	100.74
AD-02a-HF5US-07	0.00	76.58	0.00	0.03	12.97	0.06	0.78	0.06	0.50	4.15	4.80	0.00	0.06	99.71
AD-02a-HF5US-08	0.00	76.41	0.01	0.04	12.95	0.04	0.71	0.05	0.50	4.15	4.77	0.26	0.11	100.20
AD-02a-HF5US-09	0.00	75.98	0.01	0.08	13.18	0.05	0.78	0.11	0.52	4.14	4.81	0.19	0.09	100.60
AD-02b-HF5US-01	0.04	75.96	0.02	0.04	13.10	0.04	0.74	0.05	0.33	4.53	4.77	0.22	0.10	99.35
AD-02b-HF5US-02	0.00	76.02	0.00	0.05	13.07	0.03	0.72	0.08	0.33	4.65	4.91	0.00	0.09	100.23
AD-02b-HF5US-03	0.00	76.52	0.00	0.08	13.11	0.04	0.78	0.10	0.37	3.97	4.96	0.00	0.06	99.45
AD-02b-HF5US-04	0.03	76.56	0.02	0.09	13.15	0.01	0.74	0.07	0.41	3.98	4.77	0.11	0.07	100.49
AD-02b-HF5US-05	0.02	76.73	0.01	0.10	13.13	0.02	0.65	0.05	0.24	4.02	4.98	0.00	0.06	100.11
AD-02b-HF5US-06	0.03	76.57	0.02	0.04	13.01	0.18	0.70	0.08	0.33	4.02	4.81	0.11	0.07	99.21
AD-02b-HF5US-07	0.02	76.41	0.01	0.04	13.03	0.06	0.80	0.06	0.40	4.21	4.76	0.10	0.07	98.30
AD-02b-HF5US-08	0.00	76.35	0.04	0.11	13.19	0.11	0.76	0.06	0.38	4.15	4.68	0.09	0.05	99.57
AD-02b-HF5US-09	0.01	76.06	0.01	0.05	13.35	0.04	0.84	0.05	0.49	4.12	4.67	0.20	0.06	100.79
AD-02a-HF24US-01	0.03	76.61	0.00	0.05	13.10	0.04	0.71	0.03	0.48	4.20	4.58	0.07	0.07	98.45
AD-02a-HF24US-02	0.00	76.32	0.01	0.02	13.22	0.07	0.79	0.06	0.43	4.06	4.86	0.04	0.09	99.68
AD-02a-HF24US-03	0.03	75.96	0.00	0.03	13.38	0.11	0.76	0.08	0.52	4.21	4.79	0.00	0.07	100.04
AD-02a-HF24US-04	0.01	76.30	0.08	0.07	13.24	0.03	0.77	0.05	0.28	4.13	4.78	0.16	0.06	98.44
AD-02a-HF24US-05	0.00	76.56	0.00	0.01	13.15	0.18	0.79	0.08	0.33	4.09	4.74	0.00	0.06	97.93
AD-02a-HF24US-06	0.00	76.13	0.01	0.04	13.54	0.02	0.80	0.08	0.41	4.07	4.73	0.04	0.09	99.56

Sample Number	P2O5	SiO2	SO2	TiO2	Al2O3	MgO	CaO	MnO	FeO	Na2O	K2O	F	Cl	N. Total
AD-02a-HF24US-07	0.03	76.61	0.02	0.08	13.16	-0.02	0.73	0.07	0.30	4.16	4.73	0.04	0.06	99.91
AD-02a-HF24US-09	0.00	76.40	0.03	0.04	13.21	0.06	0.78	0.08	0.28	4.17	4.72	0.15	0.07	101.33
AD-02b-HF24US-01	0.00	75.88	0.00	0.09	13.15	0.03	0.86	0.08	0.48	4.13	4.98	0.10	0.21	99.84
AD-02b-HF24US-03	0.03	76.16	0.02	0.09	13.26	-0.02	0.80	0.05	0.49	4.09	4.72	0.18	0.07	100.41
AD-02b-HF24US-04	0.00	76.17	0.01	0.06	13.25	0.03	0.80	0.08	0.50	4.18	4.74	0.05	0.05	99.67
AD-02b-HF24US-05	0.02	76.14	0.00	0.07	13.24	0.18	0.77	0.12	0.38	4.14	4.85	0.02	0.07	99.94
AD-02b-HF24US-06	0.00	76.17	0.00	0.11	13.22	0.04	0.78	0.02	0.40	4.14	4.87	0.12	0.05	100.50
AD-02b-HF24US-07	0.01	76.18	0.02	0.05	13.31	0.04	0.73	0.07	0.48	4.02	4.85	0.09	0.09	99.37
AD-02b-HF24US-08	0.00	76.32	0.00	0.01	13.41	0.05	0.77	0.03	0.47	4.13	4.74	0.00	0.05	100.35
AD-02b-HF24US-09	0.03	75.71	0.01	0.02	13.17	0.01	0.79	0.07	0.59	4.19	4.65	0.66	0.10	100.75
AD-02b-HF24US-10	0.03	76.04	0.01	0.04	13.38	0.05	0.76	0.04	0.52	4.18	4.77	0.05	0.08	100.67
AD-02b-HF24US-11	0.05	76.56	0.04	0.08	13.22	0.18	0.78	0.07	0.57	3.71	4.65	0.00	0.07	100.67
AD-03a-5US-01	0.00	76.30	0.01	0.06	13.35	0.00	0.73	0.09	0.41	4.03	4.74	0.14	0.12	99.26
AD-03a-5US-02	0.00	76.43	0.02	0.04	12.80	0.40	0.79	0.09	0.51	3.90	4.89	0.00	0.12	93.65
AD-03a-5US-03	0.00	76.39	0.00	0.00	13.16	0.02	0.77	0.05	0.48	4.06	4.98	0.00	0.09	94.81
AD-03a-5US-07	0.00	76.05	0.02	0.08	13.52	0.02	0.76	0.08	0.41	4.10	4.88	0.00	0.08	95.50
AD-03a-5US-08	0.00	75.07	0.00	0.06	13.15	0.03	0.73	0.08	0.35	4.17	4.70	1.52	0.14	98.02
AD-03a-5US-09	0.00	75.75	0.00	0.05	13.45	0.02	0.71	0.06	0.52	4.06	4.76	0.52	0.10	99.42
AD-04a-5US-01	0.00	75.06	0.00	0.09	13.56	0.00	0.38	0.02	0.07	3.24	7.33	0.23	0.02	99.63
AD-04a-5US-02	0.04	75.93	0.00	0.06	13.43	0.00	0.67	0.04	0.06	4.10	5.19	0.47	0.01	99.27
AD-04a-5US-05	0.00	76.43	0.02	0.03	13.27	0.00	0.58	0.02	0.08	3.74	5.78	0.01	0.02	98.02
AD-04a-5US-06	0.02	76.63	0.02	0.06	13.27	0.14	1.27	0.10	0.81	5.38	2.02	0.24	0.04	98.10
AD-04a-5US-07	0.02	76.58	0.00	0.07	13.56	0.00	0.82	0.01	0.08	4.39	4.46	0.00	0.01	98.14
AD-04a-5US-08	0.05	76.35	0.02	0.07	13.61	0.00	0.89	0.00	0.24	4.46	4.20	0.10	0.03	99.40
AD-04a-5US-09	0.00	76.91	0.01	0.06	13.51	0.02	1.02	0.06	0.32	4.87	3.06	0.14	0.01	99.72
AD-04a-5US-10	0.03	76.54	0.00	0.08	13.42	0.02	0.95	0.02	0.33	4.74	3.58	0.28	0.01	99.39
AD-04a-5US-11	0.00	76.40	0.01	0.04	13.57	0.10	1.06	0.05	0.47	5.01	3.09	0.18	0.01	98.11
AD-04a-5US-12	0.00	76.17	0.03	0.06	13.40	0.06	0.91	0.09	0.44	4.46	4.28	0.09	0.02	99.09
AD-04b-5US-1	0.03	75.40	0.02	0.03	13.37	0.01	0.50	0.09	0.36	3.19	6.82	0.02	0.15	99.11
AD-04b-5US-2	0.04	75.97	0.01	0.11	13.82	0.08	1.09	0.14	0.74	6.15	1.58	0.19	0.08	97.64
AD-04b-5US-4	0.00	75.51	0.00	0.04	13.34	0.00	0.63	0.09	0.73	3.33	6.27	0.07	0.00	99.23
AD-04b-5US-5	0.00	76.10	0.00	0.08	12.98	0.03	0.48	0.09	0.28	3.19	6.57	0.13	0.06	99.01
AD-04b-5US-9	0.05	78.26	0.00	0.10	12.16	0.00	0.50	0.03	0.12	3.01	5.76	0.00	0.00	98.41
AD-05-5US-01	0.00	76.69	0.00	0.08	13.31	0.03	0.48	0.13	0.54	4.28	4.25	0.19	0.03	97.00
AD-05-5US-02	0.00	76.70	0.00	0.07	13.13	0.03	0.44	0.15	0.50	4.37	4.36	0.21	0.04	97.05
AD-05-5US-03	0.01	76.89	0.01	0.06	13.20	0.00	0.44	0.16	0.51	4.41	4.26	0.00	0.05	97.47

Sample Number	P2O5	SiO2	SO2	TiO2	Al2O3	MgO	CaO	MnO	FeO	Na2O	K2O	F	Cl	N. Total
AD-05-5US-04	0.00	76.38	0.00	0.08	13.05	0.04	0.52	0.14	0.56	4.29	4.40	0.46	0.06	97.38
AD-05-5US-05	0.00	76.66	0.00	0.04	13.16	0.03	0.45	0.15	0.50	4.14	4.51	0.29	0.05	97.75
AD-05-5US-06	0.02	76.60	0.00	0.05	13.12	0.03	0.48	0.18	0.48	4.34	4.54	0.11	0.05	97.41
AD-05-5US-07	0.00	76.99	0.00	0.08	13.00	0.01	0.46	0.13	0.44	4.08	4.56	0.22	0.02	96.66
AD-05-5US-08	0.00	76.74	0.00	0.08	13.23	0.00	0.46	0.09	0.53	4.32	4.36	0.13	0.05	97.18
AD-05-5US-09	0.02	76.72	0.00	0.04	13.14	0.02	0.51	0.16	0.53	4.26	4.37	0.18	0.04	97.52
AD-05-5US-10	0.00	76.87	0.00	0.06	13.14	0.04	0.44	0.12	0.50	4.08	4.52	0.18	0.05	97.29
AD-05-5US-11	0.00	76.48	0.03	0.04	13.31	0.01	0.45	0.12	0.54	4.28	4.53	0.17	0.03	97.37
AD-05-5US-12	0.03	76.28	0.01	0.08	13.48	0.02	0.45	0.17	0.44	4.20	4.50	0.30	0.04	97.81
AD-05-5US-13	0.02	76.81	0.02	0.03	13.13	0.01	0.42	0.12	0.50	4.37	4.41	0.11	0.05	96.96
AD-05-5US-14	0.00	76.61	0.01	0.09	13.22	0.00	0.44	0.13	0.52	4.32	4.37	0.26	0.03	97.38
AD-05-5US-15	0.01	76.69	0.01	0.10	13.13	0.03	0.45	0.13	0.48	4.32	4.22	0.35	0.06	97.00
AD-05-5US-19	0.00	76.87	0.03	0.00	13.07	0.04	0.46	0.20	0.48	3.94	4.54	0.32	0.04	96.37
AD-05-5US-20	0.00	76.60	0.01	0.02	13.19	0.02	0.41	0.14	0.52	4.38	4.49	0.18	0.03	96.43
AD-06a-5US-01	0.03	76.05	0.00	0.03	13.06	0.02	0.17	0.14	0.76	4.32	4.55	0.81	0.06	96.54
AD-06a-5US-02	0.02	76.18	0.00	0.04	12.89	0.00	0.22	0.18	0.54	4.22	4.58	1.08	0.04	96.99
AD-06a-5US-03	0.03	76.37	0.00	0.06	12.89	0.00	0.22	0.15	0.48	4.19	4.62	0.89	0.08	96.88
AD-06a-5US-04	0.03	75.67	0.00	0.04	13.41	0.00	0.23	0.15	0.46	4.52	4.59	0.84	0.07	95.17
AD-06a-5US-07	0.00	75.03	0.02	0.06	12.84	0.00	0.39	0.25	1.62	4.11	4.61	1.03	0.06	97.86
AD-06a-5US-09	0.00	76.58	0.02	0.08	13.02	0.02	0.40	0.09	0.37	4.08	4.79	0.50	0.05	97.49
AD-06a-5US-10	0.03	76.31	0.01	0.06	12.89	0.00	0.43	0.15	0.37	3.84	5.26	0.58	0.08	96.89
AD-06a-5US-11	0.01	75.52	0.16	0.08	13.17	0.00	0.61	0.14	0.42	4.65	4.51	0.39	0.34	95.36
AD-06a-5US-12	0.00	76.80	0.02	0.06	13.06	0.04	0.42	0.21	0.40	4.24	4.49	0.21	0.04	98.26
AD-06a-5US-13	0.02	76.57	0.00	0.06	13.13	0.00	0.42	0.18	0.42	4.32	4.60	0.27	0.02	99.72
AD-06b-5US-01	0.00	75.84	0.00	0.06	12.99	0.00	0.42	0.19	0.84	4.16	4.56	0.91	0.02	97.29
AD-06b-5US-03	0.00	75.75	0.01	0.04	13.56	0.00	0.41	0.08	0.37	4.57	4.25	0.93	0.02	95.49
AD-06b-5US-04	0.00	76.10	0.00	0.03	12.69	0.03	0.42	0.12	0.46	4.54	4.74	0.68	0.17	99.59
AD-06b-5US-05	0.00	75.68	0.02	0.10	13.27	0.00	0.39	0.21	0.45	4.01	4.93	0.91	0.04	95.44
AD-06b-5US-06	0.00	76.52	0.00	0.05	12.77	0.09	0.34	0.16	0.38	4.31	4.45	0.86	0.06	96.37
AD-06c-5US-01	0.00	76.16	0.00	0.05	13.20	0.01	0.44	0.17	0.39	4.32	4.86	0.33	0.06	98.37
AD-06c-5US-02	0.00	76.04	0.02	0.04	13.51	0.00	0.49	0.11	0.49	4.32	4.71	0.21	0.06	97.14
AD-06c-5US-03	0.01	76.32	0.00	0.08	13.05	0.01	0.43	0.15	0.43	4.22	4.73	0.50	0.06	100.01
AD-06c-5US-04	0.00	76.03	0.00	0.04	13.20	0.01	0.47	0.20	0.45	4.17	4.70	0.68	0.05	96.85
AD-06c-5US-05	0.00	76.67	0.00	0.00	13.10	0.02	0.43	0.16	0.44	4.21	4.74	0.20	0.04	98.61
AD-06c-5US-06	0.00	76.17	0.00	0.04	13.46	0.00	0.42	0.16	0.40	4.55	4.45	0.29	0.05	99.54
AD-06c-5US-07	0.00	76.82	0.02	0.01	13.28	0.03	0.40	0.18	0.40	4.13	4.65	0.03	0.06	96.82

Sample Number	P2O5	SiO2	SO2	TiO2	Al2O3	MgO	CaO	MnO	FeO	Na2O	K2O	F	Cl	N. Total
AD-06c-5US-09	0.00	76.72	0.03	0.06	13.01	0.00	0.43	0.15	0.41	4.25	4.69	0.19	0.06	96.54
AD-06d-5US-02	0.00	76.48	0.00	0.05	13.20	0.01	0.47	0.16	0.33	4.20	4.74	0.31	0.05	97.91
AD-06d-5US-03	0.01	76.31	0.00	0.08	13.11	0.03	0.43	0.18	0.43	4.08	4.80	0.51	0.04	99.21
AD-06d-5US-04	0.00	76.66	0.00	0.03	12.99	0.03	0.47	0.18	0.40	4.20	4.80	0.20	0.03	99.18
AD-06d-5US-05	0.03	76.22	0.00	0.08	13.21	0.00	0.43	0.17	0.42	4.36	4.73	0.32	0.06	95.52
AD-06d-5US-06	0.05	76.30	0.00	0.11	13.28	0.00	0.41	0.15	0.38	4.08	4.77	0.42	0.05	98.00
AD-06d-5US-07	0.00	76.50	0.02	0.07	12.99	0.04	0.44	0.17	0.45	4.07	4.76	0.45	0.04	99.22
AD-06d-5US-08	0.00	75.15	0.04	0.04	13.45	0.14	0.45	0.15	0.41	4.65	4.33	1.14	0.04	99.22
AD-06d-5US-09	0.00	76.13	0.00	0.07	13.32	0.00	0.42	0.22	0.41	4.22	4.83	0.32	0.07	99.51
AD-06d-5US-10	0.00	76.49	0.00	0.04	13.13	0.05	0.38	0.16	0.42	4.21	4.81	0.25	0.05	98.86
AD-06a-24US-01	0.00	76.63	0.03	0.08	12.94	0.05	0.43	0.14	0.42	4.06	4.92	0.23	0.05	100.53
AD-06a-24US-02	0.00	76.42	0.03	0.04	13.04	0.04	0.49	0.17	0.45	4.26	4.86	0.16	0.04	100.66
AD-06a-24US-03	0.00	76.77	0.00	0.06	12.89	0.03	0.48	0.15	0.45	4.25	4.75	0.12	0.03	99.38
AD-06a-24US-04	0.00	76.73	0.03	0.08	12.81	0.02	0.47	0.11	0.42	4.22	4.83	0.25	0.03	100.44
AD-06a-24US-05	0.04	76.19	0.02	0.10	12.84	0.00	0.46	0.12	0.45	4.17	4.78	0.72	0.05	100.74
AD-06a-24US-06	0.00	76.46	0.09	0.06	12.76	0.15	0.48	0.13	0.44	4.27	4.78	0.28	0.06	100.50
AD-06a-24US-07	0.00	76.65	0.04	0.05	13.05	0.00	0.48	0.12	0.34	4.15	4.76	0.26	0.05	99.04
AD-06a-24US-08	0.00	76.64	0.00	0.04	12.92	0.01	0.44	0.12	0.38	4.31	4.79	0.27	0.04	100.34
AD-06a-24US-09	0.00	76.65	0.01	0.07	12.88	0.04	0.48	0.12	0.33	4.25	4.83	0.31	0.03	99.16
AD-06b-24US-01	0.00	76.92	0.02	0.05	12.85	0.00	0.45	0.11	0.41	4.19	4.81	0.16	0.02	99.06
AD-06b-24US-03	0.00	77.03	0.01	0.04	12.65	0.00	0.42	0.14	0.41	4.02	4.89	0.30	0.05	99.96
AD-06b-24US-04	0.02	76.91	0.00	0.06	12.72	0.00	0.47	0.09	0.42	4.18	4.91	0.13	0.08	100.26
AD-07a-5US-01	0.06	75.03	0.02	0.06	13.49	0.00	0.32	0.04	0.11	3.79	6.72	0.19	0.17	97.97
AD-07a-5US-02	0.06	75.15	0.04	0.04	13.59	0.01	0.58	0.01	0.14	4.55	5.52	0.22	0.09	98.57
AD-07a-5US-03	0.04	76.22	0.02	0.02	13.30	0.00	0.51	0.10	0.13	4.67	4.83	0.04	0.11	97.35
AD-07a-5US-04	0.00	77.47	0.00	0.08	13.08	0.00	0.58	0.08	0.14	4.82	3.63	0.08	0.05	98.60
AD-07a-5US-05	0.03	75.00	0.00	0.05	12.83	0.00	0.44	0.08	0.12	4.56	4.09	2.79	0.01	101.71
AD-07a-5US-06	0.00	76.89	0.01	0.06	12.67	0.00	0.48	0.13	0.26	4.27	4.54	0.63	0.05	99.63
AD-07a-5US-07	0.06	75.14	0.02	0.07	13.08	0.07	0.28	0.28	0.90	3.94	5.77	0.25	0.16	98.59
AD-07a-5US-08	0.02	75.65	0.00	0.06	12.81	0.12	0.56	0.12	0.38	4.43	4.40	1.39	0.06	98.48
AD-07a-5US-09	0.00	76.36	0.03	0.07	12.67	0.00	0.65	0.08	0.62	4.61	4.24	0.65	0.00	97.68
AD-07a-5US-10	0.02	76.59	0.00	0.08	12.83	0.00	0.30	0.15	0.16	3.80	5.69	0.24	0.15	98.22
AD-08a-5US-01	0.01	76.27	0.00	0.05	13.25	0.03	0.66	0.11	0.37	3.64	5.49	0.01	0.10	95.05
AD-08a-5US-03	0.00	76.20	0.00	0.07	13.28	0.00	0.63	0.07	0.44	3.72	5.30	0.22	0.07	96.07
AD-08a-5US-04	0.03	75.98	0.01	0.07	13.33	0.00	0.64	0.07	0.40	3.80	5.45	0.10	0.11	95.84
AD-08b-5US-01	0.00	76.13	0.01	0.15	13.36	0.00	0.65	0.06	0.38	3.65	5.40	0.14	0.08	95.19

Sample Number	P2O5	SiO2	SO2	TiO2	Al2O3	MgO	CaO	MnO	FeO	Na2O	K2O	F	Cl	N. Total
AD-08b-5US-03	0.00	75.93	0.01	0.08	13.39	0.00	0.59	0.15	0.32	3.76	5.52	0.14	0.10	95.74
AD-08b-5US-04	0.00	75.87	0.00	0.02	13.48	0.00	0.65	0.07	0.42	3.73	5.53	0.16	0.07	95.78
AD-08b-5US-05	0.00	75.72	0.00	0.08	13.16	0.08	0.80	0.06	0.54	3.73	5.54	0.19	0.11	95.47
AD-08b-5US-06	0.05	75.69	0.01	0.00	13.35	0.00	0.68	0.04	0.31	3.81	5.65	0.29	0.12	95.43
AD-08b-5US-07	0.00	75.98	0.01	0.12	13.37	0.00	0.65	0.10	0.26	3.73	5.59	0.09	0.09	95.94
AD-08b-5US-08	0.00	76.04	0.01	0.05	13.38	0.00	0.47	0.06	0.42	3.76	5.53	0.20	0.07	96.28
AD-08c-5US-01	0.03	76.12	0.00	0.05	13.33	0.02	0.55	0.08	0.41	3.72	5.51	0.13	0.06	95.61
AD-08c-5US-02	0.05	75.98	0.00	0.09	13.56	0.00	0.57	0.07	0.31	3.72	5.38	0.15	0.12	95.08
AD-08c-5US-03	0.00	76.04	0.00	0.07	13.19	0.06	0.54	0.09	0.48	3.75	5.57	0.13	0.09	95.71
AD-08c-5US-04	0.00	75.94	0.00	0.08	13.29	0.09	0.61	0.10	0.43	3.72	5.45	0.19	0.08	96.21
AD-08c-5US-06	0.06	76.20	0.01	0.05	13.29	0.00	0.50	0.11	0.32	3.75	5.52	0.09	0.10	95.31
AD-08c-5US-07	0.05	76.23	0.00	0.08	13.38	0.01	0.62	0.02	0.34	3.61	5.38	0.18	0.09	95.15
AD-08c-5US-08	0.00	76.10	0.00	0.03	13.39	0.02	0.64	0.08	0.45	3.75	5.47	0.01	0.07	94.23
AD-08c-5US-09	0.00	76.59	0.03	0.05	13.52	0.02	0.62	0.08	0.49	2.86	5.60	0.06	0.09	95.29
AD-09b-5US-01	0.12	75.89	0.09	0.10	13.16	0.01	0.43	0.12	0.31	4.02	5.45	0.09	0.21	93.26
AD-09b-5US-02	0.00	76.39	0.03	0.00	13.36	0.01	0.35	0.08	0.37	3.95	5.29	0.11	0.05	94.25
AD-09b-5US-03	0.02	76.66	0.00	0.06	12.72	0.01	0.82	0.10	0.62	3.85	4.90	0.13	0.10	94.46
AD-09c-5US-02	0.00	76.35	0.02	0.08	13.30	0.02	0.79	0.08	0.55	3.72	4.91	0.09	0.09	95.73
AD-09c-5US-06	0.02	76.29	0.00	0.08	13.64	0.00	0.54	0.17	0.56	4.33	4.30	0.00	0.06	93.99
AD-10a-5US-01	0.02	75.93	0.01	0.09	13.49	0.00	0.77	0.09	0.53	4.00	4.88	0.11	0.09	98.35
AD-10a-5US-02	0.02	76.09	0.02	0.07	13.28	0.04	0.73	0.06	0.62	4.07	4.83	0.08	0.09	97.44
AD-10a-5US-03	0.01	76.15	0.01	0.05	13.29	0.08	0.70	0.08	0.67	4.01	4.83	0.08	0.06	95.71
AD-10a-5US-04	0.01	76.36	0.00	0.01	13.31	0.05	0.76	0.05	0.56	3.93	4.79	0.11	0.06	95.77
AD-10a-5US-05	0.00	76.07	0.03	0.05	13.33	0.03	0.74	0.09	0.56	3.98	4.90	0.14	0.09	97.63
AD-10a-5US-06	0.00	76.03	0.00	0.04	13.50	0.06	0.76	0.07	0.55	4.03	4.88	0.02	0.07	97.70
AD-10a-5US-07	0.05	76.14	0.01	0.08	13.36	0.05	0.71	0.08	0.58	3.90	4.85	0.10	0.10	97.25
AD-10a-5US-08	0.04	76.26	0.00	0.12	13.44	0.02	0.74	0.08	0.52	3.92	4.68	0.12	0.06	95.08
AD-10a-5US-09	0.00	76.39	0.00	0.09	13.25	0.02	0.75	0.13	0.55	4.03	4.70	0.02	0.06	95.62
AD-10a-5US-10	0.05	75.72	0.00	0.04	13.53	0.06	0.78	0.09	0.53	3.98	5.04	0.08	0.09	96.52
AD-10a-5US-11	0.00	76.30	0.02	0.08	13.35	0.05	0.76	0.06	0.49	3.93	4.81	0.07	0.06	96.69
AD-10a-5US-12	0.00	75.98	0.02	0.05	13.43	0.03	0.76	0.10	0.57	4.10	4.81	0.06	0.08	95.79
AD-10a-5US-13	0.00	76.18	0.00	0.02	13.37	0.03	0.72	0.09	0.49	4.12	4.76	0.16	0.07	94.94
AD-10a-5US-14	0.00	76.10	0.01	0.05	13.40	0.05	0.74	0.06	0.53	3.82	5.00	0.17	0.05	94.98
AD-10a-5US-15	0.02	76.23	0.00	0.05	13.42	0.05	0.78	0.06	0.55	3.98	4.79	0.00	0.07	95.42
AD-10a-5US-16	0.02	76.06	0.02	0.02	13.37	0.02	0.81	0.07	0.55	4.11	4.90	0.01	0.05	95.25
AD-10a-5US-17	0.03	75.95	0.01	0.09	13.43	0.03	0.74	0.11	0.49	4.12	4.78	0.14	0.07	97.58

Sample Number	P2O5	SiO2	SO2	TiO2	Al2O3	MgO	CaO	MnO	FeO	Na2O	K2O	F	Cl	N. Total
AD-10b-5US-01	0.00	76.21	0.01	0.06	13.33	0.05	0.75	0.08	0.52	4.00	4.84	0.07	0.09	95.42
AD-10b-5US-02	0.05	76.36	0.00	0.09	13.40	0.02	0.76	0.08	0.52	3.88	4.68	0.07	0.08	95.31
AD-10b-5US-03	0.01	76.32	0.00	0.05	13.43	0.01	0.73	0.12	0.50	3.95	4.73	0.06	0.08	95.22
AD-10b-5US-04	0.01	76.00	0.00	0.05	13.57	0.06	0.76	0.11	0.49	4.01	4.75	0.09	0.10	94.54
AD-10b-5US-05	0.04	75.99	0.00	0.06	13.38	0.07	0.79	0.07	0.55	3.96	4.90	0.14	0.05	95.80
AD-10b-5US-06	0.00	76.27	0.04	0.07	13.36	0.01	0.76	0.04	0.51	3.99	4.87	0.00	0.09	95.38
AD-10b-5US-07	0.00	75.98	0.00	0.06	13.50	0.02	0.79	0.05	0.60	3.98	4.89	0.07	0.06	95.46
AD-10b-5US-08	0.05	76.04	0.00	0.09	13.39	0.04	0.72	0.08	0.60	3.92	4.92	0.07	0.08	95.32
AD-10c-5US-01	0.02	76.11	0.01	0.06	13.41	0.04	0.77	0.05	0.50	4.14	4.68	0.14	0.05	95.07
AD-10c-5US-02	0.00	75.82	0.02	0.08	13.57	0.00	0.75	0.04	0.44	4.20	4.85	0.17	0.07	93.67
AD-10c-5US-03	0.00	75.77	0.00	0.05	13.56	0.03	0.79	0.09	0.62	4.08	4.76	0.17	0.08	95.29
AD-10c-5US-04	0.04	75.94	0.00	0.07	13.42	0.03	0.76	0.09	0.60	4.05	4.87	0.05	0.09	95.35
AD-10c-5US-05	0.00	76.31	0.03	0.03	13.33	0.03	0.74	0.08	0.48	4.04	4.78	0.09	0.07	95.51
AD-10c-5US-06	0.05	76.27	0.03	0.06	13.29	0.03	0.73	0.05	0.50	4.08	4.70	0.12	0.08	95.41
AD-10c-5US-07	0.00	76.09	0.00	0.07	13.39	0.03	0.73	0.10	0.49	4.09	4.73	0.21	0.07	94.86
AD-11a-5US-02	0.00	76.38	0.01	0.07	13.91	0.04	0.49	0.02	0.51	6.37	2.12	0.04	0.03	97.91
AD-11a-5US-04	0.00	76.49	0.00	0.09	13.39	0.00	0.67	0.02	0.31	3.80	4.96	0.14	0.11	95.41
AD-11a-5US-05	0.00	75.73	0.00	0.10	13.58	0.02	0.66	0.06	0.43	3.99	5.19	0.17	0.07	96.07
AD-11a-5US-06	0.00	76.17	0.02	0.11	13.40	0.03	0.62	0.09	0.42	3.88	5.14	0.07	0.04	96.70
AD-11a-5US-07	0.02	76.08	0.00	0.12	13.38	0.04	0.62	0.07	0.53	3.85	5.13	0.09	0.07	97.78
AD-11a-5US-08	0.01	75.96	0.02	0.04	13.54	0.04	0.66	0.10	0.45	3.98	5.05	0.08	0.06	97.82
AD-11a-5US-09	0.00	76.32	0.00	0.05	13.41	0.04	0.62	0.09	0.39	3.86	5.14	0.00	0.08	95.85
AD-11a-5US-10	0.00	76.07	0.02	0.04	13.46	0.01	0.71	0.11	0.49	3.86	5.13	0.03	0.06	98.36
AD-11a-5US-11	0.00	77.54	0.00	0.06	13.51	0.04	1.42	0.04	0.50	6.17	0.71	0.00	0.02	97.17
AD-11a-5US-12	0.04	76.35	0.02	0.03	13.42	0.02	0.46	0.11	0.27	4.01	5.15	0.03	0.10	95.54
AD-11a-5US-14	0.01	77.78	0.00	0.08	13.07	0.02	0.94	0.10	0.50	6.55	0.84	0.09	0.03	96.98
AD-11a-5US-15	0.00	76.37	0.00	0.03	13.38	0.02	0.63	0.08	0.39	3.80	5.13	0.09	0.10	95.80
AD-11a-5US-16	0.01	77.18	0.01	0.08	13.41	0.03	1.00	0.04	0.51	6.31	1.29	0.10	0.02	97.89
AD-11a-5US-17	0.00	76.29	0.00	0.07	13.41	0.00	0.49	0.05	0.27	3.90	5.31	0.11	0.11	95.49
AD-11a-5US-18	0.00	77.57	0.00	0.06	13.33	0.03	1.28	0.02	0.50	6.25	0.76	0.18	0.02	97.47
AD-11b-5US-01	0.02	76.10	0.00	0.10	13.43	0.00	0.67	0.07	0.38	3.81	5.20	0.12	0.08	97.95
AD-11b-5US-02	0.01	76.22	0.00	0.07	13.29	0.03	0.69	0.09	0.38	4.00	5.00	0.12	0.10	97.00
AD-11b-5US-03	0.02	76.18	0.02	0.09	13.33	0.01	0.68	0.08	0.31	3.89	5.13	0.14	0.13	96.06
AD-11b-5US-04	0.05	77.46	0.03	0.06	13.27	0.03	1.42	0.05	0.57	4.95	2.04	0.04	0.02	97.18
AD-11b-5US-05	0.03	76.40	0.02	0.08	13.23	0.03	0.68	0.08	0.34	3.82	5.15	0.07	0.07	95.43
AD-11b-5US-06	0.03	76.22	0.00	0.08	13.29	0.04	0.66	0.03	0.45	3.88	5.10	0.16	0.07	95.84

Sample Number	P2O5	SiO2	SO2	TiO2	Al2O3	MgO	CaO	MnO	FeO	Na2O	K2O	F	Cl	N. Total
AD-11b-5US-07	0.01	75.97	0.00	0.10	13.61	0.03	0.73	0.07	0.39	3.71	5.18	0.15	0.06	94.71
AD-11b-5US-08	0.02	76.22	0.02	0.11	13.29	0.04	0.71	0.05	0.44	3.85	5.01	0.19	0.06	95.23
AD-11b-5US-09	0.02	76.12	0.03	0.08	13.61	0.05	0.72	0.06	0.26	3.87	5.08	0.02	0.08	95.50
AD-11b-5US-10	0.00	76.19	0.01	0.04	13.47	0.01	0.76	0.03	0.33	3.84	5.11	0.09	0.12	97.18
AD-11b-5US-11	0.00	76.17	0.01	0.08	13.42	0.04	0.73	0.09	0.37	3.78	5.17	0.06	0.07	96.99
AD-11b-5US-12	0.01	76.07	0.00	0.07	13.48	0.02	0.72	0.05	0.41	3.83	5.09	0.16	0.08	97.44
AD-11b-5US-13	0.02	76.06	0.00	0.03	13.45	0.05	0.75	0.05	0.41	3.87	5.10	0.13	0.07	98.16
AD-11b-5US-14	0.00	75.84	0.01	0.03	13.67	0.05	0.67	0.06	0.37	3.84	5.21	0.15	0.09	96.67
AD-11a-24US-01	0.01	76.31	0.02	0.08	13.04	0.03	0.76	0.07	0.37	3.83	5.25	0.13	0.07	98.59
AD-11a-24US-02	0.00	76.24	0.00	0.07	13.23	0.02	0.73	0.08	0.43	3.78	5.11	0.18	0.07	98.57
AD-11a-24US-03	0.00	76.56	0.00	0.07	12.98	0.01	0.77	0.06	0.35	3.88	5.19	0.05	0.07	100.10
AD-11a-24US-04	0.00	76.28	0.02	0.06	13.10	0.00	0.81	0.08	0.44	3.98	5.13	0.00	0.08	99.85
AD-11a-24US-05	0.03	76.20	0.02	0.03	13.34	0.07	0.73	0.08	0.37	3.85	5.13	0.05	0.08	99.02
AD-11a-24US-06	0.00	76.25	0.03	0.08	13.14	0.15	0.75	0.03	0.27	3.84	5.12	0.29	0.08	100.19
AD-11a-24US-08	0.00	76.41	0.00	0.11	13.07	0.02	0.75	0.08	0.29	3.78	5.12	0.24	0.10	97.85
AD-11b-24US-01	0.03	76.25	0.02	0.08	13.14	0.01	0.76	0.05	0.27	3.77	5.24	0.20	0.13	99.82
AD-11b-24US-02	0.03	76.34	0.00	0.07	13.16	0.04	0.76	0.05	0.40	3.83	5.14	0.03	0.11	99.85
AD-11b-24US-03	0.02	76.20	0.00	0.08	13.05	0.04	0.80	0.08	0.31	3.84	5.27	0.20	0.08	100.12
AD-11b-24US-04	0.00	76.19	0.01	0.07	13.18	0.03	0.76	0.06	0.40	3.93	5.17	0.08	0.10	100.08
AD-12a-5US-01	0.02	76.65	0.00	0.06	13.13	0.03	0.47	0.20	0.54	4.20	4.40	0.25	0.04	96.00
AD-12a-5US-02	0.00	76.24	0.01	0.06	13.16	0.03	0.48	0.16	0.48	4.13	4.66	0.55	0.05	96.26
AD-12a-5US-03	0.07	75.07	0.00	0.03	12.27	0.03	0.47	0.19	0.54	4.12	4.40	2.79	0.03	97.90
AD-12a-5US-04	0.00	76.81	0.00	0.03	12.98	0.01	0.45	0.15	0.55	4.26	4.40	0.31	0.04	96.72
AD-12a-5US-05	0.00	77.01	0.04	0.07	13.04	0.01	0.44	0.14	0.51	4.09	4.60	0.00	0.05	95.71
AD-12a-5US-06	0.06	76.07	0.01	0.03	12.96	0.03	0.42	0.14	0.49	3.92	4.78	1.04	0.06	96.13
AD-12a-5US-07	0.02	76.78	0.00	0.06	13.24	0.01	0.43	0.15	0.48	4.08	4.55	0.17	0.03	95.76
AD-12b-5US-01	0.00	76.86	0.04	0.05	13.15	0.00	0.47	0.17	0.52	4.22	4.39	0.12	0.01	95.85
AD-12b-5US-02	0.00	76.77	0.01	0.09	13.20	0.01	0.45	0.18	0.48	4.19	4.39	0.18	0.04	95.80
AD-12b-5US-03	0.00	76.40	0.00	0.06	13.19	0.00	0.43	0.15	0.56	3.88	4.91	0.36	0.05	96.97
AD-12b-5US-04	0.00	77.20	0.02	0.08	12.12	0.04	0.47	0.17	0.58	3.73	5.13	0.44	0.02	94.69
AD-12b-5US-05	0.00	76.45	0.00	0.06	13.01	0.00	0.51	0.14	0.49	3.79	5.29	0.24	0.03	94.71
AD-12b-5US-06	0.04	77.20	0.01	0.04	13.08	0.02	0.54	0.11	0.49	3.28	5.03	0.08	0.08	95.44
AD-12b-5US-07	0.07	76.46	0.00	0.01	13.29	0.01	0.48	0.14	0.49	4.00	4.81	0.19	0.05	95.44
AD-12b-5US-08	0.02	77.44	0.00	0.08	11.89	0.00	0.49	0.17	0.57	4.24	4.62	0.47	0.02	93.33
AD-12b-5US-09	0.00	76.74	0.02	0.05	13.32	0.00	0.45	0.16	0.52	4.19	4.42	0.09	0.05	94.70
AD-12b-5US-10	0.02	76.87	0.01	0.01	12.93	0.05	0.43	0.14	0.47	3.96	4.63	0.41	0.05	96.10

Sample Number	P2O5	SiO2	SO2	TiO2	Al2O3	MgO	CaO	MnO	FeO	Na2O	K2O	F	Cl	N. Total
AD-12b-5US-11	0.00	76.58	0.00	0.00	13.23	0.00	0.49	0.17	0.47	4.21	4.40	0.40	0.05	95.34
AD-12b-5US-12	0.00	76.47	0.00	0.08	13.18	0.02	0.49	0.15	0.54	4.29	4.47	0.28	0.03	95.31
AD-12b-5US-14	0.04	76.55	0.01	0.06	13.21	0.00	0.48	0.16	0.45	4.24	4.45	0.29	0.04	96.18
AD-12b-5US-13	0.04	76.62	0.01	0.07	13.21	0.00	0.44	0.16	0.51	4.14	4.59	0.16	0.03	96.44
AD-12b-5US-15	0.03	75.94	0.02	0.10	13.23	0.01	0.48	0.12	0.48	4.23	4.48	0.85	0.03	95.97
AD-12b-5US-16	0.00	76.75	0.03	0.07	13.07	0.02	0.42	0.16	0.48	4.12	4.55	0.25	0.06	96.34
AD-12b-5US-17	0.00	78.97	0.00	0.06	13.47	0.00	0.47	0.14	0.60	1.63	4.47	0.16	0.03	92.40
AD-12c-5US-01	0.00	76.53	0.00	0.01	13.11	0.00	0.47	0.16	0.51	4.51	4.52	0.12	0.05	100.16
AD-12c-5US-02	0.05	76.03	0.01	0.05	13.28	0.00	0.41	0.14	0.48	4.61	4.36	0.53	0.05	100.52
AD-12c-5US-03	0.00	76.49	0.00	0.07	13.22	0.02	0.43	0.19	0.52	4.56	4.40	0.09	0.01	100.31
AD-12c-5US-04	0.00	77.00	0.00	0.05	12.69	0.00	0.51	0.16	0.48	4.50	4.42	0.18	0.02	97.75
AD-12c-5US-05	0.00	76.18	0.01	0.08	13.00	0.01	0.57	0.17	0.54	4.44	4.85	0.06	0.10	88.56
AD-12c-5US-06	0.00	75.02	0.02	0.05	13.30	0.00	0.44	0.11	0.39	5.38	3.99	1.24	0.06	105.42
AD-12c-5US-07	0.00	76.38	0.00	0.01	13.31	0.03	0.47	0.17	0.48	4.51	4.39	0.20	0.06	99.78
AD-12c-5US-08	0.02	75.50	0.00	0.05	13.29	0.00	0.44	0.18	0.46	4.47	4.31	1.25	0.04	99.64
AD-12c-5US-09	0.01	76.24	0.02	0.08	13.25	0.05	0.58	0.22	0.46	4.37	4.51	0.11	0.11	96.21
AD-12c-5US-10	0.02	76.30	0.02	0.10	13.15	0.00	0.44	0.15	0.49	4.49	4.56	0.24	0.04	100.03
AD-12c-5US-11	0.02	76.01	0.01	0.02	13.43	0.02	0.41	0.13	0.71	4.51	4.46	0.24	0.03	98.67
AD-12c-5US-12	0.00	76.63	0.00	0.06	13.05	0.00	0.43	0.16	0.43	4.51	4.45	0.22	0.06	97.76
AD-12c-5US-14	0.00	75.59	0.01	0.05	12.89	0.00	0.44	0.11	0.45	4.38	4.26	1.79	0.04	101.10
AD-12c-5US-15	0.03	76.51	0.04	0.03	13.08	0.00	0.45	0.16	0.44	4.56	4.41	0.26	0.04	99.98
AD-12c-5US-16	0.00	76.57	0.02	0.08	13.17	0.02	0.46	0.12	0.51	4.44	4.43	0.15	0.03	99.98
AD-12c-5US-17	0.00	76.62	0.02	0.08	13.31	0.03	0.45	0.14	0.56	4.40	4.28	0.06	0.06	99.82
AD-12d-5US-04	0.00	76.99	0.02	0.11	12.87	0.00	0.48	0.17	0.48	4.23	4.60	0.00	0.05	95.20
AD-12d-5US-05	0.04	76.71	0.00	0.11	13.08	0.00	0.43	0.18	0.53	4.00	4.48	0.40	0.05	97.06
AD-12d-5US-06	0.00	75.96	0.00	0.08	13.33	0.09	0.45	0.18	0.90	4.38	4.38	0.22	0.04	98.60
AD-12-5US-01	0.03	75.52	0.00	0.06	13.32	0.01	0.44	0.09	0.49	4.53	4.44	0.28	0.03	99.24
AD-12-5US-02	0.00	75.88	0.01	0.06	13.17	0.03	0.45	0.19	0.45	4.50	4.40	0.16	0.04	99.35
AD-12-5US-03	0.01	76.04	0.00	0.03	13.07	0.02	0.40	0.21	0.52	4.61	4.37	0.40	0.06	99.75
AD-12a-24US-01	-0.02	76.84	0.02	0.07	12.86	0.08	0.45	0.12	0.33	4.35	4.50	0.32	0.04	98.20
AD-12a-24US-02	-0.03	76.38	0.02	0.06	13.16	0.04	0.47	0.11	0.37	4.44	4.49	0.39	0.04	97.21
AD-12a-24US-03	0.01	76.63	0.02	0.03	13.15	0.05	0.47	0.14	0.31	4.52	4.35	0.27	0.04	99.10
AD-12a-24US-04	0.00	76.76	0.00	0.05	13.08	0.02	0.43	0.14	0.28	4.63	4.55	0.01	0.04	100.19
AD-12a-24US-05	0.01	76.52	0.00	0.04	13.11	0.03	0.49	0.14	0.58	4.38	4.32	0.31	0.04	100.59
AD-12a-24US-06	0.01	76.74	0.00	-0.02	12.89	0.04	0.52	0.14	0.46	4.56	4.33	0.24	0.05	99.20
AD-12a-24US-07	0.02	76.80	0.01	0.05	13.03	0.08	0.47	0.15	0.42	4.40	4.52	0.00	0.04	98.05

Sample Number	P2O5	SiO2	SO2	TiO2	Al2O3	MgO	CaO	MnO	FeO	Na2O	K2O	F	Cl	N. Total
AD-12a-24US-08	-0.01	76.54	0.00	0.06	13.04	0.08	0.49	0.14	0.48	4.41	4.45	0.23	0.04	99.50
AD-12a-24US-09	-0.03	76.63	0.03	0.03	12.92	0.06	0.38	0.16	0.46	4.53	4.60	0.17	0.03	100.08
AD-12a-24US-10	-0.02	76.54	0.01	0.06	12.99	0.10	0.48	0.17	0.49	4.52	4.47	0.13	0.02	100.83
AD-12b-24US-01	0.04	76.66	0.00	0.03	13.03	0.03	0.45	0.12	0.51	4.32	4.57	0.16	0.05	98.44
AD-12b-24US-02	-0.01	76.65	0.01	0.10	12.99	0.01	0.40	0.11	0.45	4.32	4.56	0.30	0.06	99.72
AD-12b-24US-03	-0.03	76.54	0.03	0.05	13.25	0.03	0.45	0.14	0.34	4.37	4.63	0.13	0.05	100.09
AD-12b-24US-04	0.03	76.21	0.00	0.12	13.04	0.03	0.49	0.13	0.45	4.35	4.69	0.38	0.04	99.79
AD-12b-24US-05	0.00	76.64	0.01	0.07	12.99	0.12	0.46	0.15	0.35	4.50	4.48	0.18	0.03	98.41
AD-12b-24US-06	-0.01	76.30	0.02	0.09	13.21	0.06	0.48	0.11	0.35	4.60	4.51	0.25	0.05	100.68
AD-12b-24US-07	0.01	78.08	0.02	0.05	13.27	0.06	0.51	0.13	0.39	2.50	4.58	0.29	0.04	99.85
Valles Caldera obsidian data														
AD-20a-24US-01	0.04	75.63	0.01	0.22	13.19	0.20	0.82	0.05	0.95	4.00	4.74	0.03	0.14	100.13
AD-20a-24US-02	0.00	76.13	0.00	0.23	12.81	0.16	0.88	0.03	0.97	3.83	4.82	0.08	0.07	98.69
AD-20a-24US-03	0.06	76.26	0.00	0.20	12.93	0.16	0.83	0.03	1.00	3.66	4.82	0.00	0.05	98.41
AD-20a-24US-04	0.04	76.30	0.00	0.19	13.11	0.16	0.71	0.05	0.87	3.66	4.86	0.00	0.06	99.09
AD-20a-24US-05	0.07	76.22	0.00	0.19	12.77	0.13	0.79	0.05	0.88	3.81	5.01	0.04	0.04	97.19
AD-20b-24US-01	0.04	75.54	0.01	0.11	13.34	0.16	1.21	0.07	0.87	4.10	4.47	0.03	0.06	98.35
AD-20b-24US-02	0.06	76.24	0.01	0.24	12.88	0.14	0.78	0.01	0.98	3.82	4.80	0.00	0.05	99.10
AD-20b-24US-03	0.02	76.13	0.00	0.16	12.94	0.14	0.74	0.03	0.92	3.92	4.96	0.01	0.03	98.11
AD-20b-24US-05	0.03	75.79	0.00	0.28	13.02	0.16	0.76	0.00	0.87	3.96	4.99	0.09	0.05	96.09
AD-21a-24US-01	0.00	76.64	0.01	0.07	12.45	0.02	0.38	0.08	0.97	4.28	4.87	0.11	0.14	98.69
AD-21a-24US-03	0.01	76.52	0.00	0.10	12.47	0.02	0.34	0.06	1.00	4.14	5.05	0.15	0.15	99.63
AD-21a-24US-04	0.00	76.92	0.00	0.11	12.31	0.01	0.35	0.09	0.75	4.22	5.03	0.08	0.11	97.86
AD-21a-24US-06	0.04	76.06	0.00	0.12	12.67	0.09	0.34	0.08	0.93	4.29	5.11	0.17	0.10	96.55
AD-21a-24US-07	0.04	77.33	0.03	0.07	11.84	0.02	0.34	0.02	0.90	4.25	5.01	0.06	0.11	97.95
AD-21a-24US-08	0.03	76.75	0.03	0.11	12.48	0.04	0.34	0.06	0.76	4.24	4.97	0.07	0.12	98.89
AD-22a-24US-01	0.01	76.61	0.00	0.15	12.49	0.04	0.36	0.04	0.81	4.28	4.93	0.15	0.13	98.12
AD-22a-24US-02	0.04	74.88	0.01	0.06	12.37	2.23	0.36	0.01	0.94	3.94	5.03	0.04	0.09	100.85
AD-22a-24US-03	0.00	76.63	0.00	0.12	12.41	0.06	0.33	0.05	0.96	4.06	5.08	0.20	0.10	98.74
AD-22a-24US-04	0.01	76.45	0.00	0.08	12.67	0.02	0.33	0.06	0.85	4.20	5.21	0.00	0.11	97.50
AD-22a-24US-05	0.00	76.93	0.00	0.08	12.66	0.02	0.33	0.04	0.79	3.95	5.09	0.00	0.10	99.20
AD-22a-24US-06	0.00	77.00	0.00	0.09	12.56	0.05	0.35	0.07	0.76	3.91	5.07	0.03	0.11	99.56
AD-22a-24US-07	0.01	76.68	0.00	0.01	12.58	0.04	0.37	0.08	0.91	4.08	5.09	0.07	0.08	99.57
AD-22a-24US-08	0.00	76.23	0.00	0.10	12.72	0.03	0.34	0.06	0.94	4.09	5.17	0.20	0.12	97.50
AD-23b-24US-01	0.02	76.47	0.01	0.11	12.56	0.03	0.33	0.06	1.07	4.25	4.82	0.15	0.11	100.30
AD-23b-24US-02	0.01	76.43	0.00	0.10	12.67	0.03	0.35	0.00	1.04	4.27	4.84	0.13	0.12	98.54

Sample Number	P2O5	SiO2	SO2	TiO2	Al2O3	MgO	CaO	MnO	FeO	Na2O	K2O	F	Cl	N. Total
AD-23b-24US-03	0.02	76.74	0.01	0.08	12.52	0.03	0.37	0.04	1.02	4.29	4.78	0.02	0.09	99.95
AD-23b-24US-04	0.00	76.70	0.00	0.12	12.51	0.03	0.32	0.02	1.02	4.33	4.85	0.00	0.10	100.07
AD-23b-24US-05	0.00	76.76	0.00	0.09	12.45	0.02	0.37	0.02	0.93	4.29	4.89	0.08	0.10	99.77
AD-23b-24US-06	0.01	76.57	0.01	0.15	12.52	0.03	0.33	0.06	1.00	4.28	4.78	0.15	0.12	99.32
AD-23b-24US-07	0.00	76.46	0.00	0.15	12.69	0.02	0.33	0.04	0.93	4.09	4.97	0.23	0.09	100.03
AD-23b-24US-08	0.02	76.47	0.02	0.13	12.31	0.01	0.37	0.11	1.04	4.11	5.26	0.04	0.11	100.15
AD-23a-24US-01	0.08	76.64	0.00	0.05	12.54	0.00	0.36	0.04	1.04	4.22	4.77	0.14	0.13	98.93
AD-23a-24US-02	0.04	76.93	0.00	0.11	12.45	0.02	0.33	0.02	0.97	4.12	4.85	0.03	0.11	98.67
AD-23a-24US-03	0.04	76.56	0.00	0.08	12.46	0.02	0.36	0.04	1.06	4.32	4.83	0.10	0.12	99.09
AD-23a-24US-04	0.01	76.75	0.02	0.10	12.48	0.00	0.32	0.02	0.99	4.23	4.86	0.12	0.09	98.56
AD-23a-24US-05	0.00	76.52	0.00	0.06	12.57	0.01	0.39	0.03	1.05	4.27	4.93	0.04	0.11	99.78
AD-23a-24US-06	0.00	76.57	0.03	0.11	12.48	0.03	0.33	0.05	0.83	4.33	4.92	0.21	0.10	99.80
AD-23a-24US-07	0.00	76.64	0.02	0.09	12.50	0.03	0.33	0.03	1.01	4.22	4.87	0.12	0.13	99.30
AD-23a-24US-08	0.01	76.64	0.00	0.15	12.57	0.02	0.30	0.08	0.95	4.16	4.78	0.23	0.12	99.63
AD-23a-24US-09	0.02	76.69	0.02	0.07	12.42	0.02	0.35	0.04	0.94	4.29	4.93	0.07	0.12	99.57
AD-23a-24US-10	0.00	76.73	0.00	0.08	12.60	0.02	0.38	0.02	1.11	4.20	4.61	0.15	0.12	99.43
AD-23a-24US-11	0.00	76.58	0.00	0.09	12.68	0.02	0.37	0.00	1.01	4.23	4.78	0.12	0.13	99.43
AD-23a-24US-12	0.00	76.91	0.03	0.02	12.38	0.00	0.36	0.04	0.97	4.28	4.81	0.11	0.09	99.25
AD-23a-24US-13	0.02	76.86	0.00	0.06	12.52	0.02	0.36	0.06	0.95	4.27	4.67	0.08	0.13	99.73
AD-23a-24US-14	0.00	76.68	0.01	0.10	12.48	0.01	0.35	0.09	0.95	4.32	4.76	0.12	0.11	99.28
AD-23a-24US-15	0.00	76.57	0.03	0.10	12.44	0.04	0.37	0.04	0.96	4.34	4.80	0.20	0.12	99.58
AD-23a-24US-16	0.00	76.89	0.00	0.08	12.45	0.01	0.42	0.03	0.97	4.23	4.77	0.04	0.10	99.70
AD-23a-24US-17	0.00	76.46	0.01	0.12	12.55	0.02	0.34	0.01	1.03	4.33	4.85	0.17	0.10	99.99
AD-23a-24US-18	0.00	76.73	0.00	0.09	12.50	0.01	0.34	0.05	0.92	4.27	4.82	0.11	0.13	99.33
AD-23a-24US-19	0.05	76.49	0.02	0.06	12.62	0.01	0.38	0.02	0.95	4.36	4.83	0.10	0.11	99.23
AD-23a-24US-20	0.04	76.79	0.02	0.09	12.37	0.02	0.34	0.07	0.98	4.30	4.78	0.06	0.13	99.57
AD-23a-24US-21	0.02	76.57	0.04	0.13	12.55	0.01	0.36	0.06	0.94	4.29	4.85	0.07	0.12	99.48
AD-23a-24US-22	0.00	76.23	0.01	0.14	12.71	0.02	0.32	0.08	0.94	4.26	4.94	0.23	0.13	100.45
AD-24a-24US-01	0.04	76.65	0.00	0.12	12.49	0.02	0.33	0.09	1.05	4.31	4.77	0.02	0.12	99.14
AD-24a-24US-02	0.03	76.91	0.00	0.02	12.46	0.04	0.34	0.07	1.08	4.18	4.74	0.00	0.13	99.36
AD-24a-24US-03	0.00	76.74	0.01	0.12	12.39	0.04	0.34	0.07	1.00	4.31	4.76	0.11	0.12	99.81
AD-24a-24US-04	0.02	76.58	0.02	0.09	12.55	0.06	0.33	0.04	1.01	4.21	4.82	0.13	0.15	100.00
AD-24a-24US-05	0.04	76.68	0.00	0.08	12.54	0.03	0.33	0.06	0.92	4.35	4.73	0.13	0.10	99.22
AD-24a-24US-06	0.01	76.34	0.09	0.08	12.43	0.02	0.38	0.06	1.06	4.44	4.72	0.19	0.19	99.13
AD-24a-24US-07	0.00	76.69	0.00	0.13	12.54	0.00	0.34	0.03	1.08	4.24	4.82	0.00	0.13	98.91
AD-24a-24US-08	0.00	76.69	0.01	0.13	12.50	0.05	0.32	0.06	0.99	4.19	4.86	0.09	0.11	98.78

Sample Number	P2O5	SiO2	SO2	TiO2	Al2O3	MgO	CaO	MnO	FeO	Na2O	K2O	F	Cl	N. Total
AD-24a-24US-09	0.03	76.65	0.00	0.14	12.39	0.06	0.37	0.07	0.84	4.48	4.73	0.11	0.14	99.94
AD-24Ma-24US-01	0.00	76.64	0.00	0.06	12.53	0.02	0.35	0.08	0.93	4.32	4.91	0.06	0.11	99.37
AD-24Ma-24US-02	0.00	76.73	0.00	0.10	12.52	0.01	0.38	0.03	0.97	4.28	4.75	0.09	0.12	100.19
AD-24Ma-24US-04	0.00	76.58	0.03	0.05	12.54	0.01	0.33	0.06	1.00	4.28	4.97	0.03	0.12	99.82
AD-24Ma-24US-05	0.00	76.72	0.02	0.06	12.49	0.01	0.38	0.02	1.04	4.28	4.79	0.07	0.11	97.68
AD-24Ma-24US-06	0.00	76.51	0.01	0.11	12.65	0.03	0.29	0.07	1.01	4.13	4.82	0.25	0.12	99.32
AD-24Ma-24US-07	0.00	76.43	0.02	0.12	12.57	0.05	0.40	0.07	1.01	4.41	4.69	0.05	0.18	99.42
AD-24Ma-24US-08	0.00	76.69	0.02	0.12	12.48	0.03	0.35	0.07	1.07	4.27	4.69	0.10	0.13	99.14
AD-24Ma-24US-09	0.00	76.81	0.03	0.09	12.53	0.03	0.30	0.04	0.98	4.16	4.88	0.03	0.13	99.82
AD-24Ma-24US-10	0.00	77.50	0.00	0.08	11.48	0.03	0.32	0.08	0.98	4.32	5.00	0.09	0.12	98.08
AD-24Ma-24US-11	0.04	76.76	0.02	0.08	12.49	0.03	0.37	0.07	0.89	4.23	4.66	0.27	0.09	99.24
AD-24Ma-24US-12	0.05	76.74	0.01	0.15	12.37	0.04	0.38	0.06	0.97	4.24	4.77	0.09	0.14	98.57
AD-24Ma-24US-13	0.00	76.49	0.00	0.08	12.57	0.04	0.33	0.05	1.02	4.29	4.82	0.18	0.13	99.62
AD-24Ma-24US-14	0.00	76.65	0.00	0.07	12.50	0.03	0.35	0.07	1.01	4.29	4.72	0.18	0.12	99.75
AD-24Ma-24US-15	0.00	76.52	0.01	0.12	12.56	0.04	0.35	0.07	1.01	4.25	4.75	0.22	0.10	99.79
AD-24Ma-24US-16	0.02	76.93	0.00	0.08	12.50	0.03	0.34	0.06	1.00	4.23	4.58	0.10	0.11	99.28
AD-26a-24US-02	0.00	76.60	0.01	0.05	12.48	0.02	0.38	0.07	1.07	4.16	4.84	0.20	0.10	100.15
AD-26a-24US-03	0.00	76.27	0.05	0.14	12.70	0.02	0.32	0.07	0.97	4.37	4.90	0.07	0.12	99.61
AD-26a-24US-04	0.00	76.38	0.01	0.10	12.56	0.02	0.36	0.07	1.03	4.37	4.79	0.14	0.16	99.55
AD-26a-24US-05	0.00	76.22	0.02	0.08	12.98	0.14	0.33	0.03	1.08	4.22	4.69	0.11	0.12	99.55
AD-26a-24US-06	0.00	76.42	0.00	0.08	12.70	0.03	0.36	0.11	1.06	4.20	4.76	0.15	0.14	98.78
AD-26a-24US-07	0.00	76.65	0.00	0.08	12.33	0.02	0.36	0.02	1.08	4.28	4.90	0.17	0.12	99.81
AD-26a-24US-08	0.03	76.61	0.01	0.11	12.57	0.03	0.39	0.07	0.98	4.29	4.81	0.00	0.11	99.92
AD-26a-24US-09	0.00	75.61	0.00	0.11	13.64	0.03	0.37	0.08	0.90	4.26	4.71	0.15	0.13	101.23
AD-26a-24US-10	0.00	76.44	0.00	0.09	12.39	0.04	0.41	0.08	1.03	4.39	4.87	0.15	0.11	99.83
AD-26b-5US-01	0.00	76.58	0.00	0.12	12.56	0.03	0.40	0.04	0.84	4.32	4.95	0.02	0.12	98.54
AD-26b-5US-02	0.00	76.21	0.00	0.12	12.68	0.04	0.34	0.08	0.93	4.45	4.90	0.13	0.12	100.31
AD-26b-5US-03	0.05	76.52	0.00	0.07	12.73	0.04	0.28	0.08	0.72	4.44	4.94	0.03	0.11	99.41
AD-26b-5US-04	0.00	76.38	0.02	0.14	12.72	0.01	0.39	0.10	0.82	4.40	4.73	0.17	0.12	99.63
AD-26b-5US-05	0.00	76.07	0.00	0.13	12.84	0.03	0.29	0.10	0.79	4.48	5.02	0.15	0.11	100.11
AD-26b-5US-06	0.01	76.35	0.01	0.11	12.69	0.02	0.36	0.11	0.79	4.39	5.04	0.00	0.12	99.39
AD-26b-5US-07	0.00	76.94	0.03	0.12	11.84	0.02	0.35	0.08	0.90	4.47	5.03	0.12	0.10	98.82
AD-26b-5US-08	0.01	76.30	0.00	0.20	12.77	0.02	0.34	0.06	0.82	4.42	4.83	0.11	0.11	99.76
AD-26b-5US-09	0.02	76.35	0.02	0.13	12.78	0.03	0.35	0.03	0.79	4.44	4.80	0.12	0.13	99.52
AD-26b-5US-10	0.00	76.47	0.00	0.16	12.64	0.05	0.38	0.03	0.75	4.31	5.02	0.02	0.15	98.44
AD-26b-5US-11	0.02	76.26	0.00	0.10	12.85	0.04	0.39	0.07	0.81	4.41	4.88	0.08	0.09	99.99

Sample Number	P2O5	SiO2	SO2	TiO2	Al2O3	MgO	CaO	MnO	FeO	Na2O	K2O	F	Cl	N. Total
AD-26b-5US-12	0.00	77.02	0.04	0.14	12.36	0.05	0.28	0.04	0.80	4.09	4.87	0.18	0.11	98.48
AD-26b-5US-13	0.00	76.28	0.02	0.14	12.86	0.02	0.27	0.09	0.66	4.39	5.01	0.14	0.11	99.37
AD-26b-5US-14	0.03	76.41	0.00	0.12	12.75	0.03	0.32	0.08	0.72	4.28	4.95	0.21	0.10	100.23
AD-26b-5US-15	0.00	76.20	0.00	0.13	12.77	0.04	0.37	0.10	0.93	4.34	4.96	0.04	0.12	99.63
AD-26b-5US-16	0.00	76.29	0.02	0.10	12.65	0.03	0.36	0.06	0.75	4.41	5.00	0.18	0.15	97.01
AD-26b-5US-17	0.00	76.42	0.00	0.07	12.86	0.06	0.34	0.02	0.88	4.41	4.74	0.04	0.13	99.03
AD-26b-5US-18	0.01	76.44	0.03	0.10	12.77	0.04	0.32	0.08	0.76	4.39	4.84	0.07	0.15	99.39
AD-28a-24US-01	0.00	76.14	0.01	0.24	13.07	0.11	0.78	0.02	0.83	3.76	4.88	0.11	0.05	99.70
AD-28a-24US-02	0.07	76.27	0.10	0.19	12.96	0.03	0.72	0.04	0.54	3.77	5.12	0.15	0.05	98.69
AD-28a-24US-03	0.06	76.10	0.00	0.21	13.16	0.04	0.74	0.04	0.70	3.85	5.02	0.00	0.08	99.73
AD-28a-24US-04	0.00	76.68	0.00	0.20	12.96	0.07	0.69	0.06	0.66	3.73	4.88	0.00	0.07	99.04
AD-28a-24US-05	0.04	76.56	0.00	0.20	12.98	0.04	0.59	0.05	0.67	3.69	5.04	0.07	0.07	99.48
AD-28a-24US-06	0.04	76.45	0.01	0.19	12.88	0.10	0.74	0.00	0.82	3.72	4.99	0.01	0.06	99.01
AD-28a-24US-07	0.03	76.50	0.03	0.17	12.81	0.05	0.68	0.05	0.68	3.88	4.97	0.11	0.03	99.45
AD-28a-24US-09	0.04	76.43	0.00	0.16	13.02	0.12	0.69	0.05	0.87	3.68	4.91	0.00	0.05	98.31
AD-28a-24US-10	0.04	76.71	0.01	0.24	12.77	0.05	0.68	0.06	0.69	3.73	4.91	0.07	0.05	98.91
AD-28a-24US-11	0.02	76.78	0.02	0.20	12.97	0.01	0.69	0.04	0.62	3.62	4.96	0.00	0.06	98.43
AD-30a-24US-02	0.00	75.87	0.00	0.21	13.08	0.23	0.94	0.03	1.12	3.67	4.79	0.00	0.06	98.54
AD-30a-24US-03	0.02	75.69	0.06	0.24	13.25	0.09	0.75	0.08	0.98	3.82	4.94	0.02	0.06	99.30
AD-30a-24US-04	0.04	76.21	0.00	0.20	13.02	0.14	0.88	0.10	0.98	3.75	4.64	0.00	0.05	97.87
AD-30a-24US-05	0.01	75.78	0.03	0.27	13.26	0.16	0.75	0.05	0.99	3.92	4.73	0.00	0.05	96.04
AD-30a-24US-06	0.04	75.75	0.02	0.22	13.07	0.08	0.75	0.02	1.00	3.63	5.16	0.17	0.09	97.29
AD-30a-24US-07	0.00	75.96	0.00	0.24	13.28	0.04	0.68	0.00	0.84	3.66	5.21	0.03	0.07	98.17
AD-30a-24US-08	0.00	75.96	0.00	0.19	12.95	0.18	0.96	0.02	1.06	3.78	4.74	0.07	0.09	98.99
AD-30a-24US-09	0.01	75.75	0.00	0.24	13.23	0.19	0.79	0.03	1.01	3.85	4.80	0.04	0.07	97.95
AD-30a-24US-10	0.05	75.79	0.00	0.24	13.15	0.08	0.84	0.09	1.02	3.81	4.86	0.00	0.07	98.69
AD-30a-24US-12	0.04	75.55	0.00	0.26	13.29	0.10	0.76	0.05	0.89	3.89	4.95	0.14	0.08	99.14
AD-30a-24US-13	0.03	75.76	0.02	0.23	13.21	0.08	0.74	0.00	0.88	3.87	5.04	0.07	0.06	99.38
AD-31b-5US-01	0.00	76.73	0.01	0.22	12.76	0.10	0.77	0.08	0.38	3.16	5.62	0.11	0.06	96.33
AD-31b-5US-02	0.05	76.41	0.05	0.16	12.94	0.07	0.78	0.03	0.35	3.20	5.70	0.19	0.07	96.53
AD-31b-5US-03	0.04	76.60	0.00	0.16	12.96	0.10	0.83	0.00	0.58	3.31	5.36	0.00	0.06	96.39
AD-31b-5US-04	0.05	76.49	0.02	0.22	12.84	0.12	0.75	0.03	0.48	3.18	5.66	0.11	0.04	97.48
AD-31b-5US-05	0.00	75.04	0.02	0.29	13.51	0.26	1.08	0.04	0.86	3.39	5.37	0.07	0.07	96.50
AD-31b-5US-06	0.05	75.53	0.02	0.26	13.36	0.13	1.00	0.06	0.45	3.28	5.78	0.00	0.06	96.98
AD-31b-5US-07	0.00	77.01	0.01	0.16	12.66	0.07	0.75	0.04	0.39	3.27	5.46	0.09	0.08	96.59
AD-31b-5US-08	0.01	75.96	0.02	0.23	13.16	0.10	0.92	0.04	0.50	3.27	5.65	0.07	0.08	95.77

Sample Number	P2O5	SiO2	SO2	TiO2	Al2O3	MgO	CaO	MnO	FeO	Na2O	K2O	F	Cl	N. Total
AD-31b-5US-09	0.05	75.81	0.01	0.19	12.80	0.19	0.86	0.03	1.17	3.28	5.44	0.06	0.10	95.84
AD-31b-5US-10	0.01	76.88	0.01	0.22	12.74	0.08	0.80	0.03	0.47	3.22	5.47	0.00	0.06	96.49
AD-31c-5US-03	0.00	76.54	0.01	0.19	12.96	0.11	0.84	0.02	0.46	3.40	5.41	0.00	0.05	95.17
AD-31c-5US-05	0.00	76.78	0.02	0.17	12.86	0.09	0.83	0.01	0.51	3.28	5.36	0.03	0.06	95.60
AD-31c-5US-08	0.03	76.61	0.02	0.20	12.82	0.11	0.81	0.04	0.66	3.30	5.35	0.00	0.05	96.27
AD-31c-5US-09	0.02	76.65	0.00	0.18	13.03	0.07	0.82	0.05	0.41	3.35	5.39	0.00	0.05	96.17
AD-31c-5US-11	0.02	76.76	0.00	0.20	12.81	0.10	0.81	0.04	0.63	3.16	5.33	0.07	0.06	95.25
Transects														
AD-10g-5US-01	-0.02	75.80	0.05	0.07	13.26	0.09	0.84	0.04	0.72	4.03	4.89	0.05	0.15	94.09
AD-10g-5US-02	0.02	76.16	0.01	0.08	13.37	0.02	0.79	0.06	0.50	3.94	4.75	0.19	0.10	96.23
AD-10g-5US-03	0.02	76.12	0.00	0.08	13.29	0.03	0.81	0.09	0.51	3.99	4.90	0.06	0.08	95.88
AD-10g-5US-04	0.02	76.06	0.00	0.01	13.34	0.02	0.73	0.10	0.51	3.95	5.03	0.14	0.08	96.11
AD-10g-5US-05	-0.02	76.20	0.01	0.08	13.33	0.02	0.72	0.06	0.50	3.94	4.97	0.09	0.08	96.26
AD-10g-5US-06	-0.01	76.23	0.00	0.04	13.28	0.03	0.77	0.10	0.45	4.06	4.82	0.11	0.08	97.01
AD-10g-5US-07	0.03	76.06	-0.01	0.06	13.27	0.03	0.78	0.10	0.51	4.07	4.89	0.10	0.09	98.02
AD-10g-5US-08	-0.01	75.94	0.02	0.10	13.39	0.02	0.77	0.06	0.55	4.04	4.99	0.05	0.07	98.25
AD-10g-5US-09	-0.08	75.72	-0.01	0.04	13.44	0.03	0.79	0.08	0.52	4.06	5.15	0.09	0.08	99.19
AD-10g-5US-10	-0.05	75.97	0.00	0.11	13.29	0.05	0.79	0.10	0.58	4.11	4.90	-0.01	0.08	98.96
AD-10g-5US-11	0.03	75.95	0.02	0.07	13.36	0.04	0.75	0.08	0.52	4.12	4.96	0.02	0.07	98.49
AD-10g-5US-12	0.01	75.95	0.02	0.06	13.37	0.02	0.77	0.07	0.57	4.07	5.00	-0.03	0.08	97.98
AD-10g-5US-13	0.04	75.79	0.01	0.07	13.49	0.03	0.76	0.02	0.53	4.07	4.91	0.24	0.05	98.39
AD-10g-5US-14	-0.03	75.95	0.02	0.09	13.43	0.03	0.76	0.07	0.54	4.05	4.88	0.09	0.09	98.63
AD-10g-5US-15	-0.02	75.67	0.01	0.05	13.36	0.04	0.74	0.10	0.58	4.16	4.90	0.31	0.07	98.66
AD-10g-5US-16	0.03	76.06	0.02	0.05	13.36	0.04	0.78	0.07	0.58	4.10	4.86	0.03	0.05	98.73
AD-10g-5US-17	0.02	75.91	0.02	0.10	13.35	0.03	0.73	0.08	0.60	4.11	4.93	0.06	0.07	98.45
AD-10g-5US-18	0.01	76.06	0.02	0.05	13.47	0.02	0.74	0.09	0.46	4.10	4.80	0.10	0.08	97.86
AD-10g-5US-19	0.00	75.97	0.00	0.07	13.42	0.01	0.80	0.11	0.51	4.03	4.99	-0.05	0.07	97.48
AD-10g-5US-20	0.05	76.04	0.01	0.01	13.28	0.04	0.80	0.13	0.54	4.30	4.64	0.08	0.07	96.58
AD-10g-5US-21	0.00	76.32	0.00	0.03	13.02	0.02	0.81	0.06	0.53	4.07	4.92	0.12	0.07	96.46
AD-10g-5US-22	-0.01	76.32	0.00	0.04	13.43	0.02	0.76	0.06	0.57	3.62	4.81	0.24	0.10	96.28
AD-10g-5US-23	0.01	75.97	0.01	0.08	13.46	0.01	0.77	0.08	0.53	4.14	4.83	0.00	0.09	95.35
AD-10g-5US-24	0.02	78.10	0.01	0.03	11.06	0.02	0.79	0.08	0.49	4.24	4.99	0.12	0.06	92.77
AD-10g-5US-25	0.01	76.18	0.03	0.13	13.25	0.01	0.84	0.10	0.48	3.82	5.04	-0.02	0.09	86.95
AD-10g-5US-26	0.02	75.95	0.00	0.06	13.20	0.04	0.83	0.10	0.53	4.21	4.88	0.12	0.07	98.03
AD-10g-5US-27	0.02	76.00	0.01	0.05	13.41	0.03	0.73	0.06	0.44	4.14	4.85	0.18	0.07	97.65
AD-10g-5US-28	-0.02	75.99	0.01	0.04	13.34	0.04	0.73	0.04	0.57	4.11	4.82	0.24	0.06	98.68

Sample Number	P2O5	SiO2	SO2	TiO2	Al2O3	MgO	CaO	MnO	FeO	Na2O	K2O	F	Cl	N. Total
AD-10g-5US-29	0.00	75.80	-0.03	0.08	13.30	0.03	0.80	0.09	0.55	4.09	4.71	0.47	0.08	97.79
AD-10g-5US-30	0.00	75.96	0.02	0.06	13.31	0.04	0.78	0.08	0.47	4.13	4.88	0.19	0.08	98.66
AD-10g-5US-31	-0.03	76.19	-0.01	0.06	13.25	0.02	0.76	0.07	0.51	4.06	5.01	-0.04	0.07	98.26
AD-10g-5US-32	0.03	76.06	0.00	0.06	13.28	0.06	0.82	0.05	0.56	4.03	4.79	0.20	0.06	98.37
AD-10g-5US-33	0.01	76.06	0.00	0.07	13.23	0.02	0.72	0.10	0.51	4.21	4.93	0.06	0.07	98.24
AD-10g-5US-34	0.03	75.98	0.02	0.05	13.19	0.03	0.81	0.07	0.63	4.10	5.00	0.01	0.08	98.01
AD-10g-5US-35	0.01	76.05	0.02	0.07	13.30	0.02	0.76	0.03	0.50	4.14	5.00	-0.02	0.08	98.16
AD-10g-5US-36	-0.01	75.99	0.03	0.08	13.38	0.02	0.79	0.08	0.59	4.13	4.81	0.02	0.08	97.07
AD-10g-5US-37	0.01	75.86	0.00	0.04	13.35	0.05	0.84	0.08	0.48	4.11	5.05	0.07	0.07	96.44
AD-10g-5US-38	0.03	75.96	0.02	0.04	13.35	0.02	0.78	0.04	0.59	4.02	5.05	-0.04	0.09	96.05
AD-10g-5US-39	0.04	75.96	-0.02	0.06	13.47	0.03	0.76	0.06	0.56	3.96	4.88	0.05	0.16	94.20
AD-10g-5US-40	0.02	76.07	0.01	0.07	13.27	0.02	0.80	0.05	0.46	3.99	5.06	0.02	0.16	94.23
AD-10g-5US-41	0.03	76.32	0.05	0.04	13.30	0.03	0.74	0.16	0.42	3.91	4.91	0.00	0.08	95.65

Notes:

5US= Five minute ultrasonic bath in DI water

5HF= Five minute ultrasonic bath in HF followed by a five minute ultrasonic bath in DI water

24US= Twenty-four hour ultrasonic bath in DI water

AA= Twenty-four hour air abrasion treatment followed by a five minute ultrasonic bath in DI water

Table B.3. Electron microprobe analysis of feldspar.

Valles Cladera Sanidine Data

Sample Number	SiO2	BaO	Al2O3	CaO	SrO	FeO	Na2O	K2O	Total
AD-25-01-01	68.38	0.02	20.92	0.98	0.03	0.20	8.57	4.40	103.49
AD-25-01-02	25.58	0.04	9.68	0.68	0.00	0.20	5.48	2.77	44.42
AD-25-01-03	62.28	0.02	19.83	1.19	0.03	0.20	8.84	3.70	96.10
AD-25-01-04	99.64	0.01	0.37	0.00	0.04	0.00	0.18	0.08	100.32
AD-25-02-01	67.25	0.00	20.49	0.96	0.02	0.21	7.93	4.80	101.66
AD-25-02-02	67.00	0.00	20.96	1.34	0.03	0.20	8.51	3.76	101.79
AD-25-02-03	63.25	0.01	19.76	1.35	0.03	0.20	7.57	3.62	95.79
AD-25-02-04	66.71	0.02	20.45	1.05	0.00	0.21	8.04	4.46	100.94
AD-25-02-05	100.08	0.02	0.32	0.00	0.00	0.02	0.10	0.09	100.63
AD-25-02-06	68.15	0.04	20.50	0.63	0.02	0.19	7.68	5.90	103.12
AD-27-01-01	66.88	0.06	20.02	0.48	0.00	0.17	6.61	7.23	101.45
AD-27-01-02	66.55	0.00	20.31	1.10	0.04	0.22	8.17	4.45	100.85
AD-27-01-03	67.18	0.00	20.60	1.14	0.02	0.22	8.22	4.38	101.76
AD-27-01-04	66.45	0.04	20.57	1.35	0.01	0.17	8.21	3.95	100.74
AD-27-01-05	66.57	0.00	20.37	0.95	0.00	0.18	7.80	5.16	101.02
AD-27-02-01	66.86	0.08	20.62	0.96	0.00	0.17	7.74	5.08	101.52
AD-27-02-02	66.25	0.08	19.36	0.43	0.04	0.14	5.84	8.02	100.16
AD-27-02-03	67.19	0.05	20.86	1.19	0.04	0.20	8.25	4.35	102.14
AD-54-01	65.40	0.05	19.39	0.37	0.00	0.15	6.07	7.94	99.36
AD-54-02	64.53	0.10	19.21	0.37	0.05	0.12	5.86	8.07	98.30
AD-54-03	66.58	0.00	20.65	1.05	0.00	0.10	8.12	4.46	100.96
AD-54-04	66.29	0.11	19.47	0.30	0.00	0.11	5.70	8.35	100.34
AD-54-05	66.15	0.08	19.39	0.39	0.00	0.12	6.00	7.88	100.01
AD-54-06	65.24	0.00	20.39	0.98	0.00	0.14	8.07	4.61	99.43
AD-54-07	65.37	0.00	19.34	0.34	0.00	0.11	5.89	8.00	99.05
AD-54-08	66.52	0.05	19.58	0.41	0.05	0.15	6.12	7.87	100.74
AD-54-09	66.67	0.06	19.40	0.29	0.00	0.11	5.87	8.08	100.48
AD-54-10	66.18	0.07	20.10	1.04	0.00	0.13	8.02	4.23	99.78
AD-54-11	65.37	0.00	19.28	0.31	0.00	0.08	5.77	8.35	99.16
AD-54-12	66.62	0.06	19.41	0.30	0.00	0.13	5.81	8.27	100.59
AD-54-13	67.07	0.06	19.49	0.31	0.00	0.13	6.07	8.26	101.40
AD-54-15	66.36	0.06	20.07	0.92	0.00	0.11	7.86	4.80	100.17

Sample Number	SiO2	BaO	Al2O3	CaO	SrO	FeO	Na2O	K2O	Total
AD-54-16	65.00	0.07	19.35	0.39	0.00	0.10	6.18	7.65	98.73
AD-54-17	64.86	0.00	20.09	1.08	0.05	0.13	7.93	4.42	98.56
AD-54-18	66.62	0.00	19.42	0.30	0.00	0.12	6.10	7.99	100.54
AD-54-19	65.72	0.09	19.69	0.45	0.00	0.11	6.41	7.60	100.07
AD-54-21	65.08	0.00	20.55	1.20	0.00	0.12	8.35	3.67	98.99
AD-55-01	65.51	0.00	19.29	0.35	0.00	0.13	5.94	7.91	99.13
AD-55-02	66.73	0.13	19.57	0.32	0.08	0.10	6.26	8.01	101.19
AD-55-04	66.38	0.09	19.54	0.33	0.00	0.14	5.92	8.28	100.68
AD-55-05	66.48	0.00	19.46	0.35	0.05	0.11	6.22	7.92	100.59
AD-55-06	66.15	0.08	20.52	1.20	0.06	0.12	8.55	4.07	100.74
AD-55-08	66.34	0.06	19.49	0.32	0.00	0.11	6.17	8.11	100.60
AD-55-09	67.03	0.00	19.66	0.27	0.06	0.08	6.12	8.31	101.53
AD-55-10	66.22	0.11	19.51	0.34	0.00	0.10	6.10	7.95	100.33
AD-55-11	66.61	0.00	20.62	1.10	0.00	0.11	8.19	4.19	100.81
AD-55-12	65.90	0.00	19.35	0.37	0.00	0.10	6.05	8.00	99.77
AD-55-13	65.18	0.00	20.34	1.11	0.00	0.16	8.11	4.08	98.98
AD-55-14	67.09	0.12	19.89	0.48	0.00	0.11	6.80	7.27	101.76
AD-55-15	66.52	0.08	20.23	0.87	0.00	0.13	7.84	5.12	100.78
AD-55-16	66.00	0.13	19.54	0.35	0.00	0.12	5.90	8.23	100.26
AD-55-17	66.54	0.00	19.62	0.35	0.00	0.13	6.06	8.11	100.80
AD-55-18	67.11	0.05	19.85	0.30	0.00	0.14	6.11	8.40	101.96
AD-55-21	66.44	0.09	19.60	0.38	0.05	0.09	6.12	8.11	100.87
AD-55-22	66.37	0.00	19.50	0.32	0.00	0.14	6.11	8.08	100.51
AD-55-24	66.31	0.00	20.51	1.17	0.07	0.10	8.35	4.16	100.68
AD-55-25	66.08	0.00	21.14	1.81	0.00	0.17	9.27	2.18	100.64
AD-55-26	65.79	0.11	19.40	0.30	0.00	0.08	5.65	8.44	99.78
AD-55-22	66.37	0.00	19.50	0.32	0.00	0.14	6.11	8.08	100.51
AD-55-24	66.31	0.00	20.51	1.17	0.07	0.10	8.35	4.16	100.68
AD-55-25	66.08	0.00	21.14	1.81	0.00	0.17	9.27	2.18	100.64
AD-55-26	65.79	0.11	19.40	0.30	0.00	0.08	5.65	8.44	99.78

Appendix B. Table B.4: Electron microprobe precision of standard analyses and accepted values.

	VG-568			Orthoclase		
Number of Analyses:	23					
	Average	Standard Deviation	Accepted Value	Average	Standard Deviation	Accepted Value
SiO_2	76.04	±0.70	76.71	64.54	±0.58	64.79
TiO_2	0.09	±0.03	0.12			
Al_2O_3	12.06	±0.18	12.06	16.67	±0.10	16.72
FeO	1.11	±0.05	1.23	1.78	±0.04	1.88
MnO	0.04	±0.02	0.03			
MgO	0.03	±0.04				
CaO	0.43	±0.04	0.50	0.00	±0.01	
Na_2O	4.00	±0.26	3.75	0.93	±0.04	0.91
K_2O	4.99	±0.13	4.89	15.72	±0.11	15.49
P_2O_5	0.01	±0.01				
F	0.24	±0.10				
SO_2	0.04	±0.02				
Cl	0.10	±0.02				
SrO				0.00	±0.02	
BaO				0.05	±0.02	0.05

APPENDIX C.1: AR-AR PREPARATION TECHNIQUES

A more complete description of sample preparation techniques for the Ar-Ar dating method is described below. For full irradiation statistics including sample numbers per irradiated package, correction factors, irradiation positions and times, and sensitivities for the furnace and laser during analysis see Table C.1.

Calcium and potassium salts were irradiated with samples and monitors to measure interfering reactions produced while in the reactor. Six monitor sanidine crystals were fused per monitor position and averaged to determine the J value per crystal location. A sine curve was then fit to the disk to give appropriate J values to all samples. It was shown that a 3-4% gradient in the J factor is present from the NM-183 irradiation due not being rotated properly, thus affecting the No Agua samples slightly.

All samples were analyzed at the New Mexico Institute of Mining and Technology using a Mass Analyzer Products (MAP) 215-50 with extended geometry. The automated, all-metal vacuum extraction line consists of two stages, connected to the spectrometer. All gas is run through the second stage, which consists of two SAES GP-50 getters operating at temperatures of 450° C and 20° C to remove reactive gasses. Furnace samples were also subjected to one other getter from the first stage, operating at a temperature of ~450° C. All gas was exposed to a ~2000° C W filament and a cold finger operating at a temperature of -140° C. Signals were multiplied in the mass spectrometer using an electron multiplier; sensitivities are listed in Table C.1. All runs were corrected for backgrounds and isotopic fits. System blanks and background for the

CO_2 laser averaged 2_E-16±9_E-18, 5_E-18±7_E-19, 6_E-19±2_E-19, 9_E-19±2_E-19, and 1_E-18±1_E-19 moles at masses 40, 39, 38, 37, and 36 respectively based on air shots measured periodically throughout the analysis. When using the furnace, the average system blanks for masses 40, 39, 38, 37, and 36 were 1_E-15±1_E-17, 1_E-17±1_E-18, 1_E-18±3_E-19, 3_E-18±4_E-19, and 3_E-18±4_E-19 moles respectively All $^{40}Ar/^{39}Ar$ data in this study is reported at the 2σ confidence level and ages were determined using the decay constants and atmospheric intercept suggested by Steiger and Jager (1977). Peak intensities of argon isotopes were measured in seven cycles. Masses 36, 37, and 38 were isotopically fit to a linear curve, whereas masses 39 and 40 were fit to either a linear or parabolic fit depending on the behavior of the peak regressions. The background was fit to an average Y ± the standard deviation or by bracketing blanks; isotopic fits were then applied to the background corrections. All of the corrections were then applied to unknowns.

Full raw data from all Ar-Ar analyses can be seen in Tables C.2 through C.4. Table C.2 through C.4 are listed according to extraction method used. Included in each analysis is the J factor for the sample, the discrimination value, the irradiation package number including disk, and the lab I.D. number. Sample weights are listed for multiple-step heating schedules. All isotopic ratios have been corrected for blank, radioactive decay and mass discrimination, but have not been corrected for interfering reactions. Appendix C.5 shows ideograms and spectra of individual samples used in this study.

Appendix C. Table C.1: Irradiation data including position and duration, monitor age used, correction factors, samples from each package, and furnace and laser sensitivity durnig the times of analyses per irradiation package.

Irradiation	NM-160	NM-172	NM-183	NM-190	NM-193
Reactor Facility	Texas A&M	Texas A&M	McMaster	Texas A&M	Texas A&M
Position	D3	D3	C5	D3	D3
Time irradiated	7 hrs	7 hrs	3.5 mWhrs	1 hr	1hr
Monitor Age (Ma)	27.84	27.84	28.02	28.02	28.02
Correction Factors:					
(36Ar/37Ar)Ca	0.00028±0.000005	0.00028±0.00005	0.00028±0.000005	0.00068±0.00002	0.00028±1e-05
(39Ar/37Ar)Ca	0.0007±0.00002	0.0007±0.00002	0.00077±0.00002	0.00029±0.000005	0.0007±5e-05
(40Ar/39Ar)K	0.0002±0.0003	0.0002±0.0003	0.00008±0.00003	0.00002±0.000005	0±0.0004
Samples Irradiated	AD-54--AD-55	AD-50--AD-53	AD-01--AD-12	AD-21--AD-28	AD-20, 30, 31
Furnace Sensitivity	2.6E-16	2.6E-16	1.9E-16	1.9E-16	3.0E-16
Laser Sensitivity	1.4E-16	1.5E-16	1.0E-16	1.1E-16	1.7E-16

Appendix C. Table C.2. $^{40}Ar/^{39}Ar$ furnace and laser step-heat analytical data.

	ID	Temp (°C)	$^{40}Ar/^{39}Ar$	$^{37}Ar/^{39}Ar$	$^{36}Ar/^{39}Ar$ (x 10^{-3})	$^{39}Ar_K$ (x 10^{-15} mol)	K/Ca	$^{40}Ar^*$ (%)	^{39}Ar (%)	Age (Ma)	±1σ (Ma)
	AD-02 5HF, , 29.63 mg, J=0.0008785±0.43%, D=1.005±0.001, NM-183G, Lab#=55240-15										
xi	A	650	26.32	0.0737	79.44	5.77	6.9	10.7	2.4	4.47	0.26
xi	B	750	11.53	0.0734	30.76	6.3	7.0	21.0	4.9	3.83	0.18
xi	C	850	11.39	0.0749	30.04	12.1	6.8	22.0	9.9	3.95	0.11
xi	D	885	11.33	0.0747	30.19	13.2	6.8	21.1	15.3	3.78	0.11
	E	910	11.32	0.0739	30.02	13.9	6.9	21.5	21.0	3.836	0.099
	F	950	11.29	0.0724	29.65	17.8	7.1	22.2	28.3	3.965	0.087
	G	1025	11.33	0.0752	29.82	27.9	6.8	22.1	39.8	3.961	0.079
	H	1100	11.17	0.0744	29.33	39.5	6.9	22.3	56.0	3.933	0.071
	I	1210	11.74	0.0738	30.93	40.0	6.9	22.0	72.4	4.084	0.073
xi	J	1250	11.97	0.0729	31.06	38.9	7.0	23.2	88.3	4.390	0.075
xi	K	1300	10.99	0.0723	27.06	8.8	7.1	27.2	91.9	4.71	0.13
xi	L	1350	12.49	0.0746	33.34	2.19	6.8	21.0	92.8	4.14	0.42
xi	M	1700	12.80	0.0782	32.74	17.5	6.5	24.3	100.0	4.91	0.10
	Integrated age ± 2σ			n=13		243.7	6.9	K2O=3.60%		4.13	0.14
	Plateau ± 2σ	steps E-I		n=5	MSWD=1.14	139.1	6.9 ±0.2		57.1	3.97	0.08
	Isochron±2σ	steps E-I		n=5	MSWD=0.57		$^{40}Ar/^{36}Ar$=	359.9±88.8		0.92	1.28
	AD-02 5US, , 31.4 mg, J=0.0008657±0.37%, D=1.005±0.001, NM-183G, Lab#=55241-01										
	A	650	13.31	0.0722	36.37	4.35	7.1	19.2	1.8	3.97	0.23
	B	750	9.117	0.0749	22.02	5.90	6.8	28.5	4.3	4.04	0.17
	C	850	8.983	0.0741	21.49	18.551	6.9	29.2		4.08	0.10
	D	885	8.868	0.0757	21.69	10.4	6.7	27.6	16.4	3.80	0.11
	E	910	9.168	0.0772	22.45	4.31	6.6	27.5	18.2	3.92	0.22
	F	950	8.838	0.0742	21.49	7.9	6.9	28.0	21.5	3.85	0.13
	G	1025	8.896	0.0749	21.29	24.0	6.8	29.1	31.6	4.031	0.064
	H	1100	9.068	0.0764	21.79	31.4	6.7	28.9	44.7	4.071	0.062
	I	1210	9.032	0.0744	21.88	48.6	6.9	28.3	65.0	3.971	0.055
xi	J	1250	9.238	0.0736	21.64	45.5	6.9	30.7	84.1	4.403	0.056
xi	K	1300	8.909	0.0720	20.42	15.7	7.1	32.1	90.6	4.453	0.080
xi	L	1350	9.801	0.0721	22.87	1.75	7.1	30.9	91.4	4.71	0.49
xi	M	1700	9.270	0.0765	21.79	20.6	6.7	30.4	100.0	4.384	0.072
	Integrated age ± 2σ			n=13		238.9	6.8	K2O=3.38%		4.15	0.10
	Plateau ± 2σ	steps A-I		n=9	MSWD=0.89	155.4	6.8 ±0.3		65.0	4.00	0.07
	Isochron±2σ	steps A-I		n=9	MSWD=0.99		$^{40}Ar/^{36}Ar$=	295.1±20.4		4.01	0.67
	AD-02 5HF, , 13.78 mg, J=0.0008785±0.43%, D=1.005±0.001, NM-183G, Lab#=55240-16										
	A	5	12.27	0.0726	32.80	7.7	7.0	20.9	5.3	4.05	0.11
	B	10	11.88	0.0747	31.69	42.1	6.8	21.1	34.2	3.953	0.067
	C	12	12.67	0.0739	33.87	60.9	6.9	20.9	76.0	4.187	0.070
xi	D	14	11.40	0.0742	29.38	29.3	6.9	23.7	96.1	4.266	0.067
xi	E	17	11.54	0.0737	29.40	3.95	6.9	24.6	98.9	4.48	0.15
xi	F	20	11.23	0.0696	27.71	0.74	7.3	27.0	99.4	4.79	0.68
xi	G	23	10.94	0.0668	25.72	0.277	7.6	30.4	99.5	5.3	1.8
xi	H	27	9.841	0.0679	18.57	0.277	7.5	44.2	99.7	6.9	1.8
xi	I	30	8.741	0.0660	21.17	0.251	7.7	28.3	99.9	3.9	1.9
xi	J	50	6.997	0.0644	11.66	0.130	7.9	50.7	100.0	5.6	3.7
	Integrated age ± 2σ			n=10		145.6	6.9	K2O=4.62%		4.15	0.14
	Plateau ± 2σ	steps A-C		n=3	MSWD=2.87	110.6	6.9 ±0.2		76.0	4.06	0.15
	Isochron±2σ	steps A-C		n=3	MSWD=0.03		$^{40}Ar/^{36}Ar$=	363.4±65.9		0.5	3.0
	AD-30 blk 24US, Obsidian, 7.4 mg, J=0.0001756±0.18%, D=1.003±0.001, NM-193K, Lab#=56068-01										
	A	4	10.61	0.0814	32.17	0.219	6.3	10.5	4.7	0.35	0.40
	B	8	1.255	0.0927	1.395	0.898	5.5	67.8	24.2	0.269	0.095

C	10	1.298	0.1151	2.009	1.200	4.4	55.0	50.2	0.226	0.074
D	12	1.421	0.2242	1.837	1.104	2.3	63.1	74.1	0.284	0.079
E	14	2.014	0.4674	5.743	0.473	1.1	17.7	84.3	0.11	0.18
F	16	2.213	0.4762	1.392	0.194	1.1	83.2	88.5	0.58	0.45
G	20	1.733	0.4006	3.520	0.289	1.3	41.9	94.8	0.23	0.30
H	30	4.922	0.7998	10.96	0.241	0.64	35.6	100.0	0.55	0.36
Integrated age ± 2σ			n=8		4.62	2.1	K2O=1.36%		0.22	0.11
Plateau ± 2σ	steps A-H		n=8	MSWD=0.32	4.62	3.3 ±4.5		100.0	0.257	0.088
Isochron±2σ	steps A-H		n=8	MSWD=0.34		$^{40}Ar/^{36}Ar$=	315.5±84.1		0.24	0.11

AD-30 clr 24US, Obsidian, 13.2 mg, J=0.0001747±0.18%, D=1.003±0.001, NM-193K, Lab#=56067-01

A	4	49.35	0.0784	83.50	0.106	6.5	50.0	35.0	7.76	0.92
B	8	22.43	0.0929	45.49	0.163	5.5	40.1	88.7	2.83	0.58
C	10	18.69	0.0851	25.81	0.025	6.0	59.2	96.9	3.5	3.5
D	12	87.78	0.8738	563.7	0.005	0.58	-89.7	98.5	-25.0	24.4
E	14	81.12	0.5380	291.9	0.005	0.95	-6.3	100.1	-1.6	18.2
F	16	443.6	0.0344	2639.8	0.001	14.8	-75.9	100.3	-109.3	571.8
G	20	-1345.5240	7.752	-12319.8000	0.000	0.066	-170.6	100.2	611.1	######
Xi H	30	-4286.6370	5.687	-14245.6400	-0.001	0.090	1.8	100.0	-24.4	186.1
Integrated age ± 2σ			n=8		0.303	6.0	K2O=0.05%		2.2	1.7
Plateau ± 2σ	steps A-G		n=7	MSWD=3.68	0.304	5.8 ±10.3		100.2	4.2	1.9
Isochron±2σ	steps A-G		n=7	MSWD=1.75		$^{40}Ar/^{36}Ar$=	604.3±279.6		-1.22	0.92

AD-20 Nite, Obsidian, 15.2 mg, J=0.0001743±0.18%, D=1.003±0.001, NM-193K, Lab#=56066-01

xi A	3	45.53	0.1275	70.75	0.264	4.0	54.1	1.3	7.73	0.44
xi B	5	16.45	0.1202	8.289	3.01	4.2	85.2	15.9	4.401	0.052
C	8	6.641	0.1057	5.216	11.60	4.8	76.9	72.1	1.606	0.015
D	10	8.415	0.1252	10.20	3.14	4.1	64.3	87.3	1.701	0.044
xi E	12	23.87	0.1068	51.46	0.581	4.8	36.3	90.1	2.72	0.19
xi F	14	18.76	0.0940	62.07	0.367	5.4	2.3	91.9	0.13	0.28
xi G	16	23.78	0.1101	76.16	0.285	4.6	5.4	93.3	0.41	0.36
xi H	20	18.03	0.0614	62.11	0.477	8.3	-1.8	95.6	-0.10	0.20
xi I	30	22.71	0.0949	75.59	0.904	5.4	1.7	100.0	0.12	0.17
Integrated age ± 2σ			n=9		20.6	4.7	K2O=2.99%		1.996	0.040
Plateau ± 2σ	steps C-D		n=2	MSWD=4.23	14.742	4.667±1.062		71.5	1.62	0.058
Isochron±2σ	steps C-D		n=2	MSWD=0.00		$^{40}Ar/^{36}Ar$=	356.4±69.0		1.507	0.128

AD-31, Obsidian, 26.9 mg, J=0.0001762±0.23%, D=1.003±0.001, NM-193K, Lab#=56069-01

A	3	48.59	0.0851	162.3	1.289	6.0	1.3	1.8	0.20	0.16
B	5	5.151	0.0837	17.43	10.96	6.1	0.1	17.1	0.002	0.018
C	8	5.125	0.0861	17.25	20.7	5.9	0.7	45.9	0.011	0.013
D	10	5.446	0.0970	18.41	18.6	5.3	0.2	71.8	0.004	0.014
E	12	4.901	0.0988	16.49	12.12	5.2	0.7	88.7	0.012	0.017
F	14	5.235	0.1103	17.23	4.20	4.6	2.9	94.6	0.049	0.035
G	16	4.750	0.1095	15.09	1.68	4.7	6.3	96.9	0.096	0.064
H	20	5.170	0.1184	18.62	0.979	4.3	-6.3	98.3	-0.103	0.099
I	30	6.249	0.1115	21.20	1.209	4.6	-0.1	100.0	-0.002	0.081
Integrated age ± 2σ			n=9		71.7	5.5	K2O=5.81%		0.014	0.021
Plateau ± 2σ	steps A-I		n=9	MSWD=0.77	71.7	5.5 ±1.4		100.0	0.010	0.015
Isochron±2σ	steps A-I		n=9	MSWD=0.70		$^{40}Ar/^{36}Ar$=	299.4±7.1		-0.012	0.011

AD-50, Obsidian, D2:172, 70.20 mg obsidian, J=0.0007275±0.11%, D=1.005±0.001, NM-172, Lab#=54425-01

Xi A	5	1.646	0.0327	2.844	6.7	15.6	49.1	1.2	1.061	0.019
B	10	0.9536	0.0335	0.1988	76.3	15.2	94.1	15.4	1.178	0.003
C	15	0.9155	0.0324	0.0517	186.2	15.7	98.6	50.0	1.185	0.002
D	17	0.9239	0.0332	0.0727	126.5	15.4	98.0	73.5	1.188	0.002
E	20	0.9315	0.0327	0.0987	104.0	15.6	97.2	92.8	1.188	0.002
F	23	1.249	0.0327	1.185	32.9	15.6	72.2	98.9	1.183	0.006
G	27	1.982	0.0333	3.653	6.1	15.3	45.7	100.0	1.188	0.020

	Integrated age ± 2σ		n=7		538.8	15.5	K2O=4.05%			1.184	0.004
	Plateau ± 2σ	steps B-G	n=6	MSWD=1.75	532.1	15.5 ±0.4		98.8		1.185	0.004
	Isochron±2σ	steps B-G	n=6	MSWD=2.08		$^{40}Ar/^{36}Ar$=	294.1±6.0			1.186	0.003
	AD-51, Obsidian, D1:172, 62.40 mg obsidian, J=0.0007282±0.11%, D=1.005±0.001, NM-172, Lab#=544424-01										
Xi	A	5	16.23	0.0333	52.85	8.0	15.3	3.8	1.8	0.81	0.11
Xi	B	10	1.274	0.0320	1.385	74.7	15.9	68.1	18.5	1.139	0.006
	C	15	1.878	0.0334	3.345	107.3	15.3	47.5	42.4	1.172	0.008
	D	17	1.239	0.0335	1.184	84.2	15.2	72.0	61.3	1.172	0.005
	E	20	1.133	0.0325	0.8392	87.4	15.7	78.4	80.8	1.166	0.004
	F	23	1.205	0.0334	1.094	68.0	15.3	73.4	96.0	1.162	0.004
	G	25	1.432	0.0334	1.868	10.6	15.3	61.7	98.3	1.160	0.013
	H	27	1.812	0.0341	3.268	3.6	15.0	46.9	99.2	1.115	0.028
Xi	I	30	1.996	0.0323	3.753	3.8	15.8	44.6	100.0	1.169	0.027
	Integrated age ± 2σ		n=9		447.6	15.5	K2O=3.78%			1.157	0.012
	Plateau ± 2σ	steps C-H	n=6	MSWD=1.33	361.1	15.4 ±0.5		80.7		1.166	0.006
	Isochron±2σ	steps C-H	n=6	MSWD=1.58		$^{40}Ar/^{36}Ar$=	296.1±5.1			1.165	0.010
	AD-52, Obsidian, D3:172, 73.49 mg obsidian, J=0.0007284±0.11%, D=1.005±0.001, NM-172, Lab#=54426-01										
Xi	A	5	3.331	0.0325	8.920	5.9	15.7	21.0	1.0	0.917	0.031
Xi	B	10	0.9711	0.0335	0.3263	65.7	15.3	90.4	12.6	1.153	0.003
	C	15	0.9775	0.0334	0.2829	224.4	15.3	91.8	52.1	1.178	0.002
	D	17	0.9333	0.0331	0.1496	142.6	15.4	95.6	77.2	1.172	0.002
	E	20	0.9103	0.0330	0.0778	94.2	15.5	97.8	93.8	1.169	0.003
	F	23	0.9304	0.0332	0.1385	31.8	15.4	95.9	99.4	1.172	0.004
	G	27	1.022	0.0347	0.4797	3.6	14.7	86.4	100.0	1.161	0.015
	Integrated age ± 2σ		n=7		568.2	15.4	K2O=4.08%			1.169	0.005
	Plateau ± 2σ	steps C-G	n=5	MSWD=2.06	496.6	15.4 ±0.6		87.4		1.173	0.004
	Isochron±2σ	steps C-G	n=5	MSWD=0.80		$^{40}Ar/^{36}Ar$=	323.7±23.9			1.167	0.006
	AD-53, Obsidian, D4:172, 70.03mg obsidian, J=0.00073±0.10%, D=1.005±0.001, NM-172, Lab#=54427-01										
Xi	A	5	1.759	0.0333	3.183	7.3	15.3	46.7	1.3	1.081	0.019
Xi	B	10	1.990	0.0331	3.824	76.5	15.4	43.4	14.9	1.136	0.010
Xi	C	15	4.066	0.0329	11.16	258.2	15.5	18.9	61.0	1.014	0.020
	D	17	1.062	0.0330	0.6401	112.3	15.5	82.5	81.0	1.154	0.003
	E	20	1.077	0.0327	0.6936	86.9	15.6	81.2	96.5	1.151	0.004
	F	23	1.276	0.0333	1.368	18.1	15.3	68.6	99.8	1.152	0.009
Xi	G	27	1.195	0.0285	0.4383	1.4	17.9	89.4	100.0	1.406	0.044
	Integrated age ± 2σ		n=7		560.8	15.5	K2O=4.21%			1.086	0.022
	Plateau ± 2σ	steps D-F	n=3	MSWD=0.09	217.4	15.5 ±0.3		38.8		1.153	0.005
	Isochron±2σ	steps D-F	n=3	MSWD=0.17		$^{40}Ar/^{36}Ar$=	294.6±20.3			1.153	0.019

Notes:

Isotopic ratios corrected for blank, radioactive decay, and mass discrimination, not corrected for interfering reactions.
Errors quoted for individual analyses include analytical error only, without interfering reaction or J uncertainties.
Integrated age calculated by summing isotopic measurements of all steps.
Integrated age error calculated by quadratically combining errors of isotopic measurements of all steps.
Plateau age is inverse-variance-weighted mean of selected steps.
Plateau age error is inverse-variance-weighted mean error (Taylor, 1982) times root MSWD where MSWD>1.
Plateau error is weighted error of Taylor (1982).
Decay constants and isotopic abundances after Steiger and Jäger (1977).
symbol preceding sample ID denotes analyses excluded from plateau age calculations.
Weight percent K_2O calculated from ^{39}Ar signal, sample weight, and instrument sensitivity.
Ages calculated relative to FC-2 Fish Canyon Tuff sanidine interlaboratory standard at 28.02 Ma
Decay Constant (LambdaK (total)) = 5.543e-10/a
Correction factors for NM-172:
$(^{39}Ar/^{37}Ar)_{Ca}$ = 0.0007 ± 2e-05
$(^{36}Ar/^{37}Ar)_{Ca}$ = 0.00028 ± 5e-06

$(^{36}Ar/^{39}Ar)_K$ = 0.012
$(^{40}Ar/^{39}Ar)_K$ = 0.0002 ± 0.0003
Correction factors for NM-183:
$(^{39}Ar/^{37}Ar)_{Ca}$ = 0.00077 ± 2e-05
$(^{36}Ar/^{37}Ar)_{Ca}$ = 0.000276 ± 5e-06
$(^{38}Ar/^{39}Ar)_K$ = 0.0127
$(^{40}Ar/^{39}Ar)_K$ = 0.03 ± 0.002
Correction factors for NM-193:
$(^{39}Ar/^{37}Ar)_{Ca}$ = 0.0007 ± 5e-05
$(^{36}Ar/^{37}Ar)_{Ca}$ = 0.00028 ± 1e-05
$(^{38}Ar/^{39}Ar)_K$ = 0.013
$(^{40}Ar/^{39}Ar)_K$ = 0 ± 0.0004

5US= short ultrasonic, 24US= long ultrasonic, AA= air abrasion, and 5HF= HF preparation treatments respectively

Appendix C. Table C.3. $^{40}Ar/^{39}Ar$ analytical data of the two-step heating schedule for obsidian.

	ID	$^{40}Ar/^{39}Ar$	$^{37}Ar/^{39}Ar$	$^{36}Ar/^{39}Ar$ (x 10^{-3})	$^{39}Ar_K$ (x 10^{-15} mol)	K/Ca	$^{40}Ar^*$ (%)	Age (Ma)	±1σ (Ma)
	AD-01 24US, , J=0.000876±0.12%, D=1.005±0.001, NM-183AAAA, Lab#=55248								
	16B	3.778	0.0336	8.445	0.119	15.2	33.5	2.0	1.1
	08B	4.903	0.0497	10.29	0.116	10.3	37.7	2.9	1.3
	19A	7.772	0.0480	19.15	1.102	10.6	27.0	3.30	0.20
	04A	6.988	0.0425	16.23	1.688	12.0	31.1	3.42	0.13
	11A	9.640	0.0431	25.13	1.849	11.8	22.8	3.46	0.17
	20B	6.908	0.0423	15.77	0.576	12.1	32.3	3.51	0.32
	12B	5.565	0.0468	11.21	1.835	10.9	40.2	3.52	0.13
	18A	4.476	0.0419	7.515	1.381	12.2	50.2	3.52	0.16
	21A	5.833	0.0447	12.10	1.140	11.4	38.5	3.53	0.16
	15B	9.524	0.0438	24.49	0.735	11.7	23.8	3.57	0.26
	21B	4.858	0.0422	8.644	0.648	12.1	47.2	3.60	0.23
	07A	4.815	0.0429	8.370	1.548	11.9	48.4	3.66	0.13
	02A	6.497	0.0460	14.01	2.815	11.1	36.0	3.680	0.087
	13B	7.264	0.0439	16.60	1.099	11.6	32.3	3.68	0.19
	17A	5.155	0.0423	9.459	1.201	12.1	45.6	3.69	0.18
	17B	5.067	0.0437	8.916	3.282	11.7	47.8	3.800	0.089
	11B	8.063	0.0439	19.05	2.075	11.6	30.0	3.80	0.13
	13A	8.323	0.0464	19.92	1.594	11.0	29.1	3.81	0.16
	20A	6.587	0.0437	14.04	1.264	11.7	36.8	3.81	0.18
	15A	12.24	0.0449	33.17	1.642	11.4	19.8	3.81	0.20
	22B	5.985	0.0447	11.95	1.207	11.4	40.8	3.83	0.19
	01A	2.997	0.0451	1.800	2.148	11.3	82.2	3.852	0.077
	10A	5.894	0.0440	11.44	3.063	11.6	42.4	3.928	0.066
	22A	6.912	0.0460	14.79	1.177	11.1	36.6	3.97	0.19
	14B	6.904	0.0392	14.70	0.300	13.0	36.9	4.00	0.50
	16A	6.382	0.0432	12.87	1.184	11.8	40.2	4.03	0.16
	09B	6.355	0.0439	12.75	3.138	11.6	40.5	4.047	0.086
	12A	5.964	0.0452	11.29	0.752	11.3	43.8	4.11	0.19
	14A	7.671	0.0450	16.84	1.712	11.3	34.9	4.21	0.15
	09A	8.641	0.0438	19.96	1.176	11.6	31.6	4.29	0.18
	18B	4.470	0.0371	5.760	0.312	13.8	61.8	4.33	0.42
	10B	5.067	0.0368	7.093	0.173	13.9	58.5	4.65	0.96
xi	03B	9.583	0.0170	21.01	0.049	30.0	35.0	5.3	3.4
xi	09C	6.461	0.0542	7.926	0.196	9.4	63.7	6.46	0.53
xi	03A	19.12	0.0426	29.53	1.980	12.0	54.3	16.32	0.19
	Mean age ± 2σ	n=32	MSWD=2.41			11.8 ±1.9		3.80	0.08
	AD-01 5US, , J=0.0008576±0.15%, D=1.0055±0.001, NM-183HHHH, Lab#=55252								
	12A	7.227	0.0515	17.60	0.372	9.9	27.8	3.10	0.54
	14A	10.36	0.0491	28.01	1.515	10.4	20.0	3.19	0.17
	10A	5.670	0.0492	11.90	1.721	10.4	37.8	3.30	0.15
	01A	9.086	0.0431	23.45	0.925	11.8	23.6	3.30	0.25
	01B	7.670	0.0459	18.53	2.447	11.1	28.4	3.36	0.12
	14B	7.563	0.0415	18.08	1.938	12.3	29.2	3.40	0.13
	13B	6.044	0.0417	12.92	2.033	12.2	36.6	3.40	0.13
	09B	4.489	0.0711	7.667	0.341	7.2	49.4	3.41	0.55
	15A	10.91	0.0393	29.38	1.243	13.0	20.3	3.41	0.17
	05A	10.71	0.0459	28.65	1.677	11.1	20.8	3.44	0.17
	05B	8.572	0.0346	21.31	0.313	14.7	26.4	3.48	0.63
	11A	5.335	0.0496	10.32	0.808	10.3	42.7	3.50	0.25
	08A	8.669	0.0482	21.54	1.303	10.6	26.4	3.53	0.19
	10B	5.320	0.0342	10.13	1.434	14.9	43.5	3.56	0.17
	09A	4.912	0.0511	8.676	1.223	10.0	47.6	3.60	0.17

	08B	7.904	0.0255	18.72	0.229	20.0	29.8	3.63	0.85
	06A	6.546	0.0355	14.11	1.551	14.4	36.1	3.64	0.16
	02A	6.956	0.0445	15.44	1.427	11.5	34.2	3.66	0.17
	12B	6.412	0.0432	13.58	6.873	11.8	37.2	3.674	0.060
	15B	8.400	0.0408	20.19	2.834	12.5	28.8	3.725	0.095
	04A	7.933	0.0458	18.54	0.743	11.1	30.8	3.76	0.31
	07A	9.052	0.0478	22.29	0.630	10.7	27.1	3.78	0.34
	13A	6.385	0.0373	13.18	0.785	13.7	38.8	3.81	0.27
	02B	6.609	0.0285	13.91	0.419	17.9	37.6	3.83	0.50
	03B	3.914	0.0422	4.782	3.508	12.1	63.8	3.830	0.072
	06B	6.500	0.0444	13.43	1.467	11.5	38.8	3.88	0.16
	03A	4.191	0.0387	5.523	1.074	13.2	60.9	3.92	0.19
	04B	7.380	0.0613	15.60	0.196	8.3	37.4	4.25	0.97
xi	11B	5.419	-0.1200	5.710	0.110	-	68.6	5.7	1.7
	Mean age ± 2σ	n=28	MSWD=1.65			12.1 ±5.2		3.612	0.074

AD-1 5US, Obsidian, .01 mg, J=0.0001758±0.22%, D=1.003±0.001, NM-193K, Lab#=56064

xi	15B	29.01	0.0560	71.88	0.194	9.1	26.8	2.47	0.36
	13B	38.98	0.0336	99.26	0.206	15.2	24.8	3.06	0.41
	01B	21.94	0.0375	40.97	0.429	13.6	44.8	3.12	0.17
	04B	31.63	0.0434	72.63	0.748	11.8	32.2	3.22	0.17
xi	06B	39.04	0.0202	97.57	0.198	25.3	26.2	3.24	0.38
	07B	32.23	0.0444	73.92	0.628	11.5	32.2	3.29	0.20
	09A	34.09	0.0323	79.19	0.130	15.8	31.4	3.39	0.52
	02B	22.88	0.0399	40.84	0.468	12.8	47.3	3.43	0.15
	12B	31.92	0.0425	70.74	0.771	12.0	34.5	3.49	0.16
	08B	31.77	0.0418	69.63	0.992	12.2	35.2	3.55	0.14
	03B	29.28	0.0445	61.14	0.855	11.5	38.3	3.55	0.15
	10B	36.10	0.0413	83.41	1.008	12.4	31.7	3.63	0.16
	05B	33.27	0.0426	73.82	1.259	12.0	34.4	3.63	0.13
	11B	27.27	0.0338	51.06	0.372	15.1	44.7	3.86	0.18
xi	09B	28.28	0.0208	47.22	0.121	24.5	50.7	4.54	0.54
	Mean age ± 2σ	n=12	MSWD=1.45			13.0 ±3.1		3.49	0.12

AD-02 AA, Obsidian, J=0.0008787±0.32%, D=1.0063±0.001, NM-183jj, Lab#=55245

07A	4.124	0.0679	6.087	0.927	7.5	56.3	3.65	0.32
16A	3.451	0.0743	3.517	0.686	6.9	69.9	3.79	0.42
15A	11.61	0.0764	30.99	0.475	6.7	21.0	3.86	0.67
06A	10.35	0.0746	26.68	0.668	6.8	23.7	3.88	0.48
09A	3.819	0.0674	4.469	0.881	7.6	65.5	3.93	0.34
01B	13.70	0.0770	37.88	6.187	6.6	18.2	3.95	0.12
02B	3.436	0.0925	3.089	0.417	5.5	73.6	3.97	0.71
13B	4.025	0.0690	4.956	5.199	7.4	63.6	4.024	0.063
07B	3.481	0.0742	3.107	6.450	6.9	73.7	4.029	0.053
04B	3.103	0.0746	1.788	10.746	6.8	83.2	4.047	0.032
11B	16.23	0.0762	46.10	4.456	6.7	16.0	4.10	0.15
02A	3.523	0.0786	3.101	0.845	6.5	74.1	4.10	0.35
10B	6.981	0.0712	14.80	3.946	7.2	37.2	4.10	0.11
12B	4.063	0.0745	4.910	1.656	6.9	64.3	4.11	0.18
16B	3.251	0.0735	2.149	2.617	6.9	80.6	4.11	0.11
13A	4.276	0.0832	5.623	0.522	6.1	61.1	4.11	0.56
09B	3.516	0.0760	3.031	2.009	6.7	74.6	4.12	0.15
12A	4.525	0.0768	6.331	0.859	6.6	58.6	4.17	0.34
04A	3.657	0.0666	3.328	1.270	7.7	73.2	4.20	0.23
10A	6.944	0.0777	14.36	0.952	6.6	38.8	4.25	0.34
08B	6.247	0.0736	11.81	2.538	6.9	44.1	4.34	0.14
03B	14.07	0.0758	38.13	3.405	6.7	19.8	4.41	0.15
15B	11.27	0.0707	28.59	1.452	7.2	24.9	4.43	0.25
06B	9.172	0.0735	21.48	1.862	6.9	30.7	4.44	0.19
08A	6.212	0.0728	10.95	0.668	7.0	47.9	4.68	0.45

	03A	15.09	0.0669	40.91	0.871	7.6	19.8	4.72	0.38
	01A	15.59	0.0692	42.59	0.748	7.4	19.2	4.74	0.48
	11A	15.47	0.0793	41.52	0.530	6.4	20.6	5.03	0.61
	Mean age ± 2σ	n=28	MSWD=1.12		6.9 ±0.9			4.073	0.052
	AD-02 5US, , J=0.0008657±0.37%, D=1.005±0.001, NM-183G, Lab#=55241								
	11A	14.23	0.0594	40.67	0.327	8.6	15.4	3.42	0.56
	17A	13.62	0.0748	38.22	0.398	6.8	17.0	3.60	0.48
	15A	11.03	0.0713	29.13	0.996	7.2	21.8	3.74	0.22
	19A	9.170	0.0657	22.79	0.466	7.8	26.4	3.77	0.42
	14B	15.80	0.0773	45.09	1.982	6.6	15.6	3.83	0.18
	15B	10.76	0.0735	27.96	2.772	6.9	23.1	3.86	0.11
	08B	13.74	0.0735	38.04	5.377	6.9	18.1	3.86	0.12
	22A	4.942	0.0734	8.217	0.496	7.0	50.7	3.89	0.36
	20B	5.129	0.0732	8.807	1.508	7.0	49.1	3.91	0.12
	14A	14.87	0.0764	41.69	0.473	6.7	17.0	3.94	0.43
	22B	4.774	0.0713	7.490	1.701	7.2	53.5	3.96	0.12
	21A	8.117	0.0727	18.72	0.583	7.0	31.7	4.00	0.33
	13A	6.788	0.0677	14.17	0.731	7.5	38.2	4.02	0.26
	05A	5.193	0.0710	8.704	0.625	7.2	50.3	4.06	0.27
	04B	11.74	0.0749	30.84	4.972	6.8	22.3	4.07	0.11
	09B	6.361	0.0712	12.60	1.966	7.2	41.3	4.08	0.11
	07B	4.870	0.0723	7.536	4.881	7.1	54.2	4.091	0.054
	06B	5.086	0.0724	8.246	4.333	7.0	52.0	4.099	0.056
	08A	14.20	0.0712	39.06	0.949	7.2	18.6	4.11	0.25
	16A	6.874	0.0706	14.87	0.960	7.2	35.9	3.84	0.32
	11B	13.98	0.0739	38.30	4.367	6.9	18.9	4.12	0.12
	19B	8.850	0.0707	20.93	3.461	7.2	30.0	4.124	0.097
	10B	5.381	0.0726	9.191	2.624	7.0	49.4	4.125	0.086
	03B	13.95	0.0781	38.14	2.014	6.5	19.1	4.14	0.18
	13B	6.699	0.0738	13.58	4.425	6.9	39.9	4.156	0.066
	16B	6.821	0.0734	13.99	5.113	6.9	39.3	4.161	0.062
	12B	6.381	0.0749	12.44	2.745	6.8	42.3	4.188	0.091
	09A	6.682	0.0725	13.45	0.482	7.0	40.4	4.19	0.36
	21B	8.084	0.0724	18.17	2.169	7.0	33.4	4.20	0.13
	18B	12.43	0.0740	32.88	1.530	6.9	21.7	4.20	0.21
	06A	5.391	0.0696	9.054	0.448	7.3	50.2	4.20	0.39
	02A	9.053	0.0691	21.44	1.056	7.4	29.9	4.21	0.21
	20A	5.482	0.0715	9.305	0.439	7.1	49.7	4.23	0.38
	05B	5.206	0.0721	8.335	1.716	7.1	52.6	4.25	0.12
	07A	5.045	0.0699	7.572	0.698	7.3	55.5	4.35	0.25
	18A	12.82	0.0735	33.71	0.281	6.9	22.2	4.43	0.66
	03A	12.04	0.0778	31.03	0.641	6.6	23.7	4.45	0.34
	04A	11.90	0.0722	30.52	1.059	7.1	24.1	4.45	0.21
	17B	13.38	0.0745	34.95	2.026	6.8	22.7	4.73	0.16
	02B	9.150	0.0719	20.56	1.087	7.1	33.5	4.76	0.20
	12A	7.111	0.0690	13.53	0.319	7.4	43.6	4.82	0.51
	10A	5.773	0.0792	8.762	0.344	6.4	55.1	4.93	0.53
	Mean age ± 2σ	n=42	MSWD=1.53		7.1 ±0.7			4.115	0.058
	AD-3 24US, Obsidian, .01 mg, J=0.0001749±0.16%, D=1.003±0.001, NM-193K, Lab#=56065								
xi	12A	42.90	0.0582	114.0	0.117	8.8	21.5	2.90	0.60
	07B	32.38	0.0847	68.08	0.804	6.0	37.9	3.87	0.16
	11B	40.86	0.0707	96.67	0.549	7.2	30.1	3.88	0.22
	02B	25.76	0.0704	44.67	1.399	7.2	48.8	3.96	0.10
	05B	54.64	0.0734	140.5	0.334	7.0	24.0	4.14	0.37
	13A	71.04	0.0455	194.3	0.146	11.2	19.2	4.29	0.55
	01B	39.56	0.0701	87.20	0.892	7.3	34.9	4.35	0.15
	09B	54.84	0.0622	138.8	0.732	8.2	25.2	4.35	0.22
xi	15B	64.73	0.0727	170.5	0.446	7.0	22.2	4.53	0.31
xi	12B	48.65	0.0696	115.8	0.524	7.3	29.7	4.55	0.24

xi	10B	74.95	0.0743	203.8	1.536	6.9	19.7	4.64	0.18
xi	04B	66.93	0.0695	176.2	1.351	7.3	22.2	4.68	0.16
xi	06B	70.08	0.0740	183.6	1.548	6.9	22.6	4.99	0.17
xi	13B	68.65	0.0783	178.8	0.899	6.5	23.1	4.99	0.20
xi	14B	70.01	0.0775	183.1	0.717	6.6	22.7	5.02	0.24
xi	03B	92.52	0.0743	258.2	1.639	6.9	17.5	5.11	0.18
xi	08B	66.19	0.0770	169.0	0.535	6.6	24.6	5.12	0.29
	Mean age ± 2σ	n=7	MSWD=1.42		7.7 ±3.3			4.06	0.16

AD-06 24US, , J=0.000859±0.12%, D=1.005±0.001, NM-183AAAA, Lab#=55250

18B	2.289	0.0448	1.377	0.155	11.4	82.2	2.88	0.54
19B	12.40	0.0407	35.21	0.916	12.5	15.9	3.05	0.22
22B	11.14	0.0413	30.89	1.715	12.4	17.9	3.07	0.13
22A	12.23	0.0374	34.54	0.448	13.6	16.4	3.10	0.33
18A	2.567	0.0573	1.769	0.202	8.9	79.6	3.13	0.42
19A	18.07	0.0397	54.02	0.772	12.9	11.5	3.23	0.28
21B	2.701	0.0441	1.833	0.330	11.6	79.9	3.30	0.24
04A	7.803	0.0428	18.08	1.301	11.9	31.3	3.77	0.22
20A	2.790	0.0431	1.956	0.419	11.8	79.2	3.39	0.23
10A	20.48	0.0397	61.67	0.803	12.9	10.9	3.46	0.29
05B	6.052	0.0431	12.57	8.051	11.8	38.4	3.582	0.064
02A	2.914	0.0465	1.917	0.613	11.0	80.5	3.60	0.17
08B	13.46	0.0399	37.60	2.451	12.8	17.3	3.60	0.14
03B	10.37	0.0409	27.12	2.635	12.5	22.5	3.60	0.12
04B	6.761	0.0427	14.89	2.574	11.9	34.7	3.617	0.078
21A	2.659	0.0432	0.9480	0.904	11.8	89.5	3.64	0.10
07B	2.605	0.0459	0.7548	0.947	11.1	91.5	3.650	0.086
11A	3.189	0.0478	2.699	0.662	10.7	74.9	3.66	0.15
07A	2.824	0.0427	1.417	0.712	12.0	85.2	3.68	0.11
03A	14.06	0.0355	39.44	0.812	14.4	17.0	3.69	0.22
23A	8.872	0.0405	21.76	0.626	12.6	27.3	3.74	0.21
23B	5.712	0.0433	10.95	1.774	11.8	43.1	3.795	0.080
01B	2.564	0.0435	0.2865	2.461	11.7	96.8	3.799	0.042
20B	2.548	0.0457	0.1852	0.928	11.2	98.0	3.822	0.080
11B	2.482	0.0441	-0.1099	0.591	11.6	101.5	3.85	0.16
06B	2.662	0.0445	0.4007	11.439	11.5	95.7	3.899	0.023
05A	8.130	0.0349	18.82	0.353	14.6	31.4	3.94	0.38
02B	2.624	0.0465	0.1093	9.599	11.0	99.0	3.974	0.018
01A	2.810	0.0399	0.6610	1.295	12.8	93.1	4.01	0.15
24B	2.949	0.0405	0.8507	0.692	12.6	91.5	4.14	0.11
08A	17.94	0.0380	51.46	1.205	13.4	15.1	4.20	0.23
06A	3.073	0.0407	1.109	0.595	12.5	89.4	4.21	0.18
10B	15.29	0.0374	42.21	0.607	13.7	18.3	4.32	0.32
24A	2.861	0.0421	0.0973	0.473	12.1	99.2	4.35	0.18
Mean age ± 2σ	n=34	MSWD=6.11		12.1 ±2.2			3.876	0.058

AD-11 5US, , J=0.0008623±0.13%, D=1.005±0.001, NM-183AAAA, Lab#=55249

23A	2.907	0.0634	2.399	0.810	8.0	75.6	3.38	0.19
05A	3.324	0.0633	3.501	0.482	8.1	68.8	3.52	0.35
19B	2.854	0.0600	1.828	0.119	8.5	81.1	3.6	1.4
20A	2.681	0.0622	0.9739	0.749	8.2	89.4	3.68	0.22
17B	2.683	0.0631	0.8876	1.185	8.1	90.4	3.73	0.14
22A	3.398	0.0653	3.261	0.307	7.8	71.6	3.75	0.46
16A	2.733	0.0630	0.9213	1.131	8.1	90.2	3.79	0.15
01A	7.393	0.0722	16.60	0.541	7.1	33.5	3.83	0.32
02B	2.647	0.0634	0.4784	1.653	8.1	94.9	3.86	0.10
02A	2.916	0.0587	1.361	1.130	8.7	86.3	3.87	0.15
06A	2.862	0.0640	1.061	1.004	8.0	89.2	3.93	0.18
03B	2.692	0.0669	0.4427	8.091	7.6	95.4	3.946	0.024
21B	2.681	0.0679	0.3932	3.532	7.5	95.9	3.952	0.059

19A	2.747	0.0643	0.6135	1.473	7.9	93.6	3.95	0.11
06B	2.760	0.0650	0.6454	0.837	7.9	93.3	3.96	0.17
04B	2.634	0.0651	0.1916	7.489	7.8	98.1	3.971	0.025
07B	2.825	0.0659	0.8076	2.875	7.7	91.7	3.985	0.059
08B	3.387	0.0678	2.684	0.663	7.5	76.6	4.00	0.22
07A	4.280	0.0643	5.661	1.118	7.9	60.8	4.02	0.16
01B	3.030	0.0670	1.371	7.493	7.6	86.8	4.045	0.030
16B	2.750	0.0680	0.3921	1.719	7.5	96.0	4.060	0.098
04A	3.049	0.0639	1.389	1.415	8.0	86.7	4.07	0.12
22B	2.723	0.0679	0.2314	2.777	7.5	97.8	4.092	0.061
05B	2.760	0.0643	0.2495	2.667	7.9	97.6	4.140	0.068
21A	2.984	0.0681	0.9673	0.903	7.5	90.6	4.16	0.17
08A	7.516	0.0656	16.20	1.355	7.8	36.2	4.21	0.20
18A	3.126	0.0608	1.318	1.687	8.4	87.7	4.22	0.10
03A	5.201	0.0642	8.204	0.998	7.9	53.3	4.28	0.20
23B	2.938	0.0597	-0.6425	0.099	8.5	106.8	4.8	1.3
Mean age ± 2σ	n=29	MSWD=1.74		7.9 ±0.7			3.987	0.035

AD-11 24US, Obsidian, J=0.0008605±0.28%, D=1.0055±0.001, NM-183jj, Lab#=55247

10A	3.111	0.0705	2.209	0.610	7.2	79.3	3.79	0.25
02B	2.701	0.0570	0.7062	1.164	8.9	92.7	3.84	0.13
14B	2.972	0.0728	1.522	2.933	7.0	85.2	3.887	0.053
15A	4.014	0.0732	5.039	0.512	7.0	63.0	3.89	0.30
03B	2.823	0.0754	0.9789	0.830	6.8	90.2	3.90	0.17
07A	3.018	0.0738	1.563	1.189	6.9	85.0	3.94	0.12
09A	2.996	0.0525	1.478	0.778	9.7	85.7	3.94	0.18
03A	2.705	0.0706	0.4969	0.996	7.2	95.0	3.94	0.15
08B	2.813	0.0771	0.8315	2.007	6.6	91.7	3.957	0.075
04B	2.701	0.0637	0.3904	2.693	8.0	96.2	3.984	0.057
04A	3.021	0.0612	1.430	0.706	8.3	86.3	4.00	0.19
02A	2.658	0.0677	0.1223	1.169	7.5	99.1	4.04	0.13
11A	2.995	0.0743	1.235	0.899	6.9	88.2	4.05	0.16
13B	2.724	0.0695	0.2983	1.940	7.3	97.2	4.062	0.075
15B	2.787	0.0647	0.4519	6.200	7.9	95.6	4.089	0.030
07B	2.757	0.0624	0.3459	1.800	8.2	96.7	4.091	0.083
11B	2.834	0.0698	0.5963	3.534	7.3	94.2	4.096	0.047
06B	2.854	0.0676	0.6605	4.499	7.5	93.6	4.097	0.039
14A	2.790	0.0591	0.4172	0.846	8.6	96.0	4.11	0.16
01B	2.841	0.0701	0.5864	1.679	7.3	94.3	4.111	0.091
08A	3.112	0.0727	1.413	1.371	7.0	86.9	4.15	0.11
10B	2.838	0.0648	0.4620	1.369	7.9	95.6	4.16	0.11
05B	2.759	0.0698	0.1897	1.733	7.3	98.5	4.167	0.090
12B	2.893	0.0676	0.6105	4.160	7.5	94.2	4.180	0.040
01A	3.203	0.0718	1.619	0.844	7.1	85.3	4.20	0.18
05A	2.852	0.0690	0.4264	1.344	7.4	96.0	4.20	0.11
06A	5.511	0.0782	9.394	0.766	6.5	49.6	4.22	0.23
12A	3.239	0.0584	1.190	0.708	8.7	89.5	4.45	0.20
13A	2.881	0.0720	-0.5051	0.661	7.1	105.7	4.67	0.21
Mean age ± 2σ	n=29	MSWD=1.80		7.5 ±1.5			4.077	0.044

AD-12 24US, , J=0.0008761±0.25%, D=1.0055±0.001, NM-183HHHH, Lab#=55251

09B	2.400	0.1061	2.501	0.122	4.8	69.3	2.6	1.5
05B	2.390	0.0428	1.251	0.544	11.9	84.6	3.15	0.36
06A	3.099	0.0485	3.026	0.356	10.5	71.1	3.45	0.55
02A	3.091	0.0177	2.860	0.496	28.8	72.6	3.51	0.41
07B	2.494	0.0479	0.6433	0.793	10.7	92.6	3.60	0.25
05A	2.532	0.0341	0.7463	0.681	14.9	91.4	3.61	0.30
14B	2.552	0.0427	0.6170	0.378	11.9	93.1	3.71	0.51
04B	2.820	0.0387	1.457	1.414	13.2	84.8	3.74	0.14
07A	2.710	0.0477	0.9616	1.076	10.7	89.7	3.79	0.18
04A	3.431	0.0340	3.346	0.855	15.0	71.1	3.82	0.23

	14A	3.102	0.0396	2.204	1.537	12.9	79.0	3.83	0.13
	09A	2.524	0.0464	0.2467	1.654	11.0	97.4	3.83	0.12
	15A	3.668	0.0285	4.075	0.488	17.9	67.1	3.85	0.40
	10B	2.477	0.0464	-0.1258	1.259	11.0	101.8	3.93	0.15
	02B	2.771	0.0468	0.8672	0.944	10.9	90.9	3.94	0.22
	11A	2.745	0.0526	0.6638	1.553	9.7	93.1	3.99	0.13
	13A	3.074	0.0595	1.631	0.733	8.6	84.5	4.06	0.28
	10A	2.897	0.0400	1.010	0.990	12.7	89.8	4.07	0.20
	13B	2.865	0.0461	0.3922	1.254	11.1	96.2	4.30	0.16
	08A	3.232	0.0605	1.588	0.499	8.4	85.6	4.33	0.38
xi	15B	2.843	0.0438	0.1842	4.640	11.6	98.3	4.367	0.047
	06B	3.759	0.0417	3.211	0.143	12.2	74.7	4.4	1.4
	03A	3.043	0.0397	0.7441	0.899	12.8	92.9	4.42	0.23
	03B	3.299	0.0650	0.9599	0.300	7.9	91.6	4.73	0.64
	11B	3.335	0.0972	0.6141	0.176	5.3	94.9	4.9	1.1
xi	08B	2.407	0.0037	-3.6509	0.109	136.9	145.6	5.5	1.7
xi	12A	5.006	0.0569	1.905	1.221	9.0	88.9	6.98	0.17
xi	01A	5.199	0.0619	1.342	0.907	8.2	92.6	7.55	0.23
xi	12B	5.360	0.0650	0.3330	3.650	7.8	98.4	8.271	0.062
	Mean age ± 2σ	n=23	MSWD=1.25			11.1 ±5.9		3.91	0.10

AD-21 24US, Obsidian, J=0.0001128±0.09%, D=1.0055±0.001, NM-190C, Lab#=55703

05B	14.27	0.0325	32.56	0.633	15.7	32.6	0.948	0.055
01B	9.040	0.0335	14.53	0.221	15.2	52.6	0.97	0.14
02B	8.930	0.0316	13.10	0.316	16.1	56.7	1.031	0.096
09B	10.28	0.0290	15.69	0.407	17.6	55.0	1.151	0.082
Mean age ± 2σ	n=4	MSWD=1.46			16.2 ±2.1		1.01	0.10

AD-22 24US, Obsidian, J=0.000113±0.11%, D=1.0055±0.001, NM-190C, Lab#=55705

xi	13B	429.0	0.0330	1483.6	0.933	15.4	-2.2	-1.91	0.39
xi	05B	495.1	0.0314	1703.6	1.156	16.3	-1.7	-1.71	0.44
xi	01B	160.3	0.0314	558.3	1.003	16.3	-2.9	-0.96	0.16
xi	02B	131.3	0.0340	460.1	0.718	15.0	-3.6	-0.95	0.15
xi	15B	110.9	0.0341	386.0	0.549	15.0	-2.8	-0.64	0.15
xi	09B	124.0	0.0341	429.9	0.391	15.0	-2.4	-0.62	0.18
xi	06B	169.9	0.0367	579.8	0.137	13.9	-0.8	-0.29	0.38
xi	08B	81.77	0.0308	279.3	0.683	16.6	-0.9	-0.16	0.12
xi	07B	112.6	0.0331	382.6	0.195	15.4	-0.5	-0.10	0.24
xi	11B	180.7	0.0266	612.8	0.485	19.2	-0.2	-0.07	0.21
xi	11A	188.4	0.0350	638.4	0.122	14.6	-0.1	-0.05	0.40
xi	10B	87.49	0.0335	296.7	0.900	15.2	-0.2	-0.04	0.10
xi	12B	55.30	0.0334	181.0	0.422	15.3	3.3	0.37	0.12
xi	04B	75.79	0.0344	250.0	0.311	14.8	2.5	0.39	0.17
xi	14B	53.82	0.0290	174.8	1.126	17.6	4.0	0.444	0.067
xi	16B	53.72	0.0325	173.6	0.677	15.7	4.5	0.495	0.086
	Mean age ± 2σ	n=0	MSWD=0.00			-±0.0		0.00	0.00

AD-23 24US, Obsidian, J=0.0001131±0.16%, D=1.0055±0.001, NM-190D, Lab#=55713

07A	5.864	0.0248	14.60	0.128	20.6	26.5	0.32	0.23
04A	9.001	0.0325	16.83	0.129	15.7	44.8	0.82	0.23
13A	6.178	0.0429	6.832	0.093	11.9	67.5	0.85	0.32
10A	6.367	0.0242	5.566	0.094	21.0	74.2	0.96	0.31
11B	5.924	0.0248	2.263	0.258	20.6	88.8	1.07	0.11
15A	6.424	0.0436	3.792	0.087	11.7	82.7	1.08	0.34
14A	6.327	0.0376	2.975	0.107	13.6	86.2	1.11	0.27
06B	6.002	0.0330	1.822	0.225	15.5	91.1	1.12	0.13
05B	6.572	0.0253	3.741	0.140	20.2	83.3	1.12	0.22
07B	6.015	0.0284	1.468	0.597	17.9	92.9	1.140	0.050
08B	6.086	0.0256	1.476	0.440	20.0	92.9	1.154	0.067
09B	6.021	0.0305	1.084	0.449	16.7	94.8	1.165	0.068
15B	5.613	0.0301	-0.5002	0.497	17.0	102.7	1.177	0.061

	04B	6.006	0.0319	0.7924	0.670	16.0	96.2	1.179	0.047
	10B	6.012	0.0343	0.7689	0.244	14.9	96.3	1.18	0.12
	12B	6.048	0.0306	0.8593	0.329	16.7	95.9	1.184	0.091
	14B	5.992	0.0317	0.3963	0.286	16.1	98.2	1.20	0.11
	06A	6.440	0.0241	1.675	0.132	21.2	92.4	1.21	0.22
	13B	6.041	0.0279	-0.0303	0.396	18.3	100.2	1.236	0.075
	05A	5.976	0.0222	-0.2744	0.097	23.0	101.4	1.24	0.30
	12A	6.169	0.0245	0.2182	0.115	20.8	99.0	1.25	0.25
	11A	6.330	0.0276	0.1821	0.102	18.5	99.2	1.28	0.29
	09A	6.476	0.0288	0.3300	0.135	17.7	98.6	1.30	0.22
	08A	6.724	0.0290	-1.8898	0.096	17.6	108.4	1.49	0.31
xi	16A	21.54	0.0341	6.410	0.941	15.0	91.2	4.007	0.042
	Mean age ± 2σ	n=24	MSWD=0.92			17.6 ±5.9		1.16	0.04

AD-24M, Obsidian, J=0.0001122±0.12%, D=1.0055±0.001, NM-190E, Lab#=55716

09B	7.300	0.0288	5.736	1.344	17.7	76.9	1.135	0.030
02B	10.77	0.0351	17.49	0.345	14.5	52.1	1.14	0.11
01B	7.522	0.0286	6.120	0.534	17.9	76.0	1.157	0.069
10B	8.028	0.0299	7.759	1.292	17.1	71.5	1.161	0.031
11B	9.775	0.0297	13.34	0.878	17.2	59.8	1.181	0.044
13B	7.538	0.0301	5.574	0.906	16.9	78.2	1.193	0.041
08B	8.123	0.0303	7.388	1.038	16.8	73.2	1.203	0.038
07B	6.609	0.0359	2.234	0.294	14.2	90.1	1.20	0.13
03B	7.139	0.0362	3.871	0.332	14.1	84.1	1.21	0.11
12B	8.798	0.0312	9.360	1.795	16.3	68.6	1.221	0.024
14B	7.435	0.0326	4.650	1.225	15.6	81.6	1.227	0.032
06B	10.64	0.0315	14.66	0.322	16.2	59.4	1.28	0.11
08A	13.53	0.0270	24.38	0.116	18.9	46.8	1.28	0.31
15B	10.40	0.0317	12.77	1.015	16.1	63.8	1.342	0.039
05B	8.753	0.0338	6.745	0.233	15.1	77.3	1.37	0.16
04B	8.912	0.0295	7.010	0.394	17.3	76.8	1.385	0.096
Mean age ± 2σ	n=16	MSWD=1.80			16.4 ±2.8		1.207	0.030

AD-24nm, Obsidian, J=0.000113±0.13%, D=1.0055±0.001, NM-190D, Lab#=55708

06B	5.974	0.0290	2.867	0.387	17.6	85.9	1.046	0.096
05B	5.988	0.0351	1.551	0.631	14.5	92.5	1.129	0.058
02B	6.247	0.0311	2.230	0.837	16.4	89.6	1.140	0.045
11B	6.485	0.0316	2.973	0.961	16.1	86.6	1.144	0.038
14B	6.160	0.0300	1.598	1.067	17.0	92.4	1.161	0.036
13B	7.084	0.0319	4.642	0.933	16.0	80.7	1.166	0.040
10B	7.753	0.0325	6.882	1.278	15.7	73.9	1.167	0.031
08B	6.483	0.0340	2.148	1.245	15.0	90.3	1.194	0.029
09B	6.236	0.0302	1.083	0.531	16.9	95.0	1.207	0.069
12B	6.823	0.0291	2.963	0.555	17.5	87.3	1.214	0.067
04B	6.204	0.0286	0.6800	0.282	17.8	96.9	1.22	0.12
15B	20.55	0.0304	49.15	0.792	16.8	29.4	1.230	0.061
09A	7.701	0.0267	5.589	0.108	19.1	78.6	1.23	0.32
03B	7.842	0.0311	4.727	0.427	16.4	82.3	1.315	0.086
Mean age ± 2σ	n=14	MSWD=0.66			16.6 ±2.4		1.172	0.026

AD-26, Obsidian, J=0.000113±0.11%, D=1.0055±0.001, NM-190C, Lab#=55707

13A	6.843	0.0277	5.273	0.100	18.5	77.3	1.08	0.36
02B	6.337	0.0370	3.514	0.224	13.8	83.7	1.08	0.16
12B	5.927	0.0305	1.924	0.525	16.7	90.5	1.093	0.069
07B	6.072	0.0378	1.539	0.236	13.5	92.6	1.15	0.15
08B	6.016	0.0353	1.003	0.881	14.5	95.2	1.167	0.044
04B	6.203	0.0332	1.463	0.526	15.4	93.1	1.177	0.069
10B	5.861	0.0341	0.1652	0.739	15.0	99.3	1.186	0.049
15B	6.022	0.0325	0.4843	0.845	15.7	97.7	1.199	0.043
16B	5.992	0.0292	0.3516	1.082	17.5	98.4	1.201	0.034

	13B	5.915	0.0300	0.0477	0.936	17.0	99.9	1.203	0.039
	11B	6.170	0.0282	0.8907	0.855	18.1	95.8	1.204	0.043
	03B	6.204	0.0348	0.8780	0.538	14.7	95.9	1.212	0.068
	01B	5.775	0.0347	-0.5805	0.473	14.7	103.1	1.213	0.075
	09B	5.980	0.0327	-0.3652	0.593	15.6	101.9	1.242	0.061
	16A	6.776	0.0371	2.167	0.106	13.7	90.7	1.25	0.33
	05B	6.052	0.0312	-0.9756	0.573	16.4	104.9	1.293	0.063
	09A	6.715	0.0295	-0.4919	0.108	17.3	102.3	1.40	0.32
	Mean age ± 2σ	n=17	MSWD=0.44			15.8 ±3.1		1.198	0.028
	AD-28, Obsidian, J=0.0001124±0.12%, D=1.0055±0.001, NM-190E, Lab#=55714								
xi	09A	5.699	0.0495	13.61	0.119	10.3	29.6	0.34	0.30
	08A	7.011	0.0360	5.649	0.102	14.2	76.3	1.08	0.34
	09B	5.571	0.0426	0.5229	0.765	12.0	97.4	1.100	0.048
	12B	6.021	0.0320	1.929	0.383	16.0	90.6	1.107	0.093
	08B	5.660	0.0367	0.5482	0.809	13.9	97.3	1.116	0.045
	02B	6.148	0.0338	1.882	0.495	15.1	91.1	1.135	0.073
	14B	5.932	0.0303	0.8676	0.918	16.8	95.8	1.152	0.039
	07B	6.150	0.0251	1.352	0.279	20.4	93.6	1.17	0.13
	15B	5.961	0.0363	0.2499	0.857	14.1	98.9	1.195	0.042
	10B	6.064	0.0329	0.4264	1.016	15.5	98.0	1.206	0.036
	03B	6.224	0.0265	0.8081	0.460	19.3	96.2	1.215	0.079
	13B	6.092	0.0301	0.0161	0.652	16.9	100.0	1.236	0.056
	01B	6.048	0.0308	-0.2447	1.261	16.6	101.3	1.242	0.030
	04B	6.040	0.0330	-0.3342	0.522	15.5	101.7	1.246	0.071
	05B	6.059	0.0348	-0.2731	0.418	14.7	101.4	1.247	0.086
	11B	6.121	0.0300	-0.1442	0.810	17.0	100.8	1.251	0.045
	06B	6.009	0.0289	-1.4011	0.263	17.7	107.0	1.30	0.14
	15A	6.649	0.0306	-1.7398	0.102	16.7	107.8	1.45	0.34
	10A	7.002	0.0256	-0.8332	0.109	19.9	103.6	1.47	0.33
	Mean age ± 2σ	n=18	MSWD=1.02			16.2 ±4.4		1.195	0.027

Notes:

Isotopic ratios corrected for blank, radioactive decay, and mass discrimination, not corrected for interfering react
Errors quoted for individual analyses include analytical error only, without interfering reaction or J uncertainties.
Mean age is weighted mean age of Taylor (1982). Mean age error is weighted error
of the mean (Taylor, 1982), multiplied by the root of the MSWD where MSWD>1, and also
incorporates uncertainty in J factors and irradiation correction uncertainties.
Decay constants and isotopic abundances after Steiger and Jäger (1977).
symbol preceding sample ID denotes analyses excluded from mean age calculations.
Ages calculated relative to FC-2 Fish Canyon Tuff sanidine interlaboratory standard at 28.02 Ma
Decay Constant (LambdaK (total)) = 5.543e-10/a

Correction factors for NM-183:

$(^{39}Ar/^{37}Ar)_{Ca}$ = 0.00077 ± 2e-05
$(^{36}Ar/^{37}Ar)_{Ca}$ = 0.000276 ± 5e-06
$(^{38}Ar/^{39}Ar)_{K}$ = 0.0127
$(^{40}Ar/^{39}Ar)_{K}$ = 0.03 ± 0.002

Correction factors for NM-190:

$(^{39}Ar/^{37}Ar)_{Ca}$ = 0.000289 ± 5e-06
$(^{36}Ar/^{37}Ar)_{Ca}$ = 0.00068 ± 2e-05
$(^{38}Ar/^{39}Ar)_{K}$ = 0.013
$(^{40}Ar/^{39}Ar)_{K}$ = 0 ± 0.0004

Correction factors for NM-193:

$(^{39}Ar/^{37}Ar)_{Ca}$ = 0.0007 ± 5e-05
$(^{36}Ar/^{37}Ar)_{Ca}$ = 0.00028 ± 1e-05
$(^{38}Ar/^{39}Ar)_{K}$ = 0.013
$(^{40}Ar/^{39}Ar)_{K}$ = 0 ± 0.0004

5US= short ultrasonic, 24US= long ultrasonic, 5HF= HF, and AA= air abrasion preparation treatments respectively.

Appendix C. Table C.4. $^{40}Ar/^{39}Ar$ analytical data from laser fusion of sanidine and obsidian.

	ID	$^{40}Ar/^{39}Ar$	$^{37}Ar/^{39}Ar$	$^{36}Ar/^{39}Ar$ (x 10^{-3})	$^{39}Ar_K$ (x 10^{-15} mol)	K/Ca	$^{40}Ar^*$ (%)	Age (Ma)	±1σ (Ma)
	AD-01, , J=0.0008848±0.17%, D=1.005±0.001, NM-183F, Lab#=55233								
	03	15.80	0.2252	42.88	0.072	2.3	19.8	5.0	2.5
	02	13.12	0.4404	31.76	0.078	1.2	28.6	6.0	2.5
xi	04	15.29	0.1453	3.419	0.507	3.5	93.5	22.63	0.40
	Mean age ± 2σ	n=2		MSWD=0.08		1.7 ±1.6		5.5	3.5
	AD-03 sanidine, , J=0.0008868±0.15%, D=1.005±0.001, NM-183F, Lab#=55234								
xi	06	5.973	1.657	25.27	0.072	0.31	-23.4	-2.2	2.5
xi	08	6.538	1.545	22.60	0.116	0.33	-0.7	-0.1	1.6
xi	09	7.784	1.252	26.43	0.063	0.41	0.6	0.1	2.9
	07	7.700	0.5876	22.44	0.267	0.87	14.2	1.74	0.73
	05	14.12	0.9106	43.04	0.262	0.56	10.2	2.31	0.77
	11	5.947	1.486	15.19	0.209	0.34	26.2	2.48	0.92
	12	7.032	0.8005	18.46	0.105	0.64	23.1	2.6	1.6
	14	15.12	1.170	45.32	0.097	0.44	11.9	2.9	1.9
Z	01	33.95	1.689	103.7	0.319	0.30	10.1	5.46	0.81
	Mean age ± 2σ	n=5		MSWD=0.17		0.57 ±0.40		2.2	0.9
	AD-09 sanidine, , J=0.0008777±0.13%, D=1.005±0.001, NM-183F, Lab#=55235								
	06	2.756	0.0099	1.248	5.840	51.3	86.5	3.730	0.052
	47	2.599	0.0105	0.3684	2.109	48.7	95.8	3.893	0.079
	12	3.052	0.0112	1.867	2.297	45.5	81.8	3.909	0.075
	13	2.793	0.0128	0.9194	9.497	39.9	90.2	3.942	0.040
	14	2.877	0.0124	0.9980	6.283	41.2	89.7	4.038	0.053
	09	3.000	0.0126	1.180	1.677	40.5	88.3	4.15	0.10
	15	2.711	0.0110	0.2327	9.789	46.3	97.5	4.134	0.033
	40	3.074	0.0101	1.259	4.990	50.7	87.8	4.227	0.045
	46	2.845	0.0127	0.0624	1.457	40.2	99.4	4.42	0.12
Z	45	3.743	0.0086	0.3793	2.476	59.4	97.0	5.694	0.074
Z	49	4.676	0.0097	1.730	5.110	52.4	89.0	6.537	0.089
Z	43	16.91	0.0142	42.66	0.852	35.9	25.3	6.75	0.28
Z	50	9.087	0.0097	1.685	2.710	52.6	94.5	13.504	0.077
Z	37	11.79	0.0123	3.101	3.027	41.6	92.2	17.086	0.085
	Mean age ± 2σ	n=9		MSWD=10.65		44.9 ±9.3		4.04	0.11
	AD-12, , J=0.0008665±0.17%, D=1.005±0.001, NM-183F, Lab#=55236								
	04	17.44	0.0550	4.645	0.834	9.3	92.1	24.91	0.27
	08	16.56	0.0044	1.488	1.656	116.6	97.3	24.98	0.16
	06	16.52	0.0032	0.9763	1.451	160.9	98.3	25.14	0.19
	12	16.67	0.0044	1.488	1.784	115.6	97.4	25.15	0.15
	05	16.43	0.0152	0.6655	2.451	33.6	98.8	25.15	0.11
	14	16.48	0.0019	0.7663	0.846	262.8	98.6	25.19	0.25
	10	16.57	0.0116	0.9805	1.421	44.0	98.3	25.22	0.18
	03	16.54	0.0038	0.6959	3.181	134.7	98.8	25.317	0.096
	13	16.99	0.0004	2.142	1.268	1365.3	96.3	25.34	0.20
Z	11	16.74	0.0059	0.4617	4.247	86.4	99.2	25.721	0.068
Z	09	16.89	0.0064	0.4113	2.358	79.2	99.3	25.98	0.12
Z	07	22.95	0.0038	17.90	0.437	133.0	76.9	27.35	0.47
Z	01	25.50	0.0142	2.287	5.665	36.1	97.4	38.35	0.11
Z	02	31.94	0.0109	12.92	1.075	46.7	88.0	43.40	0.34
	Mean age ± 2σ	n=9		MSWD=0.70		249.2 ±851.0		25.19	0.13

AD-25, Sanidine, J=0.0001128±0.11%, D=1.0055±0.001, NM-190B, Lab#=55700

	06	20.27	0.0747	49.84	0.407	6.8	27.4	1.130	0.088
	08	15.89	0.1062	35.01	0.672	4.8	35.0	1.133	0.057
	09	12.74	0.1084	24.00	0.632	4.7	44.5	1.153	0.052
	02	16.30	0.1214	35.44	0.391	4.2	35.9	1.192	0.082
	03	21.62	0.1220	53.27	0.643	4.2	27.3	1.201	0.059
	15	14.97	0.0690	30.14	0.937	7.4	40.6	1.237	0.043
	12	16.59	0.0660	35.06	0.742	7.7	37.6	1.271	0.048
	07	12.54	0.0883	21.00	0.360	5.8	50.6	1.292	0.095
	13	47.30	0.0860	137.8	0.490	5.9	13.9	1.343	0.099
	11	20.80	0.0876	47.99	0.510	5.8	31.9	1.349	0.069
	14	17.85	0.0955	37.07	0.691	5.3	38.7	1.407	0.052
	01	35.54	0.1007	96.50	0.322	5.1	19.8	1.43	0.11
	10	26.95	0.1092	66.61	0.380	4.7	27.0	1.483	0.094
	05	27.95	0.1066	69.87	0.179	4.8	26.2	1.49	0.19
	04	13.39	0.1029	19.82	0.228	5.0	56.4	1.54	0.13
	Mean age ± 2σ	n=15	MSWD=2.70			5.5 ±2.2		1.265	0.057
	AD-27, Sanidine, J=0.0001128±0.15%, D=1.0055±0.001, NM-190D, Lab#=55711								
	06	7.656	0.1044	9.102	0.206	4.9	65.1	1.01	0.15
	01	7.471	0.0778	8.130	0.431	6.6	68.1	1.034	0.073
	14	7.326	0.0520	6.469	0.613	9.8	74.1	1.103	0.051
	08	7.895	0.0732	8.043	0.414	7.0	70.1	1.125	0.073
	11	8.286	0.0938	9.147	0.954	5.4	67.6	1.139	0.033
	15	8.367	0.0978	9.411	0.627	5.2	67.0	1.140	0.051
	12	7.826	0.0929	7.451	1.176	5.5	72.1	1.148	0.027
	13	6.656	0.0574	3.230	0.607	8.9	85.8	1.162	0.050
	09	9.607	0.0923	13.19	0.618	5.5	59.6	1.165	0.051
	07	7.501	0.0611	5.775	0.268	8.3	77.4	1.18	0.11
	03	8.196	0.1061	8.157	0.385	4.8	70.9	1.181	0.081
	04	8.688	0.0906	9.797	0.627	5.6	66.9	1.182	0.050
	10	7.522	0.0827	5.628	0.893	6.2	78.1	1.195	0.034
	05	9.075	0.0717	10.36	0.343	7.1	66.4	1.226	0.088
	02	12.13	0.1032	18.75	0.424	4.9	54.5	1.344	0.075
	Mean age ± 2σ	n=15	MSWD=1.00			6.4 ±3.1		1.157	0.026
	AD-2 obsidian, , J=0.0008785±0.43%, D=1.005±0.001, NM-183G, Lab#=55240								
	11	3.258	0.0739	2.413	7.716	6.9	78.2	3.994	0.031
	05	9.913	0.0727	24.76	3.300	7.0	26.0	4.075	0.091
	08	3.182	0.0712	1.975	2.850	7.2	81.7	4.079	0.067
	13	14.33	0.0753	39.66	6.388	6.8	18.1	4.09	0.11
	03	3.510	0.0720	2.970	2.388	7.1	75.0	4.133	0.081
	09	9.839	0.0717	24.32	2.461	7.1	26.8	4.16	0.13
	10	13.63	0.0731	37.14	4.626	7.0	19.4	4.17	0.13
	04	13.38	0.0719	36.27	2.942	7.1	19.8	4.18	0.13
	12	9.219	0.0739	22.03	1.329	6.9	29.2	4.25	0.19
	14	14.27	0.0708	39.08	2.031	7.2	18.9	4.27	0.16
	01	11.65	0.0736	29.89	2.248	6.9	24.1	4.43	0.14
	06	14.43	0.0762	39.04	1.194	6.7	19.9	4.55	0.23
Z	07	14.18	0.0692	37.68	0.848	7.4	21.3	4.78	0.31
Z	02	17.89	0.0764	49.14	1.172	6.7	18.7	5.30	0.30
	Mean age ± 2σ	n=12	MSWD=2.00			7.0 ±0.3		4.067	0.073
	AD-55,J8:160, single crystal sanidine, J=0.0007303±0.10%, D=1.00743±0.00124, NM-160, Lab#=53771								
xi	20	4.920	0.0154	13.92	2.448	33.2	16.4	1.08	0.10
xi	05	1.208	0.0261	1.244	2.603	19.5	69.8	1.110	0.070
	08	1.024	0.0190	0.4789	2.729	26.9	86.3	1.164	0.066
	11	1.094	0.0194	0.7151	3.000	26.3	80.8	1.165	0.060
	03	0.9404	0.0158	0.1746	2.371	32.2	94.6	1.172	0.076
	06	1.364	0.0192	1.605	3.787	26.6	65.3	1.174	0.049
	10	0.9617	0.0231	0.2300	3.355	22.1	93.1	1.179	0.053
	07	0.9267	0.0203	0.0890	2.256	25.2	97.3	1.188	0.079

	33	1.006	0.0130	0.3882	4.979	39.3	88.7	1.189	0.039
	36	1.011	0.0163	0.4038	2.694	31.2	88.3	1.190	0.069
	04	0.9723	0.0200	0.2310	3.218	25.6	93.1	1.193	0.056
	22	1.309	0.0173	1.402	4.393	29.5	68.5	1.194	0.045
	01	0.9463	0.0161	0.1333	3.865	31.6	96.0	1.196	0.046
	26	1.050	0.0153	0.5221	4.202	33.3	85.4	1.196	0.045
	09	0.9647	0.0170	0.1883	1.835	30.0	94.4	1.199	0.099
	24	2.820	0.0160	6.499	2.835	31.9	31.9	1.201	0.080
	13	1.241	0.0216	1.112	3.296	23.6	73.7	1.204	0.055
	21	1.041	0.0191	0.4216	2.789	26.7	88.2	1.224	0.067
	12	1.453	0.0296	1.776	2.331	17.2	64.1	1.226	0.079
	25	1.079	0.0151	0.5394	3.815	33.8	85.3	1.227	0.050
	15	1.000	0.0226	0.2195	2.439	22.5	93.7	1.234	0.073
	27	1.101	0.0203	0.5821	2.735	25.2	84.5	1.240	0.070
	02	1.111	0.0232	0.5670	2.963	22.0	85.1	1.245	0.061
	35	1.101	0.0309	0.5693	2.937	16.5	85.0	1.247	0.064
	30	1.300	0.0341	1.207	3.134	15.0	72.8	1.262	0.061
	34	1.092	0.0163	0.4763	3.229	31.4	87.2	1.269	0.059
	14	1.245	0.0368	0.9540	1.450	13.9	77.6	1.27	0.12
	23	1.389	0.0159	1.470	2.269	32.0	68.8	1.274	0.085
	32	1.113	0.0162	0.5371	1.919	31.4	85.9	1.274	0.098
	29	1.173	0.0271	0.7366	2.990	18.8	81.6	1.276	0.063
xi	31	1.312	0.0202	1.027	3.320	25.2	77.0	1.346	0.058
xi	28	2.174	0.0438	3.719	2.379	11.7	49.6	1.438	0.087
	Mean age ± 2σ	n=28	MSWD=0.31		26.5	±12.6		1.210	0.023

AD-54, J9:160, single crystal sanidine, J=0.0007306±0.10%, D=1.00743±0.00124, NM-160, Lab#=53772

09	0.9121	0.0160	0.2175	12.450	31.9	93.1	1.119	0.041
06	1.706	0.0176	2.880	13.708	29.1	50.2	1.128	0.040
05	0.9922	0.0216	0.4640	7.401	23.6	86.4	1.129	0.068
07	0.9178	0.0160	0.0628	11.781	32.0	98.1	1.186	0.043
25	0.9406	0.0260	0.1655	10.460	19.6	95.0	1.189	0.038
15	1.541	0.0366	2.169	9.834	13.9	58.6	1.190	0.053
38	2.275	0.0316	4.672	7.673	16.2	39.4	1.193	0.061
23	1.072	0.0146	0.5766	6.368	34.9	84.2	1.201	0.062
14	0.9576	0.0216	0.1566	5.512	23.6	95.4	1.203	0.092
11	0.9379	0.0172	0.0853	6.400	29.6	97.5	1.204	0.078
20	1.024	0.0210	0.4008	7.096	24.3	88.6	1.207	0.057
36	0.9754	0.0140	0.2305	7.229	36.5	93.1	1.208	0.054
02	3.145	0.0223	7.536	7.167	22.8	29.2	1.211	0.080
37	1.084	0.0158	0.5894	4.004	32.4	84.0	1.211	0.097
04	0.9680	0.0258	0.1628	6.354	19.8	95.3	1.215	0.079
10	0.9481	0.0269	0.0939	8.697	19.0	97.3	1.215	0.057
26	1.004	0.0274	0.3048	6.394	18.7	91.3	1.219	0.060
08	1.095	0.0170	0.5597	9.830	29.9	85.0	1.226	0.052
22	1.119	0.0375	0.6641	8.654	13.6	82.7	1.232	0.045
24	1.011	0.0291	0.2674	6.654	17.5	92.4	1.242	0.058
35	1.152	0.0251	0.7175	9.028	20.3	81.8	1.253	0.050
27	0.9849	0.0203	0.1092	5.561	25.1	96.9	1.269	0.066
31	1.012	0.0190	0.1176	7.110	26.8	96.7	1.302	0.054
01	1.063	0.0257	0.2482	6.347	19.9	93.3	1.306	0.084
21	1.267	0.0126	0.9623	6.392	40.6	77.6	1.308	0.062
30	1.027	0.0139	0.1327	8.509	36.8	96.3	1.315	0.044
32	0.9628	0.0152	-0.0877	6.701	33.6	102.8	1.317	0.058
34	1.125	0.0156	0.4552	6.033	32.8	88.2	1.319	0.063
03	1.068	0.0332	0.1811	5.694	15.3	95.2	1.340	0.087
33	1.654	0.0346	2.164	4.127	14.7	61.5	1.354	0.099
12	1.384	0.0233	1.211	7.465	21.9	74.3	1.355	0.068
13	1.221	0.0174	0.6438	7.187	29.3	84.5	1.359	0.069
28	1.478	0.0249	1.415	5.698	20.5	71.9	1.413	0.070
29	1.738	0.0383	2.255	8.917	13.3	61.8	1.430	0.051

Mean age ± 2σ	n=34	MSWD=1.95	24.7 ±15.3	1.239	0.028

Notes:

Isotopic ratios corrected for blank, radioactive decay, and mass discrimination, not corrected for interfering reactions.
Errors quoted for individual analyses include analytical error only, without interfering reaction or J uncertainties.
Mean age is weighted mean age of Taylor (1982). Mean age error is weighted error
of the mean (Taylor, 1982), multiplied by the root of the MSWD where MSWD>1, and also
incorporates uncertainty in J factors and irradiation correction uncertainties.
Decay constants and isotopic abundances after Steiger and Jäger (1977).
symbol preceding sample ID denotes analyses excluded from mean age calculations.
Ages calculated relative to FC-2 Fish Canyon Tuff sanidine interlaboratory standard at 28.02 Ma
Decay Constant (LambdaK (total)) = 5.543e-10/a
Correction factors for NM-160:
$(^{39}Ar/^{37}Ar)_{Ca}$ = 0.0007 ± 2e-05
$(^{36}Ar/^{37}Ar)_{Ca}$ = 0.00028 ± 5e-06
$(^{38}Ar/^{39}Ar)_{K}$ = 0.01077
$(^{40}Ar/^{39}Ar)_{K}$ = 0.0002 ± 0.0003

Correction factors for NM-183:
$(^{39}Ar/^{37}Ar)_{Ca}$ = 0.00077 ± 2e-05
$(^{36}Ar/^{37}Ar)_{Ca}$ = 0.000276 ± 5e-06
$(^{38}Ar/^{39}Ar)_{K}$ = 0.0127
$(^{40}Ar/^{39}Ar)_{K}$ = 0.03 ± 0.002

Correction factors for NM-190:
$(^{39}Ar/^{37}Ar)_{Ca}$ = 0.000289 ± 5e-06
$(^{36}Ar/^{37}Ar)_{Ca}$ = 0.00068 ± 2e-05
$(^{38}Ar/^{39}Ar)_{K}$ = 0.013
$(^{40}Ar/^{39}Ar)_{K}$ = 0 ± 0.0004

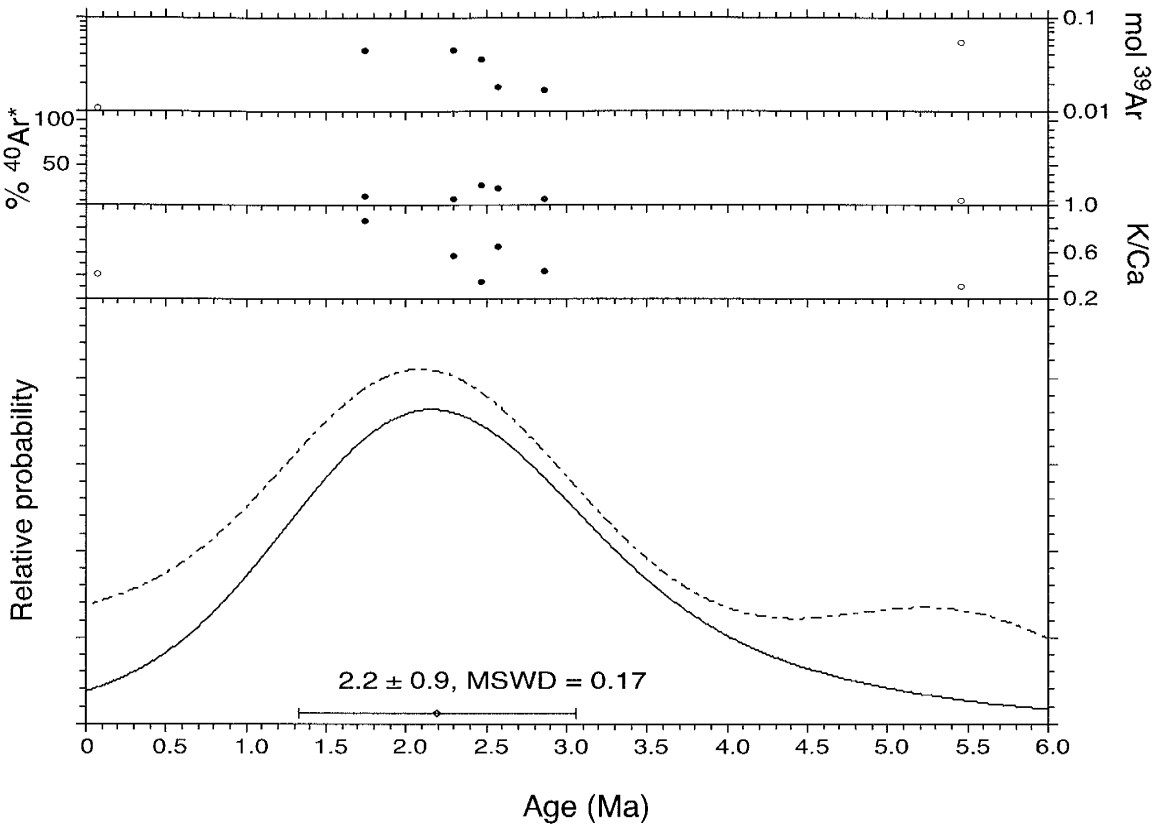

Figure C.5.1. Ideogram of plagioclase sample AD-03. This sample was not used for age calculation becasue the mineral examined was plagioclase feldspar instead of K-feldspar as known by the low K/Ca values. The impresice and inaccurate age for this sample shows why plagioclase feldspar is a poor $^{40}Ar/^{39}Ar$ dating material.

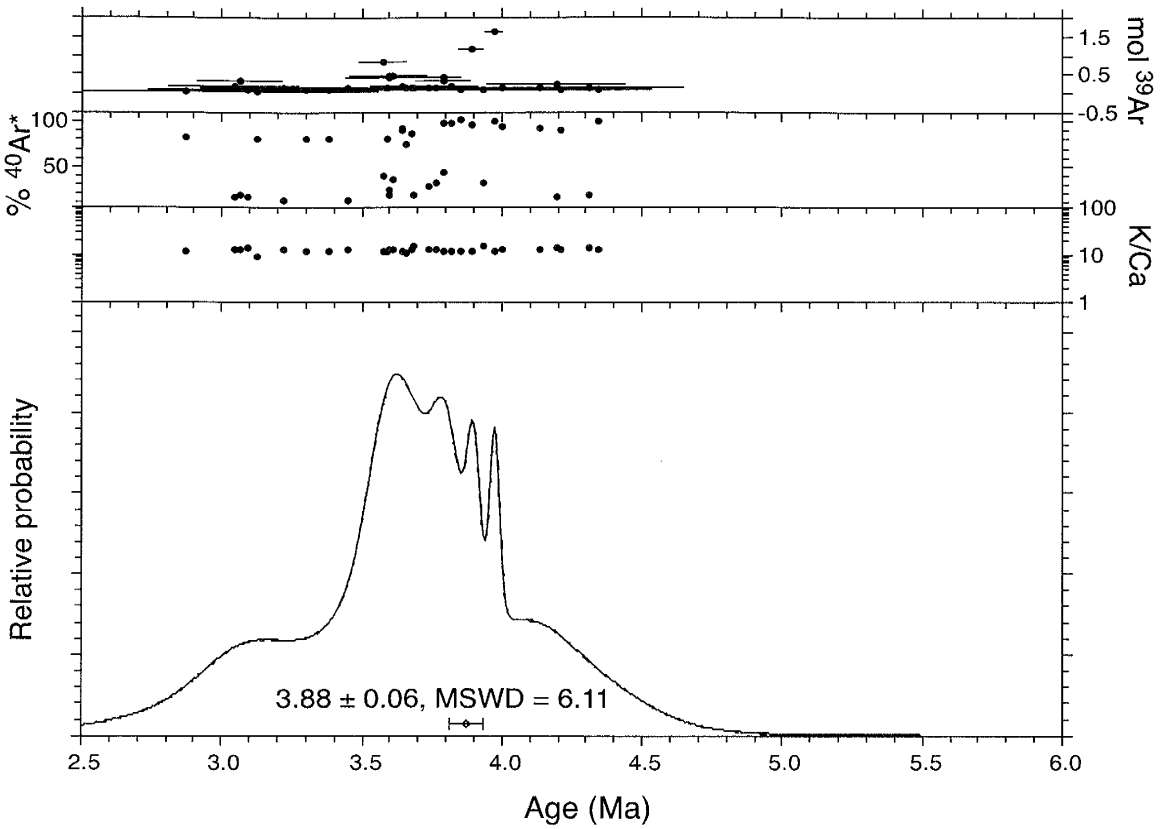

Figure C.5.2. Ideogram of obsidian sample AD-06 that forms a broad population of points. The poor MSWD is due to the scattered population; there are no outliers from this population and no points were removed from the analysis. The age overlaps other flows from the same event within uncertainty.

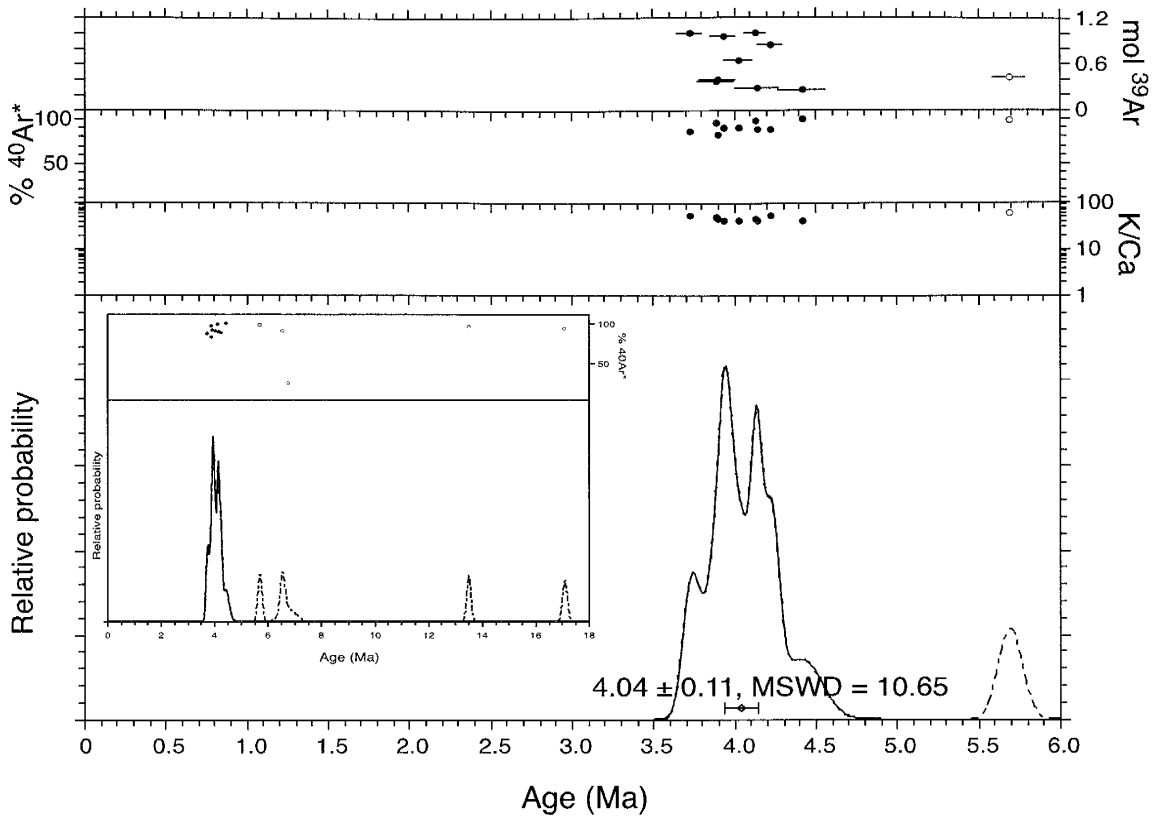

Figure C.5.3. Ideogram of sanidine sample AD-09. After many xenocrysts were removed a low-precision age was obtained at 4.04± 0.11 Ma with a MSWD of 10.65. This population of points is very scattered; the age matches other ages from the same event and therefore no attempt was made to improve the quality of this data.

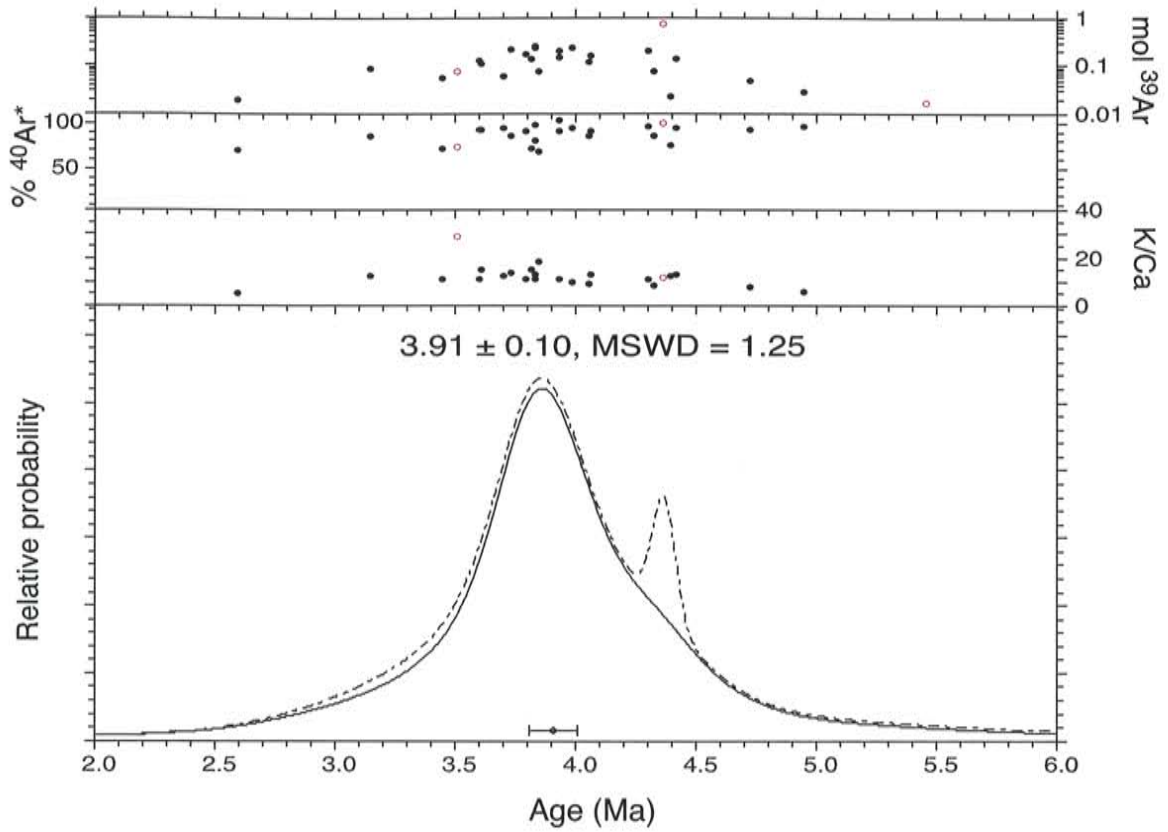

Figure C.5.4. Ideogram of obsidian sample AD-12 where three points have been removed from analysis.

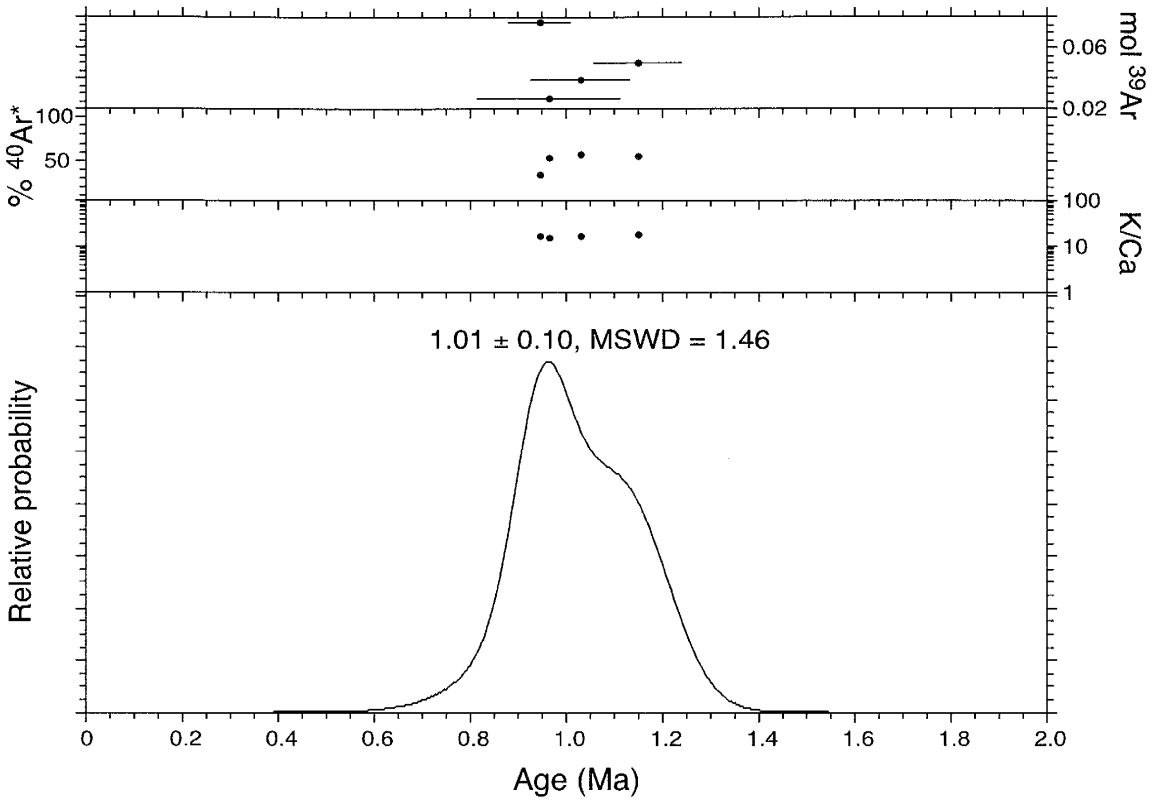

Figure C.5.5. Ideogram of obsidian sample AD-21. Although over fifteen analyses were taken from this sample, only four points made the criteria. Due to the few points used for this analysis little emphasis is placed on this data set, although the date does overlap other ages within uncertainty. This age was not used in the age calculation for the DM-W lobe.

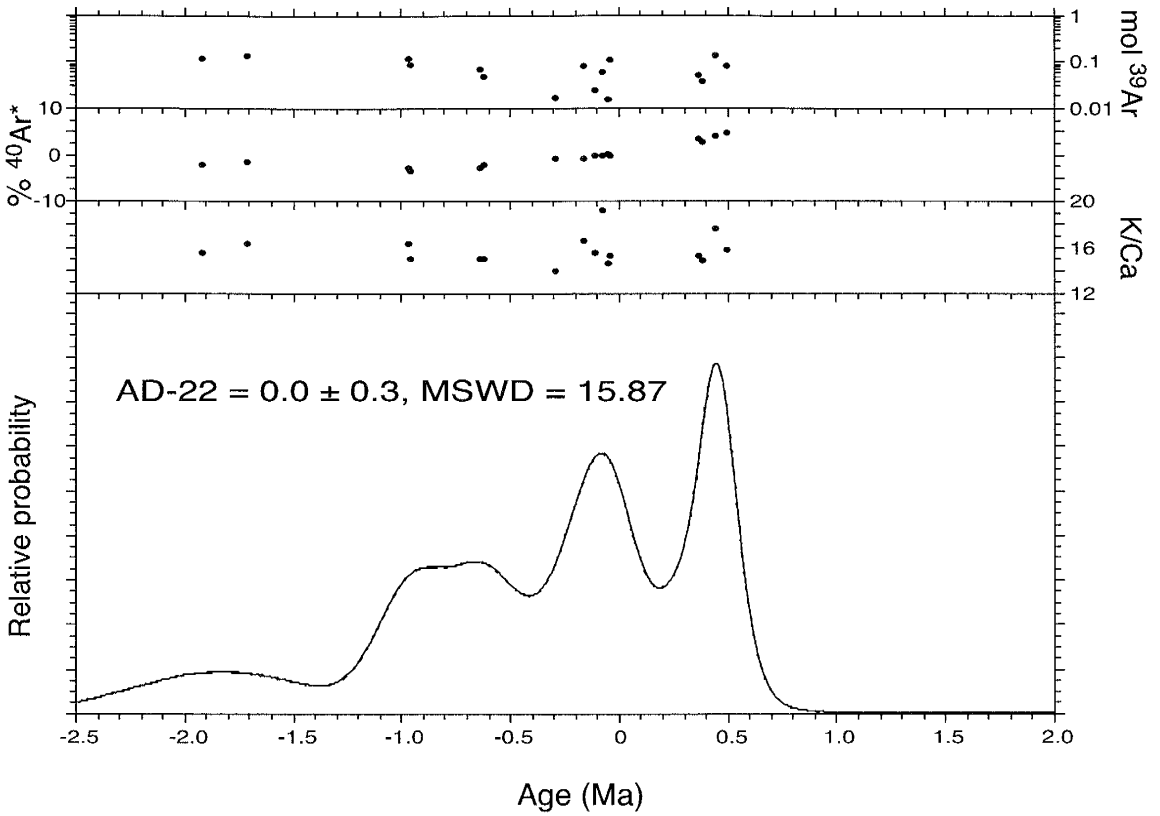

Figure C.5.6. Ideogram of obsidian sample AD-22 displaying a curve that represents a high degree of argon loss. No data from this sample met the criteria, nor was an age calculated for this sample.

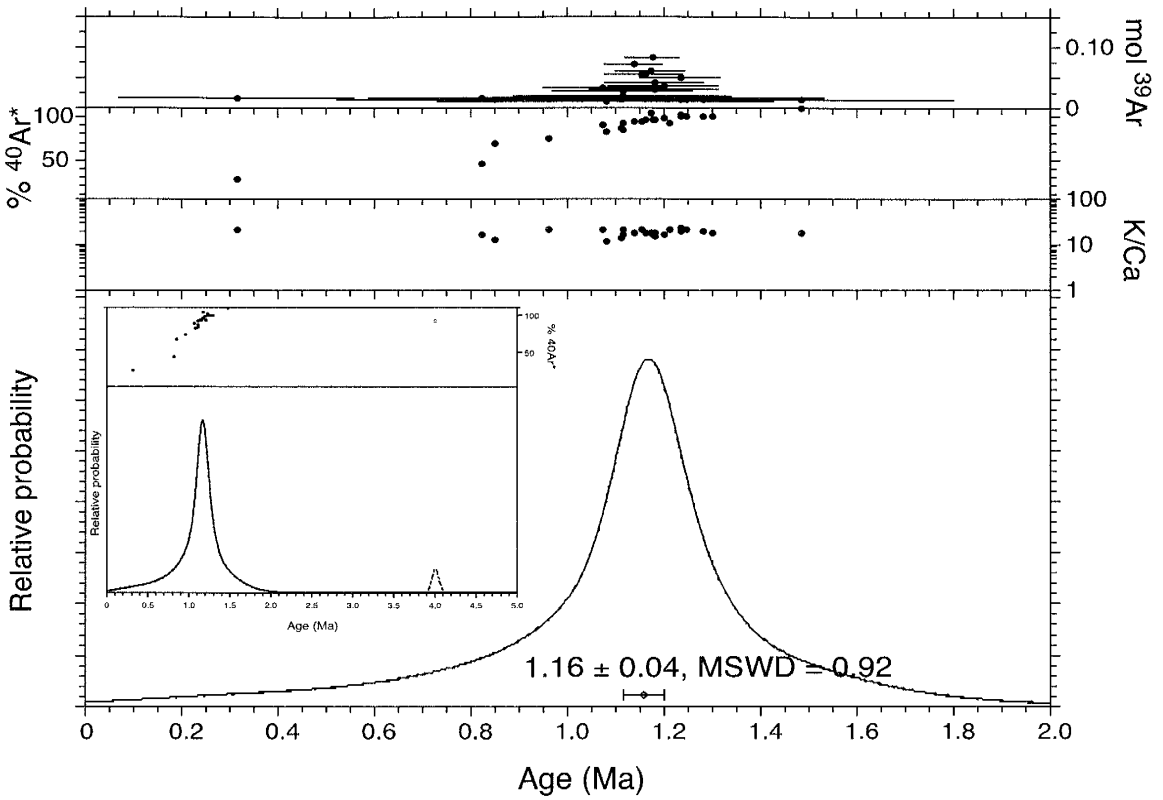

Figure C.5.7. Ideogram representing obsidian sample AD-23 where there is one xenocrystic outlier in the population (inset). After the removal of the outlier, the age becomes 1.16± 0.04 with an MSWD of 0.92. No other points were removed from the analysis.

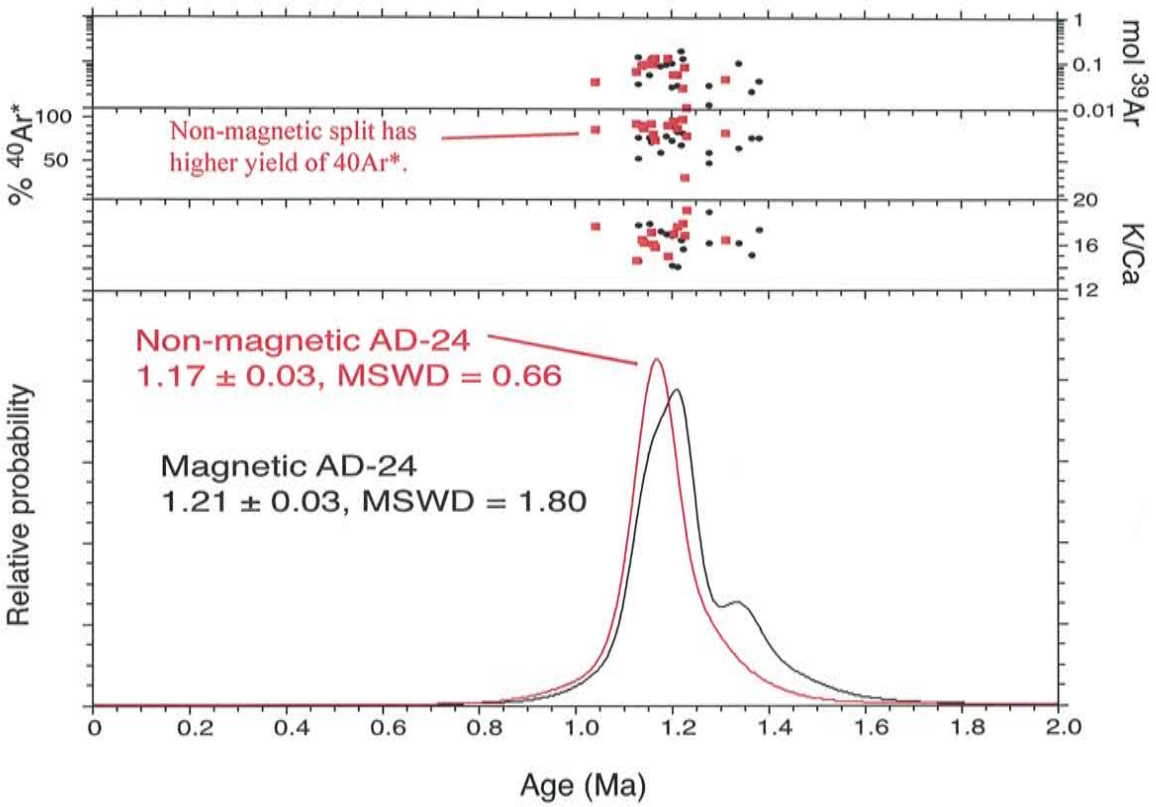

Figure C.5.8. Ideogram of the magnetic and non-magnetic sieve fractions from obsidian sample AD-24. No points were removed from either analysis because all points fell within a single population for both samples, sample ages overlap within uncertainty.

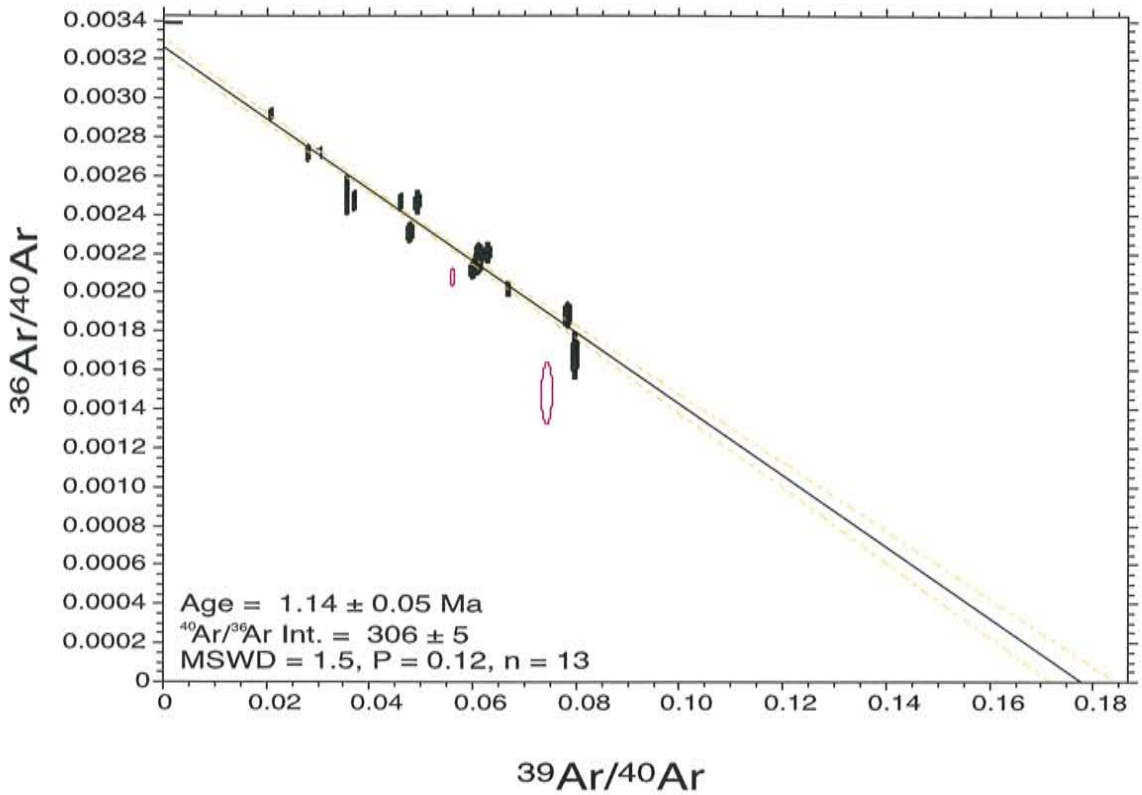

Figure C.5.9. Inverse isochron of anorthoclase sample AD-25. This sample had excess argon and an ideogram cannot take this into account, therefore an isochron age was used for this sample.

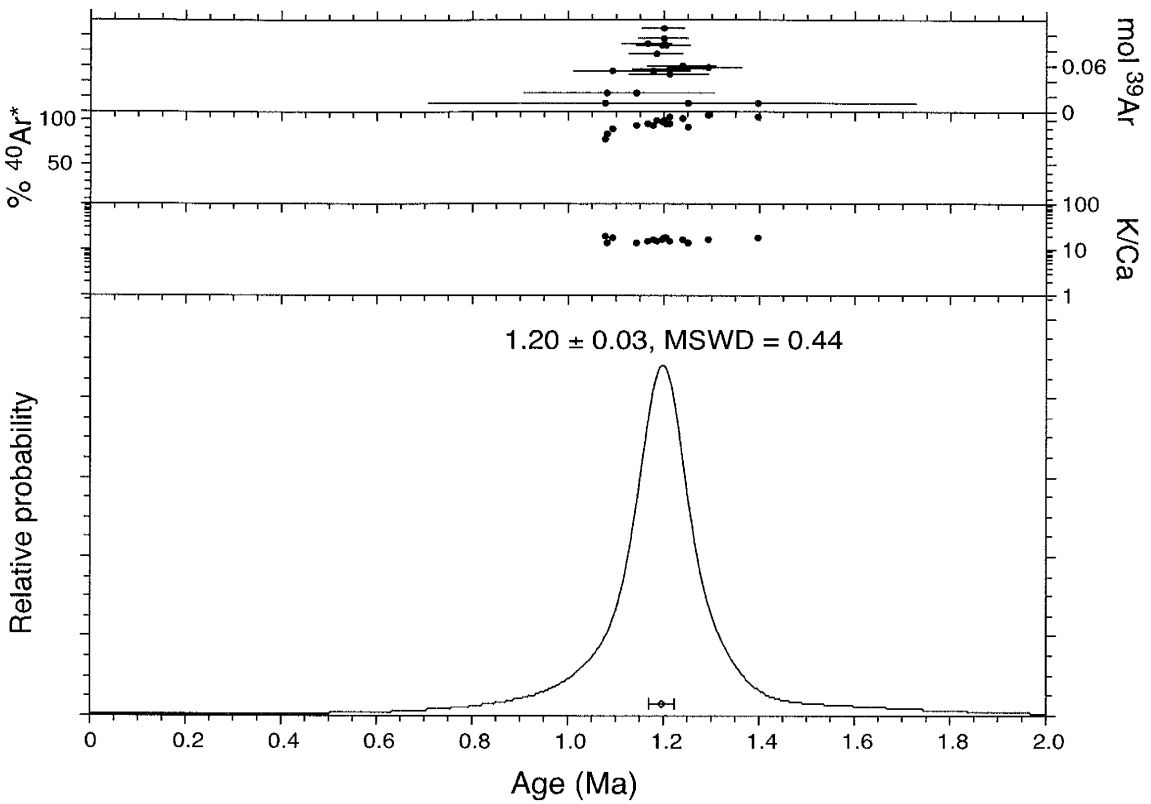

Figure C.5.10. Ideogram of obsidian sample AD-26 that displays a Gaussian curve with an age of 1.20± 0.03 Ma and a MSWD of 0.44. No points were taken out of the analysis.

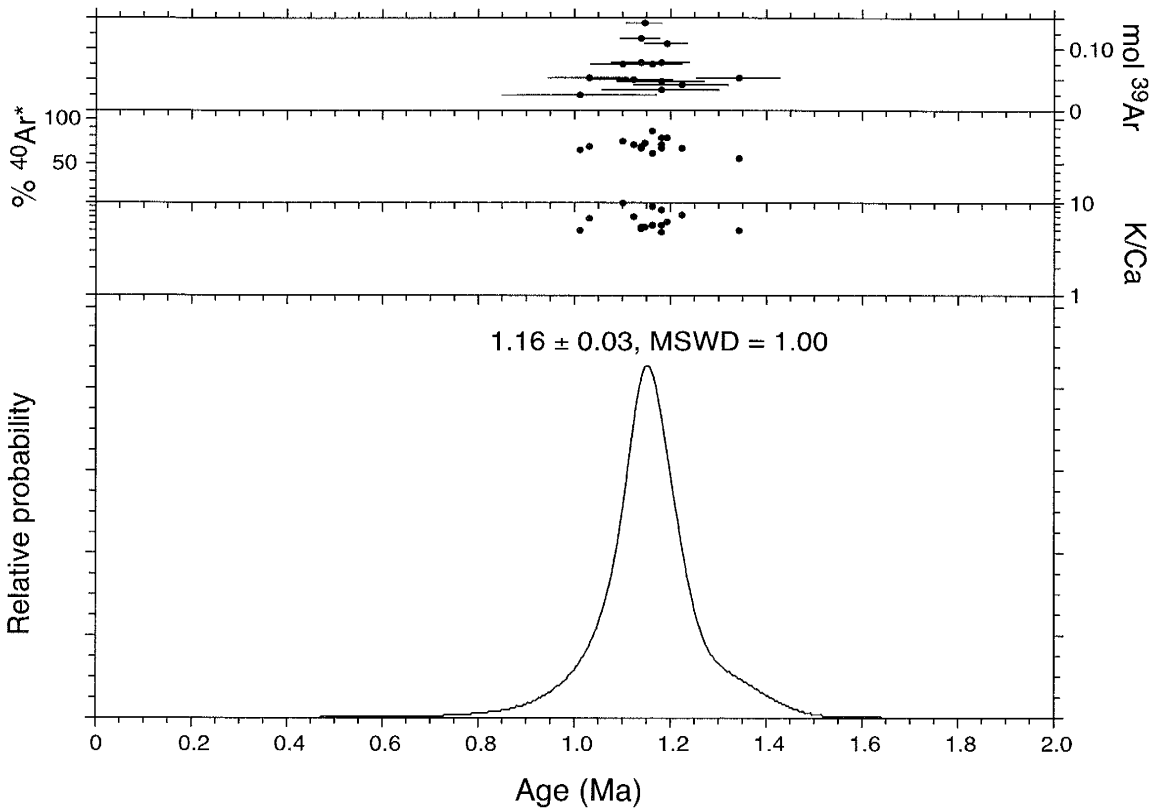

Figure C.5.11. Ideogram of anorthoclase sample AD-27 which displays a Gaussian curve that yields an age of 1.16± 0.03 Ma and a MSWD of 1.00. No points were removed from the analysis.

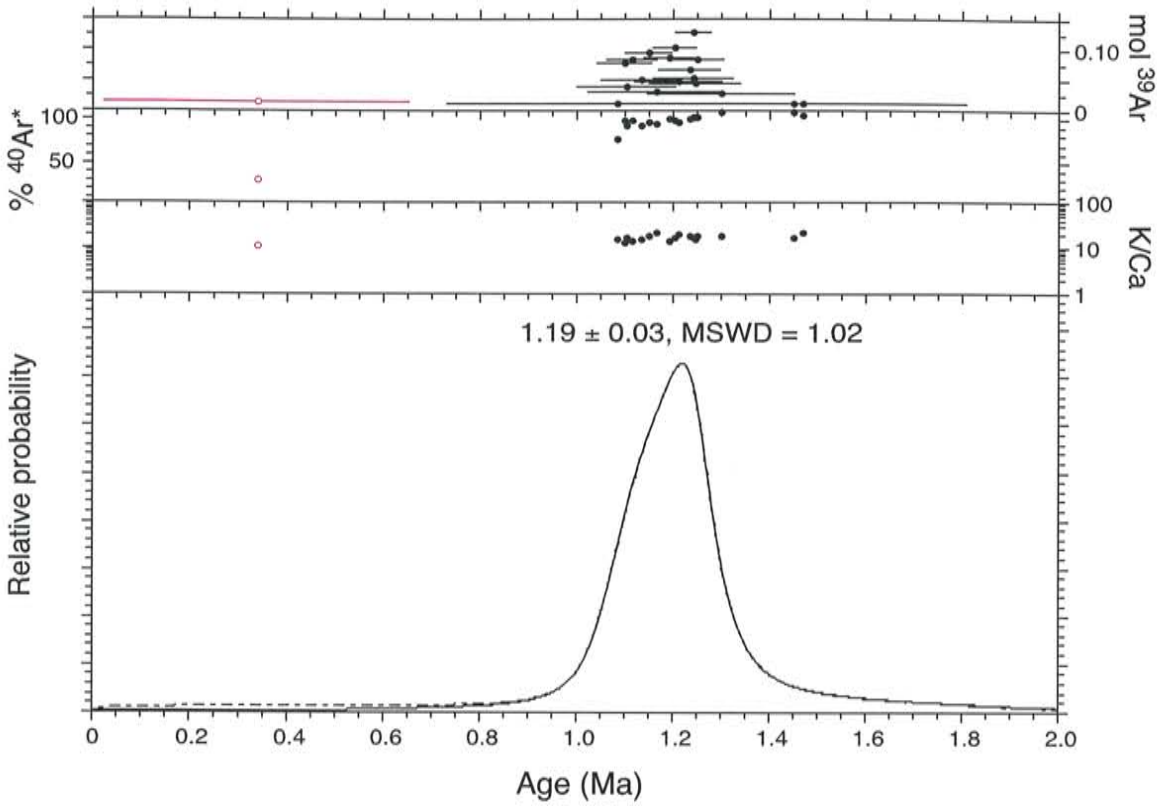

Figure C.5.12. Ideogram of obsidian sample AD-28 from the Banco Bonito formation. No points were taken out of the analysis; the Gaussian curve yields an age of 1.19± 0.03 Ma and a MSWD of 1.02, which overlaps ages from the Cerro del Medio dome. This age represents a xenocrystic age because the Banco Bonito lava is the youngest post-0.5 Ma unit associated with the Valles caldera (Self et al., 1991).

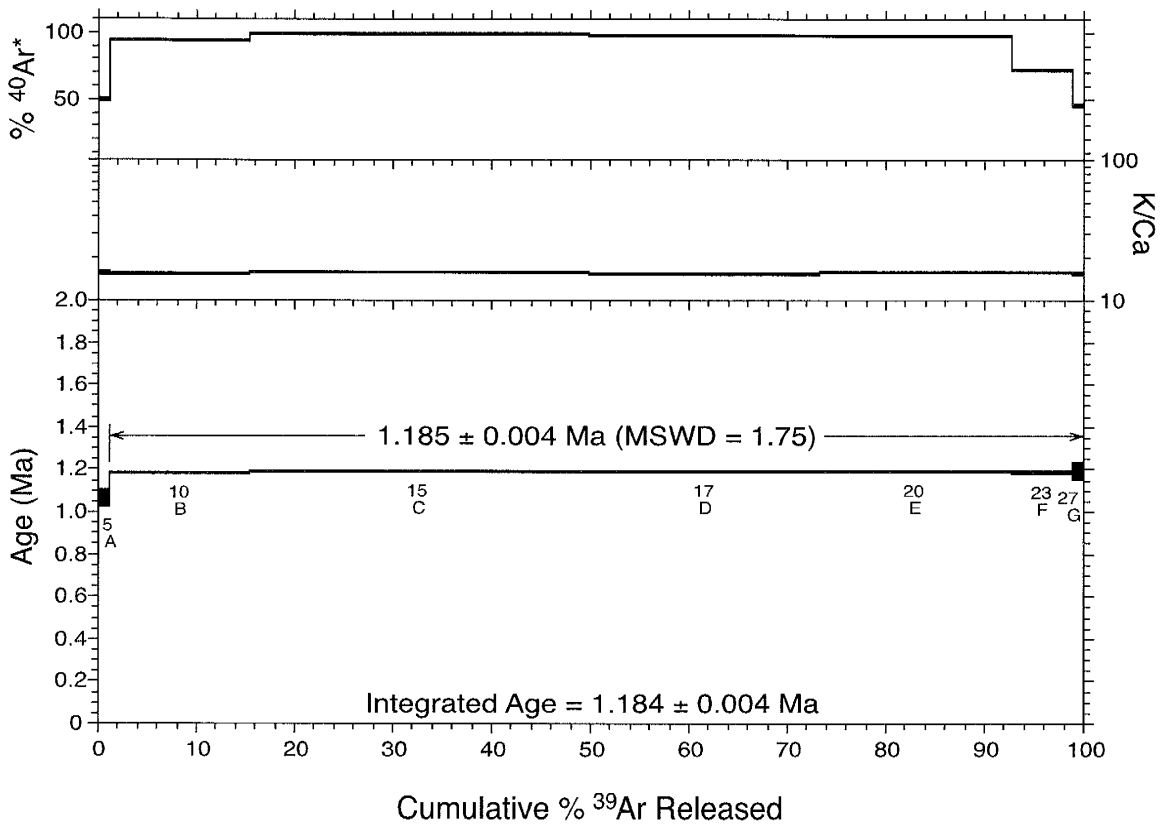

Figure C.5.13. Age spectra of obsidian sample AD-50. The flat plateau age overlaps with the integrated age for this sample; the plateau age is used for the age in this study.

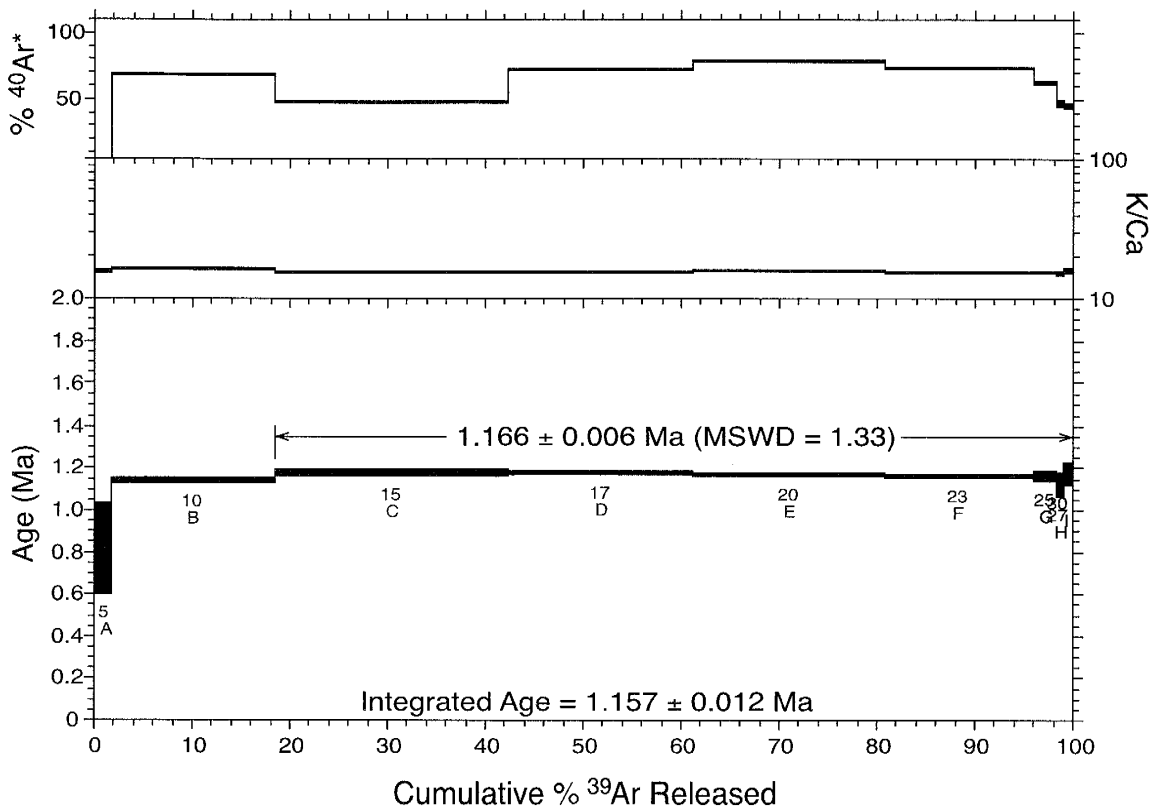

Figure C.5.14. Age spectra of obsidian sample AD-51. The nearly flat plateau age overlaps with the integrated age for this sample; the plateau age is used in this study.

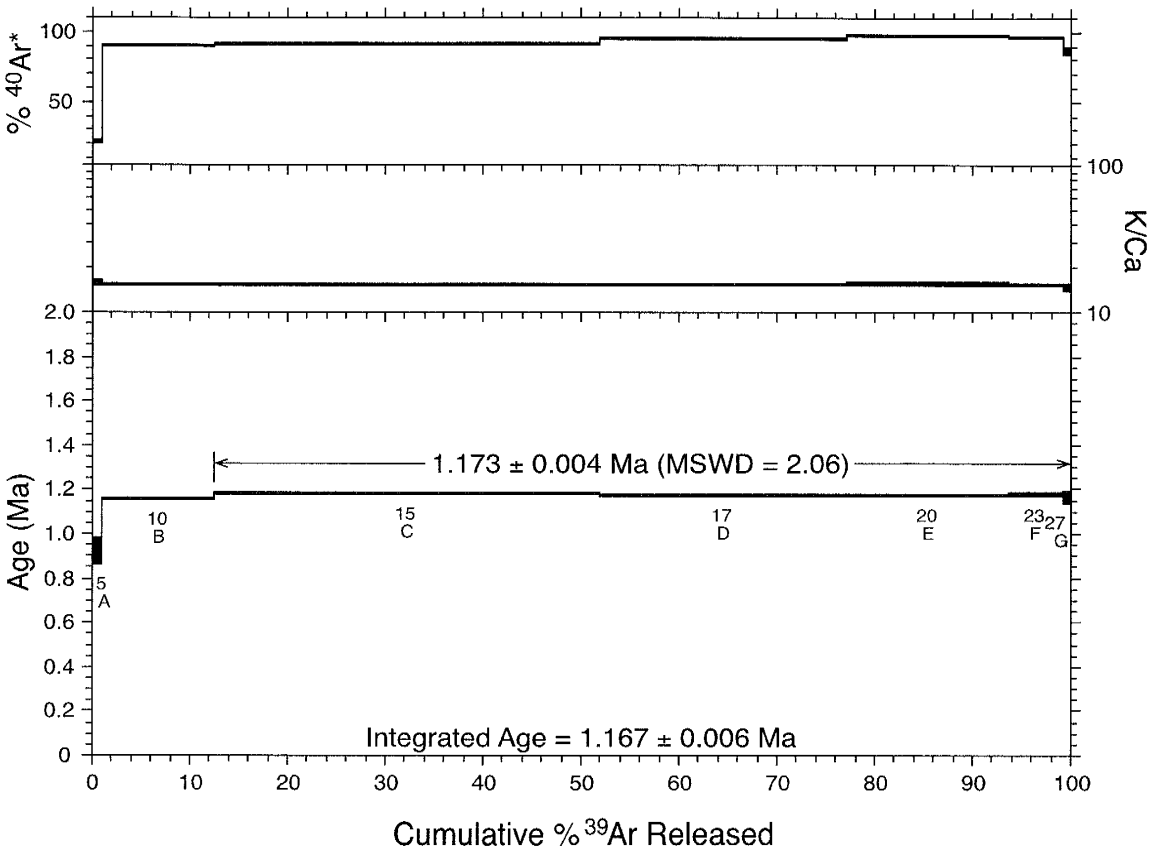

Figure C.5.15. Age spectra of obsidian sample AD-52. The flat plateau age overlaps within uncertainty with the integrated age; the high-precision plateau age is used for the age in this study.

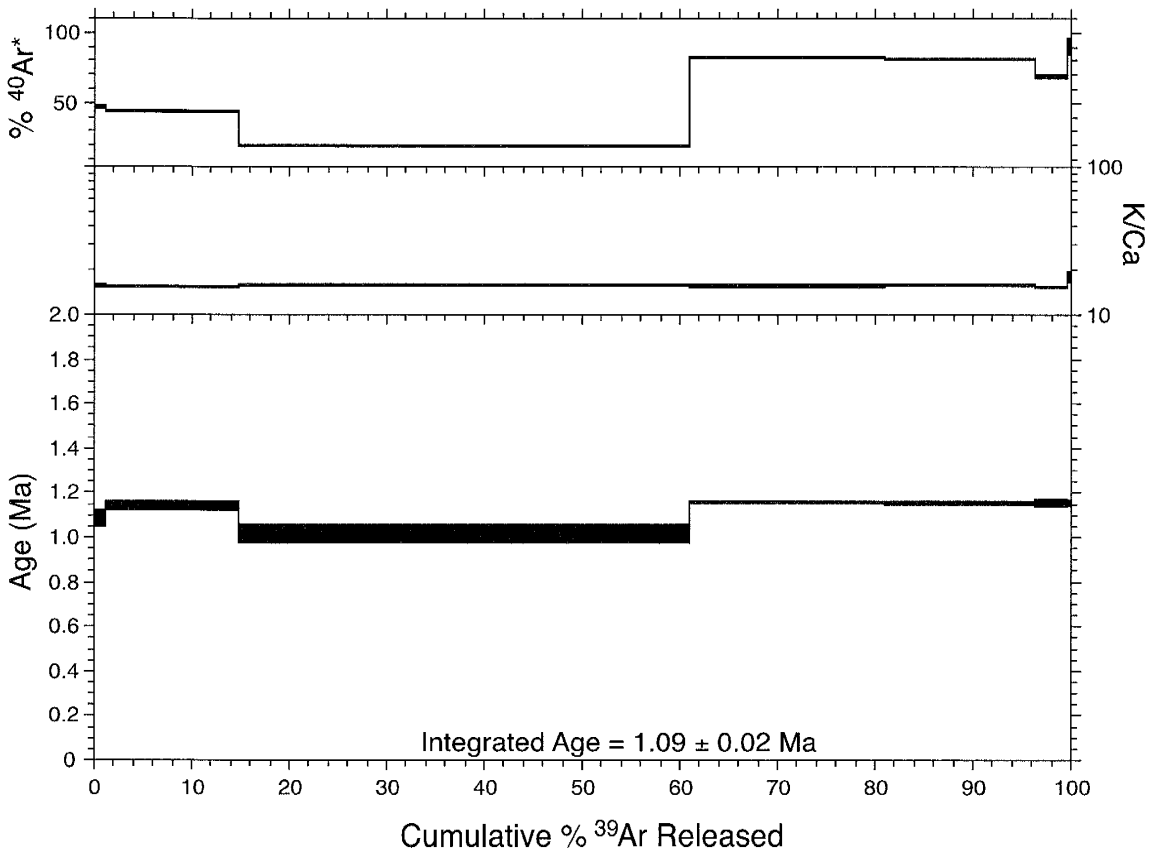

Figure C.5.16. A discordant age spectra of obsidian sample AD-53. Problems during extraction caused an inexplicable change in age and yield of $^{40}Ar^*$ during the C step. This sample was not used to calculate the age of the DM-W dome becasue of the problems encountered during analyis.

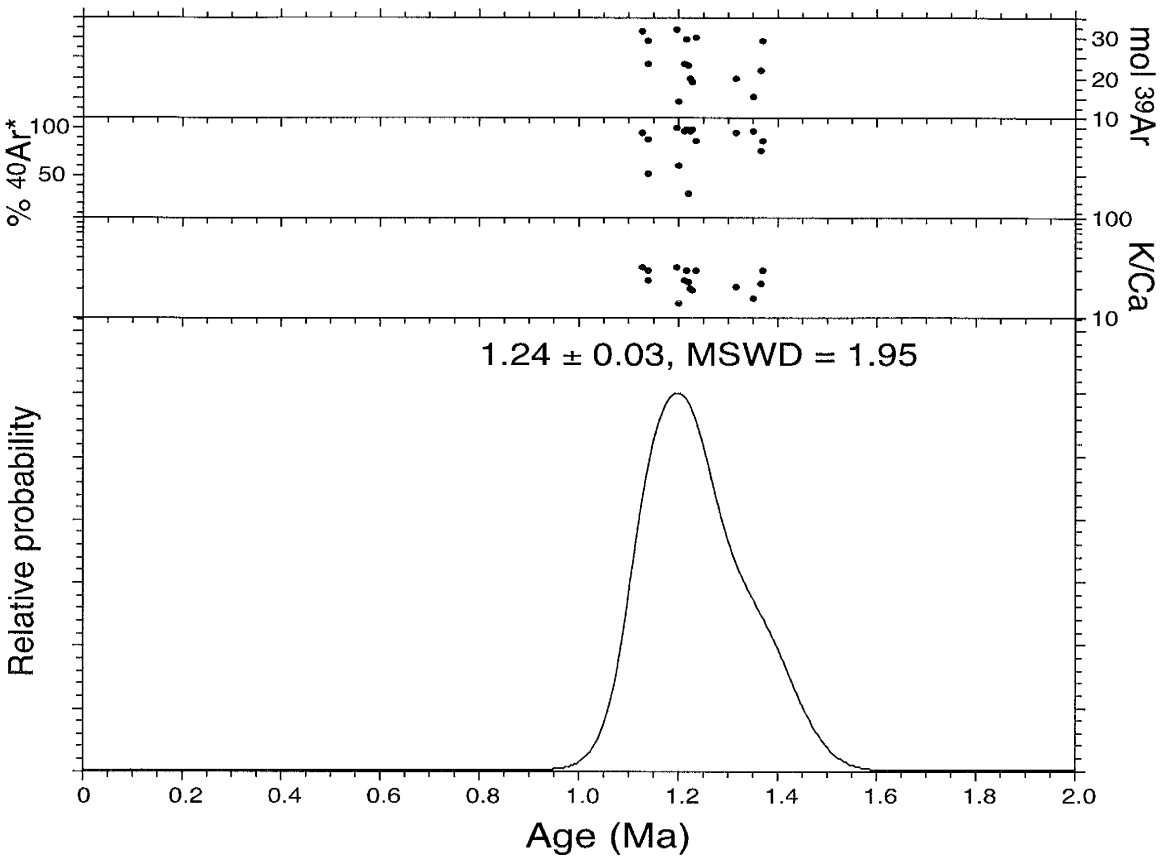

Figure C.5.17. Ideogram of sanidine sample AD-54. The curve is Gaussian although there is a slight shoulder that leans towards older ages; no points were removed from the analysis.

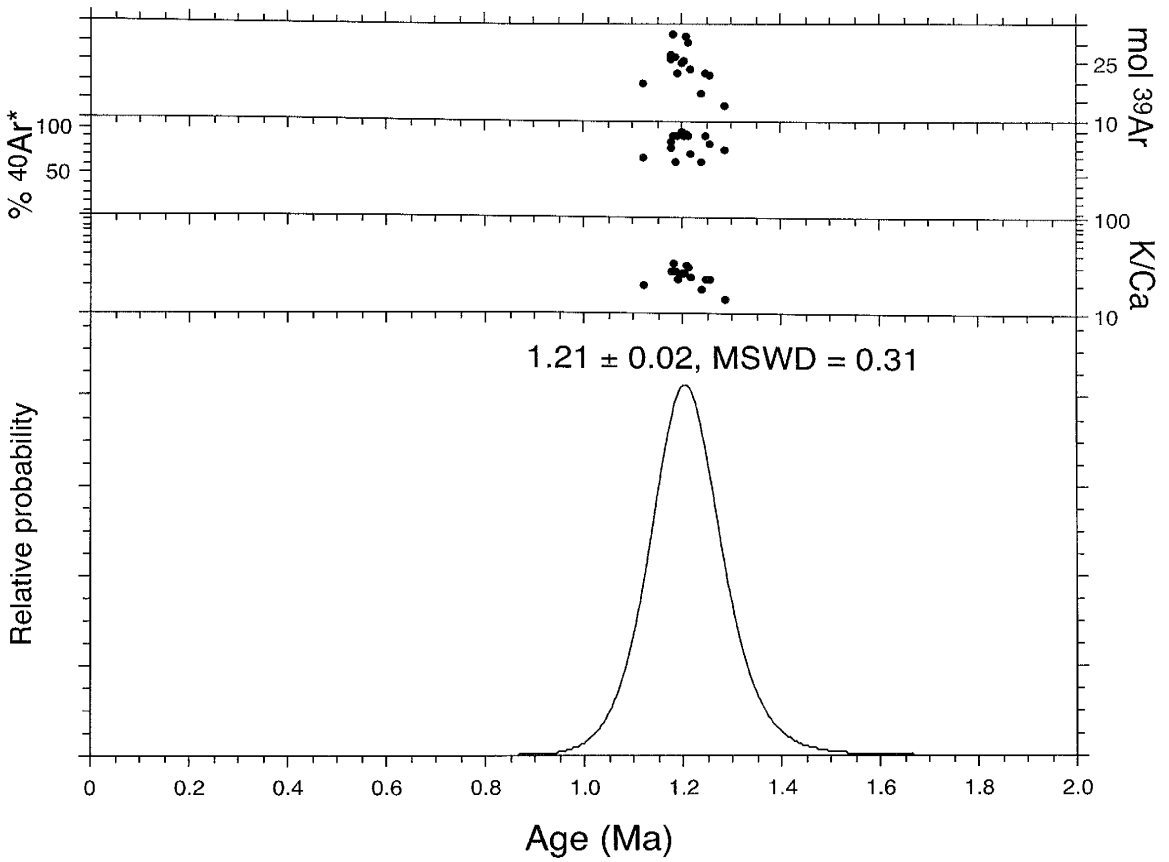

Figure C.5.18. Ideogram of sanidine sample AD-55. No points were removed from the analysis.